Engineering Aspects Of Photogrammetric Plate Measurement: Including The Development of A Novel Interferometer

A Thesis submitted for the degree of Doctor of Philosophy

by

Ian Severn

Brunel Centre for Manufacturing Metrology, Brunel University

September 1993

Acknowledgements

I would like to thank the following people at The National Physical Laboratory for their help in producing this Thesis; Dr. C.Forno, Dr. R.A.Hunt, Mr. S.Brown and Mr. S.Oldfield. I would also like to thank Dr. R.C.Spooncer and Professor B.E.Jones at Brunel University for their help.

This work was jointly funded by The Science and Engineering Council and The National Physical Laboratory.

ABSTRACT

Two different factors involved in the measurement of photogrammetric plates have been studied. A novel interferometer designed to monitor the position of a microscope stage, to be used to measure photogrammetric plates, has been built. The prototype instrument is able to give the position of the stage with a maximum error of less than 200nm.

An algorithm has been developed for a motor driven x-y microscope that is able to search a photographic plate automatically for targets, and record their positions. In a trial survey this system was able to measure the positions of the targets on the plates with an uncertainty of approximately 2μm. This result is comparable with the precision that a human operator could achieve using the same equipment, but without the fatigue effect associated with visual observation. Virtually no human interaction is necessary for the system to function.

CONTENTS

1. INTRODUCTION

Photogrammetry is a technique, based on linear perspective theory, for extracting 3-dimensional information from multiple photographs of an object. The method may be subdivided into two broad categories, close range photogrammetry and remote sensing.

Remote sensing is concerned with obtaining information about the general form of an object rather than its absolute structure. The prime use for remote sensing is in map making where aerial pictures, taken from an aeroplane or a satellite, are used to reconstruct ground features.

Close range photogrammetry is concerned with structures on a smaller scale. It can produce accurate 3-dimensional information about a shape. One of the highest measurement accuracies currently quoted is 2 parts in 10^6 (Burch & Forno 1983) which means that the position of a point inside a volume of 1 metre^3 can be determined to 2 microns. Some of the many applications of photogrammetry include medicine (Turner-Smith *et al* 1990), industrial quality control (van Voorden 1990), automated production (Rüther and Wildschek 1989), architectural surveys (Baratin *et al* 1990), and robot vision (Pinkney *et al* 1990).

1.1 Historical Development

The development of practical photogrammetry began in 1859, twenty years after Daguerre and Nièpce had independently discovered direct photographic processes. Colonel Aimé Laussedat constructed street maps of Paris using pairs of photographs

taken from the roofs of buildings in the city. By taking each photograph from the end of a baseline, he was able to work out the bearings of individual features on the photographs. Hence, he could calculate the coordinates of the point of intersection between pairs of rays. He also responsible for the first air survey. Cameras were carried in hot air balloons during mapping of the village of Buc near Versailles. Laussedat published his results at the turn of the century in three volumes (1898,1901,1903). The use of photogrammetry for map production progressed rapidly during the first world war owing to the need to produce maps quickly.

The theory of photogrammetry advanced while this practical work was being carried out, with J.H.Lambert(1901) publishing a book in which he outlined the concept of space-resection. The application of photogrammetry to industrial problems was proposed by E.Church in a series of bulletins starting in 1930. He also solved many problems concerning space resection, and developed an iterative technique for determining the location of cameras. However, until the advent of computers in the 1940s it was not possible to make full use of all the data available in a photogrammetric survey. The ability of computers to perform complex calculations quickly allowed for the use of more than two cameras, as well as making it possible to calculate various camera parameters such as distortion, focal length and orientation. Larger surveys could be conducted as the calculation process was automated.

Over the last twenty-five years tremendous advances in imaging technology have allowed photogrammetry to be used in many new fields. Modern holographic films such as Agfa 10E75, available since 1965, with their very fine grain size and high contrast,

have enabled conventional photogrammetry to be used with greater accuracy (Gates *et al* 1982). A conventional industrial survey may now be performed to an accuracy of one part in 10^5 (Dold 1990).

A special camera designed for the photogrammetric calibration of 3-coordinate measuring machines has been developed at the National Physical Laboratory. This monocentric camera, known as Centrax, is able to provide information about standard structures to an accuracy of 2 parts in 10^6 (Burch & Forno 1983,Forno 1991).

The advent of the CCD camera as a imaging medium that may be examined instantaneously has led to the development of Real-time Photogrammetry. CCD based systems have been used in applications ranging from car building (Grün 1990) to space research (Maclean *et al* 1990).

1.2 The Basis Of The Technique

Photographs of the object under investigation are taken from several different viewpoints, the relative positions of features are measured on the resulting photographic plates. A simple illustration of the technique is shown in figure 1.1. All of the rays entering the camera are considered to have passed through the centre of the camera lens system, as if it was a pinhole camera. Points lying on a particular line in space are all imaged onto a particular point on the photographic plate as shown in figure 1.1.

Point a is imaged, through the lens centre p^1 (known as the perspective centre of the camera), onto point a^1 on the first photographic plate, and point b is imaged

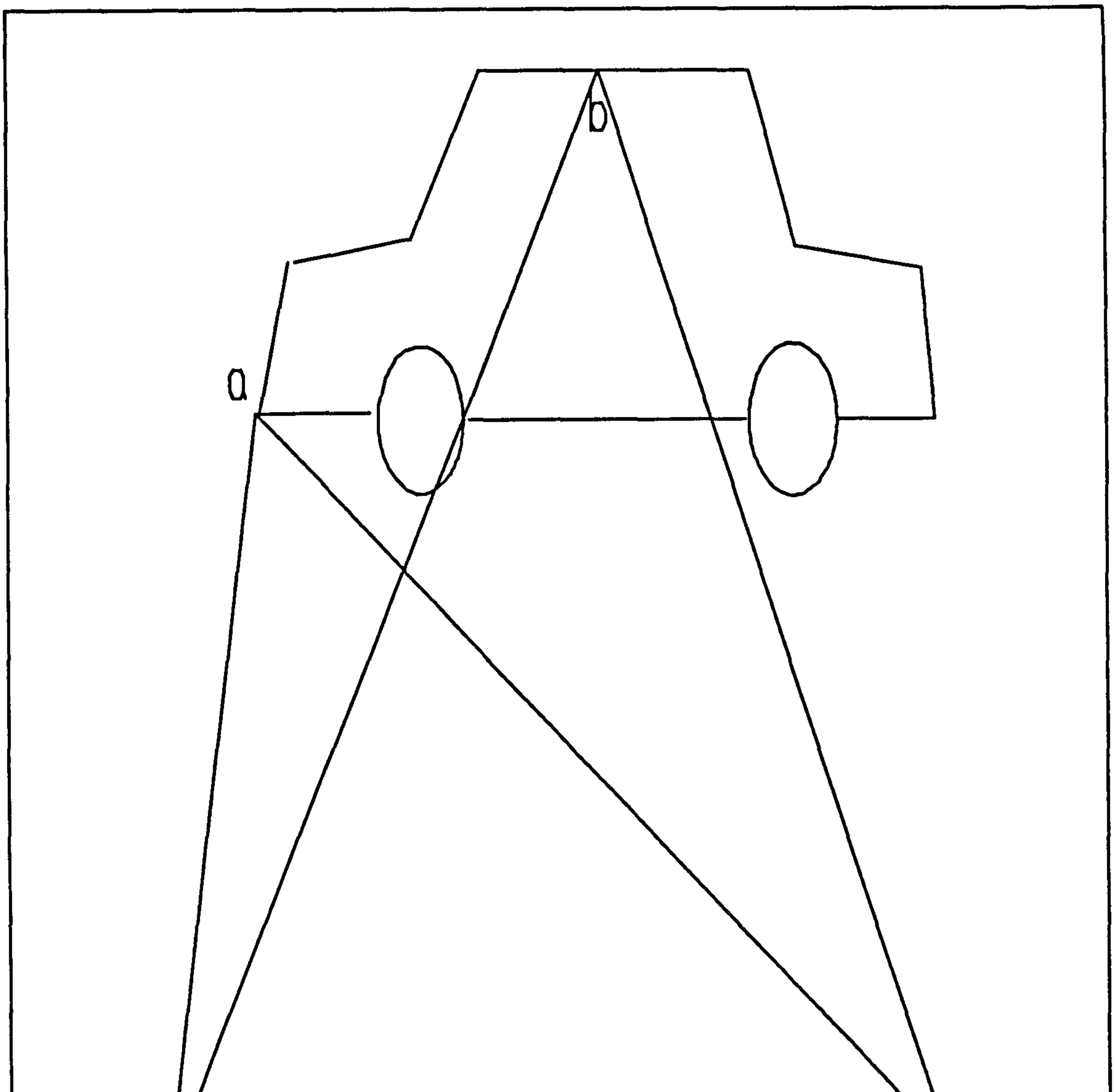

Figure 1.1: An Illustration Of Photogrammetry

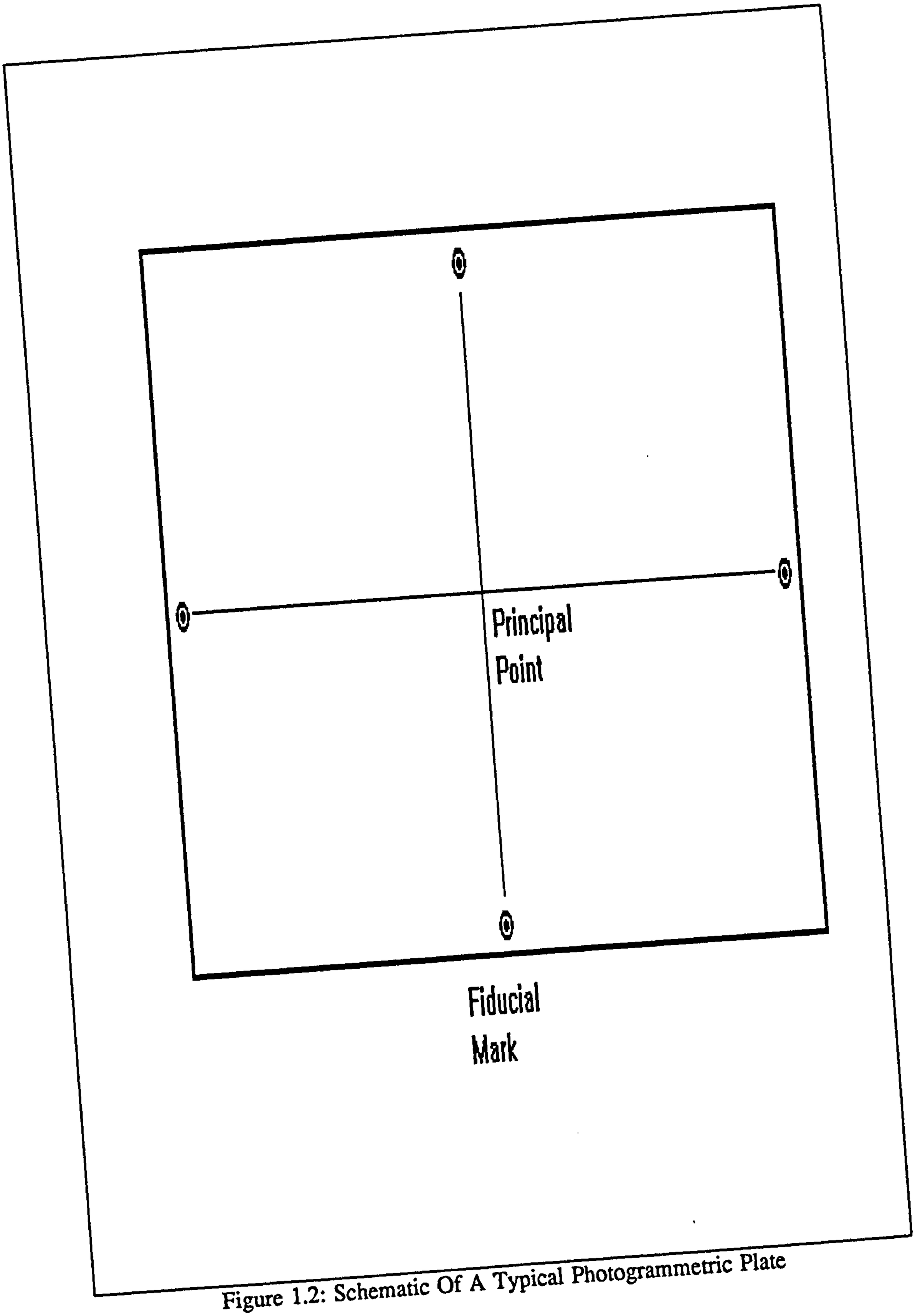

Figure 1.2: Schematic Of A Typical Photogrammetric Plate

through p^1 onto point b^1. These points are also imaged through p^2 onto points a^2 and b^2 on the second plate. The same is true for every other point on the object. The relative positions of all the points are then measured on both plates, and rays are mathematically projected back through points p^1 and p^2. The 3-dimensional coordinates of the point where corresponding rays intersect are the position of the feature being projected back through the camera lenses.

The property of the object point, the camera perspective centre and the image all lying along the same line is known as the collinearity condition. For a given point it is possible to derive an equation, known as the collinearity equation, that describes this line. If a survey contains a number of points whose positions in space are known, and whose image coordinates have been found on the relevant photograph, then it is possible to calculate the position and orientation of the camera using the collinearity equations for these points (Wolf 1984 p245). This process is known as space resection and, as previously mentioned, was devised by E.Church. The position of the camera perspective centre in space, together with its orientation are described as its exterior orientation parameters.

Fiducial Marks are superimposed at the edges of the photographic plate by photogrammetric cameras. These points provide a way to ensure that all of the points are measured in coordinate system which is consistent relative to the camera geometry. Figure 1.2 illustrates the location of these on a typical plate. A rear view of a UMK-10NF camera with its back plate removed is shown in figure 1.3. The fiducial mark exposure units are clearly shown in this picture. The principal point is defined as being

Figure 1.3: A Rear View Of A UMK-10 Camera

the point on the plate that would intercept a light ray passing along the optical axis of the camera arriving at normal incidence to the plate. Ideally, this point should coincide with the intersection of lines drawn between opposite fiducial marks. However, in practice there is usually a slight offset from this position.

The minimum number of photographs required for the reconstruction of 3-dimensional information is two, but three or four are generally taken to increase the accuracy of the survey, and as a check on the calculated coordinates. Camera properties such as lens aberrations, tilting of the photographic plate, principal distance and principal point location may be calculated from this potentially redundant information. The above properties are collectively known as the interior orientation parameters of the camera.

1.3 Object Preparation

The features appearing on the plate can be of several different types. They may be prominent features that form part of the structure of the object. Examples of this may be found in architectural surveys in which corners of bricks may be used. Surveys of this type may be regarded as totally non-invasive since no preparation of the object is necessary.

However, many objects do not have any prominent features that could be used in this manner so targets have to be superimposed on the object. There are two ways in which the targets are generally put onto the object. An array of targets may be projected on onto the object using an optical projection system. Such a method has the advantage of not interfering with the object, but there may be instabilities in the projection system. This difficulty may be overcome if the camera exposures are synchronised. There are also problems with projecting the grid onto the same points if the survey has to be repeated.

A more accurate survey can be conducted by firmly fixing targets to the object. There is no potential for instability in the target location relative to the object if this approach is used, and the targets are usually still in the same location if it proves necessary to repeat the survey. The National Physical Laboratory Photogrammetry Service and the International Airbus project (Dold 1990) are amongst the many users of this targeting method.

When using one of the targeting techniques it is advantageous to make the targets

appear much brighter than the object. It is then possible to expose the photographic plate so that the targets are imaged on the plate with little of the object being recorded. Hence, the information on the plate is more easily interpreted. The NPL group uses targets made from a retro-reflecting material called 'Scotchlite' in conjunction with an electronic ring flash held around the camera lens. Retro-reflecting materials have the property that they reflect light incident on them in a narrow cone about the direction from which it came. This enhances recorded image of the targets by causing them to be brightly exposed relative to the background.

1.4 Plate Measurement

Once the photographs have been successfully taken, it is necessary to measure the positions of various features on the photographic plates relative to each other. The accuracy with which the plates are measured is one of the major limitations to the accuracy of the technique, and it is in this area where there is the greatest difference between various groups.

There are two ways in which the photographs may be measured. They may be studied one at a time, using a mono-comparator, or in pairs using a stereo-comparator. There are advantages to both techniques, with mono-comparators generally having a better resolution than stereo systems but stereo measurements have the advantage of measuring two plates at a time.

1.4.1 Stereo viewing

The simplest way to view a stereo image is with a stereoscope and a floating point device. This type of observation relies on the photographs having been taken with the camera axes parallel to each other (parallel base photogrammetry). Figure 1.4.1 shows how a stereoscope may be used to produce a stereo model from a pair of photographs. The images a_1 and a_2 on plates 1 and 2 respectively correspond to a point 3 dimensional space. One of the observer's eyes views plate 1 while the other eye views plate 2. The brain interprets the information that it is receiving from the eyes as a three dimensional image and associates points a_1 and a_2 with point A. Similarly the brain associates b_1 and b_2, which have a greater separation, with a point B that is more distant from the plane of the photographs. This property of separation on the photographs being related to the distance from their plane of an object leads to the concept of the 'floating mark'. A piece of glass with a cross etched lightly onto it is positioned beneath each eyepiece. If the two crosses are placed on a_1 and a_2 then a combined cross will appear to be resting on feature A. If the crosses are moved towards each other, the unified cross will appear to rise towards the plane of the photographs, whilst if they are moved apart the cross will appear to go further away. By placing the crosses on corresponding points on the two photographs, and measuring the distance between them it is possible to calculate the distance from the plane of the photographs to the feature. Such measurements can be scaled by prior knowledge of the dimensions of one or more objects in the field of view.

A stereo comparator is made up of two separate stages, each with its own viewing optics. Photographs are mounted on each stage and they are viewed

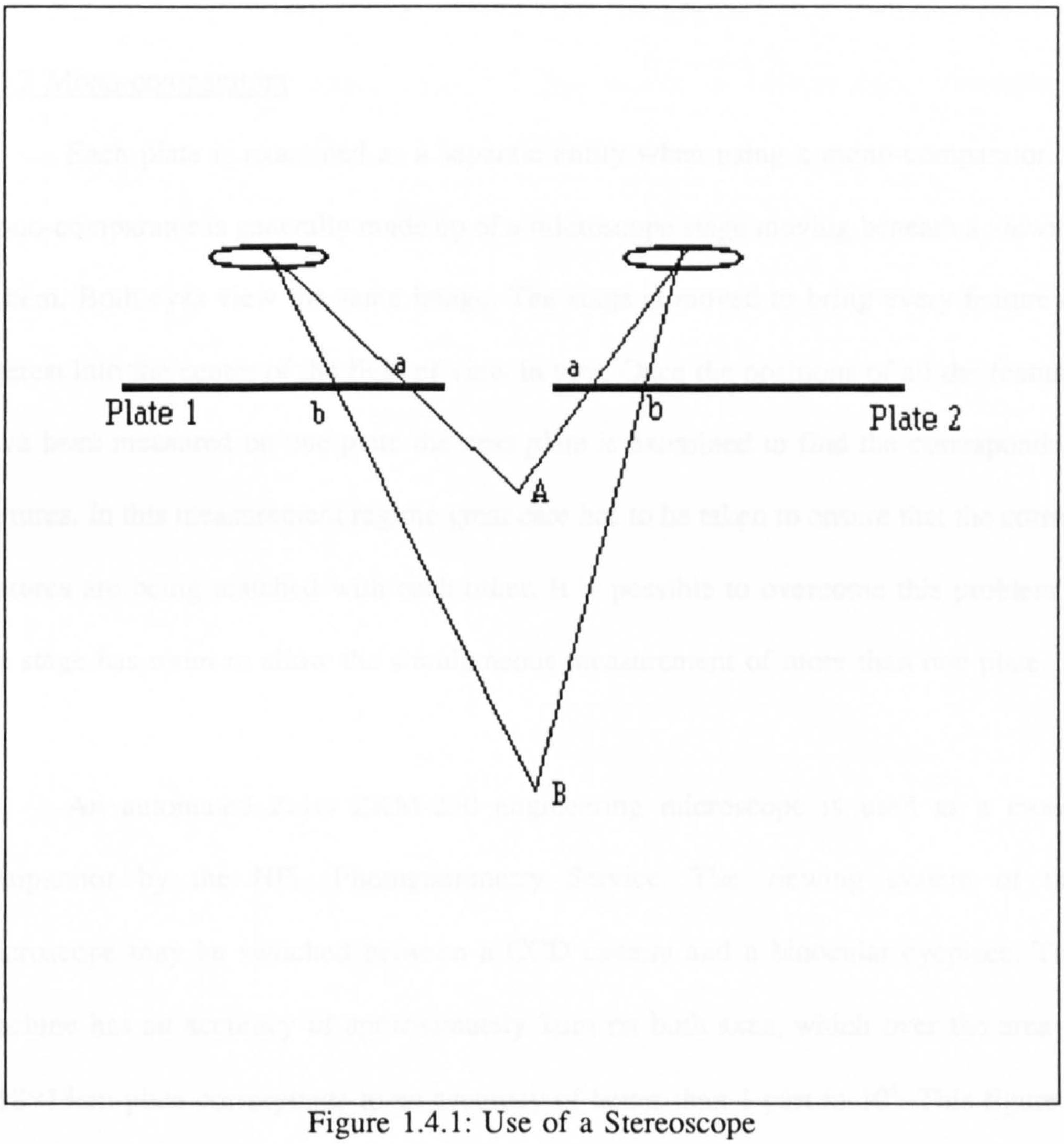

Figure 1.4.1: Use of a Stereoscope

simultaneously. The two stages are moved relative to each other until corresponding features appear in the centre of the field of view of each eyepiece. The position of each stage is recorded in this condition. A full 3-dimensional image may be built up by measuring the relative positions of all the features in the photographs.

1.4.2 Mono-comparators

Each plate is examined as a separate entity when using a mono-comparator. A mono-comparator is generally made up of a microscope stage moving beneath a viewing system. Both eyes view the same image. The stage is moved to bring every feature of interest into the centre of the field of view in turn. Once the positions of all the features have been measured on one plate the next plate is examined to find the corresponding features. In this measurement regime great care has to be taken to ensure that the correct features are being matched with each other. It is possible to overcome this problem if the stage has room to allow the simultaneous measurement of more than one plate.

An automated Zeiss ZKM-250 engineering microscope is used as a mono-comparator by the NPL Photogrammetry Service. The viewing system of this microscope may be switched between a CCD camera and a binocular eyepiece. This machine has an accuracy of approximately 1μm on both axes, which over the area of a 18×13cm plate corresponds to an accuracy of better than 1 part in 10^5. This figure is directly related to the overall accuracy with which a photogrammetric survey can be performed.

1.4.3 Automated Plate Measurement

Chapters 2 and 3 are concerned with the continuing development of high accuracy industrial photogrammetry techniques at NPL. At present, in the NPL group, an operator must manually find every target on a plate using the measuring microscope. Such a process is time consuming, a set of four plates takes about 1 week to measure, and hence expensive. Geodetic Services Inc. market a system that automatically measures the location of features on plates with an root mean square setting of approximately 0.4μm (Atkinson 1990). However, whilst this is a very good system, it is also expensive. Chapter 2 describes the development of an automated plate reading system utilising high accuracy instrumentation that was already in the possession of the National Physical Laboratory. As with the Geodetic Services system this eliminates the need for an operator to spend long periods of time finding targets, so reducing the cost of conducting a photogrammetric survey. Chapter 3 contains the details of a survey that was conducted to test the system.

1.5 Camera Limitations

The accuracy of a photogrammetric survey is limited by the quality of the optics in the photogrammetric camera. There are several limitations to the performance of a camera. They are briefly described below. A more detailed description of these factors may be found in a general optics text such as Jenkins and White (1976) or Smith (1966).

A spherical shaped lens surface deviates rays entering through its periphery more than those entering along its axis. Therefore, rays entering the periphery are brought to

a focus nearer to the lens than those passing through its centre. This problem is known as spherical aberration.

The refractive index of a material is dependent on the wavelength of light passing through it. This means that a simple lens will refract blue light more than red, a process known as dispersion. Hence different wavelengths are focused at differing points. This and spherical aberration may be greatly reduced by the use of multiple element lenses.

Astigmatism may occur when an object is offset from the optical axis of a lens by a considerable distance. Rays from the object are incident on the lens asymmetrically. The light may be resolved into two planes, the tangential or meridional plane which contains the ray passing through the centre of the lens and the optical axis, and the

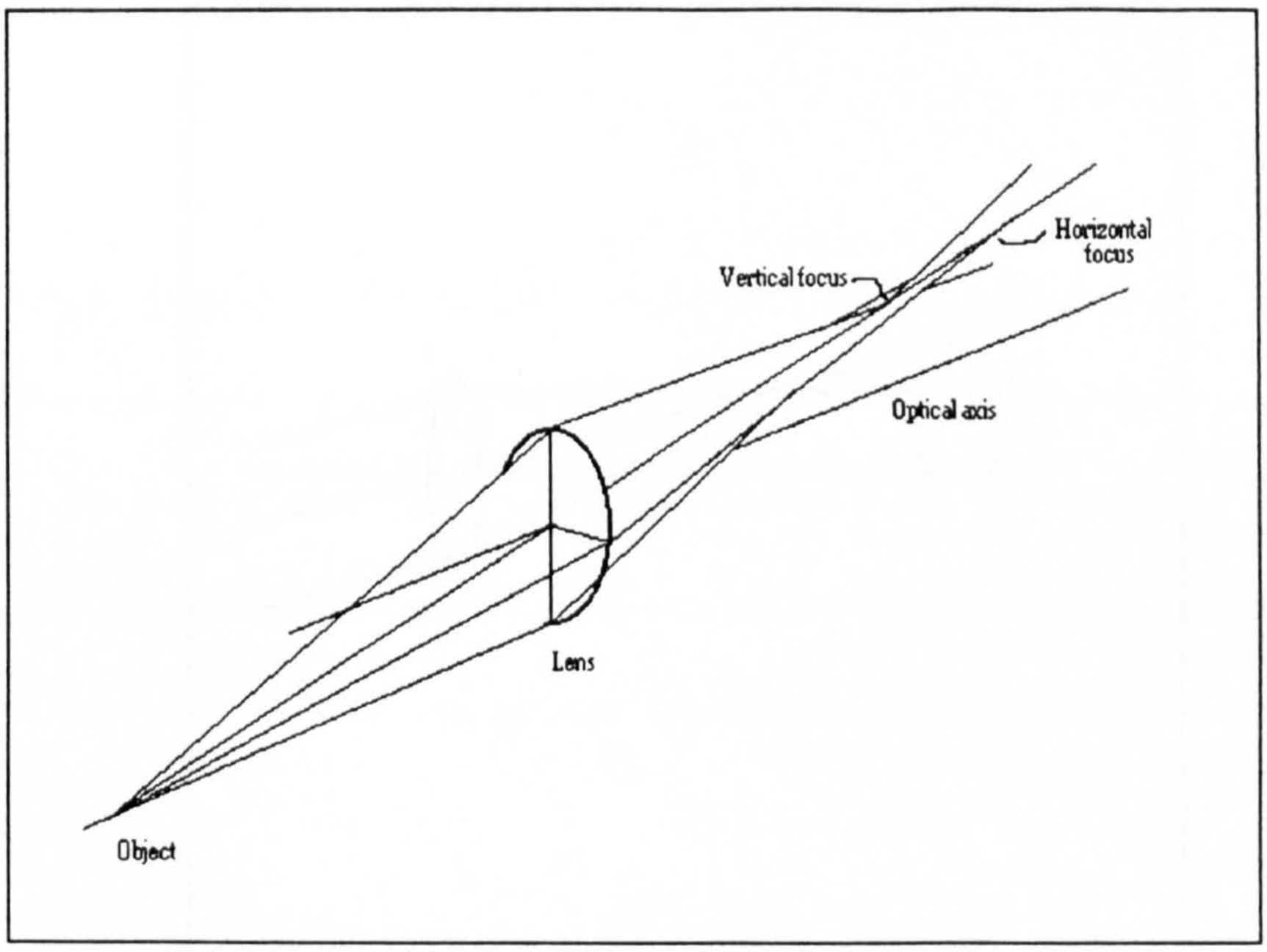

Figure 1.5.1:Astigmatism

sagital plane which is perpendicular to both the plane of the lens and the meridional plane. This is shown in figure 1.5.1. In a lens that exhibits astigmatism the light rays in these two planes are brought to different focii. The rays in the meridional plane strike the lens at a greater angle than those in the sagital plane which means that they are brought to a focus nearer to the lens. Astigmatism increases as the object moves further from the optical axis.

A further aberration that lenses are subject to is coma. This occurs when a bundle of rays are obliquely incident on a lens. Rays passing through the centre of the lens are imaged at a different distance from the optical axis to those going through the centre, as shown in figure 1.5.2. In this diagram a represents the height of the image produced by off axis rays while b represents that of the axial rays.

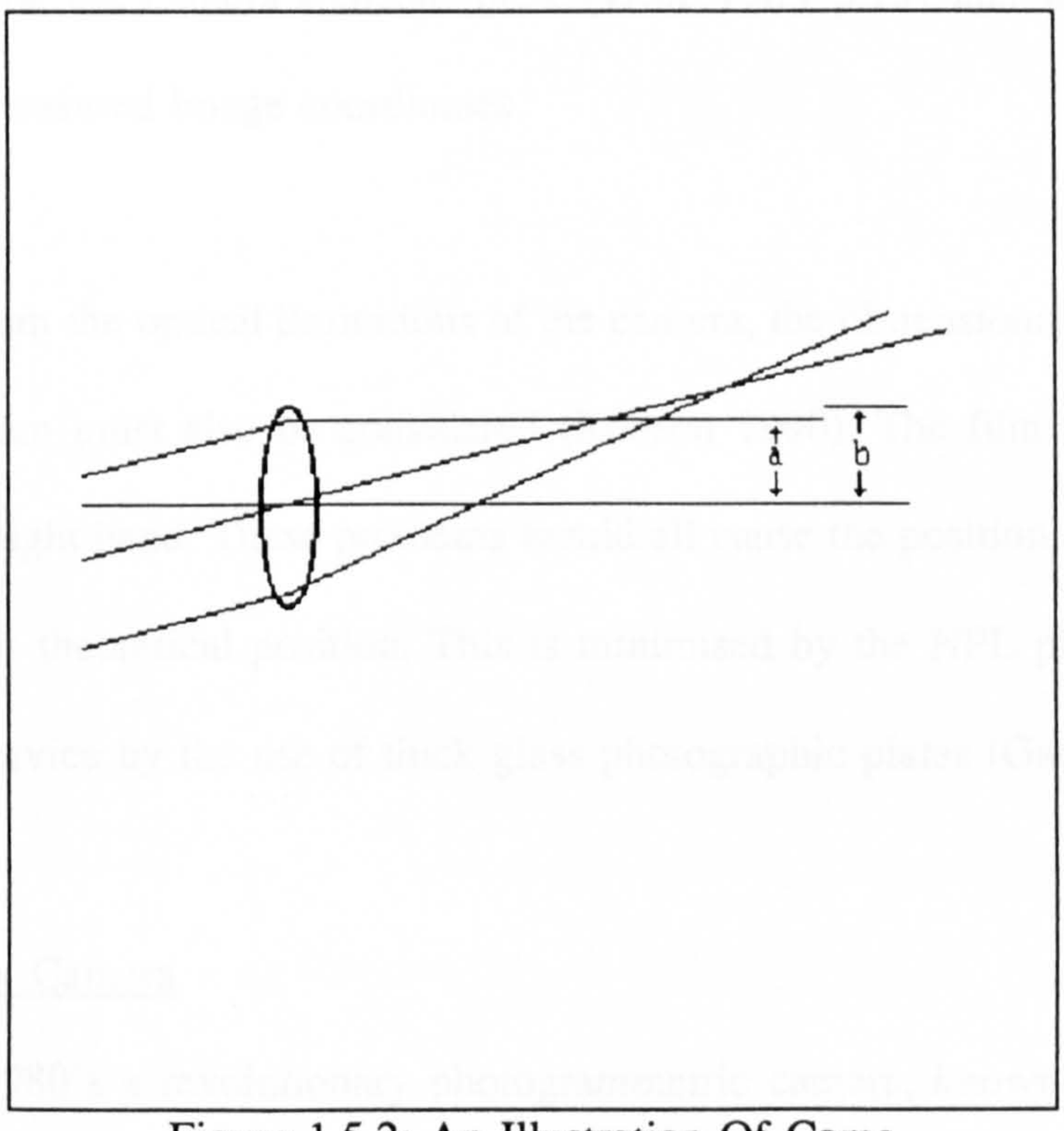

Figure 1.5.2: An Illustration Of Coma

The major effect of the aberrations discussed so far is to degrade the quality of the image through blurring. This may reduce the accuracy with which their centres can be found, but it their position in the image plane is not seriously affected. Lens distortions are more of a problem in photogrammetry as they actually cause the image to be offset from the position that a perfect lens would cause it to be imaged in. There are two types of distortion, radial in which the image is offset radially from the lens axis, and tangential distortion in which the image is offset at a tangent to the axis. Radial distortion is present in lens systems that do not have concentric symmetry and in general is minimised as a result of a compromise in correction of other aberrations. Tangential distortion is caused by errors in the alignment of lens elements. In a high quality camera such as a UMK-10NF the distortion across the field will typically be a few micrometres (Hunt 1993) but other cameras may be subject to much larger errors (Fraser and Shortis 1990). It is possible to counteract the effect of distortion errors by the calibration of the camera's image field (Wolf 1983 p.75) and making suitable corrections to measured image coordinates.

Apart from the optical limitations of the camera, the dimensional stability of the recording medium must also be considered (Robson 1990). The film may expand or contract, or it might bend. These problems would all cause the position of images to be offset from their theoretical position. This is minimised by the NPL photogrammetric measurement service by the use of thick glass photographic plates (Gates *et al* 1982).

1.6 The Centrax Camera

In the 1980's a revolutionary photogrammetric camera, known as the Centrax

Camera, which overcomes many of the limitations mentioned in the previous section, was developed at the National Physical Laboratory by J.M. Burch and C.Forno. It is not suitable for general photogrammetric applications as it requires targets that behave as point sources of light. It was designed as a low cost instrument to allow the calibration

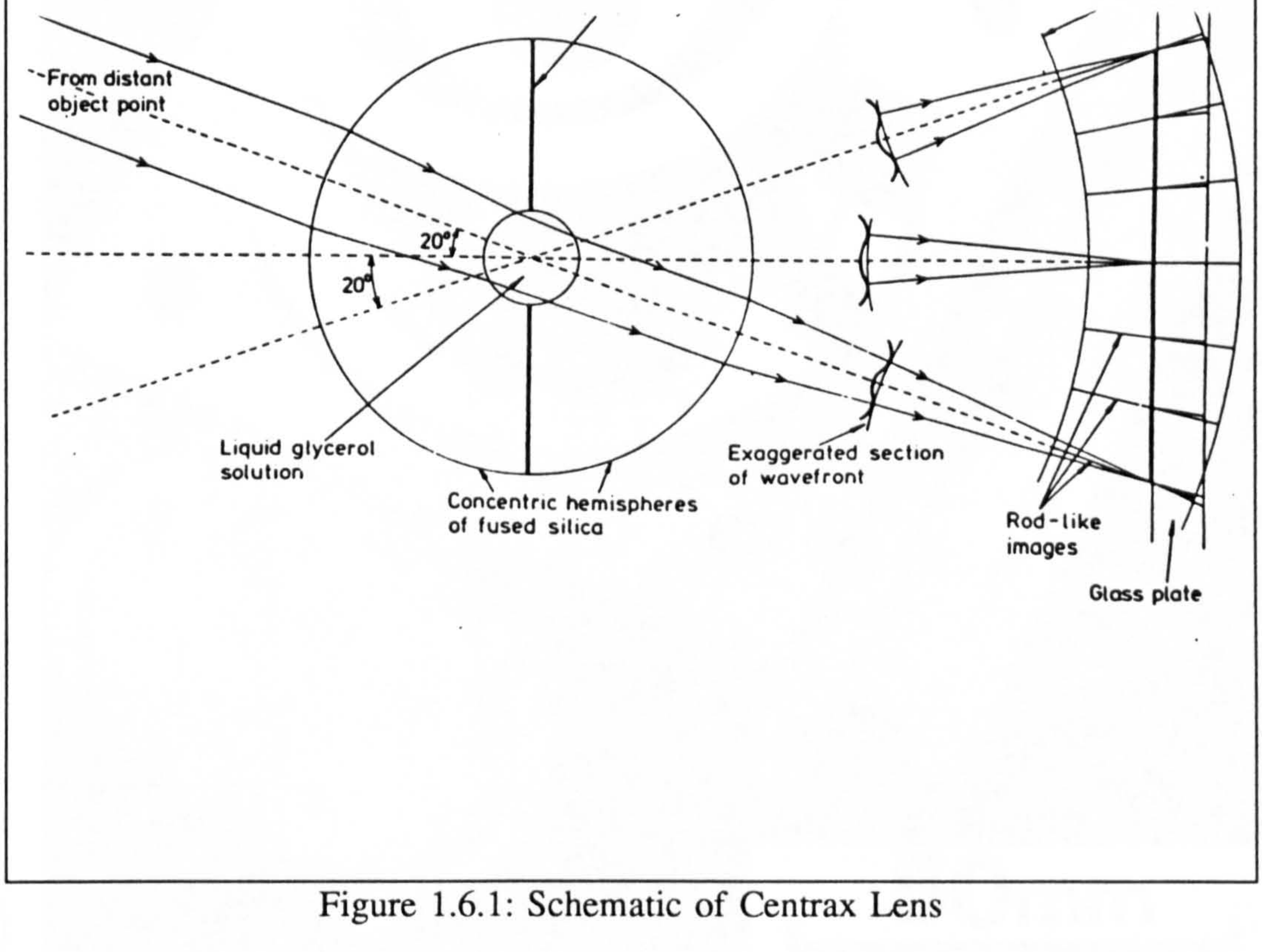

Figure 1.6.1: Schematic of Centrax Lens

of Coordinate Measuring Machines by photogrammetric means. The innovative feature of the camera is its mono-concentric lens which is shown schematically in figure 1.6.1 (figure taken from Burch and Forno 1983). A photograph of the Centrax camera is shown in figure 1.6.2. The final version consists of a central sphere made of borosilicate

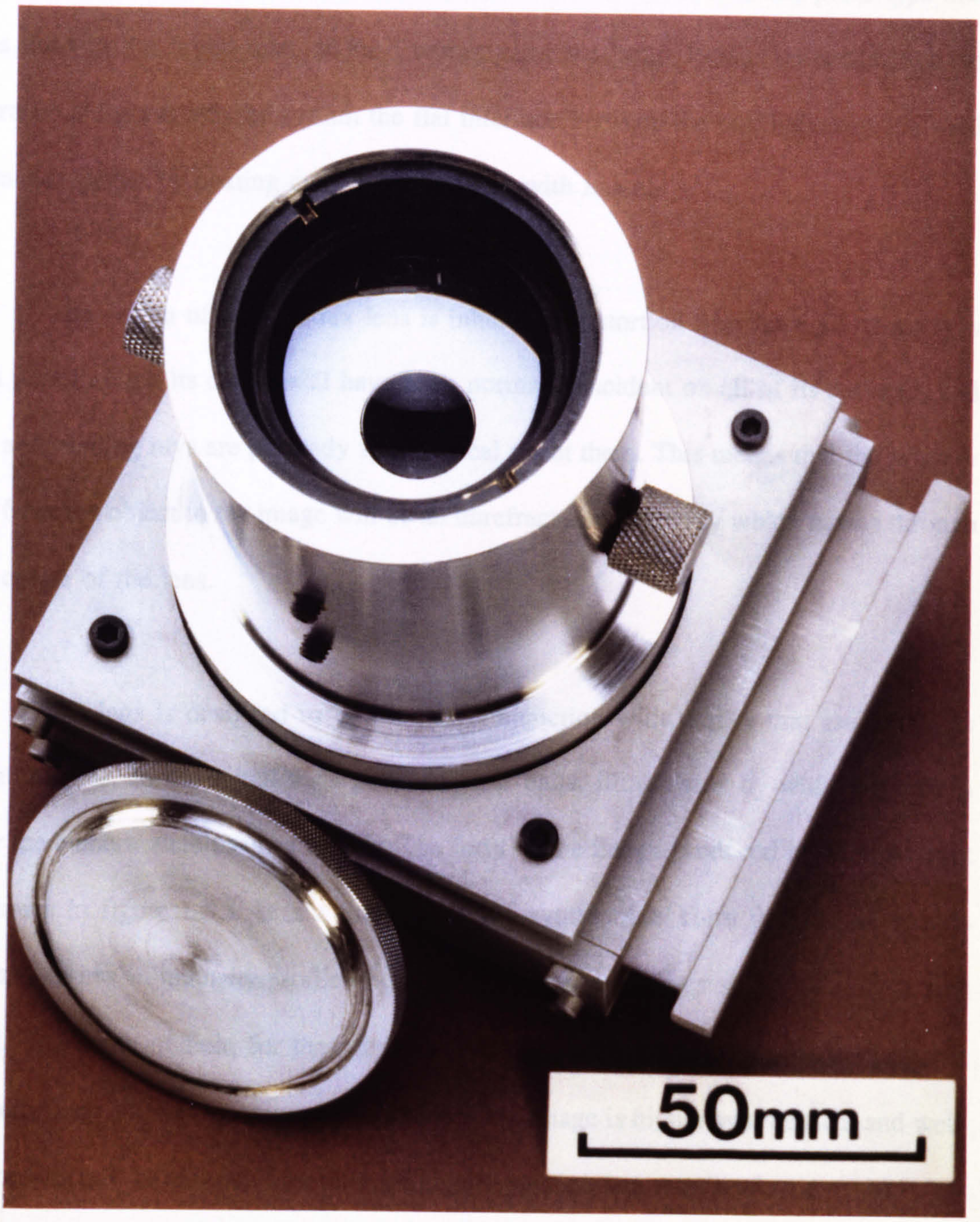

Figure 1.6.2: The Centrax Camera

crown surrounded by a pair of extra-light flint shells whose surfaces are concentric with the inner sphere. A proto-type in which the central sphere is formed from liquid glycerol solution sealed between two concentric spheres of fused silica. It is this proto-type that was used in the initial tests of the Centrax camera (Forno 1991). To ensure that no extraneous light enters the system the flat interface between the two halves of the shell is made opaque by coating one of the surfaces with nickel.

The design of the Centrax lens is inherently distortion free since all of the rays that pass through its centre will have been normally incident on all of its surfaces, and the surrounding rays are perfectly symmetrical about them. This means that the primary ray from the object to the image will be an unrefracted straight ray which passes through the centre of the lens.

The lens is designed to be used in conjunction with targets that are luminous point sources. In the initial tests polished steel balls, illuminated by white light from near the camera were used as targets. The form of the image produced by such a target is shown in figure 1.6.3. It is a sharp circularly symmetrical form that has an opaque centre and has an intensity profile in the form of a zero order Bessel function of the first kind. The depth of field for the production of such high quality, well defined images extends from 300mm to infinity. The fact that the image is highly symmetrical and well defined means that its position on a photogrammetric plate may be found to sub-micrometer precision. In initial trials (Burch and Forno 1983) a scanning laser beam system was attached to an interferometrically monitored microscope stage to attain a 50nm precision. A focused laser beam was scanned in a circle around the central spot

of the image with the transmitted intensity being measured by a two dimensional photo-sensor. With the advent of high precision CCD cameras, it is possible that it would now be feasible to capture the image using a CCD array, together with a framestore, and fit its intensity profile to a suitable Bessel function, and hence calculate its centre.

A 27 point three dimensional model, constructed from steel pillars rigidly

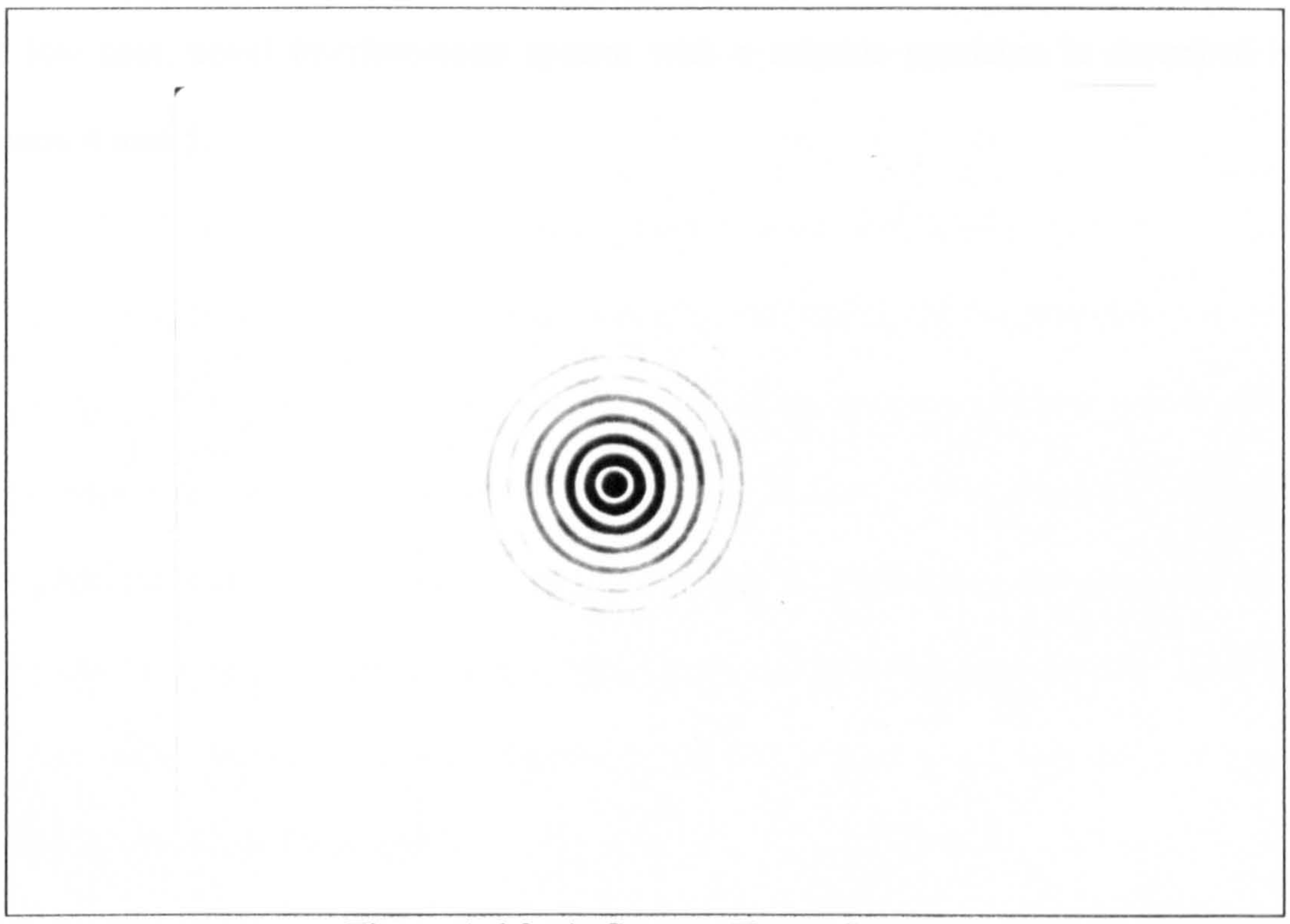

Figure 1.6.3: A Centrax Target Image

mounted on an aluminium casting was built by Burch and Forno (1984). The model was photographed from above from 4 different positions using the Centrax camera. The plates were measured using the scanning laser device in conjunction with a Zeiss microscope whose stage position is monitored by Hewlett-Packard linear interferometers. The results of the survey indicate that it is possible to carry out a photogrammetric survey, using the Centrax camera, with an accuracy of 2 parts in 10^6. However, such an

accuracy can only be achieved if the plates can be measured with suitable precision. To make any meaningful use of the Centrax camera it is necessary to have access to a microscope whose stage position is known to 50nm.

The Centrax system was designed as a low cost system, with the cameras costing about £5000 to manufacture. The measuring microscope used to measure the plates in the initial tests costs more than ten times this amount. The development of the prototype of a low cost, novel interferometer system with a suitable precision is described in chapters 4 and 5.

2. AN AUTOMATED TARGET LOCATION SYSTEM

The NPL photogrammetry group decided to automate the measurement of photogrammetric plates so that surveys could be conducted with greater efficiency. There were two potential courses of action that could have been followed once this decision had been taken. A complete commercial system, such as that marketed by Geodetic Services Inc., could be purchased, or a new system could be developed "in house".

A large amount of high precision plate measurement equipment, that could readily be adapted to form an automated system, was already in the possession of the NPL, so a decision was made to develop an automatic plate measurement system. The image processing algorithm that was developed is described in this chapter along with the experimentation that was carried out to evaluate it. Before any development was carried out a review of some of the image processing techniques already used in photogrammetry was carried out. A summary of this is also given here after a short description of the hardware used.

2.1 Hardware

The photogrammetry group at NPL possess a Zeiss ZKM measuring microscope that has been used to measure photogrammetric plates for approximately ten years. This instrument was recognised as being suitable for use in conjunction with an automatic target location algorithm. Apart from it having suitable computer interfaces, it also means that any new results can be validly compared with those of similar measurements

that have been made manually.

2.1.1 Basic Microscope Configuration

A schematic of the ZKM microscope is shown in figure 2.1.1. The stage is made up of a central glass plate held in a metal frame which moves on bearings along the x and y axes. Illumination for the plate being measured is provided by a tungsten bulb beneath the stage. The microscope optics are directly over this source. The optical system can be switched between two modes. The image can be either projected onto a CCD chip, or the operator can view it through a binocular eye-piece. When manual measurements are being made a graticule is normally inserted into the system to allow the operator to refer the image to a fixed point. However, when using image processing techniques, it is often better to remove the graticule so that only the image can be seen. The positions of any objects in the field of view are then referenced to the pixel locations.

2.1.2 The CCD System

The CCD array has 512×512 elements with 256 grey levels. When used for observations by eye, the CCD image is processed by a simple electronics circuit, and is displayed in real-time on a monochrome monitor. When the decision was taken to automate the measurement process, the output from the CCD array was fed into an image processing system that was already used for other applications by the photogrammetry group. A live image can still be displayed by the monitor after this change, so allowing compatibility between the two regimes.

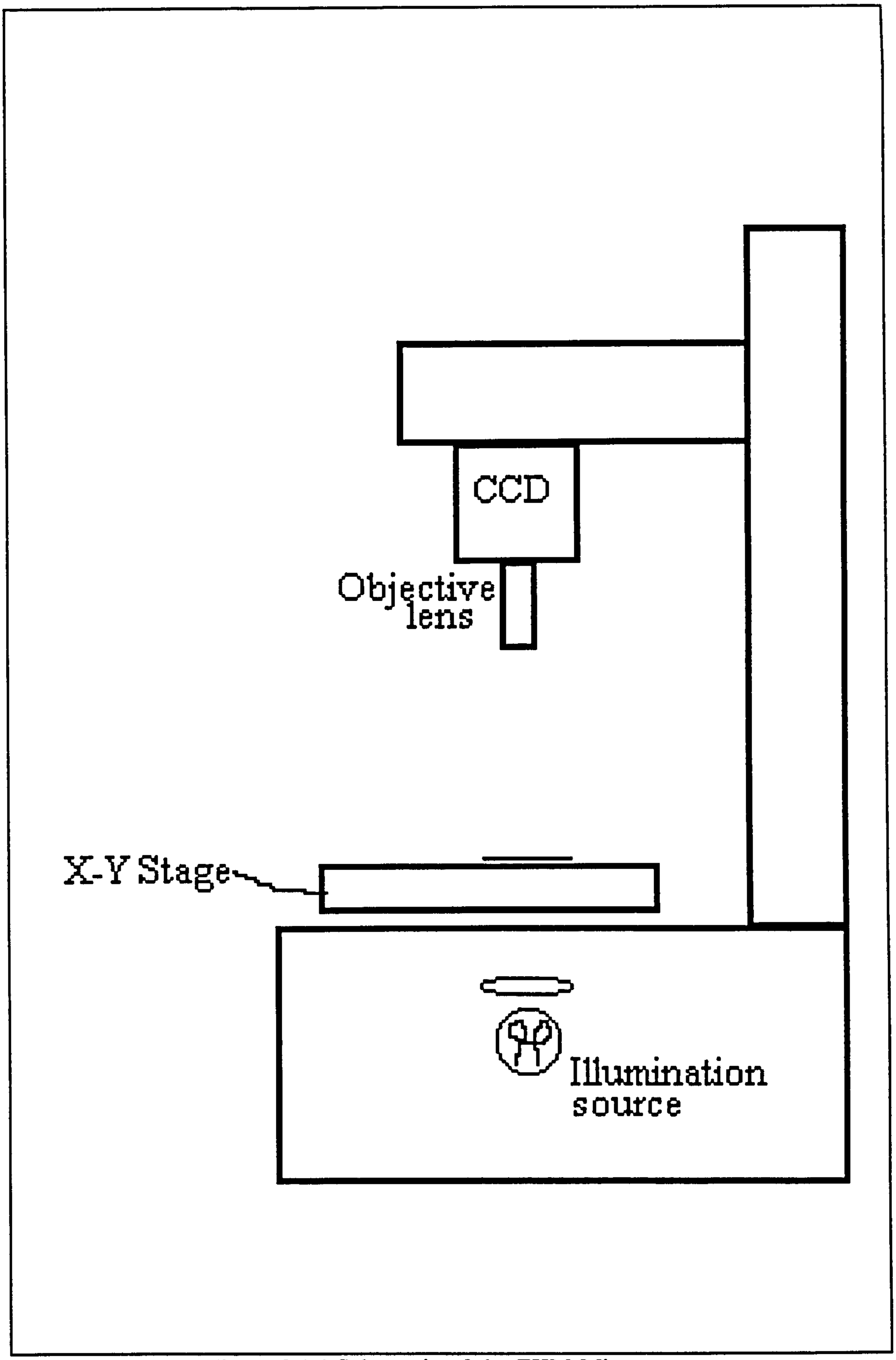

Figure 2.1.1:Schematic of the ZKM Microscope

The image processing equipment was developed and supplied by a company called Image Inspection. A 256×256 area of the CCD array is used as the input to the system, with the intensity resolution being 256 grey-scales. Image Inspection supply the product in the form of a plug in expansion board for an IBM compatible personal computer. The board was installed in an IBM compatible, Opus IV, 286 computer with a numeric co-processor. A user interface program is supplied with the equipment which allows various image processing techniques to be tested and small test programs to be written. This proved invaluable in providing a basic understanding of image processing. However, no provision is made for incorporating such programs into the sort of program that is necessary to control the microscope and record results. A set of library functions may be purchased from Image Inspection which can be used in more general programs to enable image processing tasks to be performed. These libraries are written in Microsoft C version 5.1, and can be incorporated into any program in that language. For this reason it was decided that the entire microscope control and data acquisition program should be written in Microsoft C.

2.1.3 Microscope Control System

The ZKM microscope has been automated by the addition of a linear d.c. stepper motor on each of its axes. These are controlled by an Anorad Intelligent Axis Controller. The motors were also supplied by Anorad. The controller accepts a quadrature input from each axis to determine the stage position. For further details about quadrature signals see section 4.2.3. In this case the signals are provided by moiré grating position encoders manufactured by Heidenhaim. Each of the gratings has a pitch of 10μm. The principles behind the operation of such a grating device are outlined in section 4.1.2.

The controller is connected to the serial port of the computer. This allows the position of the stage to be read by the computer and also enables instructions to be sent from the computer. To simplify the control of the microscope via the serial port, a set of serial communication libraries called *Asynch Manager* published by Blaise Computing in Microsoft C were purchased. A example of the sequence of commands that would be required to move the x axis by 1000 Anorad units is shown below.

Command character sent	Action
10	Initialise x axis
A	Address initialised axis
"1000"	Increment initialised axis by 1000 units
.	Execute move
Q	Return position of stage
31	Close all axes

It should be noted that 1 Anorad unit corresponds to 80nm.

2.2 Target Location

Several target location techniques have been used by various photogrammetrists around the world. Many of them are used in real-time applications where it is not possible to spend long periods of time analyzing images. The methods may be divided into two broad categories;-

i) Location of the centre of gravity.

ii) Fitting images to a specified geometric structure.

2.2.1 Centre Of Gravity Routines

The simplest, and perhaps most popular, procedures are based on finding the centre of gravity of the target image. The simplicity of the algorithm allows the image processing program to run relatively quickly. The basic formulae for finding the centre of gravity (x_{cg},y_{cg}) are given by;-

$$x_{cg}=\frac{1}{M}\sum_{i=1}^{n}\sum_{j=1}^{m} jw_{ij}$$

$$y_{cg}=\frac{1}{M}\sum_{i=1}^{n}\sum_{j=1}^{m} iw_{ij} \qquad 2.2.1$$

$$M=\sum_{i=1}^{n}\sum_{j=1}^{m} w_{ij}$$

Where the window under investigation is m×n pixels, the weight of pixel (i,j) is w_{ij}, and M is the total weight of the area under study.

Several photogrammetry groups use such a procedure for the location of targets (eg. Wong & Wei-Hsin 1986, Trinder 1989). A centre of gravity routine may also be

used to calculate an approximate centre before going on to use a more complex method to calculate the centre location precisely (Beyer 1987).

The major difference between the various applications is the image processing applied prior to calculating the centre of gravity. Background intensity is the major cause of error in the use of this technique. In the simplest possible implementation of the algorithm every pixel within the window contributes its weight to the centroid calculation. In some cases, such as that shown below in figure 2.2.1, this would cause the centroid to be shifted from the position that would be calculated if there were no background pixels in the window, denoted by a cross, to the position marked by a dot.

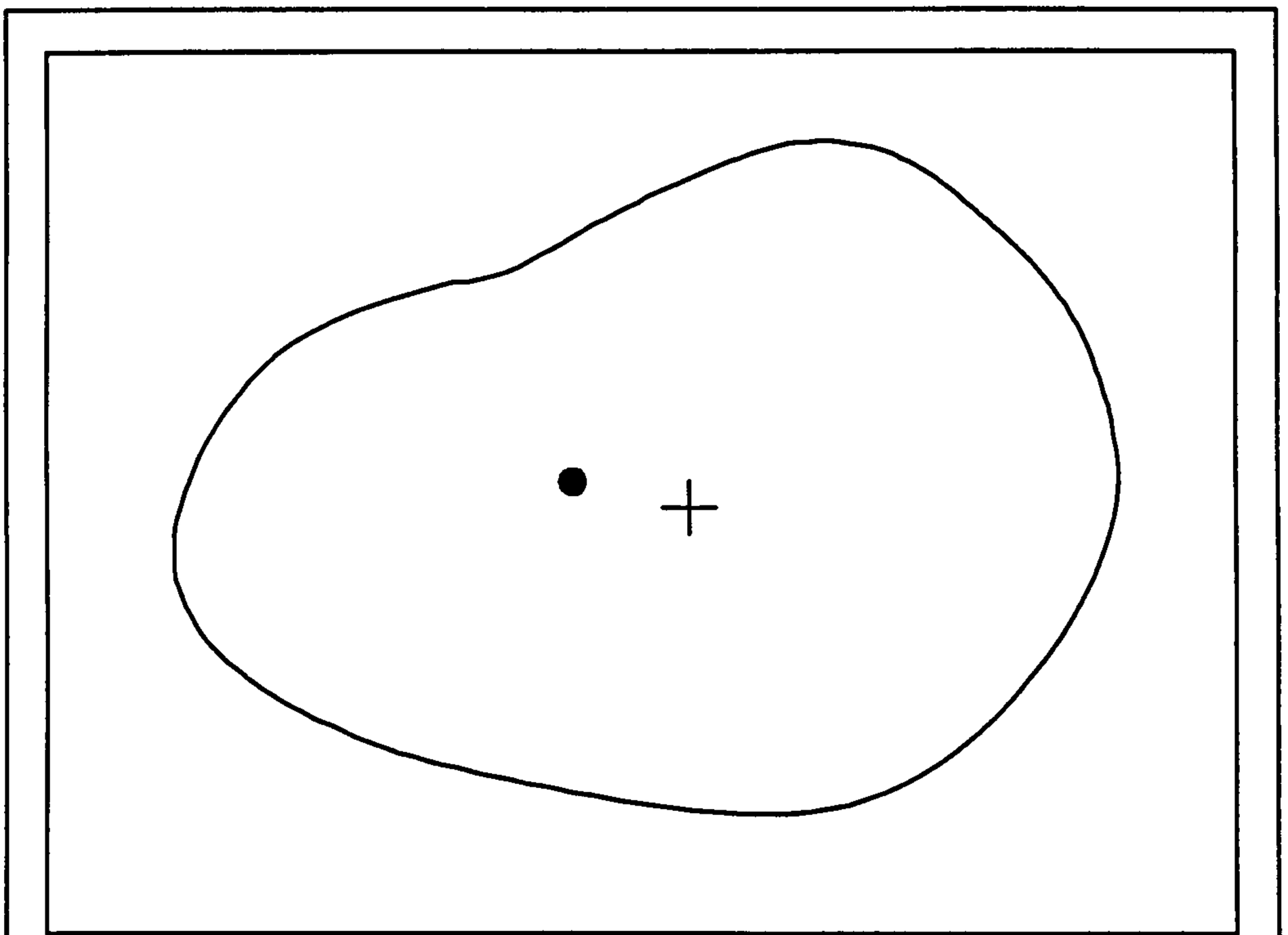

Figure 2.2.1: A Shape With A Shifted Centroid

Problems resulting from non-uniform background also occur with this technique. If there is an intensity gradient across the field of view, then the centre will appear to move towards the darker end.

2.2.1(a) Elimination Of Background

In order to overcome the contribution from background regions the window is usually thresholded to give any background pixels a zero value. The setting of the threshold is the most critical part of the technique. If it is set too high, some of the target pixels will be lost. However, if it is too low then the background will still influence the centroid position.

Wong and Wei-Hsin (1986) set the threshold at a value corresponding to:-

$$thres=\frac{minimumpixelvalue+meanpixelvalue}{2} \qquad 2.2.2$$

Trinder (1989) describes how the algorithm for calculating the centre of gravity may be improved. Each pixel value is multiplied by a weighting factor w_{ij} which depends on its position in the window. The undue influence of outer pixels is largely eliminated by this step. The modified equations are:-

$$x_{cg}=\frac{1}{M}\sum_{i=1}^{n}\sum_{j=1}^{m} jg_{ij}w_{ij}$$

$$y_{cg}=\frac{1}{M}\sum_{i=1}^{n}\sum_{j=1}^{m} ig_{ij}w_{ij} \qquad 2.2.3$$

$$M=\sum_{i=1}^{n}\sum_{j=1}^{m} g_{ij}w_{ij}$$

These corrections are said to give a half pixel improvement in accuracy.

2.2.2 Fitting Images To Shapes

Image fitting techniques may be subdivided into two categories;-

i) Methods that use information from only the perimeter of the shape.

ii) Algorithms that take into account the internal structure of the shape.

2.2.2(a) Methods Using Edge Information

Most procedures that fall into this class consist of applying an edge location operator to the image and then fitting the resultant data to a mathematical function. Many photogrammetry groups use circular targets. These targets produce almost elliptical images when viewed obliquely, so allowing the use of ellipse fitting algorithms.

An example of this is given by Fritsch(1989) who fits the perimeter of an ellipse by applying a least squares method to the following constraint equation:-

2.2.4

$$a(x_i-x_0)^2+2b(x_i-x_0)(y_i-y_0)+c(y_i-y_0)=1$$

Where (x_i,y_i) are the coordinates of the edge points, (x_0,y_0) the centre, and a,b,c the parameters which determine eccentricity and orientation.

It is reported that this gives a centring standard deviation in the range:-

$$0.05 \leq \sigma_{xy} \leq 0.10 \ \textit{Pixel Size} \qquad 2.2.5$$

Another technique for finding the centre of an ellipse is that of Zhou(1986). Here the two edge points of the ellipse on each row are recorded and their midpoint calculated. A line is calculated which passes through each of the midpoints. A similar procedure is adopted for the columns and the intersection of the two lines is at the centre as shown in figure 2.2.2.

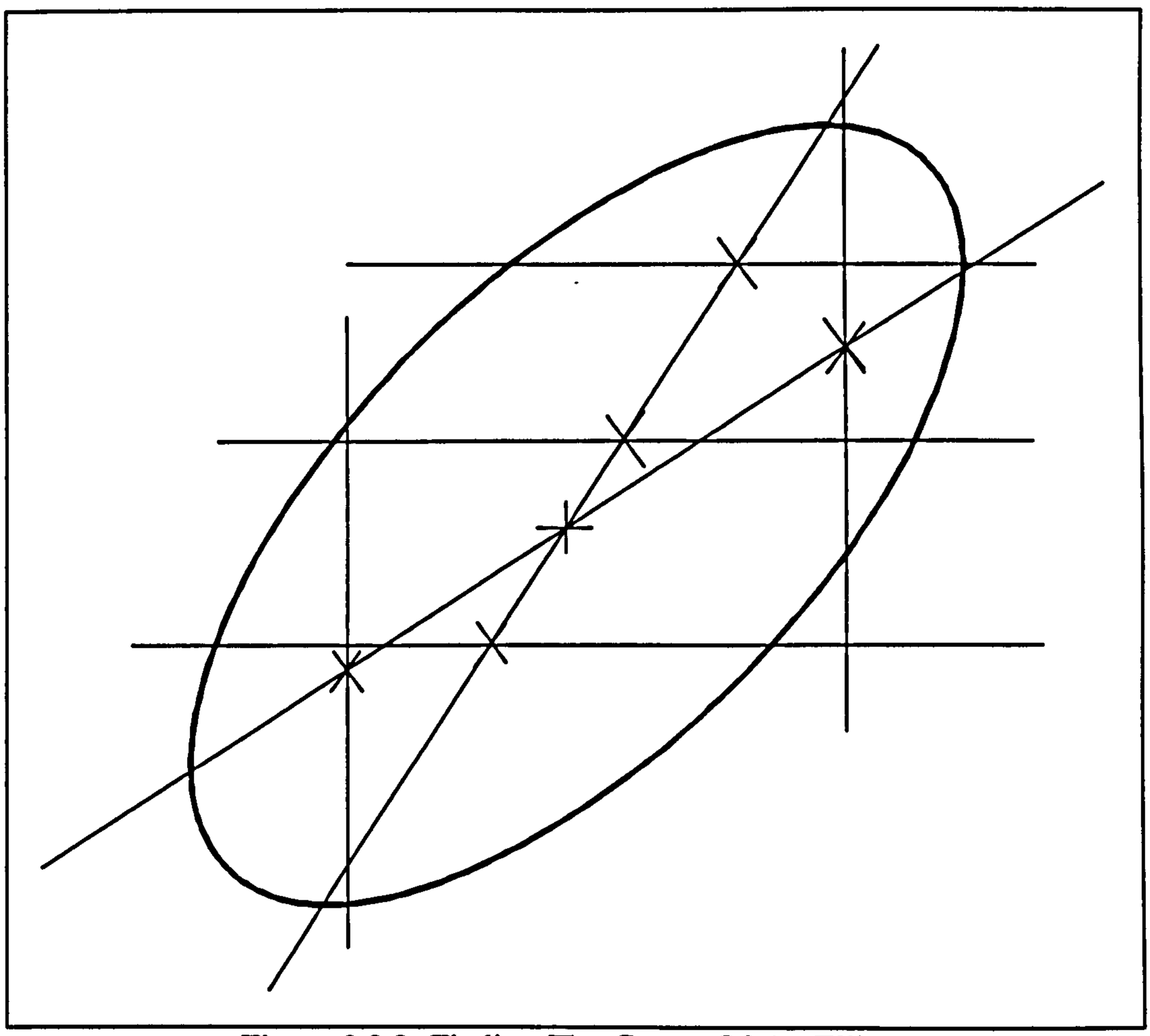

Figure 2.2.2: Finding The Centre Of An Ellipse

A standard deviation of better than 0.05 pixels is stated as the accuracy of this technique. However, in many applications the least squares method is more useful since it provides a much better error analysis so giving an indication as to the reliability with which the location of the shape has been found.

Luhmann(1986) describes another way in which shapes may be found using just edge information. This procedure has been applied to the location of crosses as well as circular targets. In the case of a cross the following procedure is adopted. A multiple ring template is superimposed on the cross. The points on each arm of the cross which intersect the rings are fitted to a polynomial using a least squares routine. The point of intersection of the polynomials is calculated as the centre of the cross. This method overcomes the problems of orientation usually associated with finding crosses. Figure 2.2.3 illustrates this technique.

An analogous operation is used to calculate the centre of circle based targets. Lines are drawn through the target, and their intersections with the edges are fitted to an ellipse using a least squares routine. The results obtained indicate an accuracy of 0.1-0.2 pixels.

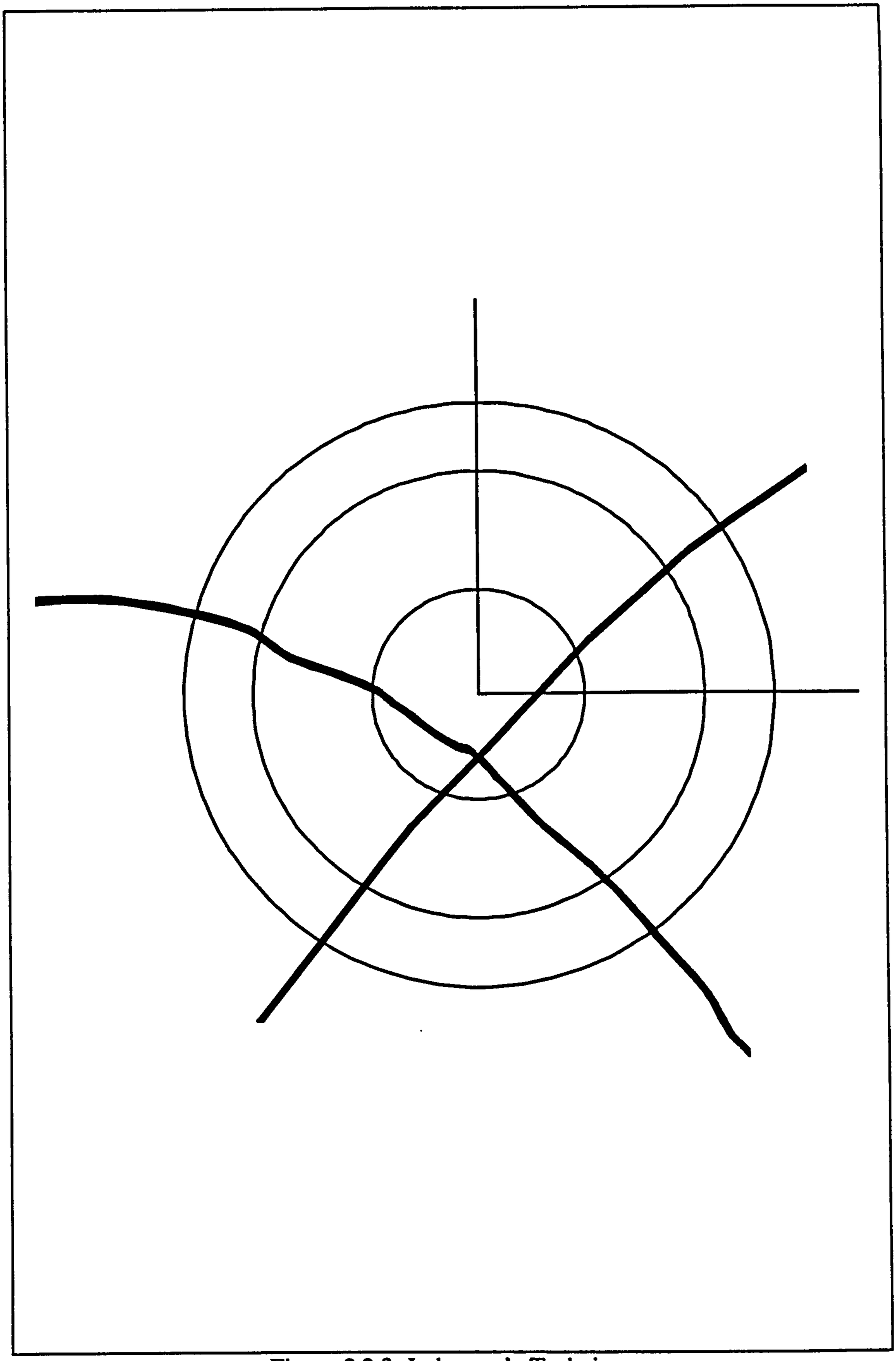

Figure 2.2.3: Luhmann's Technique

2.2.2(b) Edge Detection

All of the techniques mentioned in the previous section rely on accurately finding the edges of targets. Some of the many ways in which this may be done are outlined below.

One of the most popular edge enhancement techniques is the Sobel filter (Tabatabai & Mitchell 1984). The gradient (G) of point (i,j) is calculated using the formulae given below:-

$$G=|\langle F,W_1\rangle|+|\langle F,W_2\rangle|$$

Where $\langle A,B\rangle \equiv$ *Inner product of* A,B

$$F=\begin{pmatrix} p(i-1,j-1) & p(i,j-1) & p(i+1,j-1) \\ p(i-1,j) & p(i,j) & p(i+1,j) \\ p(i-1,j+1) & p(i,j+1) & p(i+1,j+1) \end{pmatrix} \qquad 2.2.6$$

$$W_1=\begin{pmatrix} 1 & 2 & 1 \\ 0 & 0 & 0 \\ -1 & -2 & -1 \end{pmatrix} \quad W_2=\begin{pmatrix} 1 & 0 & -1 \\ 2 & 0 & -2 \\ 1 & 0 & -1 \end{pmatrix}$$

If the edge is defined to be the line of maximum gradient around the shape it is relatively simple to locate it using this operator. However, it is necessary to interpolate the information if the edge location is required to sub-pixel accuracy.

Fritsch(1989) uses a Sobel filter to produce a gradient image and then

implements a line following algorithm to trace the lines of greatest gradient. To do this a window is defined and its centre of gravity calculated and recorded. All pixels in the window are set to zero and the window moved towards the centre of gravity. The process is then repeated. If portions of the edge are missing then an interpolation algorithm is implemented to fill in the gaps.

The Roberts filter is analogous to that of Sobel, but it only uses 2×2 matrices in the evaluation of the gradient of point (i,j). The pixel and weighting matrices used by Roberts are:-

$$F=\begin{pmatrix} f(i,j) & f(i,j+1) \\ f(i+1,j) & f(i+1,j+1) \end{pmatrix} \qquad 2.2.7$$

$$W_1=\begin{pmatrix} 1 & 0 \\ 0 & -1 \end{pmatrix} \qquad W_2=\begin{pmatrix} 0 & -1 \\ 1 & 0 \end{pmatrix}$$

2.2.2(c) Image Correlation Techniques

In some applications it is possible to match whole areas with either a known form, or another image of the same region. Such techniques offer a potentially higher level of accuracy than those previously described as they make much more use of the available information.

One simple example of the application of image correlation techniques is in the measurement of small displacements in successive video images (Bruck *et al* 1989). The

first image has an intensity profile F(x,y) at point (x,y) while that of the second image is given by $G(x^*,y^*)$. The correlation between the two images is given by a function of the form:-

$$S=1-\frac{\sum[F(x,y)*G(x^*,y^*)]}{[\sum(F(x,y)^2)*\sum(G(x^*,y^*)^2)]^{1/2}} \qquad 2.2.8$$

Assuming that the two images differ only by a translation in the plane of the camera, the two different coordinate systems are be linked by the equations:-

$$x^*=x+u+\frac{\partial u}{\partial x}\Delta x+\frac{\partial u}{\partial y}\Delta y$$
$$y^*=y+v+\frac{\partial v}{\partial x}\Delta x+\frac{\partial v}{\partial y}\Delta y \qquad 2.2.9$$

The best match occurs between the two areas of interest when the value of the function S has a minimum value. S is minimised by iteratively adjusting the values of u, v and their partial derivatives until the minimum is achieved. A Newton-Raphson type iteration(Bruck *et al 1989)* is used to perform the optimisation. It is reported that studies of the motion of a plate containing a random speckle pattern with this system were in agreement with the actual displacement to within the accuracy of the stage used.

The application of image correlation techniques to photogrammetry are complicated by the fact that the form of the images generally differ in the angle of viewing, as well as the features being translated. The main use of image correlation in photogrammetry is in matching features on a stereo pair of photographs in conjunction

with a stereo-comparator. Correlation methods have been successfully applied to this previously tedious task (Ackermann 1984, Förstner 1986).

Ackermann compares two images and the defines the optimum match to be the transformation that minimises any differences between the grey levels of corresponding pixels in the images. An iterative least squares technique is used to optimise the transformation between the two images. A standard error of better than 0.05 of a pixel is quoted as the accuracy of the algorithm implemented when used in conjunction with aerial photographs. Apart from removing the laborious task from an operator this represents a better stereo perception than a human can achieve. Not surprisingly, the accuracy of the least squares technique is reduced for areas of the photograph with less the average amount of texture. The reason for this is that the least squares method minimises differences in the image gradients as well as the pixel intensities.

2.3.1 The Basis Of CCD Cameras

A charge coupled device (CCD) is a photometrically linear, highly sensitive semi-conductor based sensor. Two dimensional arrays of individual elements are produced on single chips to enable them to be used as imaging devices. A brief outline of the operation of a single element is given below, as well as a description of how the two main types of CCD camera function.

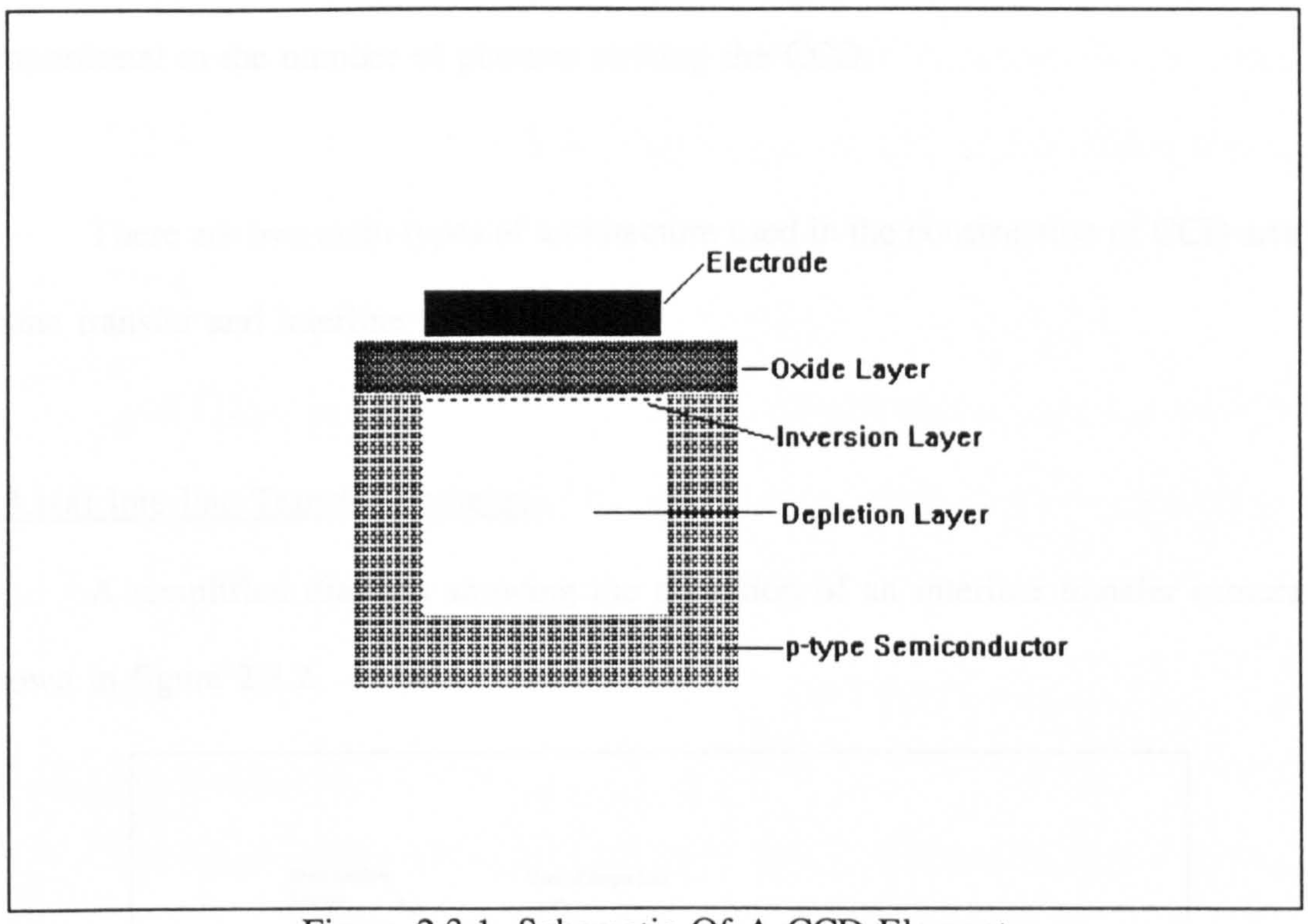

Figure 2.3.1: Schematic Of A CCD Element

Figure 2.3.1 above shows a schematic of a CCD element. The electrode is held at a bias voltage which causes the holes in the p-type material to be repelled. A depletion layer is set-up below the electrode with a depth proportional to the applied voltage. As the depth of the depletion layer increases, the surface potential becomes more positive until it reaches a level when electrons are attracted to the surface to form

a thin inversion layer. It is usual to apply a bias voltage to the electrode to ensure that the inversion threshold is always exceeded.

As photons strike the CCD element electron-hole pairs are created. The electrons so produced go into the inversion layer, which in turn causes a reduction in the surface potential. In a device of this type these electrons are the only easily available source of electrons for the inversion layer, so meaning that the surface potential is directly proportional to the number of photons striking the CCD.

There are two main types of architecture used in the construction of CCD arrays, frame transfer and interline transfer.

2.3.1(a) Interline Transfer Cameras

A simplified diagram showing the operation of an interline transfer camera is shown in figure 2.3.2.

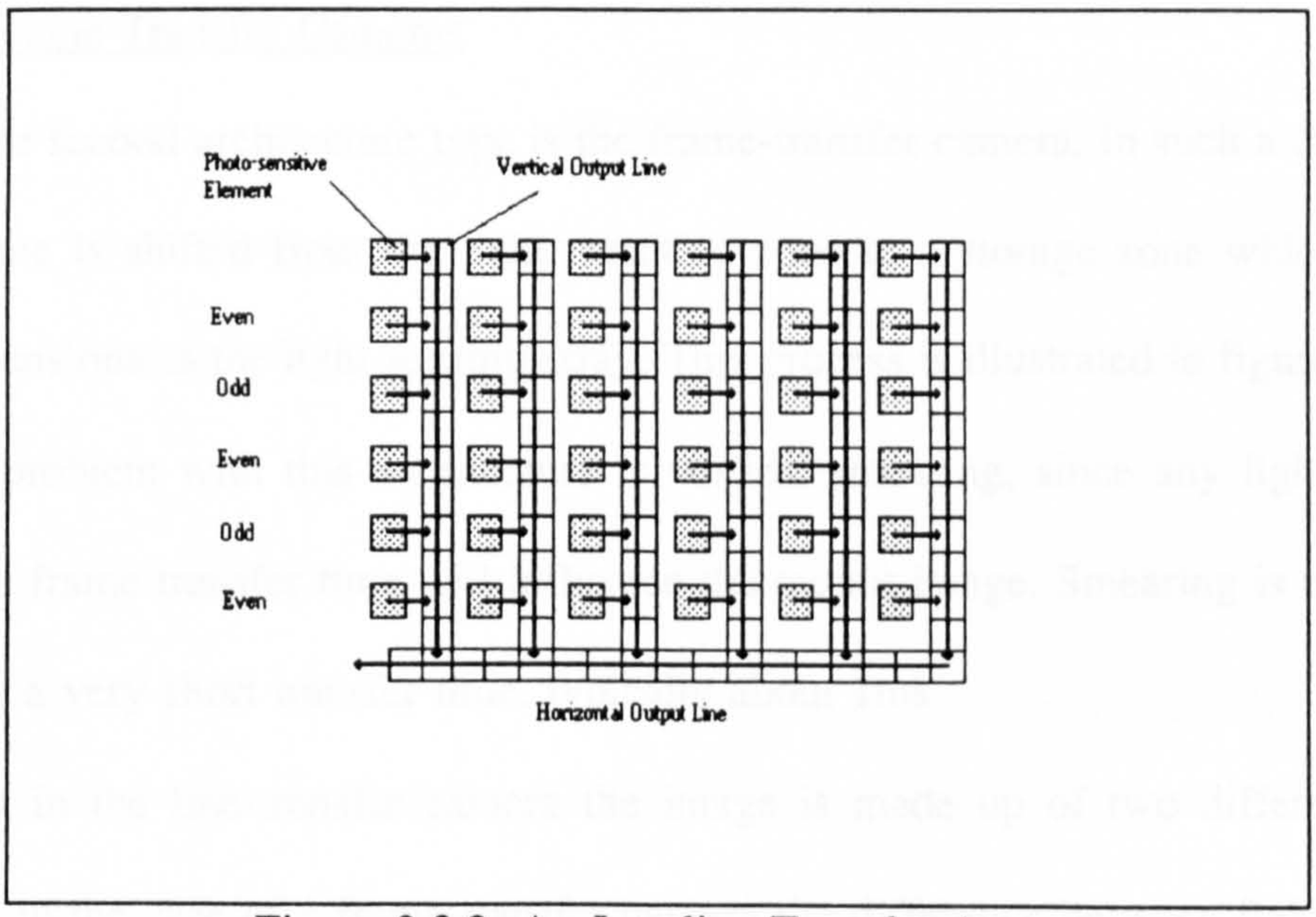

Figure 2.3.2: An Interline Transfer Array

Light is incident on the photo-sensitive elements of the array, producing a charge on each proportional to the intensity of the image at that point. Once the period, 40ms for European standard cameras, over which the incident light is averaged has elapsed, the charge is transferred from the sensitive elements into the vertical line of CCD elements. These vertical lines, as well as horizontal output lines, are shielded from the incident light.

The charges are then moved down into the horizontal output line one row at a time. A clock controls this process as well as the transfer of the charge along the horizontal line to the output port.

As is shown in figure 2.3.2, the array is divided into an odd and even field. These fields are read out alternatively (ie. One image is made up of the contents of the even field, while the next is made up of the odd field.).

2.3.1(b) Frame Transfer Cameras

The second architecture type is the frame-transfer camera. In such a camera the entire frame is shifted from the light sensitive zone to a storage zone which has the same dimensions as the light sensing array. This process is illustrated in figure 2.3.3. A potential problem with this architecture is vertical smearing, since any light incident during the frame transfer time will influence the output image. Smearing is minimised by having a very short transfer time, typically about 1ms.

As in the line-transfer camera the image is made up of two different fields. However, in the case of a frame-transfer camera the difference between fields is an

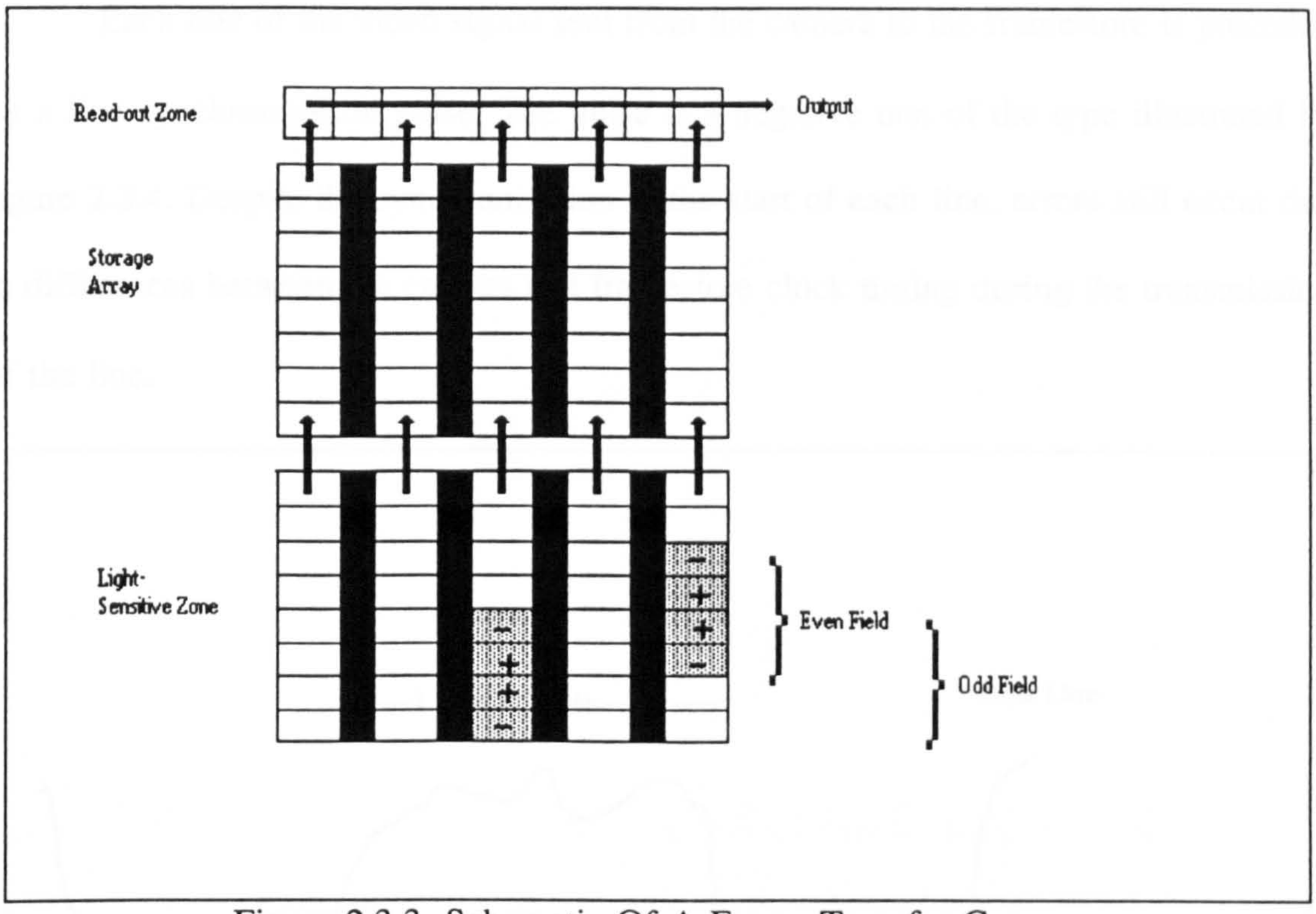

Figure 2.3.3: Schematic Of A Frame Transfer Camera

aspect of the readout timing rather than a difference between the sensing elements used. Indeed, there is a 50% overlap between the fields.

Once the image has been transferred to the storage zone it is read out in the same manner as the interline transfer array. Unlike the line-transfer camera there are no large gaps between the sensing elements, which means that the light sensitivity is enhanced by a factor of approximately 4 (Lenz 1989).

2.3.2 The Use Of CCD Cameras In Metric Applications

There are several factors that must be taken into account when a CCD camera based image processing method is used for metric purposes. The two main sources of error are line-jitter and interrogating different fields.

Each line of the video signal sent from the camera to the framestore is preceded by a line synchronisation pulse. The pulse is a negative one of the type illustrated by figure 2.3.4. Despite the synchronisation at the start of each line, errors still occur due to differences between the camera and framestore clock timing during the transmission of the line.

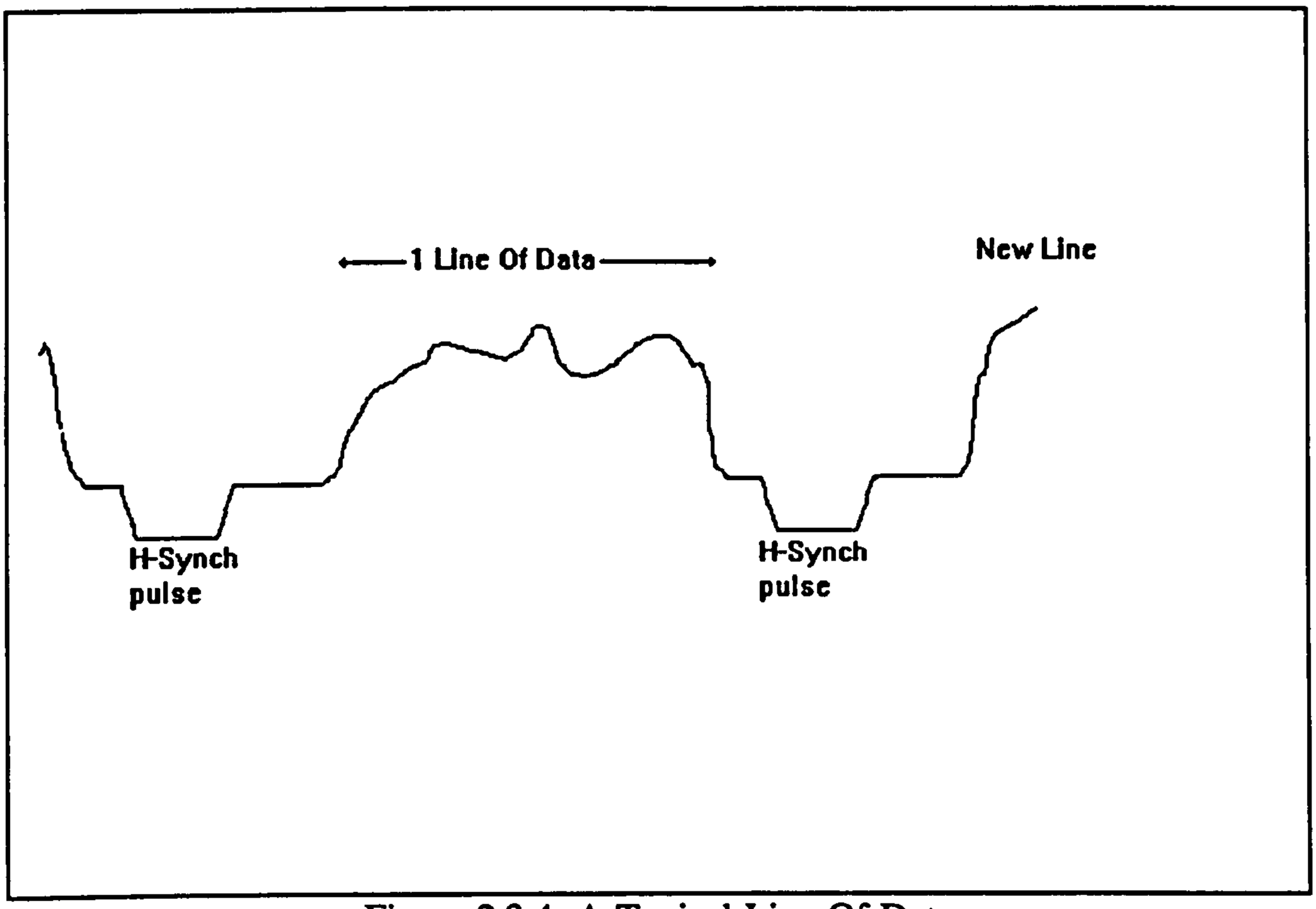

Figure 2.3.4: A Typical Line Of Data

A further problem can arise with the synchronisation pulse. If the size of the pulse varies due to power fluctuations then there may be a further contribution to the line jitter. The initial synchronisation occurs at a specified voltage level on the downwards part of the pulse. A change in the pulse voltage gives a slight change in the position of the following line of data. Such a condition is shown in figure 2.3.5. Typically the offset may be up to 0.6 of a pixel (Luhmann 1986, Beyer 1987).

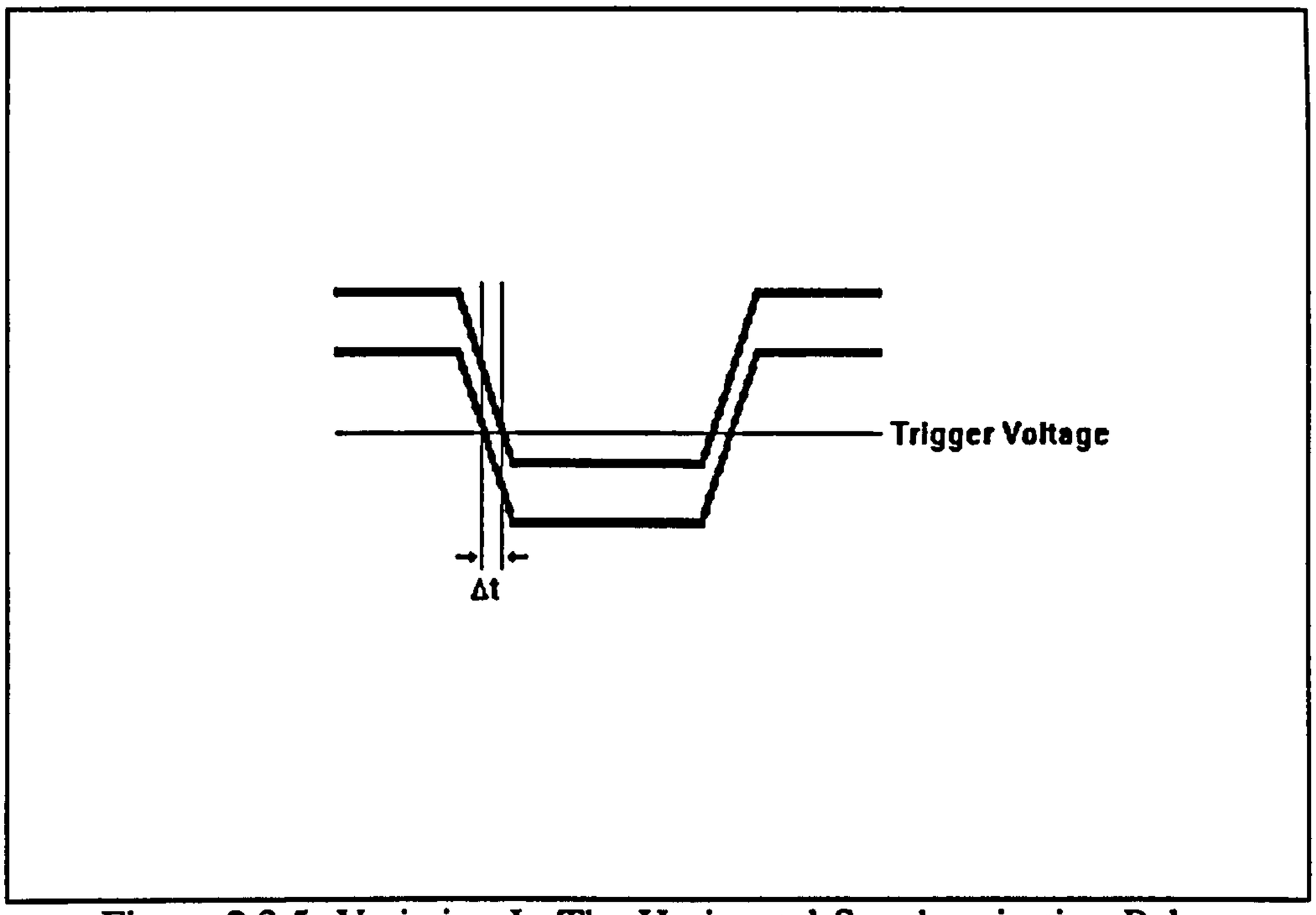

Figure 2.3.5: Variation In The Horizontal Synchronisation Pulse

A simple illustration of line jitter is to image a straight vertical line using the CCD array. The line will appear to be slightly jagged due to the framestore mapping the camera pixels incorrectly.

Line jitter is eliminated by the use of a pixel clocked system (Baltsavias *et al* 1990). In such an arrangement, a stable master clock controls both the camera and framestore. A stabilised power supply is also generally used to eliminate the problem of variable level synchronisation pulses.

An error also occurs if different fields are interrogated. This problem arises due to positions of the pixels corresponding to the two fields being offset relative to each other, as shown in figures 2.3.2 and 2.3.3. Ensuring that the same field is always interrogated totally eliminates the error.

2.4 Choice of Target Centring Technique

It emerged from the study of previous work that the most appropriate method of finding an image position is to either fit the targets to a geometric shape, in this case an ellipse, or to find the centre of gravity of the target. An algorithm of each type was developed and evaluated before a final decision as to the centring technique was taken.

2.4.1 Centre of Gravity Routine

An algorithm was developed that is able to trace around the edge of a shape, and then place a window around it. This algorithm is described in detail in section 2.5.4. It is used before the centre of gravity routine so that a window may be put around the target under investigation. Once the window has been defined the grey scale image contained within it is inverted so that the target is the most significant part of the field of view (ie has the highest grey scale values). The pixels in the window were then all interrogated to find the one with the lowest grey scale value, and this was subtracted from the value of every pixel in the window. This reduces any influence that the background may have on the calculation of the centroid. The centre of gravity is then calculated from equation 2.2.1.

2.4.2 Least Squares Best Fit Ellipse Technique

All of the targets, in a typical photogrammetric survey conducted by NPL, appear on the photographic plate in the form of either circles or ellipses. This property allowed the use of an alternative centre finding algorithm. An algorithm to fit the edge points discovered to a least squares best fit ellipse was tested. The ellipse fitting routine is based upon an algorithm described by A.B.Forbes(1987).

An ellipse of arbitrary orientation may be described by equation 2.4.1.

$$Ax^2+Bxy+Cy^2+Dx+Ey+F=0 \qquad 2.4.1$$

By placing a suitable constraint on the above equation (A+C=CONST) 2.4.1 may be rewritten as:-

$$x^2+y^2-U(x^2-y^2)-2Vxy-Rx-Sy-T=0 \qquad 2.4.2$$

$$U=cos2\alpha\frac{1-e^2}{1+e^2}, \quad V=sin2\alpha\frac{1-e^2}{1+e^2}$$

$$R=2p(1-U)-2qV, \quad S=2q(1+U)-2pV \qquad 2.4.3$$

$$T=\frac{2a^2b^2}{a^2+b^2}-\frac{pR}{2}-\frac{qS}{2}$$

Where e=eccentricity, (p,q) is the centre and α=orientation with respect to the x-axis.

If m ($m\geq5$) data points (x_i,y_i) are known then the equation of the best fit ellipse passing through them may be determined by minimising equation 2.4.4 with respect to U,V,R,S,T.

$$\sum_{i=1}^{m}\frac{\varepsilon_i^2}{N_i^2} \qquad 2.4.4$$

where

$$N_i^2=(2x_i(1-U)-2y_{iV}-R)^2+(2y_i(1+U)-2x_{iV}-S)^2 \qquad 2.4.5$$

And the residual error ε_i is given by:-

$$\varepsilon_i=(x_i^2+y_i^2)-U(x_i^2-y_i^2)-2Vx_iy_i-Rx_i-Sy_i-T \qquad 2.4.6$$

The equation is minimised using an iterative technique known as the Gauss-Newton algorithm. At each stage of the iteration it is necessary to solve a linear least squares problem to determine the correction to be made to the current best estimate for each parameter. A least squares solution method known as the "Householder" algorithm (Wilkinson & Reinsch) is used for this purpose.

Once R,S,T,U and V have been adjusted to optimise the fit of the ellipse to the data, it is straightforward to calculate the centre (p,q), the eccentricity (e), and the orientation of the ellipse (α) from equations 2.4.3.

One of the advantages of using a least squares fitting technique is the detailed error analysis that may be produced, so determining whether an image is a good match with the predicted elliptical shape. Another simple method of distinguishing targets from debris may be implemented as follows. The possible range of target eccentricities when viewed from the camera positions may be calculated. Therefore, although it was not done in this study, the calculated eccentricity may potentially be used as a check as to whether the image found is a target or debris. This check is particularly useful to prevent scratches on the photographic plate from being mistaken for images.

The major disadvantage of using an ellipse fitting routine is that only the edge points are used in the determination of the target centre. These points represent only a small part of the available information and are highly dependent upon the accuracy of the edge finding algorithm.

2.4.3 Comparison Of The Centre Finding Methods

The travelling microscope system shown schematically in figure 2.4.1 was built to compare the centre of gravity routine with the least squares ellipse fitting routine. Initially the test was performed on the centre of gravity algorithm.

A photogrammetric plate was placed on the stage with a target at the left hand-side of the field of view. The target was then moved across the visible field in a series of ten steps with its position being calculated after each step. The actual displacement was monitored by a linear displacement transducer with a resolution of 0.5μm.

The field of view of the microscope, when used in conjunction with a ×40 objective, is 45μm in the x-direction by 42.5μm in the y-direction. This area is imaged onto a 256×256 element CCD array so implying that a movement of 1 pixel corresponds to a 0.176μm movement in x and a 0.166μm movement in y.

Figure 2.4.2 shows the displacement detected by the centre of gravity algorithm for a motion of the target across field of view. The reciprocal of the gradient of the straight line graph should be equivalent to the x dimension of a single pixel. When a least squares best fit was applied to the data the equation of the line was calculated to be:-

$$y = 5.789x+26.146$$

The reciprocal of the gradient is 172.7±0.7μm/pixel which is in close agreement with the predicted value. It would be unreasonable to expect an agreement closer than this since the resolution of the displacement transducer is only 0.5μm.

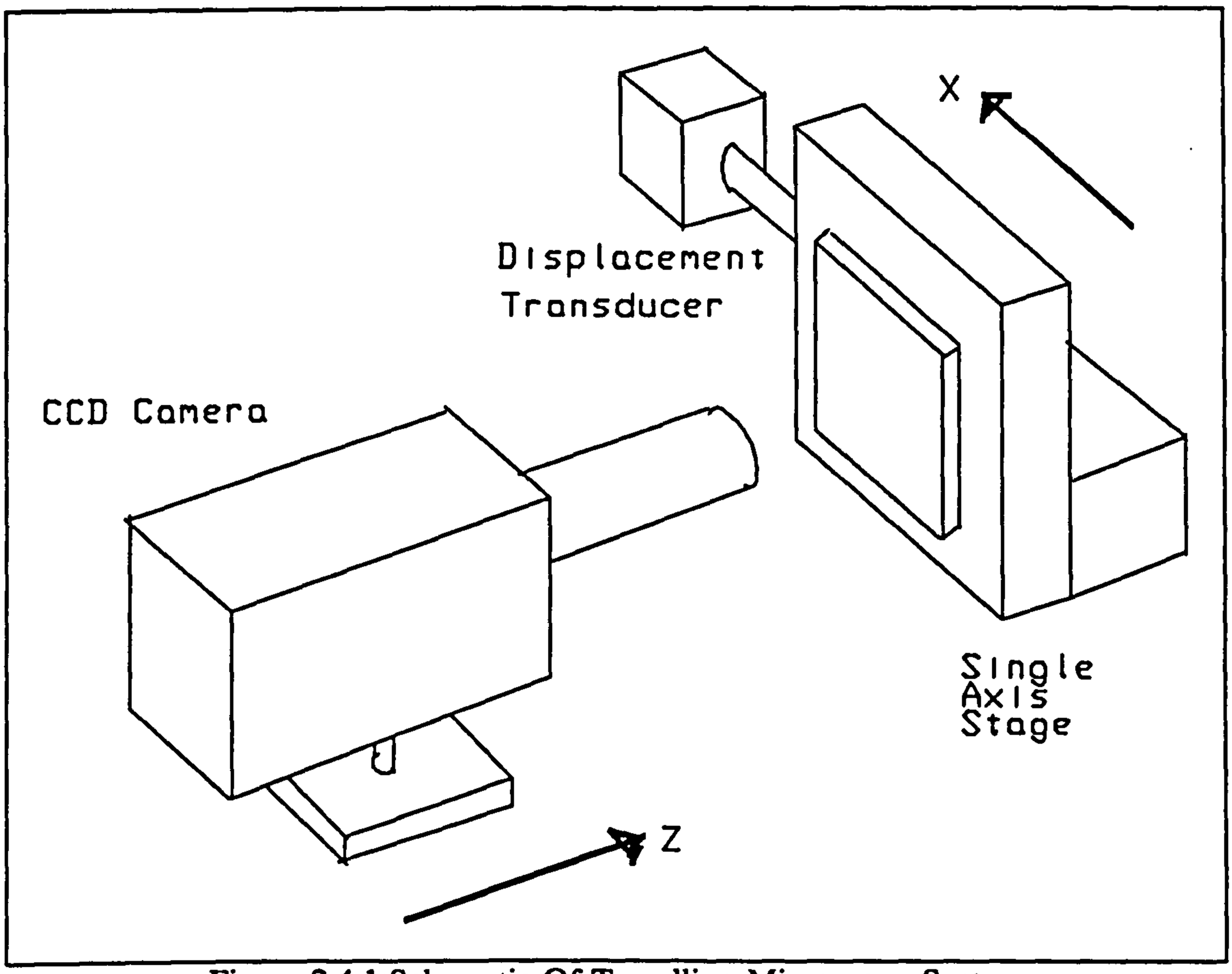

Figure 2.4.1:Schematic Of Travelling Microscope System

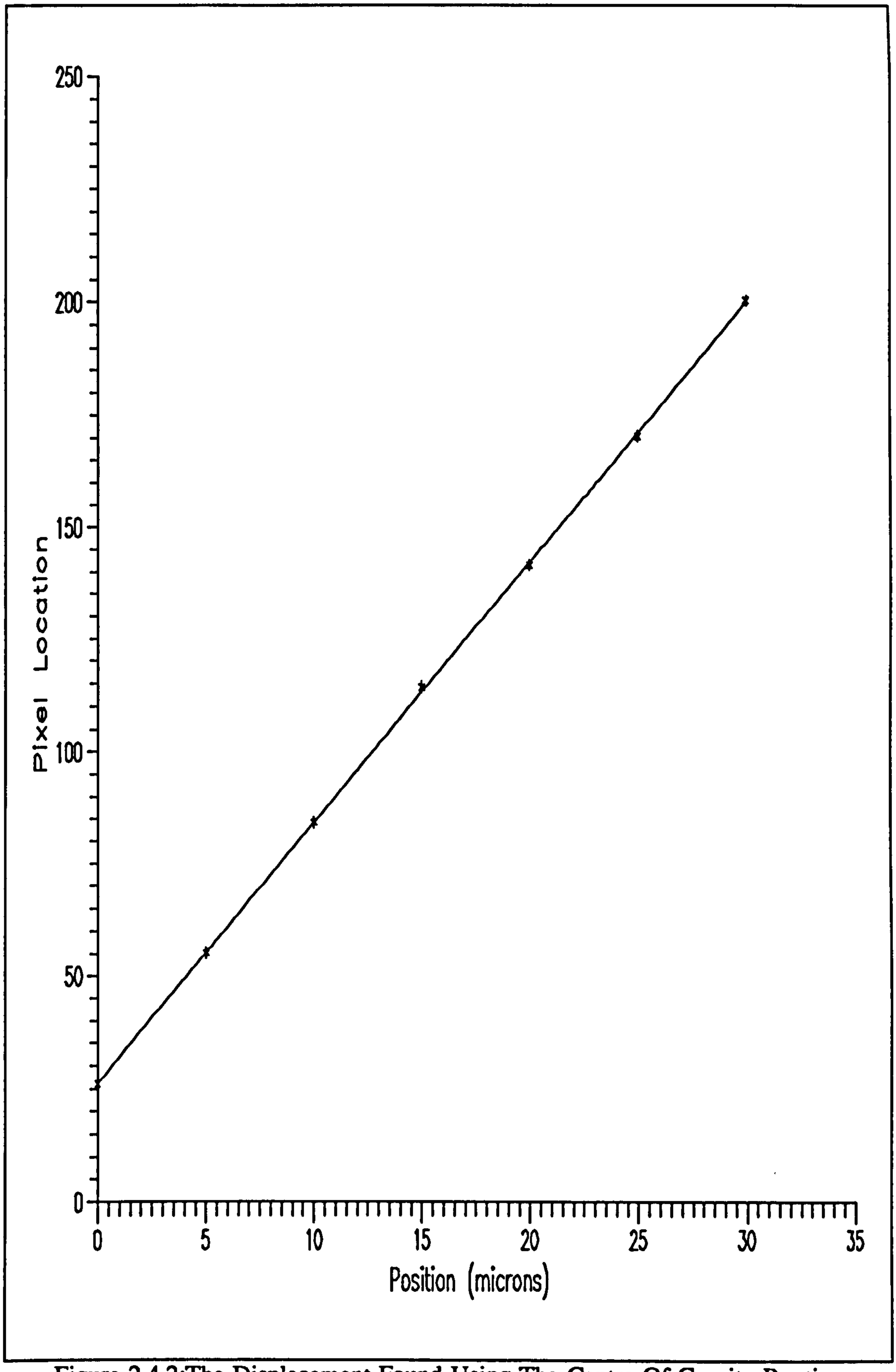

Figure 2.4.2:The Displacement Found Using The Centre Of Gravity Routine

The experiment was repeated using the ellipse fitting algorithm instead of the centre of gravity routine. In this case, the equation of the graph produced using the data was calculated to be:-

$$y = 5.760x+26.961$$

The pixel size calculated from the gradient of the graph is 173.5±1.0 μm/pixel, which is once more in close agreement with the predicted value.

The experiment failed to find any significant difference between the two techniques, since the disparity between them is below the fundamental accuracy of the experiment. However, the results strongly imply that either of the methods could be successfully used to find photogrammetric targets.

At this point, a decision was made to pursue the centre of gravity algorithm as the method for target location. There are several factors in this choice ahead of a seemingly equally accurate rival method.

i) The centre of gravity technique is intrinsically more simple.

ii) It is important that the chosen algorithm should be robust and not fail catastrophically at any time since it is anticipated that the measurements will be made overnight without an operator in attendance. The ellipse fitting routine does not satisfy this condition as well as the centre of gravity finding algorithm, as it occasionally crashes when confronted by scratches and other line features. This factor was the major influence in choosing between the two algorithms.

iii) The chosen technique is faster than ellipse fitting for highly magnified targets.

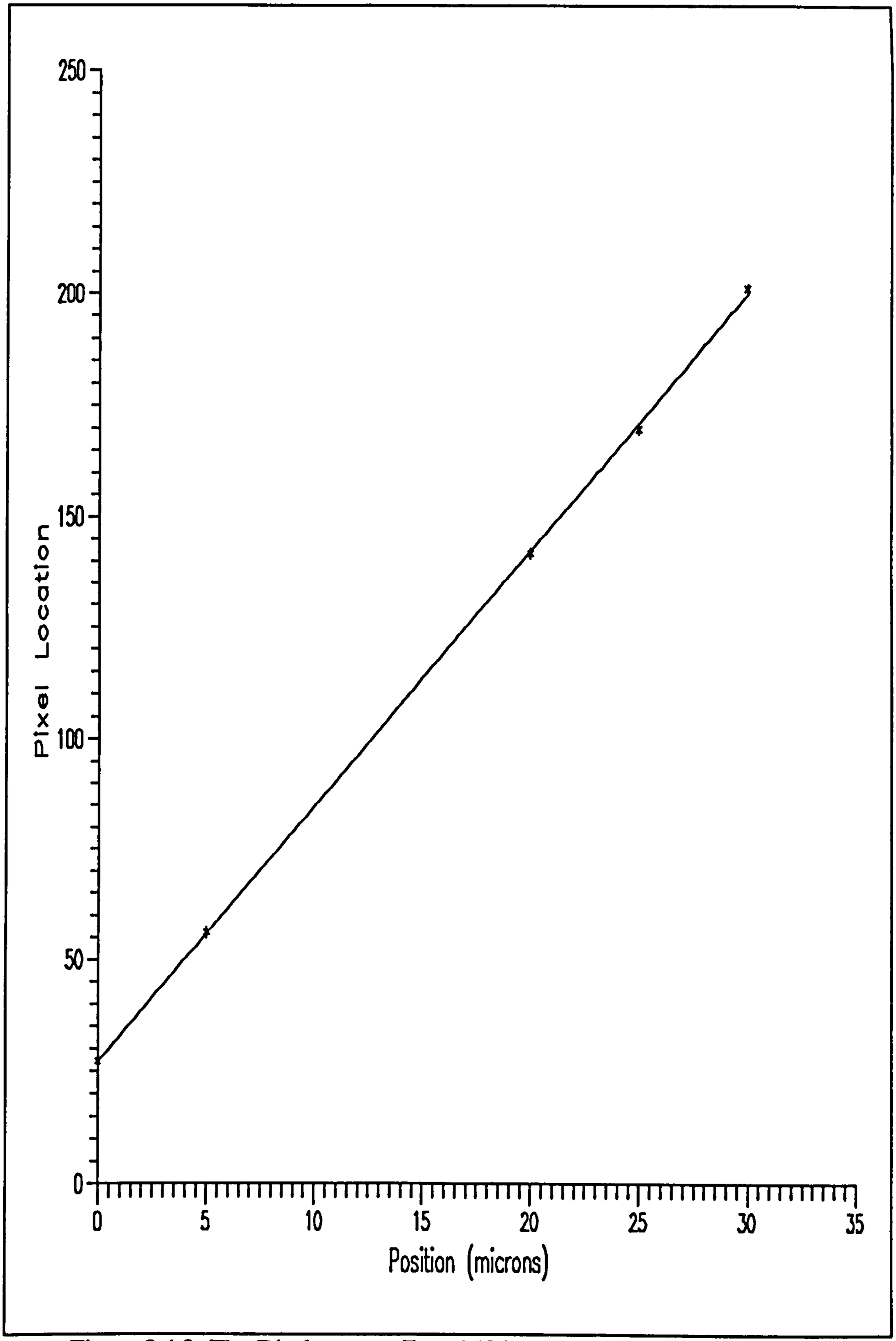

Figure 2.4.3: The Displacement Found Using The Ellipse Fitting Routine

iv) The accuracy of the ellipse fitting routine is dramatically reduced by incomplete target images and in the extreme may not recognise them as ellipses. The centre of gravity routine is less drastically affected, since more areas of the image are used in calculating the centroid.

2.5 The Plate Examination Algorithm

A package of software has been developed to measure a set of plates from a photogrammetric survey. The entire package was written in Microsoft C as part of this project. Commercial libraries were purchased to simplify communications with thee measuring microscope and to perform basic image processing commands. However, these libraries provide only very basic functions, and are used as small tools in the algorithms that are described in the following sections.

The overall flow of the collection of data is illustrated in flow-chart 1. Initially an operator is asked to select an assortment of parameters that are used in the initial search of the plate. The plate is then searched for any images using a low magnification objective lens. This process together with the algorithms that were developed for calculating the position of the images is described in the following sections. Following this initial search, the magnification of the system is increased and any images that have been found are re-examined and their positions recorded.

The plate examination algorithm is used in this manner to find the positions of all the features on each of the plates. A second program, also written as part of this study, is then used to determine which features on each of the plates correspond to each other. This target matching program, which is an epi-polar line fitting routine is described in section 2.6.

Once the points have all been found and matched, their three dimensional coordinates are calculated in the same manner as for a manually measured survey. At

NPL there are two programs available for doing this. Either the NPL bundle solution program may be used, or the General Adjustment Program (GAP), produced by the Division of Photogrammetry, The Department of Civil Engineering, at City University. An example of a complete survey is presented in chapter 3, in which such a program is used.

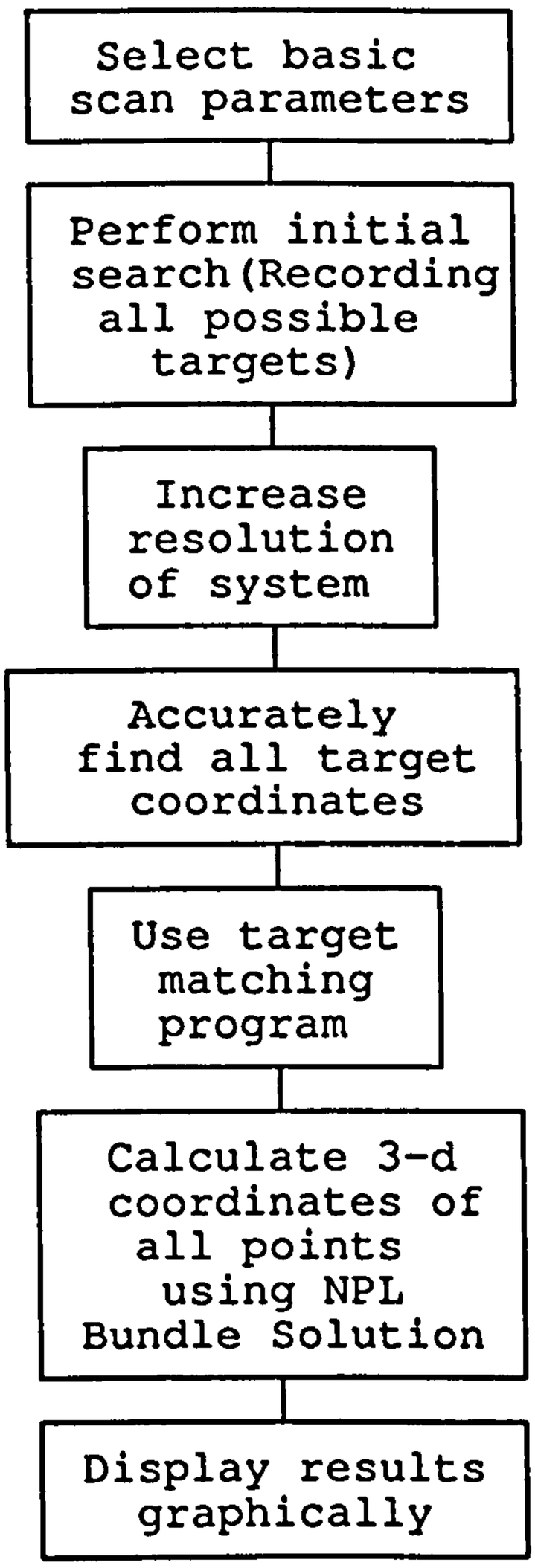

Flow-chart 1: The overall measurement process

2.5.1 Determination of Parameters for Scan

Before any meaningful measurements can be taken from the plate it is necessary for the operator to perform some simple tasks so that some important parameters are known. The order in which these tasks are carried out is shown in flowchart 2, with a more detailed description being given in the text.

2.5.1(a) Calibration of Frame

The algorithm starts by asking the operator to calibrate the field of view of the microscope. This process is essential so that positions described in terms of pixels can be expressed in real measurement units.

A live image is displayed on the output screen, and a 16×16 grid is superimposed. The operator is requested to select a feature on the image and drive the microscope until it is lined up on the second from left grid line. The microscope position corresponding to this is recorded, and the feature is moved to the second from right line whose position is also recorded. This procedure is repeated for the second from top and second from bottom lines. From the recorded position of the microscope stage when the feature corresponded to each of these lines it is possible to calculate the apparent dimensions of the pixels in both the x and y directions.

2.5.1(b) Finding the Fiducial Marks

It is important that the fiducial marks are found accurately on each plate that is measured, as these provide a reference position to which the positions of target images may be related. The operator is asked to drive the microscope stage to each of the marks

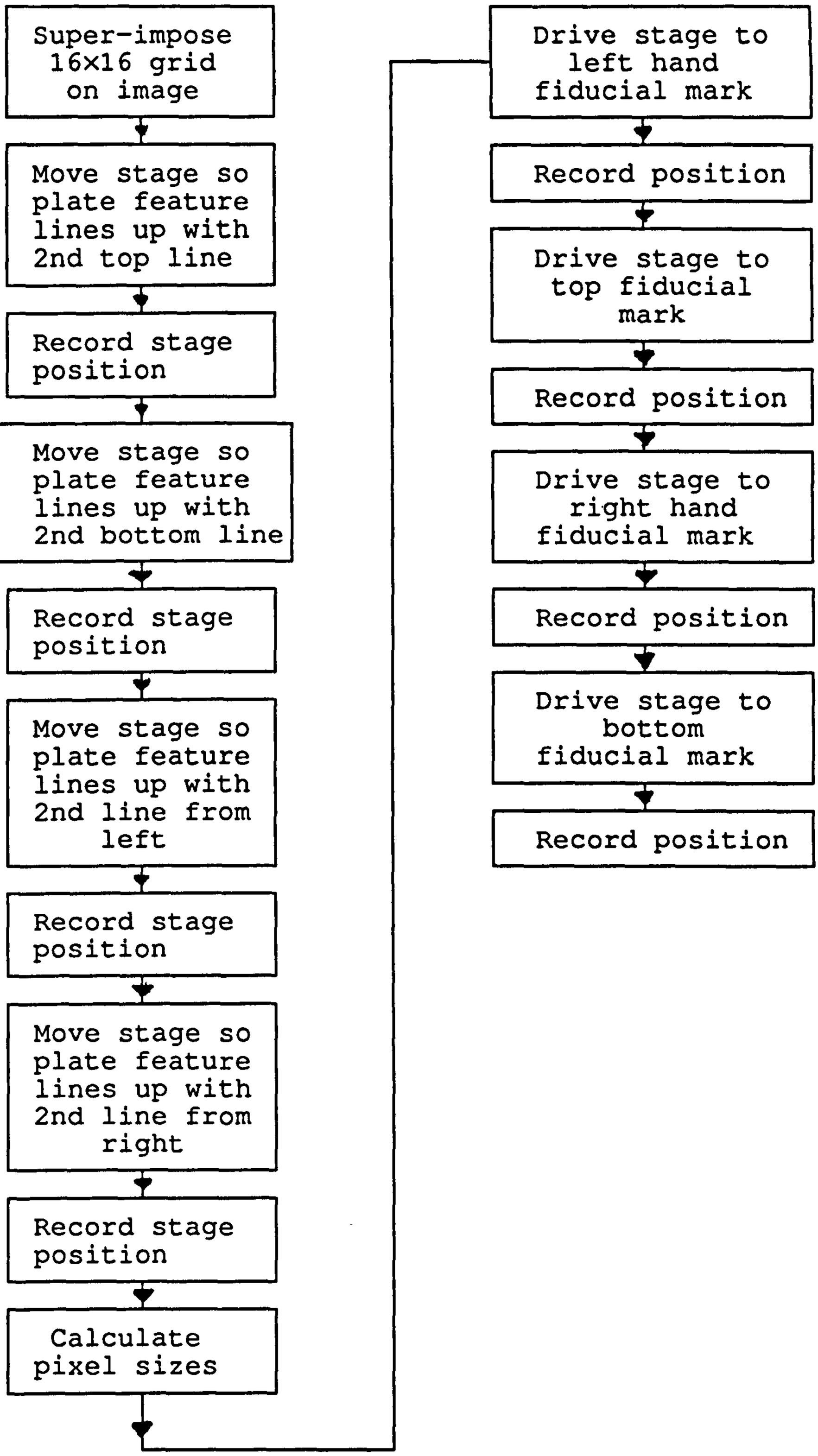

Flowchart 2: Determination of scan parameters

in rotation, starting with the left hand-side one and finishing with the bottom one. Once more a live image is produced with a 16×16 grid superimposed. Each mark is centred relative to the grid.

2.5.1(c) Determination of Scan Area

The next task that the operator is asked to perform is the selection of the area of the plate that should be searched. Once more, a live image is produced while the operator moves the microscope stage to the extremities of the search area. This completes the setting of the initial parameters, and the algorithm starts to search the selected area of the plate for targets.

2.5.2 The Initial Search

The most simple way to search the plate is to perform a raster scan. Figure 2.5.1 shows a schematic of such a scanning regime.

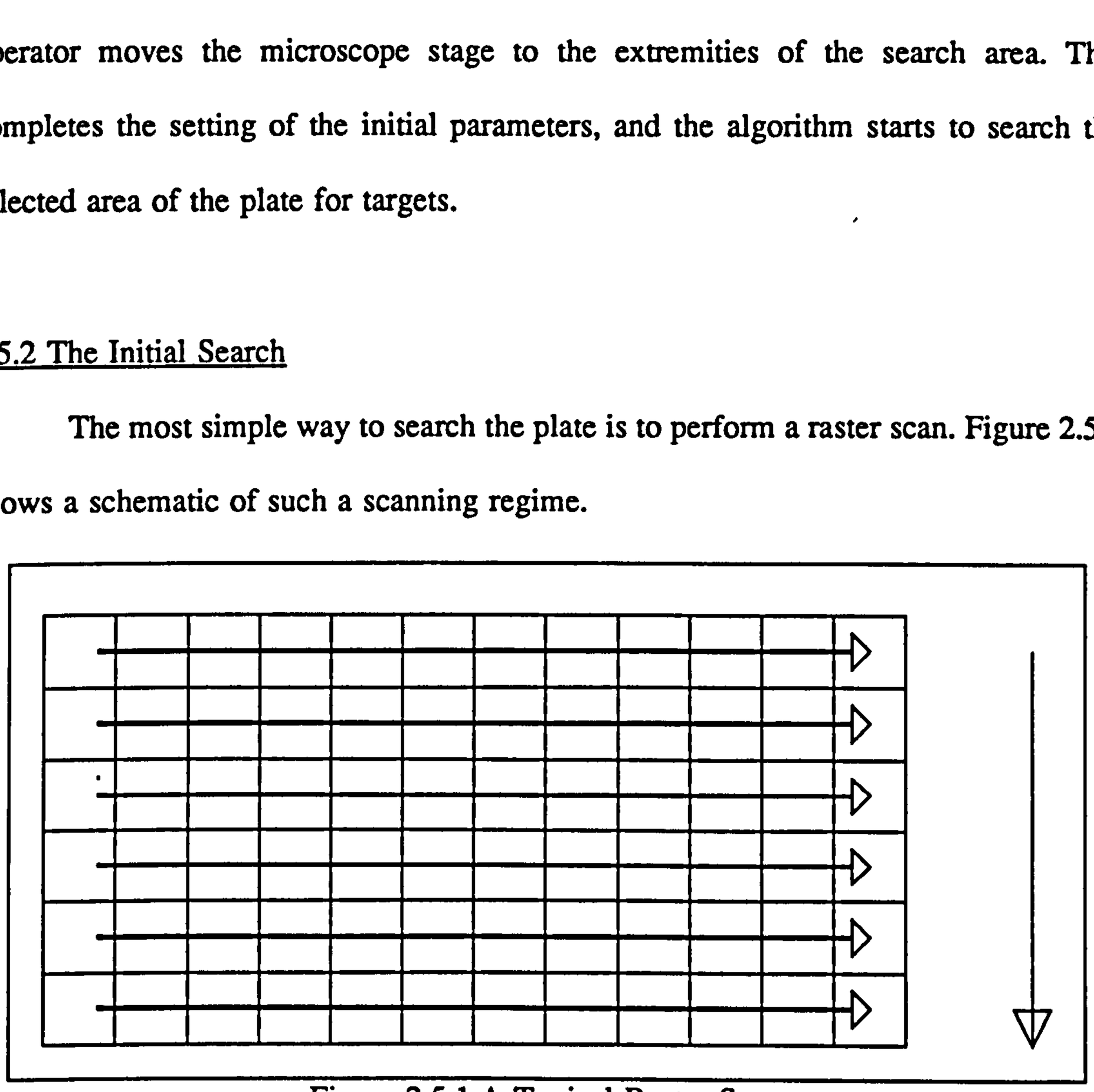

Figure 2.5.1:A Typical Raster Scan

There are two different sub-regimes that could be adopted in the scanning. The plate can either be moved continuously, or in a series of steps. The former of these

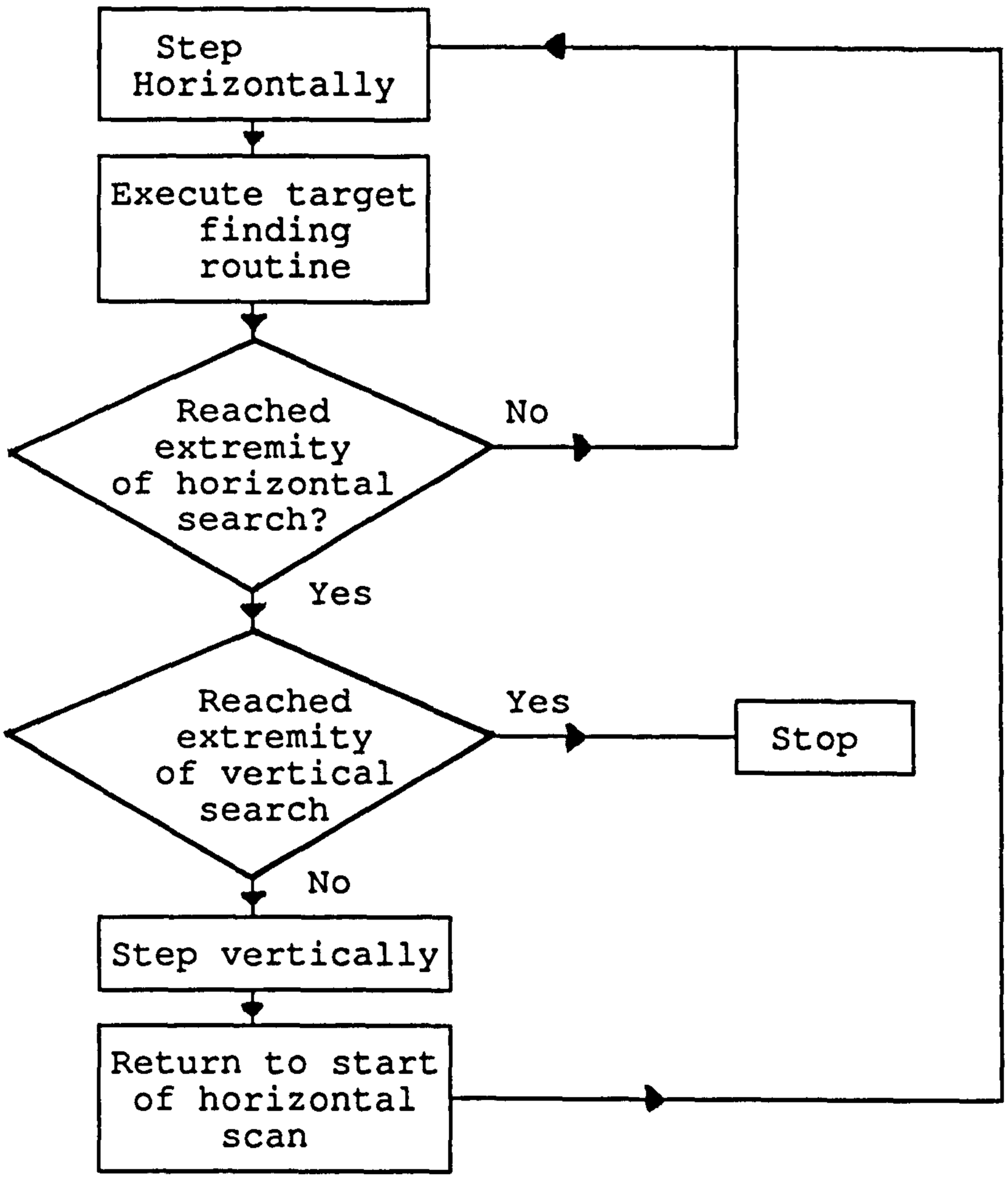

Flowchart 3: Schematic of raster scan

options has the advantage of being quicker, as well as causing less wear on the microscope stage motors. However, the uncertainty in the stage position is increased by monitoring it while in motion. Since a high level of accuracy is the prime concern of the project, the stepping protocol was adopted.

When a ×10 objective lens is used in conjunction with the microscope the field of view is 382µm × 363µm, so requiring a minimum of 147000 steps to fully scan the area of the plate where an image can be produced (Image format=120×170mm). The average time taken to analyze a frame is approximately 10 seconds, so a full investigation of a plate at ×10 magnification would take 408 hours. Whilst time is of secondary importance to accuracy this regime would clearly take too long. If an initial scan is performed with a ×1 objective the field of view is increased to 3.51mm × 3.32mm, so reducing the minimum number of steps to 1770. Hence the time to scan a full plate is reduced to approximately 5 hours.

After each step of the raster scan, the image produced by the microscope system is temporarily stored to the image processing board to allow it to be examined using the following algorithm.

2.5.3 The Algorithm For Locating The Target Centre

The most important condition that must be satisfied is that no targets should be missed. It is far better to find additional objects, which can be dismissed in the subsequent analysis, than it is to miss a target. For this reason, any filtering should be kept to a minimum.

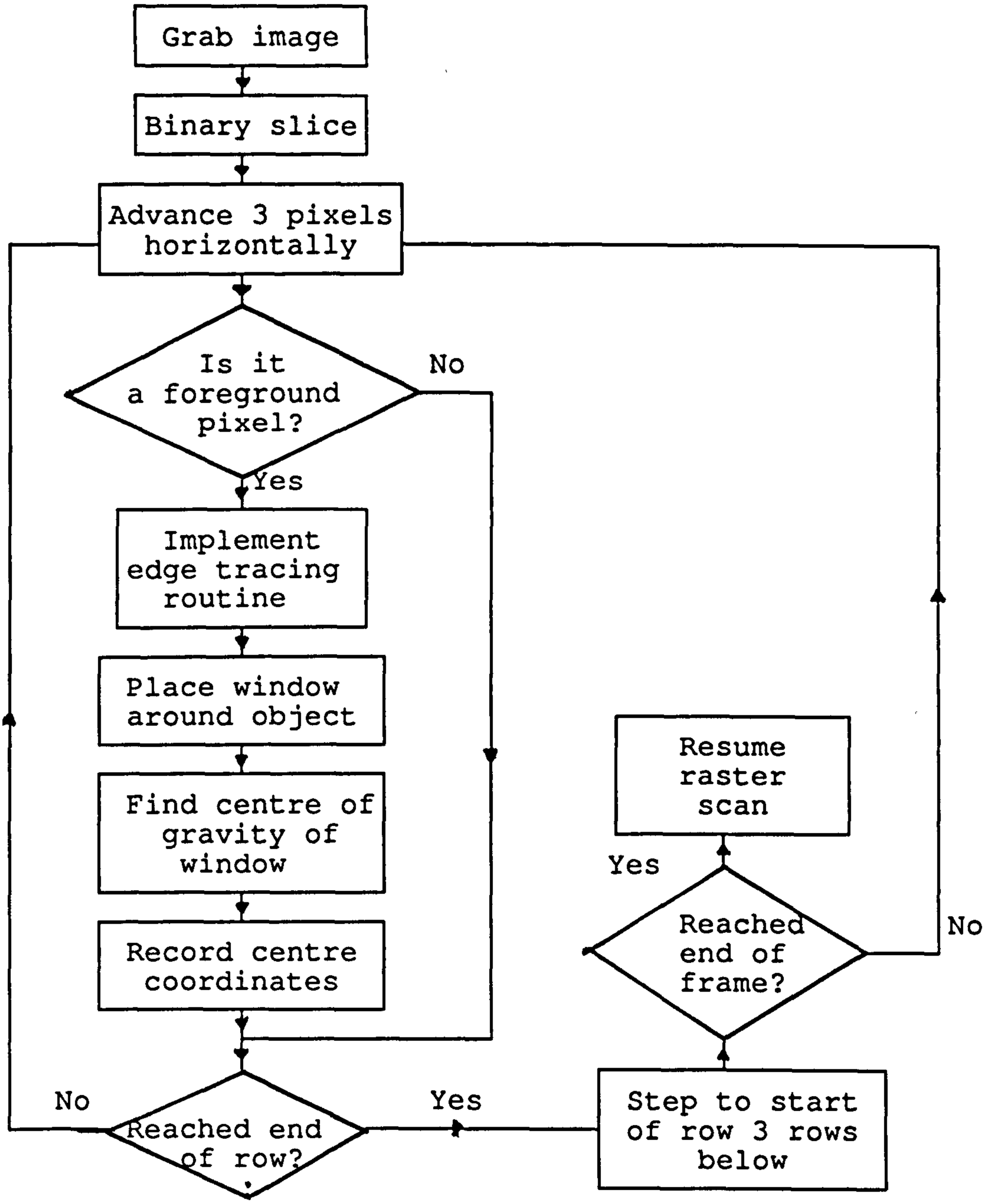

Flowchart 4: Initial target finding algorithm

Each frame is digitised into a 256×256 pixel, 256 grey-scale image. The image is already quasi-binary as the processed plate has recorded only the high contrast retro-reflecting targets attached to the structure under examination. Therefore it is relatively simple to binary-slice the image without losing information. Foreground objects, such as targets, or debris are given the intensity value 255 whilst the background is given the value 0. The threshold was set at a level corresponding to:-

$$thres = \min + \frac{mean - \min}{2.3}$$

This level was decided on after experiments in which the value now set at 2.3 was varied across a wide range, and the result of the thresholding observed. Figure 2.5.2

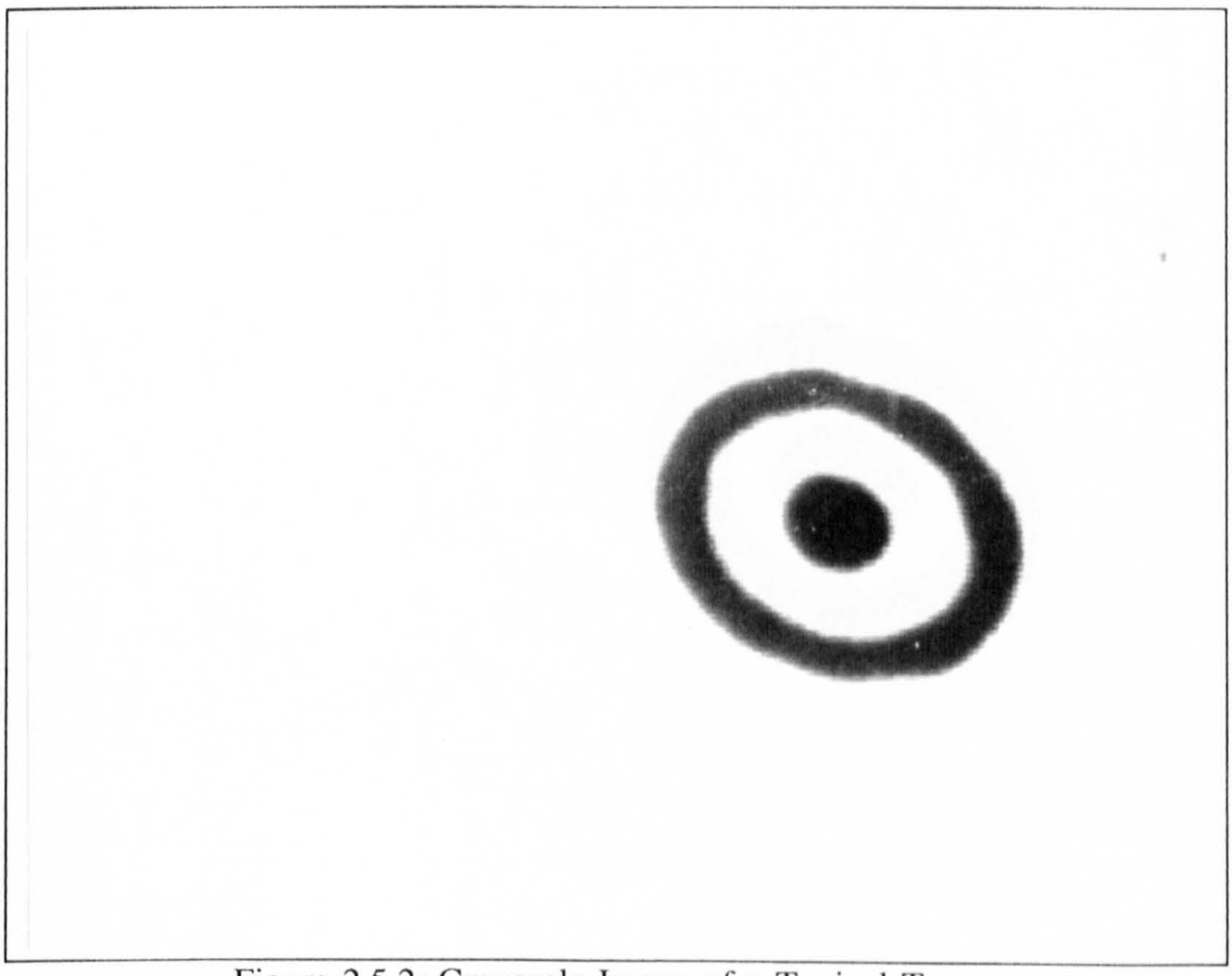

Figure 2.5.2: Greyscale Image of a Typical Target

shows a grey scale image of a typical photogrammetric target viewed using the ZKM microscope. Figures 2.5.3-2.5.6 show the results of binary slicing the image using different values for the denominator in the above equation. The values used, in the order that they are shown, are 1.8, 2.0, 2.6 and 2.8. The images produced using 2.0 and 2.6 both appear to be a good representations of the image. However, when a denominator of 1.8 is used, as in figure 2.5.4, the binary image of target starts to expand. In figure 2.5.6 (denominator of 2.8) the target features are starting to shrink. This implies that this threshold level is too low. The thresholded image is a good representation of the grey scale image when the denominator of the equation is in the range 2.0 to 2.6, so 2.3 was selected since it is in the middle of this range.

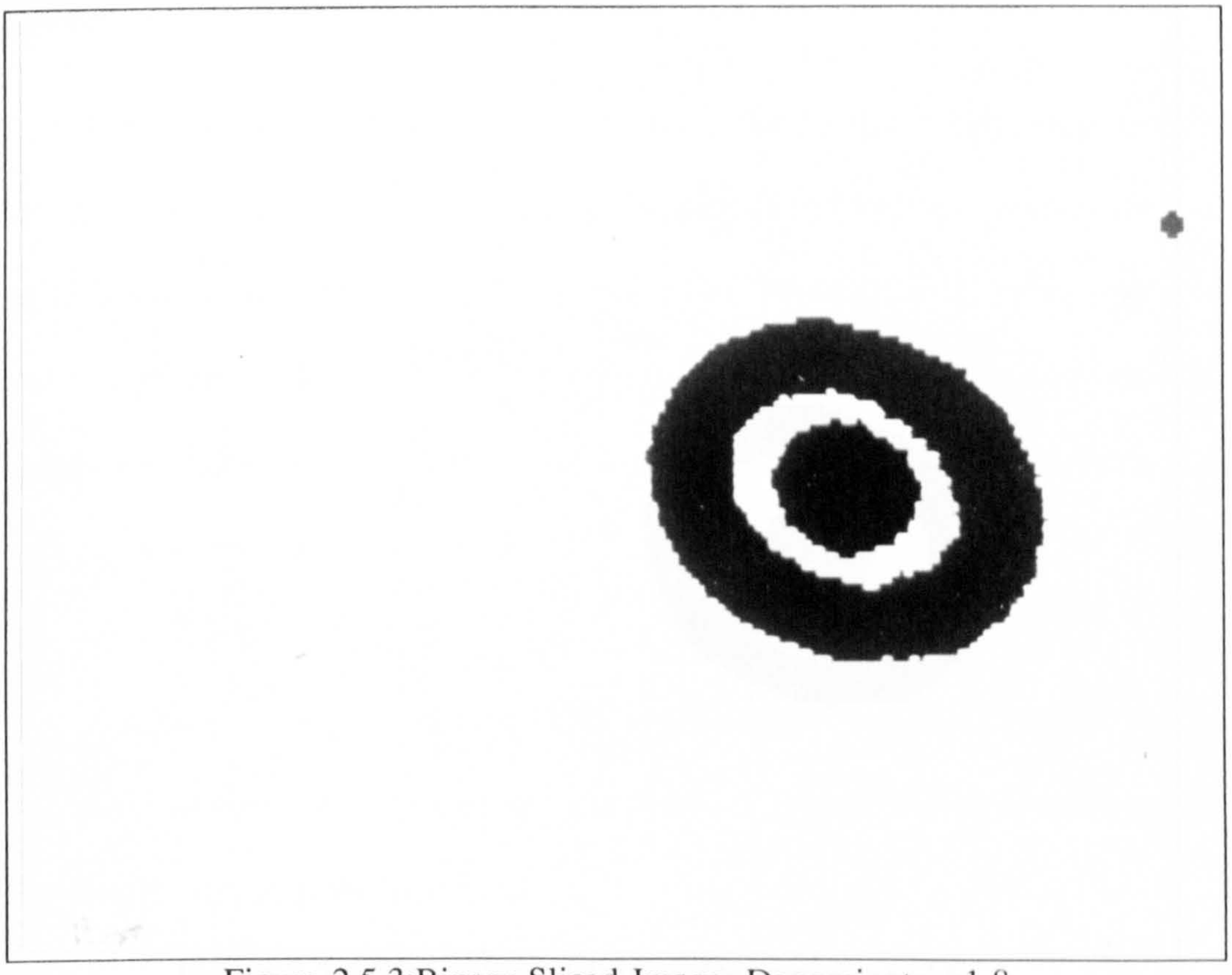

Figure 2.5.3:Binary Sliced Image. Denominator=1.8

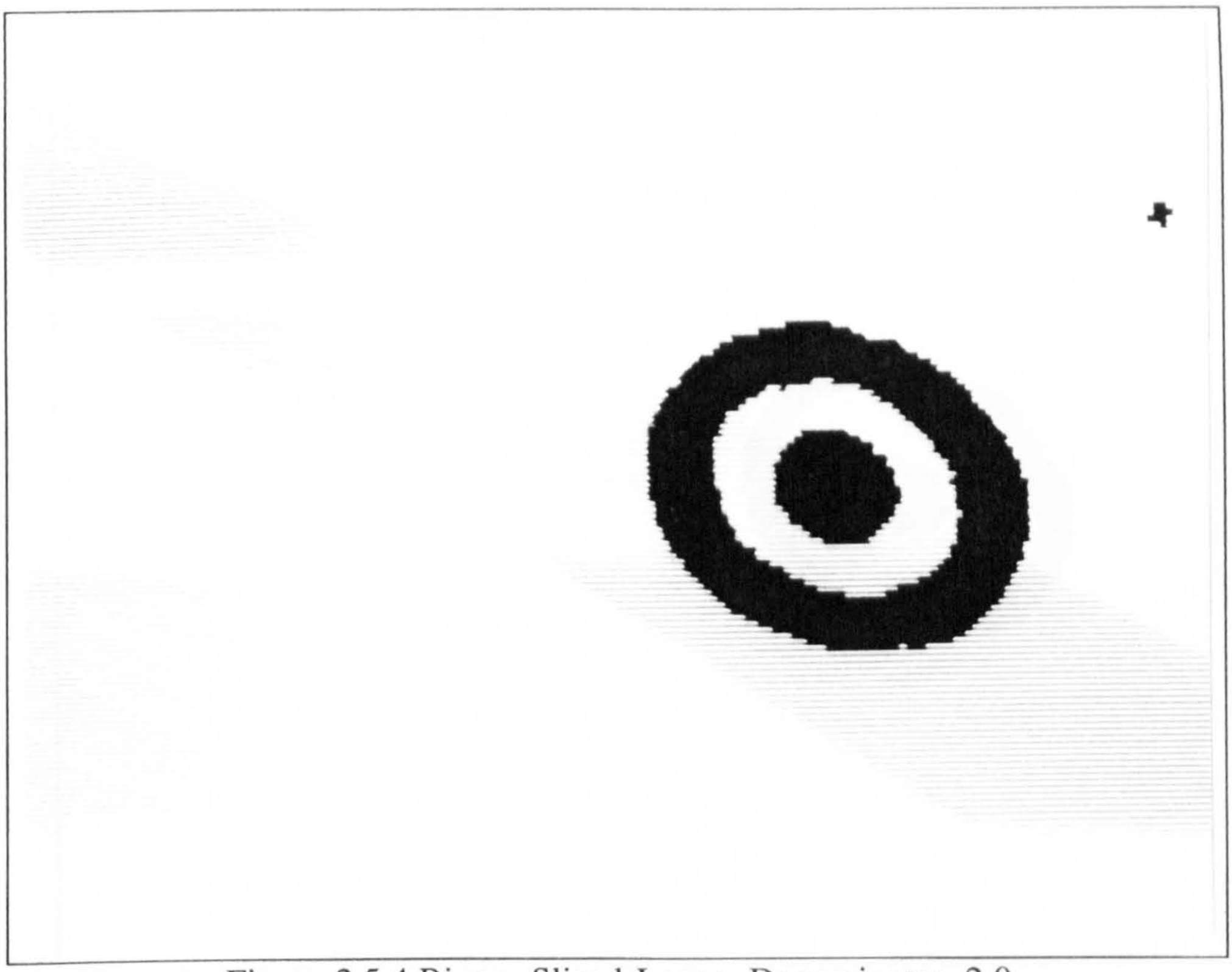

Figure 2.5.4:Binary Sliced Image. Denominator=2.0

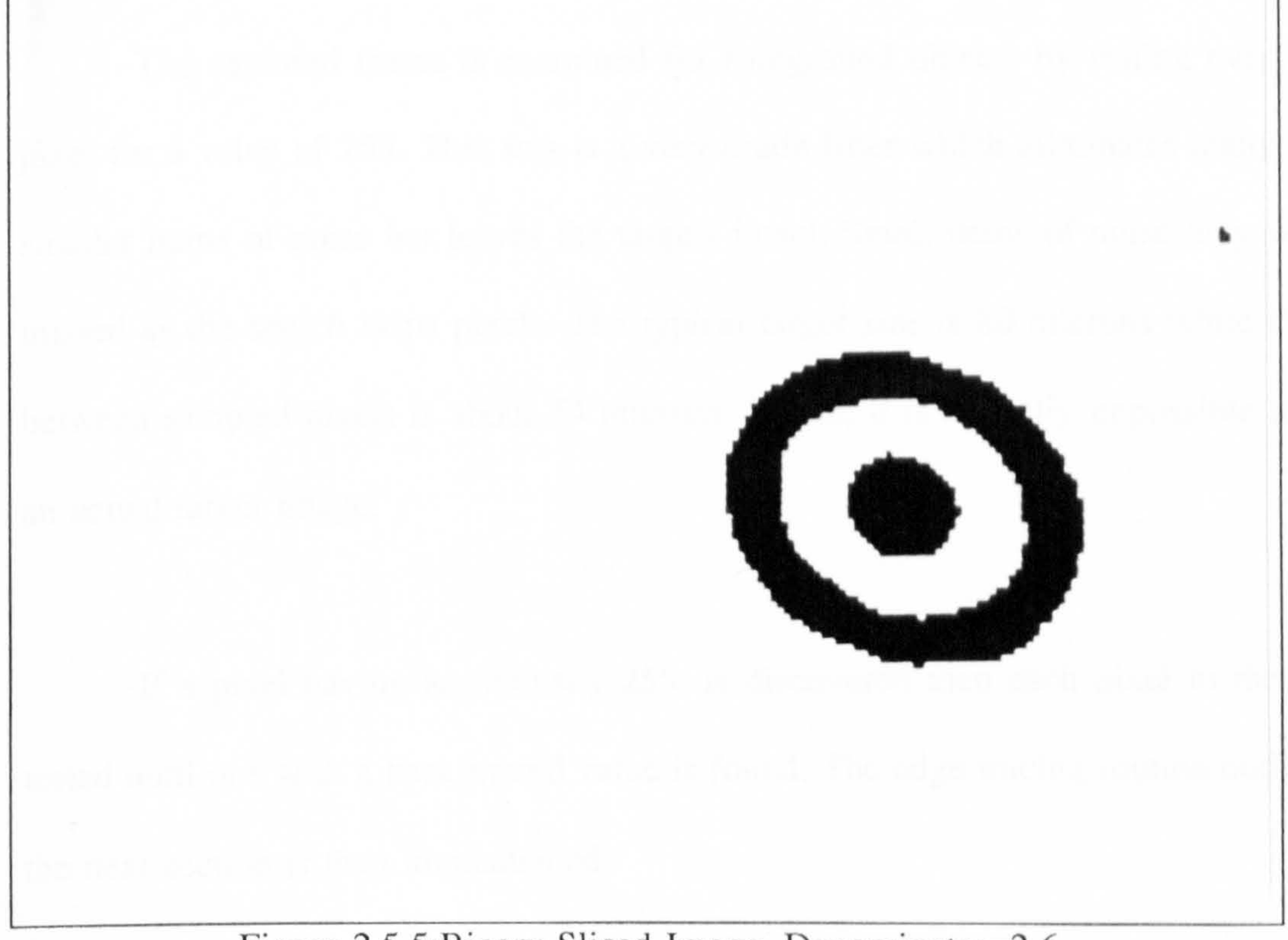

Figure 2.5.5:Binary Sliced Image. Denominator=2.6

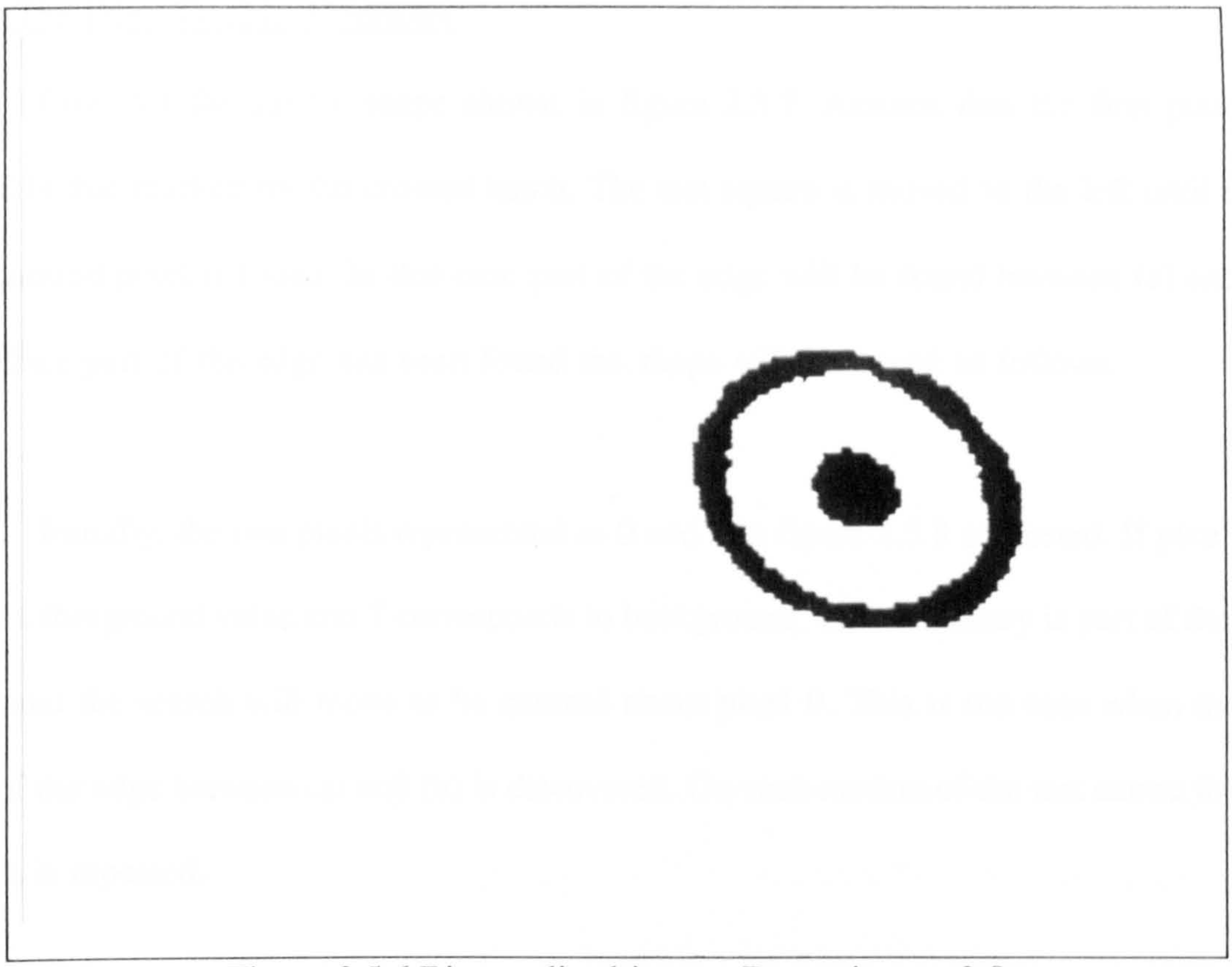

Figure 2.5.6:Binary sliced image. Denominator=2.8

The captured frame is examined for foreground objects by testing every third pixel for a value of 255. This acts is a very crude filter which eliminates many of the smaller items of noise but leaves the targets intact. Small items of noise may well be missed as the search skips pixels. The typical target size is 80 microns while the gap between sampled pixels is about 54 microns. Hence, it is virtually impossible to miss an actual target image.

If a pixel having an intensity 255, is discovered then each pixel to the left is tested until one with a background value is found. The edge tracing routine outlined in the next section is then implemented.

2.5.4 The Edge Tracing Algorithm

Consider the simple shape shown in figure 2.5.7. Assume that the first pixel found is that marked by the crossed hatch. The test square is moved to the left until a background pixel is found. In this case part of the edge will be found between (a) and (b). Once part of the edge has been found the shape will be traced as follows.

Initially, the two pixels represented as 0 and 7 in figure 2.5.8 are tested. If pixel 0 has a foreground value and 7 corresponds to background, their boundary is part of the edge and the search will move to be centred about pixel 0. This is the case when the part of the edge between (a) and (b) is discovered. On each motion of the test centre the search is repeated.

Once the search reaches corner (b), pixels 0 and 7 will both correspond to background values. Whenever this situation arises, the search moves around the grid in

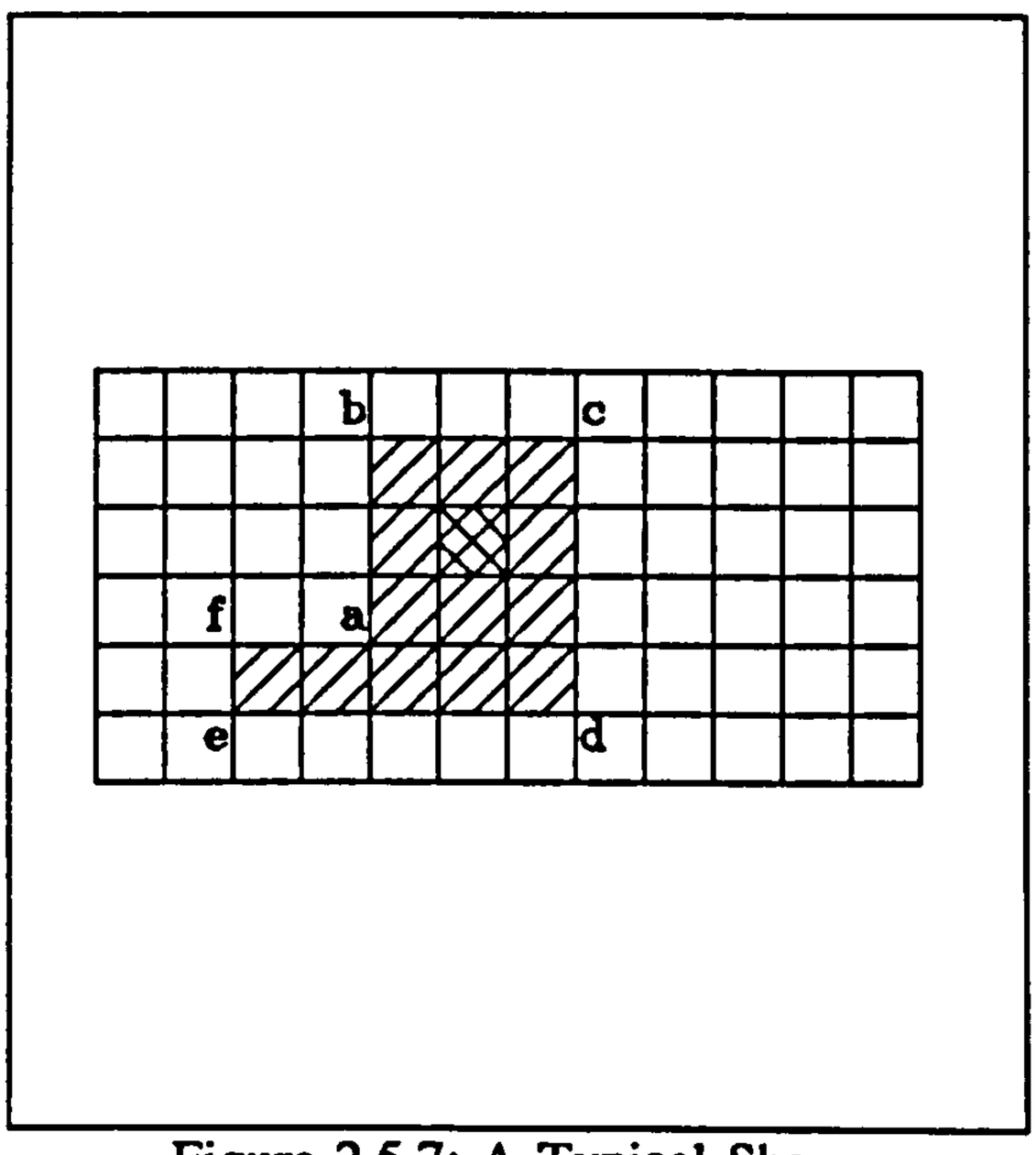

Figure 2.5.7: A Typical Shape

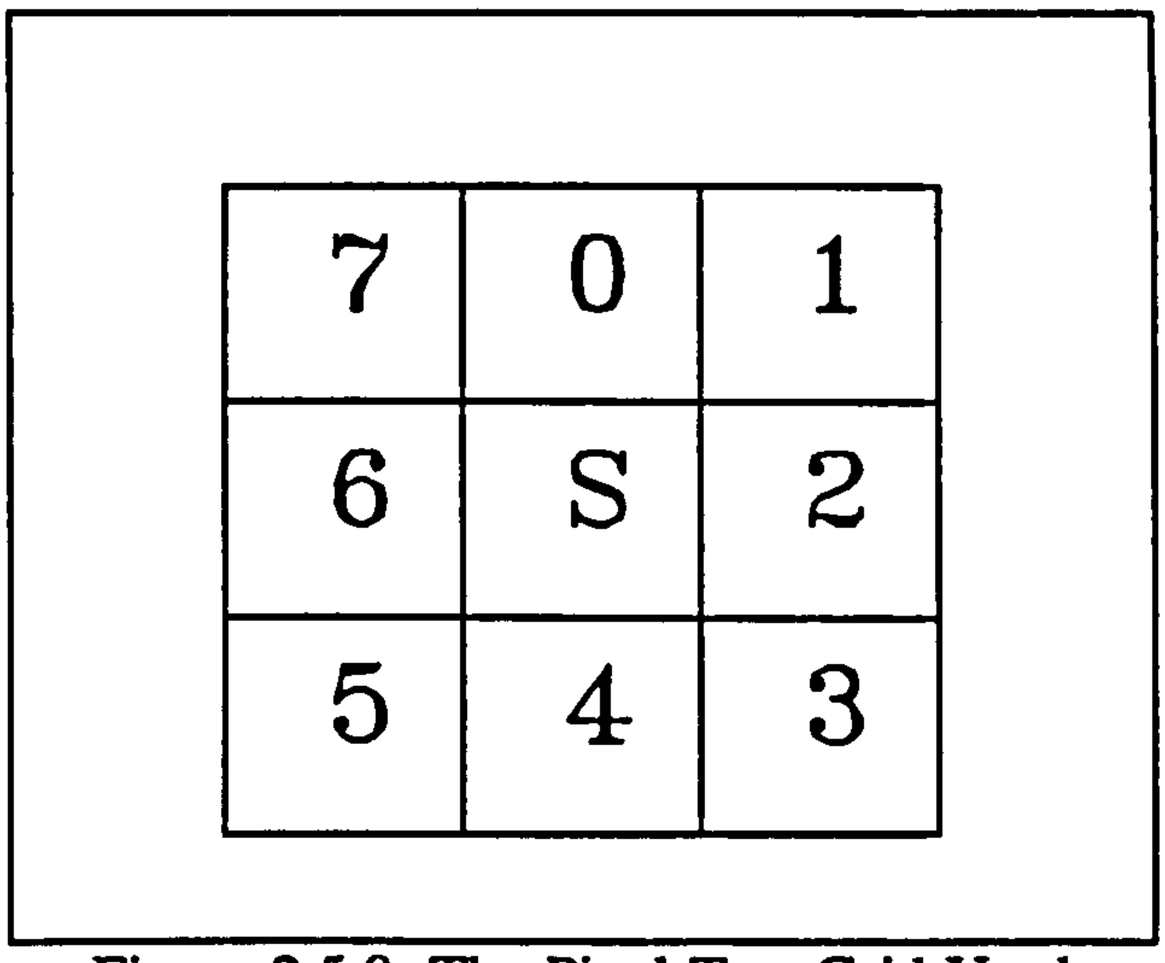

Figure 2.5.8: The Pixel Test Grid Used

a clockwise direction until a pair of pixels is found such that the most clockwise one corresponds to foreground, whilst the other is background. In this case pixels 0 and 1 will be tested following the failure of 7 and 0. They will also fail the test. Hence the search will move around to pixels 1 and 2. Here the conditions for an edge will be met since pixel 2 has a foreground value and pixel 1 is part of the background.

The search for the next portion of the edge always starts by assuming that it will lie in the same direction as the previous discovery. So, along the line from (b) to (c) the first pixel boundary to be tested will be between pixels 1 and 2. At point (c) the search will once more move clockwise to follow the edge. From there until point (d) is reached the pixel search will be on the boundary of pixels 3 and 4. Clockwise adjustment similar to those already described will occur at corners (d), (e) and (f).

Once the trace reaches (a), however, a different condition occurs. The search will have been proceeding from (f) along the boundary between pixel 1 and 2. When point (a) is reached pixels 1 and 2 will both have foreground values. The search then moves

in an anti-clockwise direction around the grid until 2 pixels are found which satisfy the criterion that only the most clockwise pixel is a foreground one. Here the condition will be met by pixels 0 and 7. The edge trace ends shortly after this when it returns to the starting point.

2.5.5 Limitations of the Edge Tracing Routine

Much effort was put into making the edge tracing algorithm robust and reliable. When the basis of the technique was first selected the basic algorithm was programmed on an IBM compatible computer in Microsoft Quick-Basic. This is a straight forward language which was unlikely to cause any problems itself. Random shapes involving concave and convex sections were drawn on the computer monitor by the program that was written. The progress of the edge tracing algorithm around the shapes was then followed on the screen.

One obvious problem that arose is that of a shape which overlaps the perimeter of the image. In this case the edge would effectively become undefined. A simple solution to this problem was achieved by effectively drawing a border 1 pixel deep around the entire image, and defining it as having a background value. This means that the edge will be traced as if it went along the side of the screen. There is no problem in using such an approach, as an object that is on the periphery of a screen will be fully on the next screen in the raster scan.

A second problem is that of an object which more than fills the screen. The targets of interest on the plate should not, under any circumstances, fall into this

category, but there is a risk that some may be obscured if this happens. In this case the program logs the microscope position so that the operator may examine it when the automatic scan has been completed.

As the program steps around the edge of a shape, it records all of the edge points in an array. The array is defined as having 5000 elements in both x and y which means that if there are more than 5000 edge points the results will not be recorded correctly. To prevent this from happening the steps around the edge are counted. If the number taken exceeds 5000 then the tracing algorithm is stopped and the microscope position is noted so that the operator can examine the area manually at the end of the program. The microscope is then stepped to the next position of the scan.

Once the algorithm had been proved in Quick-Basic it was re-coded in Microsoft C version 5.1. This allowed it to be used in conjunction with the image processing system and a CCD camera. Several shapes were drawn on blank card and their images recorded. The edge tracing algorithm was then used to follow their edges, and then draw a window around the image. Figures 2.5.9 and 2.5.10 show a binary image of such a shape and the edge that was traced around it. As can be seen from the figures, there is a good agreement between the traced edge and binary image. The algorithm was incorporated into the main program following its success in tracing the edge of every shape that it was tested with.

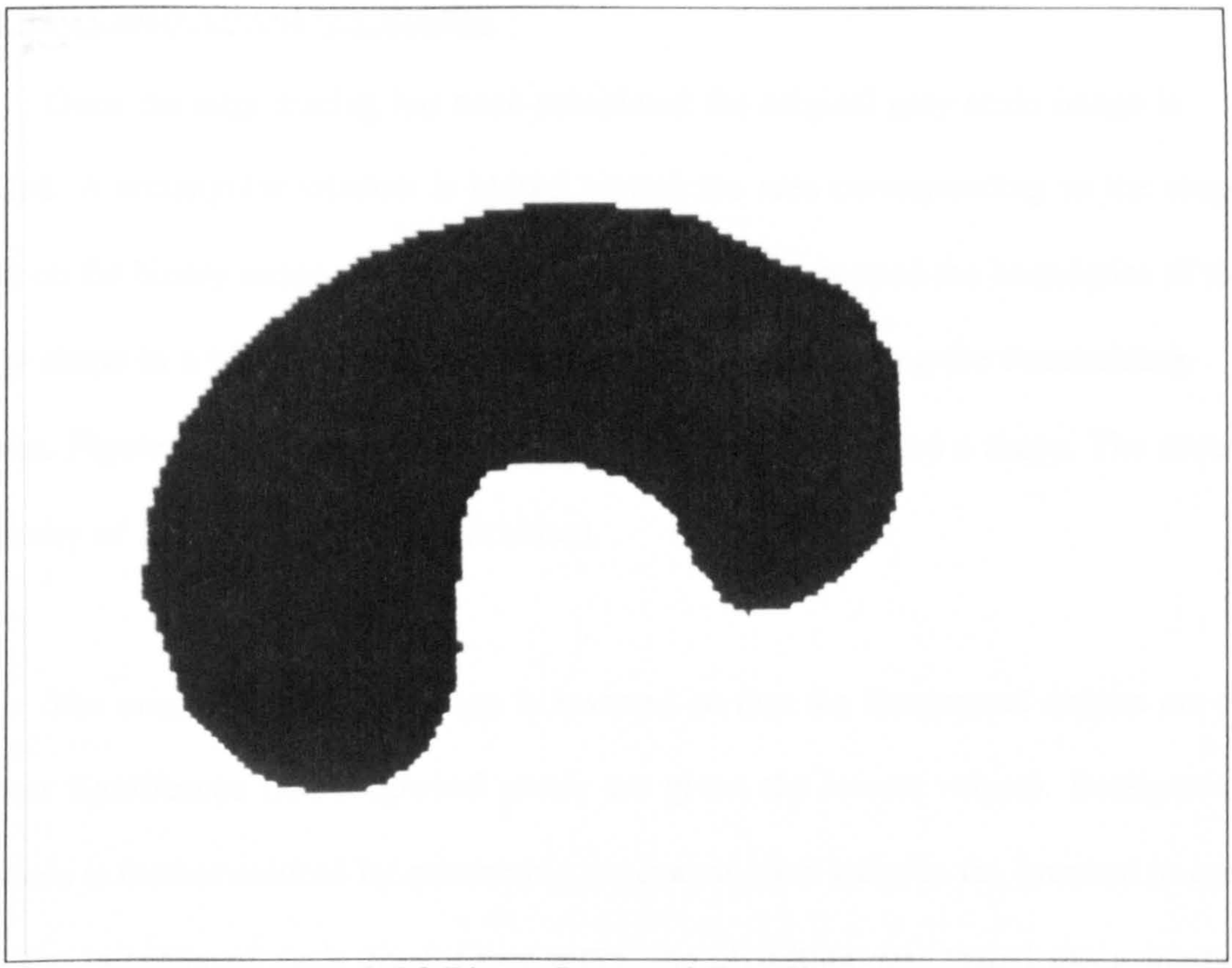

2.5.9:Binary Image of Test Shape

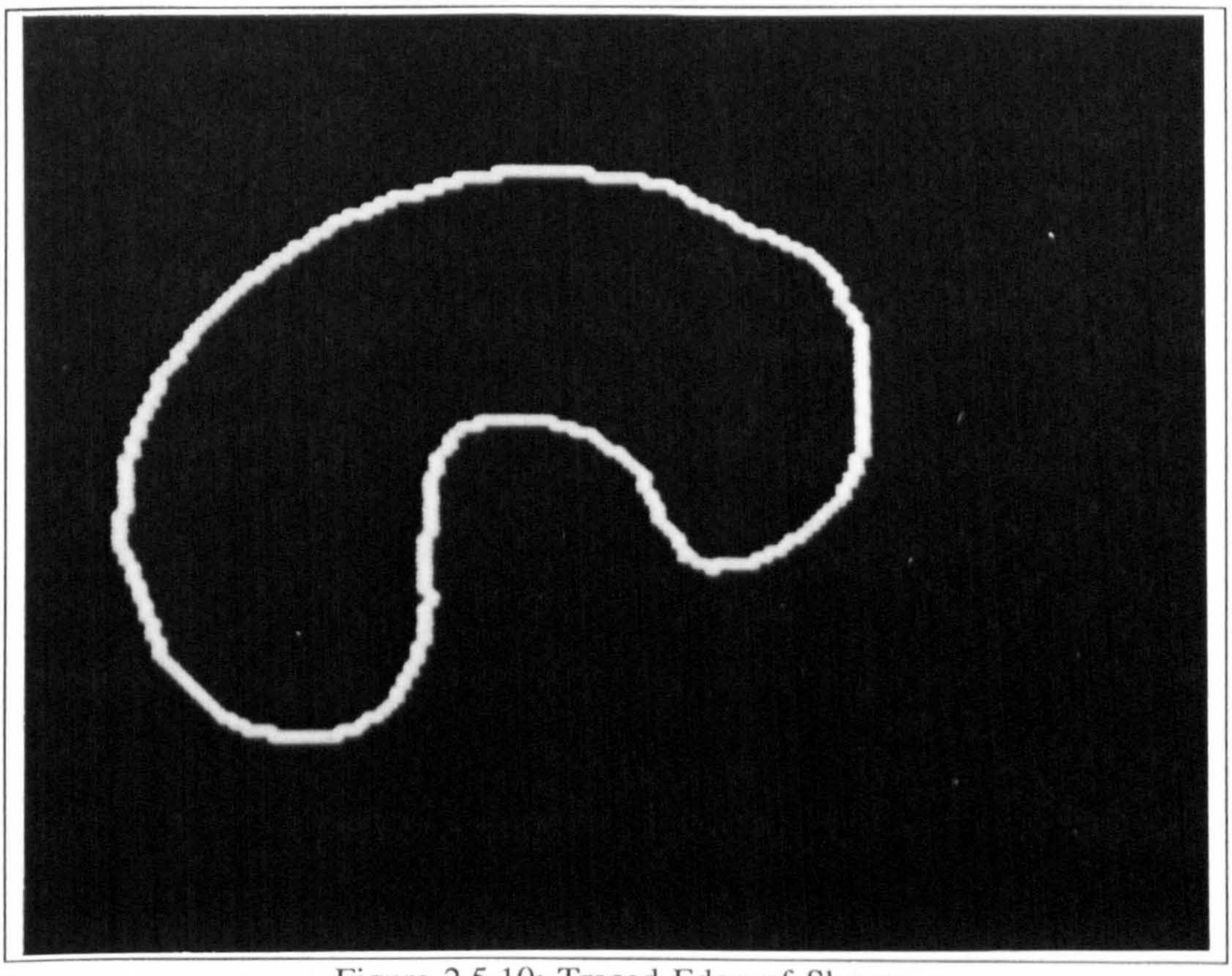

Figure 2.5.10: Traced Edge of Shape

2.5.6 The Centre Of Gravity Routine

Once the edge tracing has been completed the original grey scale image is recalled. A rectangular window is placed around the area corresponding to the shape found on the binary image. The window is made to extend beyond the boundaries of the binary shape in a bid to recover any edge information lost during the thresholding process. Figure 2.5.11 shows how a typical window would enclose a shape. The centre of gravity of the window is then calculated.

The original grey scale image is inverted so that the foreground objects are of greatest significance (ie.background pixels are given the lowest values). Background influence is further reduced by subtracting the lowest pixel value in the inverted image from the intensity of each pixel. Once more, the algorithm was tested using images drawn on blank cardboard, with a dot being drawn on the image at the calculated

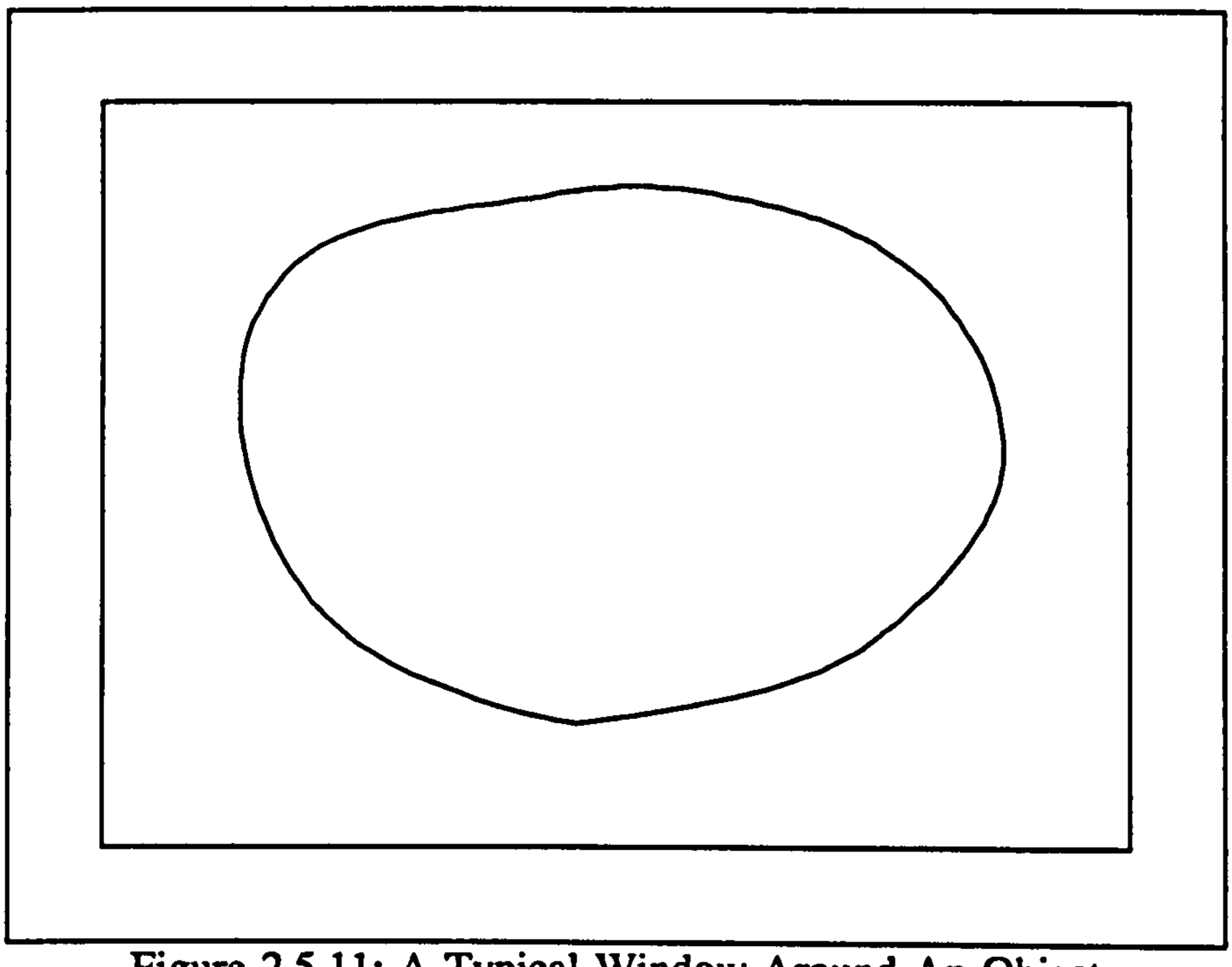

Figure 2.5.11: A Typical Window Around An Object

position of the centre of gravity. Figure 2.5.12 shows the greyscale image of a shape with a dot in the position where the algorithm calculates its centre of gravity to be.

During this initial scan the position of the microscope stage, along with the framestore coordinates of any foreground objects that are discovered, are recorded to a disk-file. An example of the disk-file produced is shown below.

x fiducial 1,y fiducial 1
x fiducial 2,y fiducial 2
x fiducial 3,y fiducial 3
x fiducial 4,y fiducial 4
x pixel size
y pixel size
Number of ground points
x microscope coordinate,xpixel offset,y microscope coordinate,y pixel offset
. . . .
. . . .
. . . .
. . . .
x microscope coordinate,xpixel offset,y microscope coordinate,y pixel offset

A typical data file from the initial scan

Figure 2.5.12:The Centre of Gravity of a Shape

2.5.7 Final Position Determination

Once the approximate positions of all the targets has been found during the raster scan it is necessary the determine their locations more accurately. The ×1 objective on the Zeiss microscope is replaced by a ×10 objective in order to increase the resolution of the system. To take into account any translation of the microscope optics during the lens changing operation, the fiducial marks are re-measured with the new lens in place using the same routine as was described in section 2.5.1(b).

A new calibration of the pixel size is made using the routine that was used prior to the initial scan. The data-file created by the raster scan is reloaded and the microscope driven in sequence to the positions of the foreground objects found by the scan. The position to which the microscope is driven (x,y) is calculated from equations 2.5.1 shown below.

$$x = x_{pos} - x_{off} - (x_{pixel} \times x_{diff})$$
$$y = y_{pos} - y_{off} - (y_{pixel} \times y_{diff}) \qquad 2.5.1$$

Where (x_{pos},y_{pos}) is the microscope position when the target was initially found, x_{off} & y_{off} are the translation due to changing the lens, x_{pixel} & y_{pixel} are the pixel sizes at the initial magnification, and (x_{diff},y_{diff}) are the initial framestore coordinates of the suspected target.

When the microscope has been moved to bring a target into the field of view the target location algorithm described in section 2.5.3 is used once more. Rather than searching the entire field of view, because the initial scan has found the approximate co-

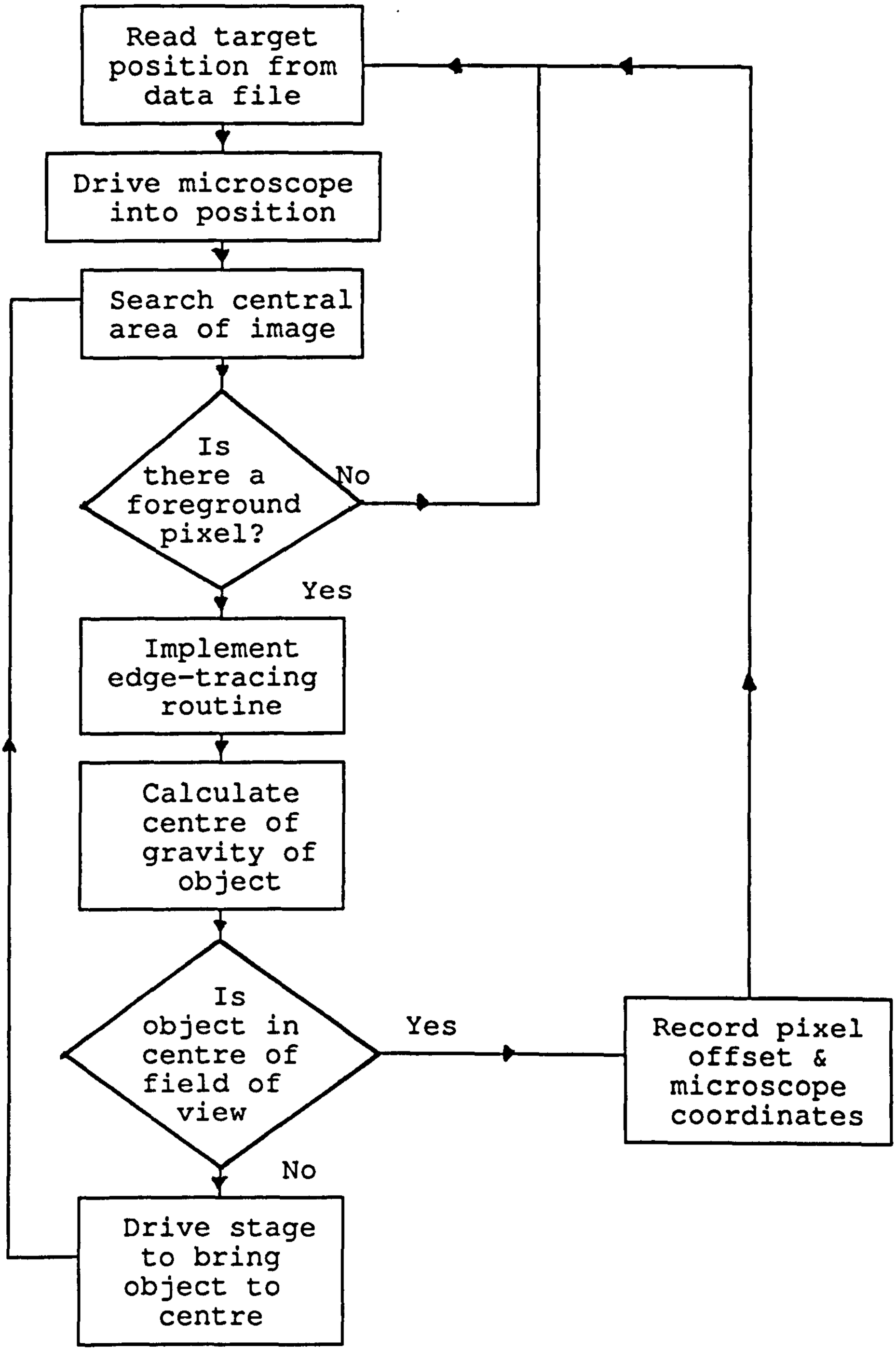

Flowchart 5: The final image processing algorithm

ordinates, it is only necessary to search a central area of 25 pixels × 25 pixels to find the target.

There are two basic approaches to recording the target position that can be adopted at this stage. Firstly, it is possible to simply record the framestore coordinates the target centre and the position of the microscope stage. This method allows the calculation of the target position, if the framestore calibration is also known. Such an approach would lead to slight inaccuracies due to distortion in the microscope lenses.

The second technique is intrinsically more accurate than the first. Here, the distance that the microscope would have to move in order to bring the target to the centre of the field of view is calculated from equations 2.5.2.

$$\Delta x = x - (x_{diff} \times x_{pixel})$$
$$\Delta y = y - (y_{diff} \times y_{pixel}) \qquad 2.5.2$$

Where x_{pixel} & y_{pixel} are the pixel dimensions at the current magnification, (x,y) are the current stage coordinates, x_{diff} & y_{diff} the pixel offset from the centre of the field of view, and Δx & Δy are the required movements.

Once the movement has been executed, the target finding algorithm is implemented once more. If the target centre still does not lie in an 8×8 pixel square at the centre of the field of view, the position refinement routine is repeated until the target is centred. When the target has been moved, so that it lies in the centre of the field of view, the coordinates of the microscope stage and any small pixel offset of the image

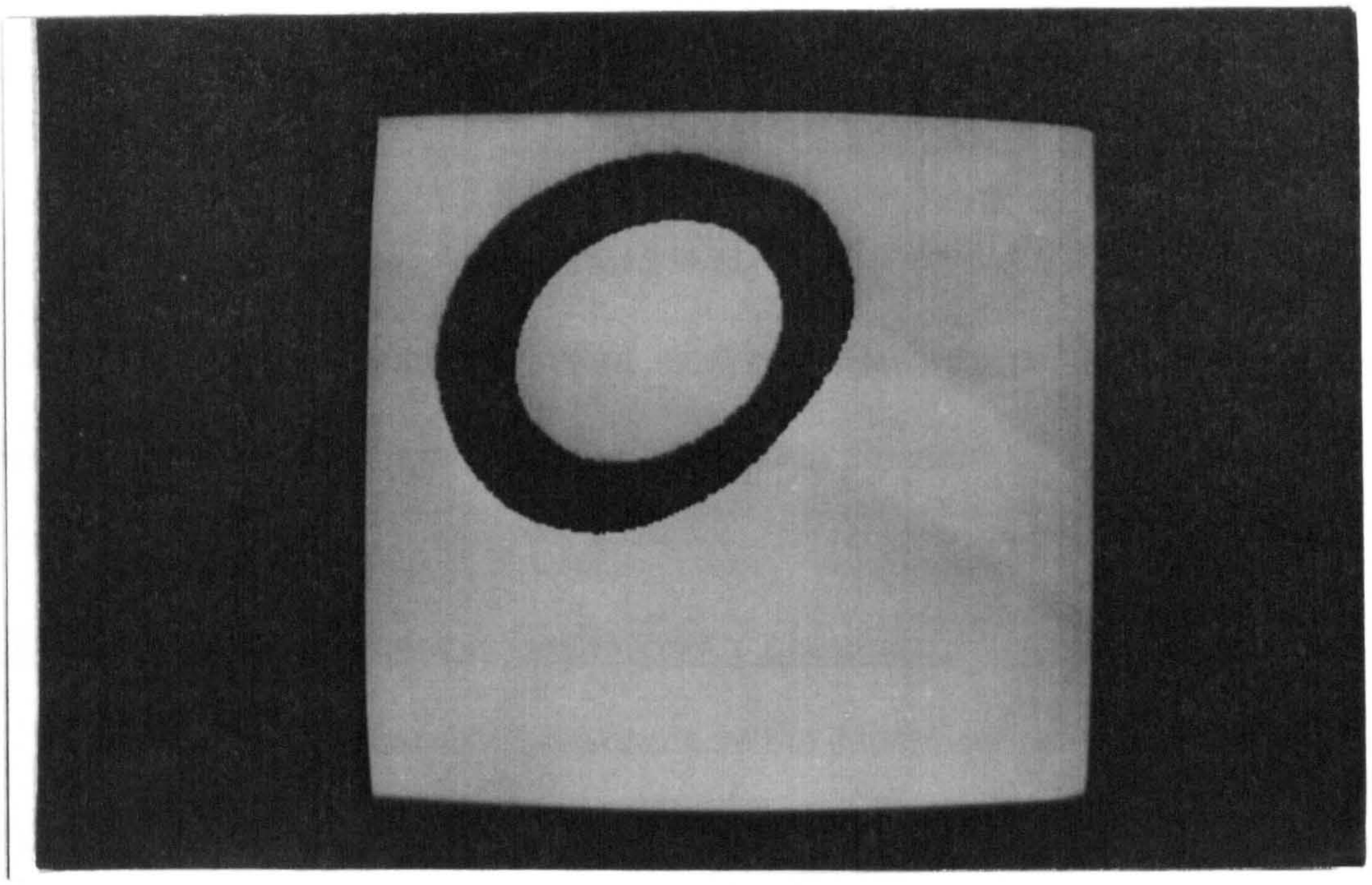

Figure 2.5.12: Target Location Before Refinement

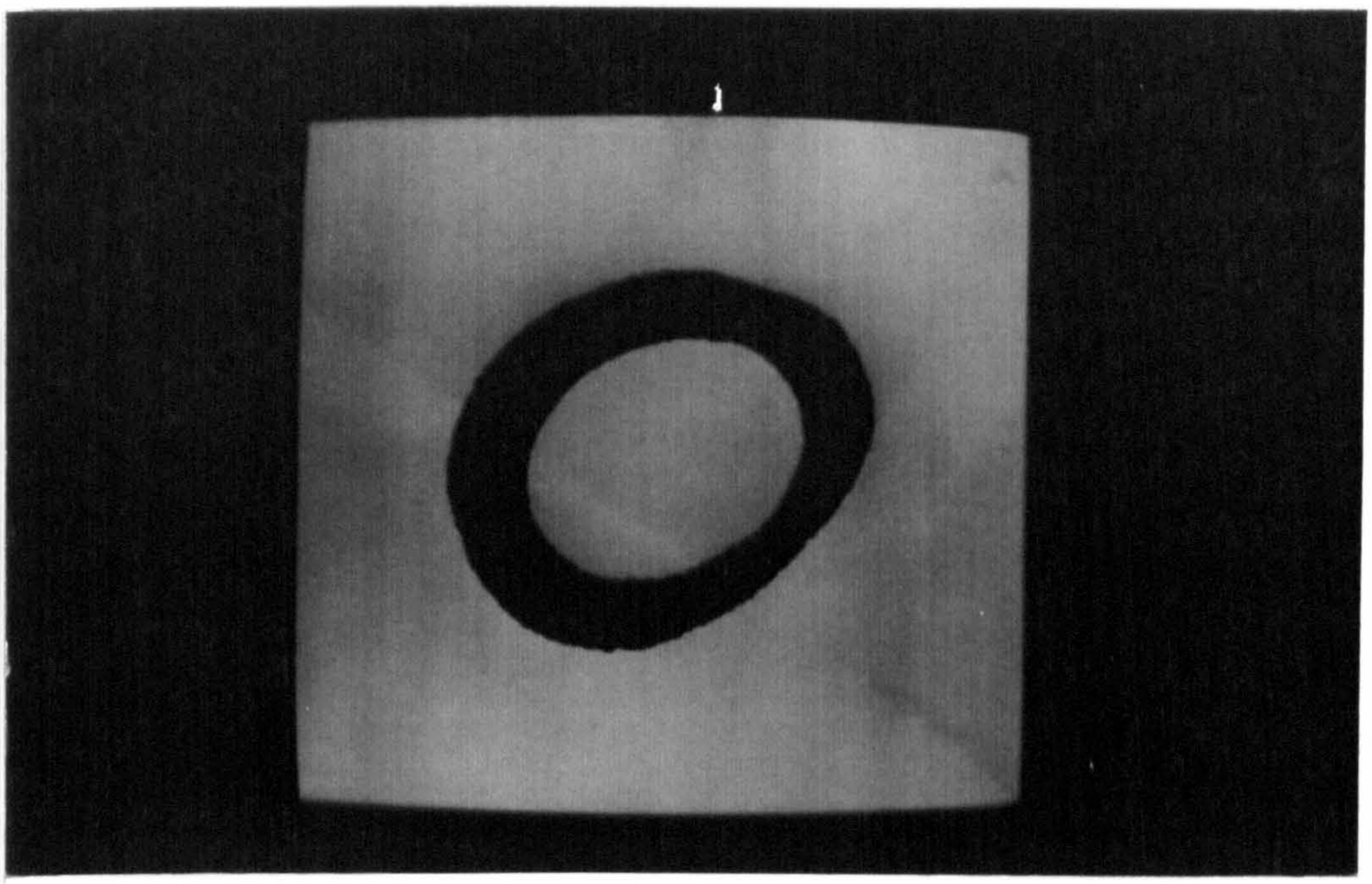

Figure 2.5.13: The Target After Being Moved To The Centre Of

The Field Of View

centre, are recorded to a disk file which has the same format to that produced by the initial scan.

The refinement process is illustrated in figures 2.5.12 and 2.5.13. In the first, a target has been brought within the field of view of the microscope. The second shows the same target having undergone the fine adjustment process.

2.5.8 Experiment To Determine Repeatability Of Location

Two separate experiments where conducted to determine the repeatability of the target finding algorithm. In the first of these tests the centroid of a target on a plate that was firmly clamped to the microscope stage was calculated 500 times. The stage was locked in position. Data was gathered over a period of approximately two hours so that any drift in both the stage position monitoring system and the CCD array would be apparent. Figures 2.5.14 and 2.5.15 show the variation in the centre of gravity of the target in the x and y directions respectively. In the case of figure 2.5.14, the x-axis there is a sharp change in first five minutes of the experiment. This is probably due to me being present in the room at the start of the test. The y-axis position seems to have been subject to a slight drift over the first forty minutes of the test, before reaching a stable value.

The maximum drift in each case is sub-pixel, 0.19 pixels in x and 0.35 pixels in y, which corresponds to a target displacement of 0.28μm in the x-direction and 0.61μm in the y-direction. These figures are below the 1μm figure that is the accuracy with

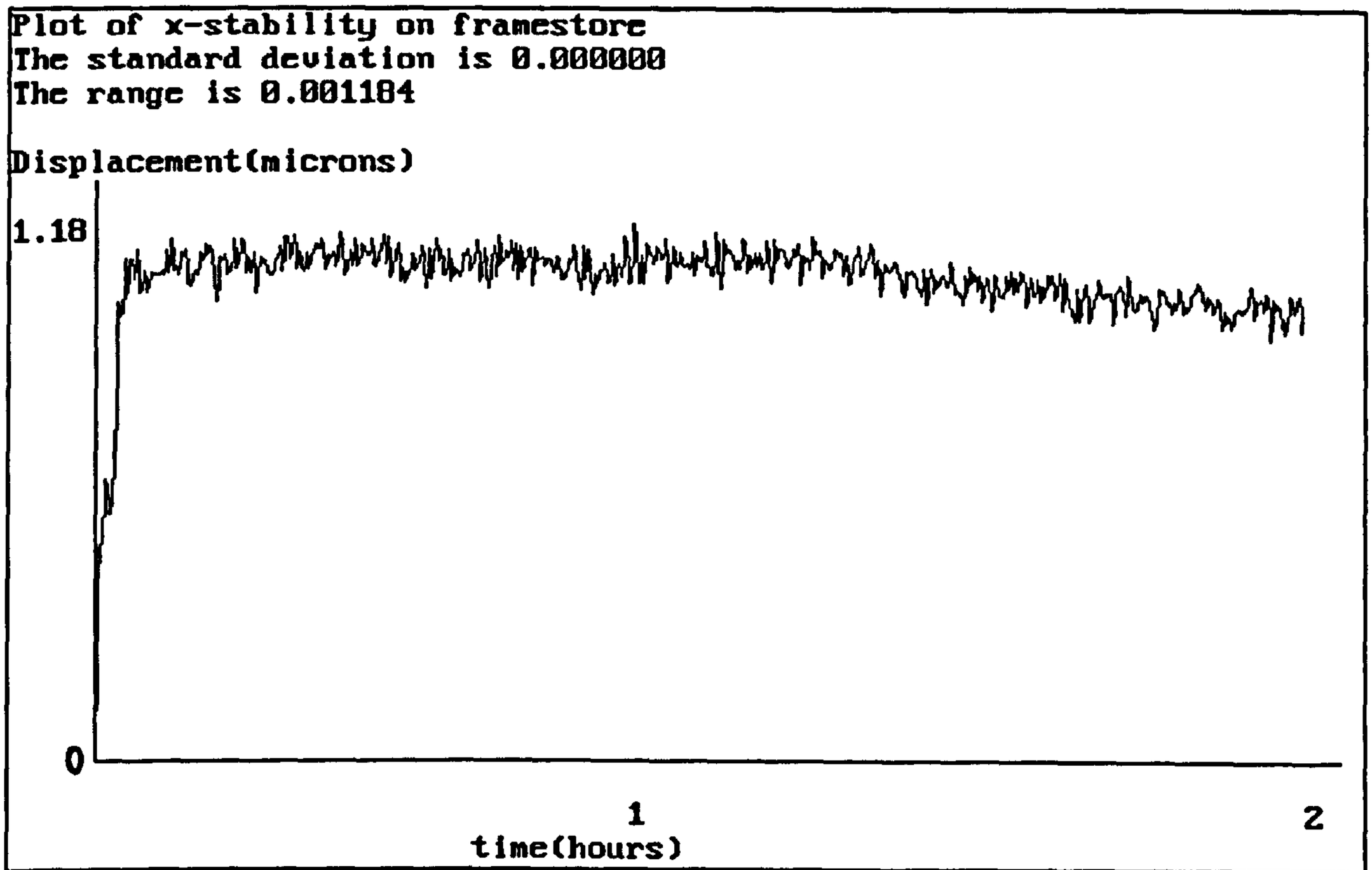

Figure 2.5.14: The Variation Of The Position Of The Target On The Framestore

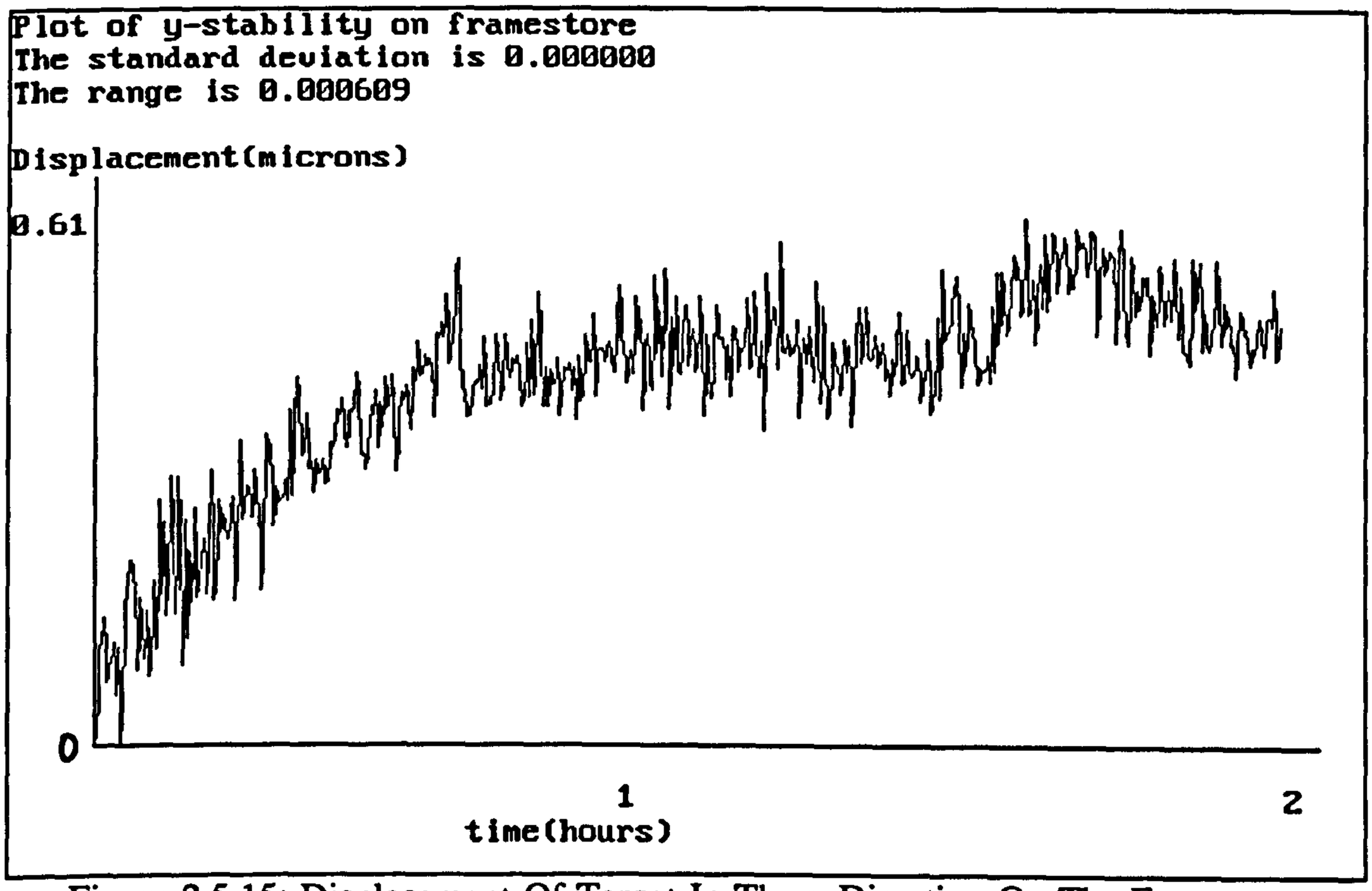

Figure 2.5.15: Displacement Of Target In The y-Direction On The Framestore

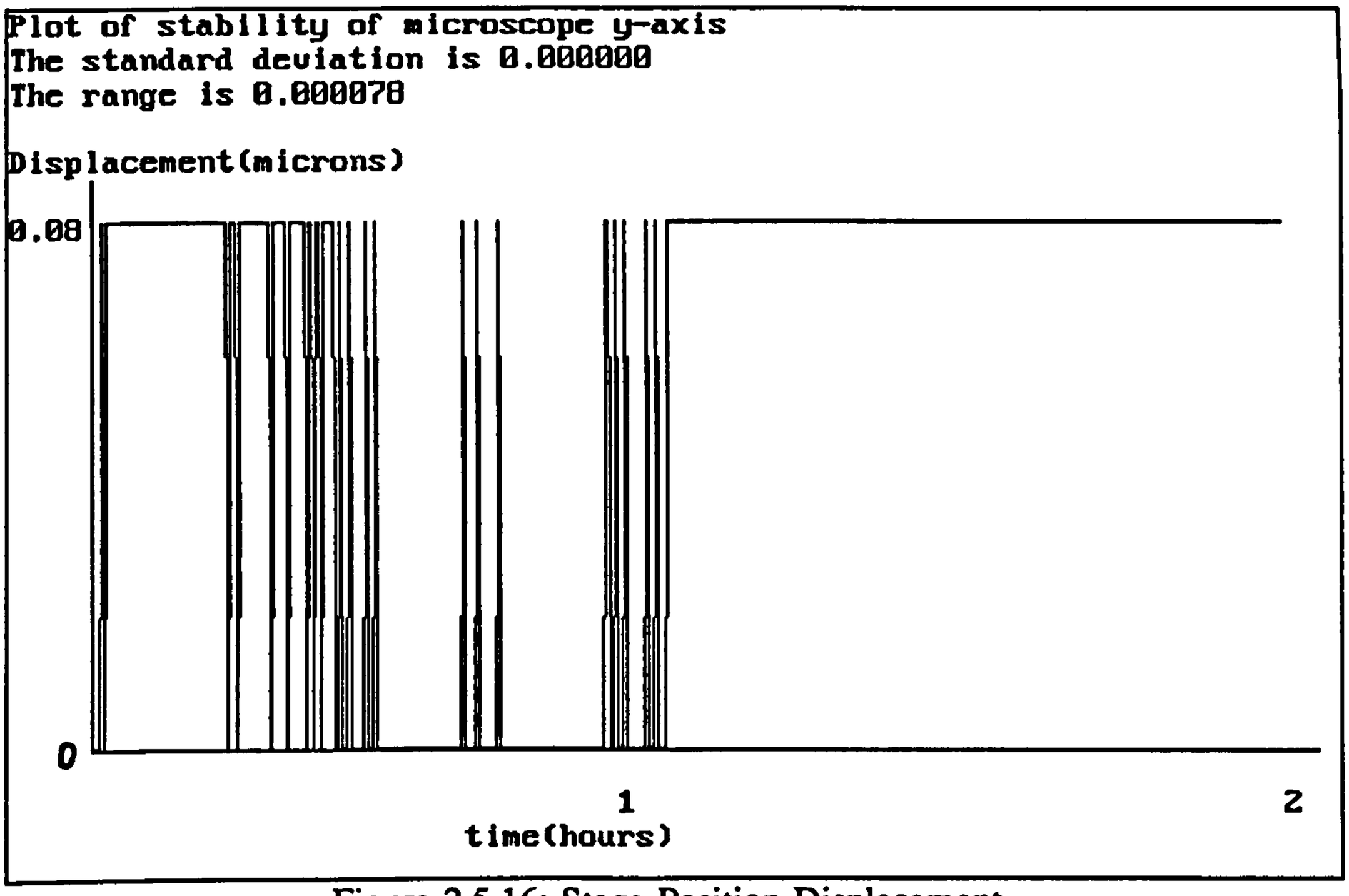

Figure 2.5.16: Stage Position Displacement

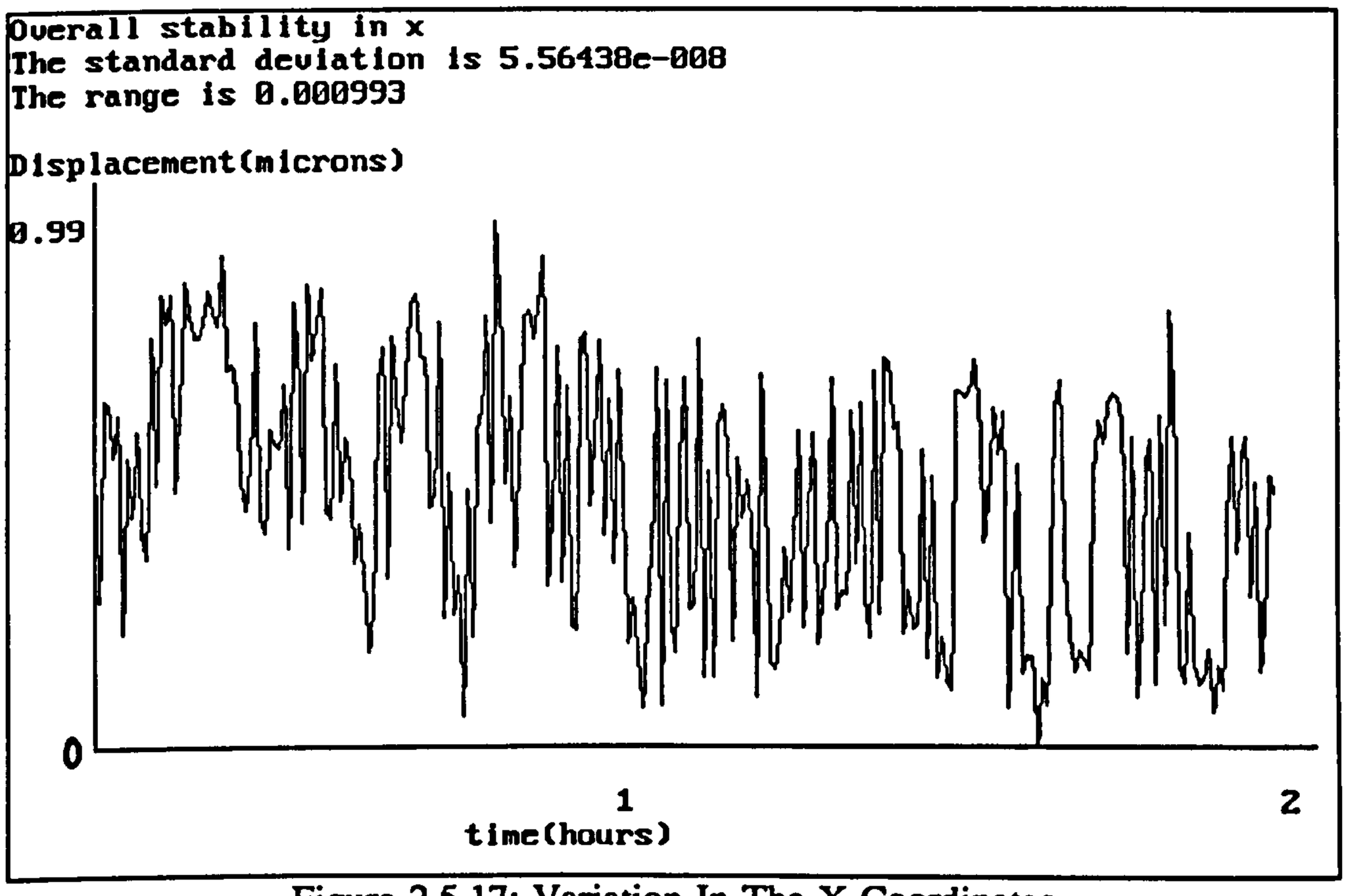

Figure 2.5.17: Variation In The X-Coordinates

which the stage can be positioned. In the best set of data obtained during the experiments using a human operator, the largest differences between readings were 1.64μm in the x-direction and 2.74μm in the y direction. In these experiments a human was asked to centre a series of six targets cyclically using the ZKM microscope. Each target was found fifteen times. Hence, there should not be any loss in the accuracy of the location of photogrammetric targets due to using the system developed here rather than a human operator.

At the same time, data was recorded to determine whether there is any drift in the actual stage position when it is firmly locked in place. The movement of the y-axis is shown in figure 2.5.16.

The only change observable from the results is a switching of the counter

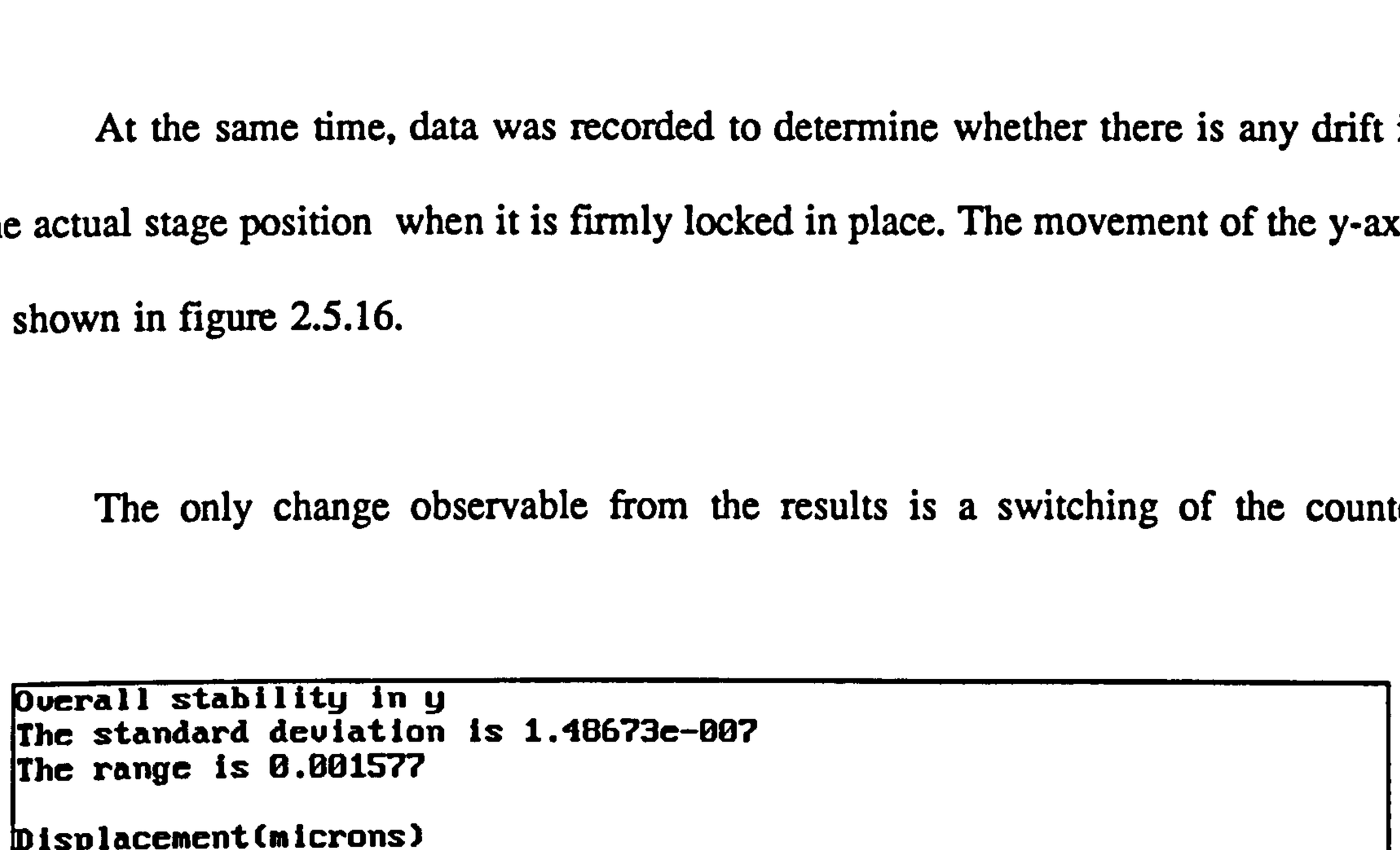

Figure 2.5.18: Variation In The Y-Coordinate

electronics between two successive counts. These manifest themselves as spikes or steps of 7.8nm which is the fundamental counting unit of the microscope counters. Therefore, any stage drift is negligible in comparison with the pixel uncertainty and is not likely to cause any problems.

The second experiment to determine repeatability tests the ability of the algorithm to re-find an object once it has been driven away from the centre of the field of view. The target is initially found using the algorithm. A random number generator is then used to select some offset co-ordinates and the stage moves to this new position. The stage then automatically returns to its initial position and the target finding routine implemented once more. The position of the target in the framestore co-ordinate system is recorded along with the position of the microscope stage. Apart from testing the image location routine, any hysteresis in the microscope movement system should also be discovered by this process.

Figure 2.5.17 shows how the x position of the target was found to vary over two hundred and fifty measurements, while figure 2.5.18 shows the same for the y-axis. The standard deviation in the readings is 0.06μm in the x-direction and 0.15μm in the y-direction. The greatest difference between any two readings is 0.99μm in the x-direction and 1.57μm in the y-direction. Experiments involving a human relocating targets give similar spreads in readings. Hence it can be claimed that the target finding algorithm developed here is able to relocate a single target as consistently as a human.

2.6.1 Target Matching

Locating the targets on each photogrammetric plate is only part of the task in developing an automated photogrammetric system. Before any meaningful use can be made of the data gathered from each plate, it is necessary to determine which object target points correspond to each target image point on all of the plates.

If a non-planar object with at least three known coordinates is imaged onto each plate, it is possible to determine the position of the cameras, as well as their orientations, in 3-dimensional space. The process of calculating the camera position is known as "space resection" and is described in appendix 1.

An image at a particular position on a plate corresponds to a straight line through space which starts at the image, passes through the perspective centre of the camera and goes on to infinity. Once the camera locations are known, it is possible to calculate the projection of this line through the perspective centre of a second camera. The projection of the line produced in this manner is imaged by the second camera as a line across the photographic plate. This line is known as the epi-polar line, and may be calculated if the perspective centres of both cameras are known. Figure 2.6.1 shows the construction of the epi-polar line.

For camera p the interior coordinates are represented by $\underline{y}^{(p)}$ and the exterior coordinates by $\underline{X}$. The origin of the interior coordinate system for camera p, $\underline{y}_0^{(p)}$, is coincident with the perspective centre of that camera, $\underline{X}_0^{(p)}$.

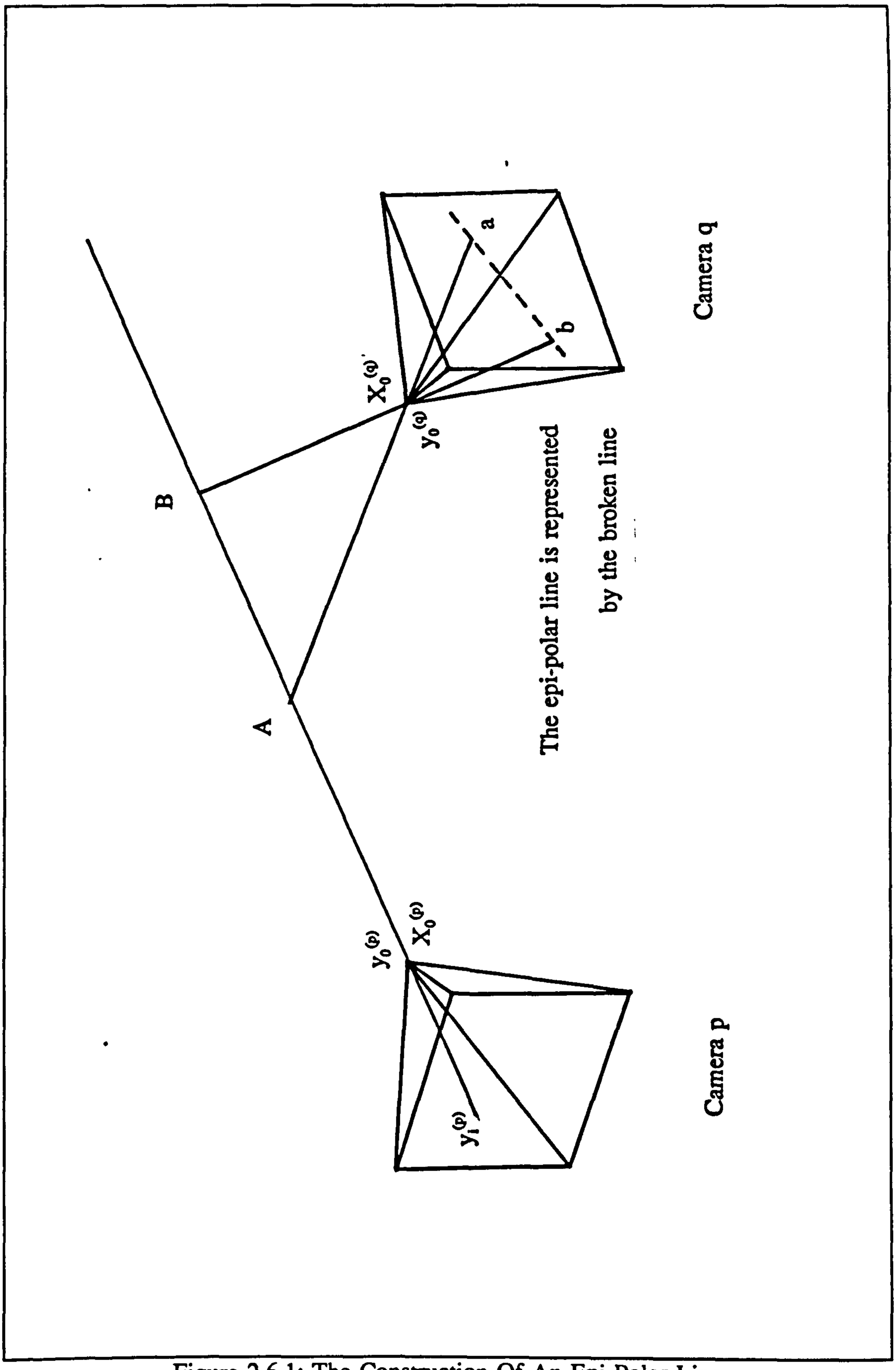

Figure 2.6.1: The Construction Of An Epi-Polar Line

A point on an object having coordinates $\underline{X}_i$ in the exterior coordinate system will be imaged through the perspective centre of camera p to the position $\underline{y}_i^{(p)}$ on the photographic plate. These coordinates are linked by the following equation:-

$$\frac{\underline{X}_i-\underline{X}_0^{(p)}}{|\underline{X}_i-\underline{X}_0^{(p)}|}=R^{(p)}\frac{(\underline{y}_0^{(p)}-\underline{y}_i^{(p)})}{|\underline{y}_0^{(p)}-\underline{y}_i^{(p)}|} \qquad 2.6.1$$

Where $\mathbf{R}^{(p)}$ is the rotation matrix for camera p.

If the distance from the perspective centre of camera p to a point i on the object is t then:-

$$\underline{X}_0^{(p)}-\underline{X}_i=-t\frac{(\underline{X}_i-\underline{X}_0^{(p)})}{|\underline{X}_i-\underline{X}_0^{(p)}|} \qquad 2.6.2$$

Hence,

$$\underline{X}_i=\underline{X}_0^{(p)}+t\frac{(\underline{X}_i-\underline{X}_0^{(p)})}{|\underline{X}_i-\underline{X}_0^{(p)}|} \qquad 2.6.3$$

From equation 2.6.1 this becomes:-

$$\underline{X}_i=\underline{X}^{(p)}+tR^{(p)}\frac{(\underline{y}_0^{(p)}-\underline{y}_i^{(p)})}{|\underline{y}_0^{(p)}-\underline{y}_i^{(p)}|} \qquad 2.6.4$$

Now consider that the object is known to lie at a distance somewhere between $t^{(p)}_{min}$ and $t^{(p)}_{max}$ from camera p. The three dimensional coordinates of points at these

distances from the camera corresponding to a plate image position $\underline{y}^{(p)}_i$ are given by:-

$$\underline{X}_{min}=\underline{X}_0^{(p)}+t_{min}^{(p)}R^{(p)}\frac{(\underline{y}_0^{(p)}-\underline{y}_i^{(p)})}{|\underline{y}_0^{(p)}-\underline{y}_i^{(p)}|}$$

$$\underline{X}_{max}=\underline{X}_0^{(p)}+t_{max}^{(p)}R^{(p)}\frac{(\underline{y}_0^{(p)}-\underline{y}_i^{(p)})}{|\underline{y}_0^{(p)}-\underline{y}_i^{(p)}|} \qquad 2.6.5$$

The positions of the images of these points in the plane of the plate of a second camera, q, may now be calculated, and hence the epi-polar line computed.

Let the coordinates with respect to the second camera be denoted by a superscript q. The distances from camera q of the maximum and minimum points in object space are given by:-

$$t_{min}^{q}=|\underline{X}_{min}-\underline{X}_0^{q}|$$

$$t_{max}^{q}=|\underline{X}_{max}-\underline{X}_0^{q}| \qquad 2.6.6$$

Equation 2.6.5 may now be written in terms of the closest possible object point to calculate the position of that image of the closest point on plate q.

$$\frac{(\underline{y}_{min}^{q}-\underline{y}_0^{q})}{|\underline{y}_{min}^{q}-\underline{y}_0^{q}|}=\tilde{R}^{(q)}\frac{(\underline{X}_0^{q}-\underline{X}_{min})}{t_{min}^{(q)}} \qquad 2.6.7$$

Where $\tilde{R}^{(q)}$ is the transpose of the rotation matrix for camera q.

For a given point, the denominator of the left hand side of the equation divided

by $t^{(q)}_{min}$ may be expressed as a constant, C, so 2.6.7 may be rewritten as:-

$$(\underline{y}^q_{min}-\underline{y}^q_0)=\tilde{R}^{(q)}(\underline{X}^q_0-\underline{X}_{min})C \qquad 2.6.8$$

$$where\ C=\frac{|\underline{y}^q_{min}-\underline{y}^q_0|}{t^{(q)}_{min}}$$

$\underline{y}_{min}^{(q)}$ must lie in the plane of the photographic plate in camera q, so the value of the third element of $\underline{y}_{min}^{(q)}-\underline{y}_0^{(q)}$ must be equal to -f, where f is the focal length of the camera. Hence the magnitude of C may be calculated by dividing -f by the third component of $(\underline{y}_{min}^{(q)}-\underline{y}_0^{(q)})$, so allowing the calculation of the other two components of $(\underline{y}_{min}^{(q)}-\underline{y}_0)$.

The calculation of $\underline{y}^q_{max}$, corresponding to the position of the most distant point, may be calculated in a similar manner using t^q_{max} rather than t^q_{min}.

The epi-polar line for point i on camera q, $\underline{r}^q_i$, is the line joining $\underline{y}^q_{min}$ and $\underline{y}^q_{max}$, and so may be calculated from:-

$$\underline{r}^q_i=\underline{y}^q_{max}-\underline{y}^q_{min} \qquad 2.6.9$$

Point i on plate p will produce an image on plate q that lies on this line. Hence, points that are found on plate q may be tested to determine whether they could correspond to point i found on plate p.

If information about the approximate distance of the object from the camera is

available, then it is possible to predict which portion of the epi-polar line contains the second image. In figure 2.6.1, for example, the object is known to lie between points A and B. If this information was not known, the epi-polar line would pass right across the plate. However, with knowledge about points A and B, the location of the plate image must lie between points a and b.

Two camera views are sufficient to produce three dimensional information about the object, but there is the risk that not all of the object points will be imaged by each camera. To counter this problem, as well as reducing the measurement uncertainty, additional cameras are often used. The use of more than two cameras also allows for the resolution of ambiguities.

It is possible that more than one image point lies on an epi-polar search line. The decision as to which point matches the original one can possibly be made with only two views, since it is likely that the incorrect image will lie on an epi-polar line corresponding to a further image point. However, if the incorrect image was not seen by the first camera then a third plate is needed to resolve the problem. Once the position of an object has been calculated from the first two photographs it is possible to predict exactly where its image should lie on further plates. Hence, by testing whether the third plate contains an image at the position predicted by each of the points located on the epi-polar line, it is possible to determine which is the correct image.

2.6.2 Application Of The Algorithm

It is much faster to search a series of epi-polar lines that may be calculated after fully measuring one plate, so it may be considered that it is only necessary to interrogate one plate completely. However, such an algorithm would be unsatisfactory since only the points found on the first plate could be found on the second. Therefore, any parts of the object not in the field of view of the first camera would be missed. In order to ensure that no points are missed it is advisable to fully search all additional plates.

The most important sets of data that must be read from each plate are the coordinates of the known object, the ground points. These points, along with the fiducial marks, are located on each plate by an operator before the automatic plate scan starts.

Having fully investigated each plate it is possible to match each point on one plate with all corresponding points which have been recorded on other plates.

A data file is created for each plate that has been measured. The data-files may then be compared cyclically using the epi-polar algorithm to match the points. If no matching point is found, successive data-files are investigated in an epi-polar manner until one is found. Once a matching image has been found, the anticipated position of that point is predicted for further data-files, so simplifying their interrogation. Not all of the points on each plate will be matched between every pair of plates, but, unless the survey has been badly designed, each point should appear on a minimum of two plates.

2.7 Limitations Of The Software

The system limitations can be divided into two categories, those of the image processing software and those of the target matching program.

2.7.1 Image Processing software

The main problems that can arise in the use of the image processing software are due to the greyscale image of an individual frame not being binary sliced correctly. If the threshold is set too high some of the information contained in the image is lost (in an extreme case a target may be missed completely). In the case of the threshold being set too low the image will becoime noisey as more pixels are given the same value as the target pixels. However, as discussed in section 2.5.3, there is a wide range of thresholds that may be selected to successfully binary slice the image. Only a change in the imaging properties of the microscope or CCD camera, or a substantial change in the illumination of the plate would cause this problem to occur.

The simplicity of the centre of gravity routine can lead to errors in finding the centre of a target if part of the target is not imaged. In the case of a 100μm diameter circular target, half of which is missing, the centre of gravity will be shifted by approximately 17μm. This represents an error that would cause the target to not be matched by the target matching program. This would cause the lose of information about the object. However, if the point is seen by two other plates it is still possible to calculate its three dimensional position.

Other potential problems are caused if the operator makes mistakes in locating

the fiducial marks or identifying the area of the plate to be searched. If the fiducial marks are not correctly found it would prove extremely difficult to reference the image coordinate system to that of the camera. Incorrectly identifying the area to be searched could lead to some points not being found be the search.

2.7.2 Target Matching Program

One fundamental limitation of the system developed here is its reliance on knowing the three dimensional coordinates of at least four ground points. This requirement could be easily modified to three points. Without this information it would fail to calculate the camera positions, and hence would not be able to match the points found on the plates. Similarly, if an error has been made in calculating the ground points, the camera positions will be incorrectly computed and once more it would not be able to match corresponding target images. Hence there is a great reliance on the technique used to determine the three dimensional coordinates, usually a theodolite survey. However, as long as the theodolite survey is conducted competently, as would be expected from the people carrying out such operations, there should not be any problem with this part of the system. The precision of a good theodolite survey is in the range 1 part in 10^4 to 1 part in 10^5 depending on the conditions.

Another potential problem may arise in calculating the camera position, but once more this is easily overcome by taking care in setting up the experiment. If the ground points are collinear it is not possible to calculate the the camera position. The uncertainty in the camera position decreases as the points move away from a condition of collinearity. In the method of calculating the camera position adopted here the three

points out of the four specified ground points that are the furthest away from collinearity are used. Therefore, it would be possible to alter the algorithm to require only three ground points. A measure of the collinearity of the points is to project their positions into the image plane of the camera. The three points which form the triangle of largest area in that plane are the furthest from collinearity (Hunt 1983,1984). The image positions of the points on the plate corresponding to the ground points are known from the plate measurement process, so it is trivial to calculate which combination of ground points produces the triangle of largest area in that plane. These are then used in the calculation of the camera position.

3. VERIFICATION OF THE TARGET FINDING ALGORITHM

Figure 3.1.1 shows a rowing boat that was selected as the first object to be surveyed using the automated target location program. Shortly after the survey was conducted the NPL Photogrammetry section used the boat to compete in a 22 mile river race from Richmond-upon-Thames to Greenwich. Out of 118 entrants, 'Ewanderput', as the boat is called, finished second

3.1.1 Object Preparation

One hundred retro-reflecting targets, of a concentric circle design, were fixed to one side of the upturned boat. The diameter of the outer ring was 5mm. At a range of 2 metres these targets produce images on the plate with a diameter of 125μm, slightly larger than usual. A more typical image size is approximately 80μm.

As well as the targets on the boat, two additional targets were placed on posts behind the boat to act as ground points for the camera location algorithm. Four further ground points were placed on the boat with numbers to identify them. Figure 3.1.1 is a picture of the boat and ground points.

3.1.2 Theodolite Survey Of Ground Points

Two Wild T2000S theodolites were used to conduct a survey of the 6 ground points to allow for the locations of the cameras to be calculated. So that scale could be attributed to the subsequent survey, a standard 1 metre length bar was also placed in the field of view, and its two ends found using the theodolites. The three dimensional co-

ordinates of the ground points were calculated on-line using an in house package ofprograms on a Toshiba T1200 portable computer (Morley 1990). A co-ordinate framework is also established by the program. As shown in figure 3.1.2 the x-axis is defined to be along the line from theodolite 1 to theodolite 2, the z-axis is vertical, and the y-axis is defined so that the co-ordinate system is right-handed. For simplicity, this co-ordinate set was adopted by the automated photogrammetric survey. In this survey the x-axis is approximately in line with the keel of the boat.

3.1.3 The Photography

To allow for a full coverage of one side of the boat it was decided that four photographs would be taken. A single UMK10N camera was moved around between the chosen camera stations. The first two photographs were taken from approximately the same positions as had been used for the theodolites. The two other camera positions were at each end of the boat, as is illustrated by figure 3.1.3.

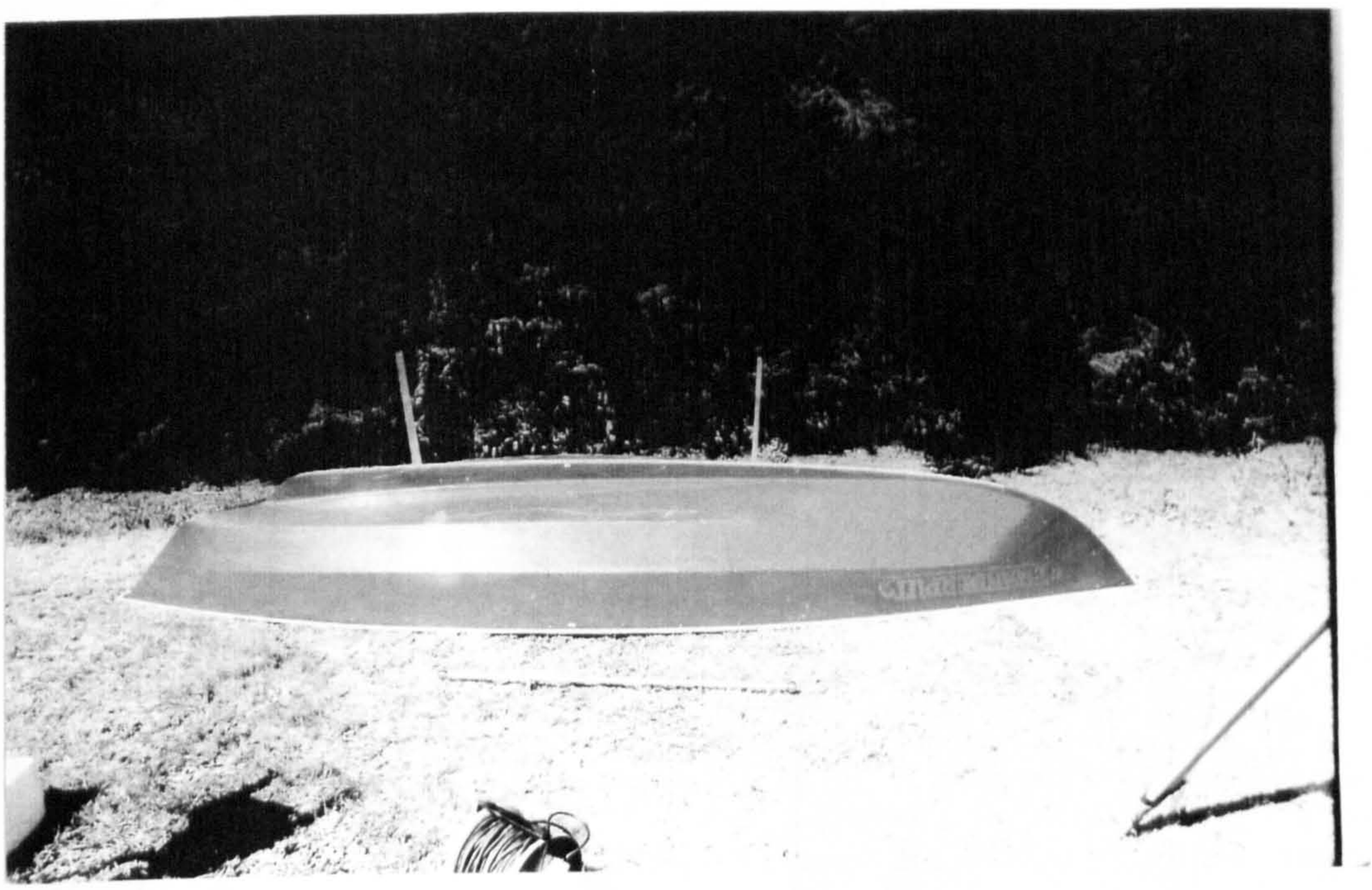

Figure 3.1.1:The Boat And Ground Point Posts

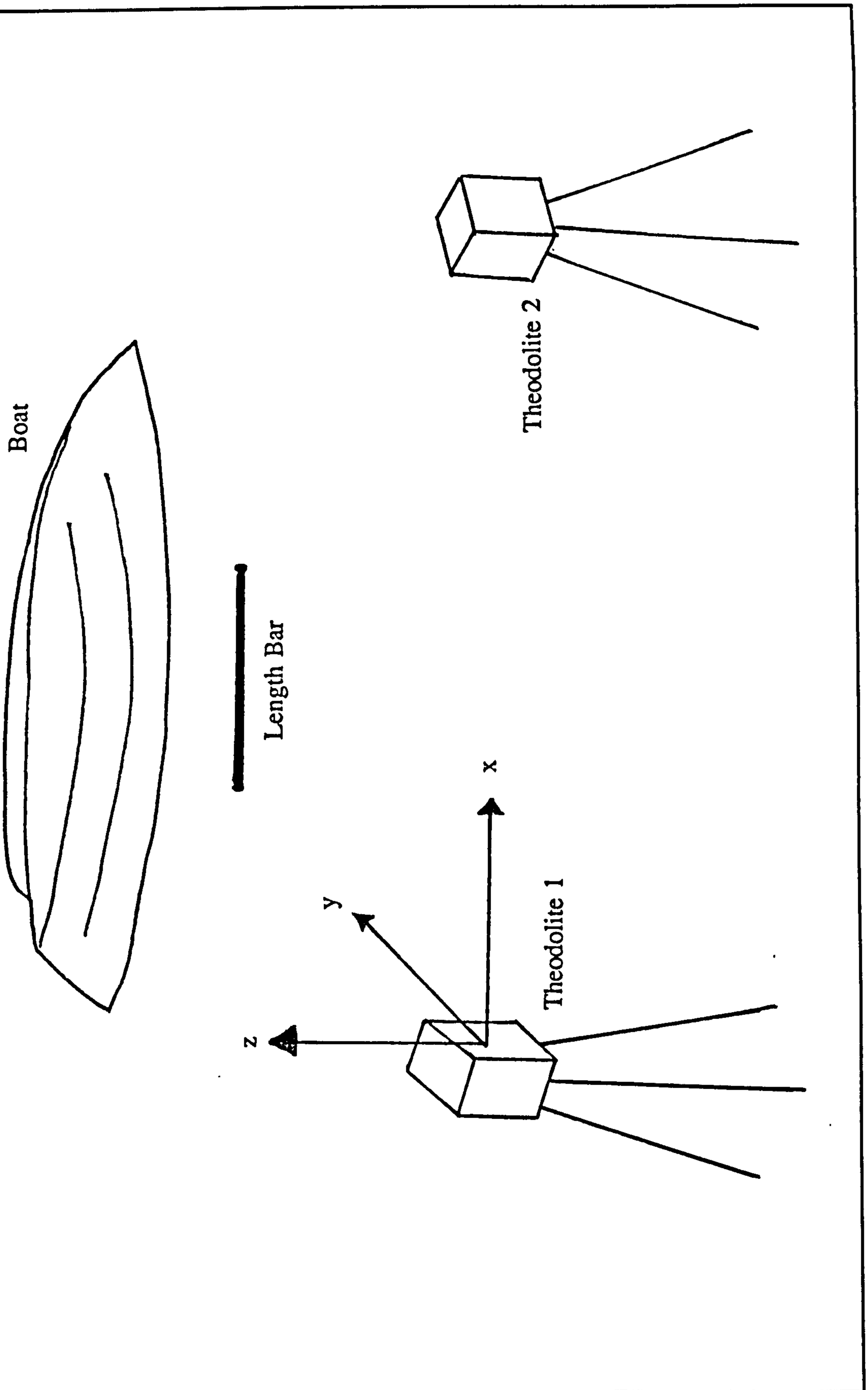

Figure 3.1.2:The Coordinate System

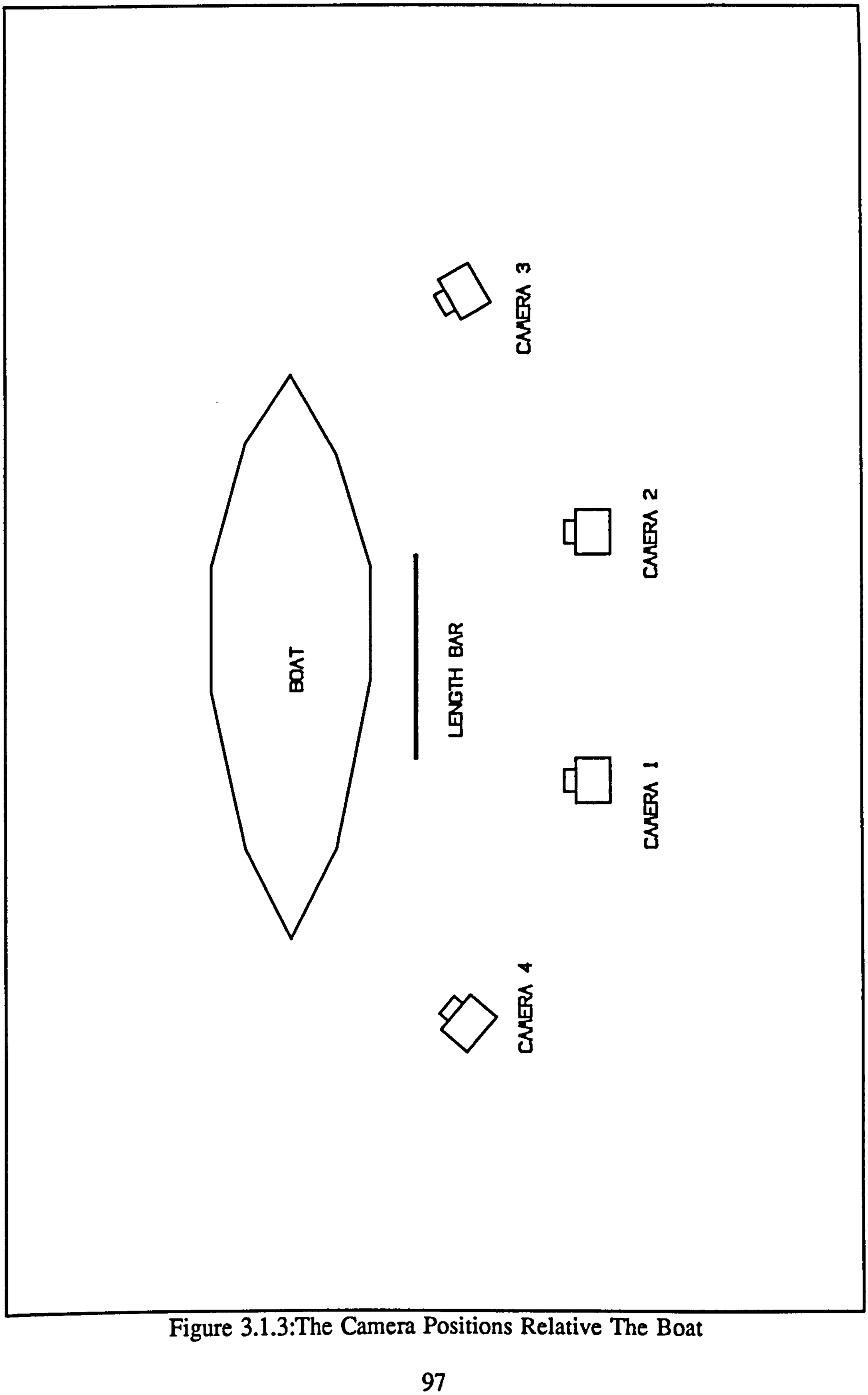

Figure 3.1.3:The Camera Positions Relative The Boat

3.1.4 Plate Measurement

Once the plates had been developed, they were interrogated on the Zeiss ZKM measuring microscope using the automated target location algorithm. Initially, the whole of the first plate was raster scanned in the search for targets. This procedure took approximately 5½ hours to complete. In this first full test of the algorithm virtually every single mark on the emulsion was found during the raster scan, which meant that the high resolution target location process was slowed since it had to attempt to find the centres of many items of debris. In this case the final target location took approximately 8 hours to complete, and located a total number of 531 objects. Owing to the excessive number of targets found a new regime was adopted for the measurement of the remaining three plates.

The initial raster scanning routine was amended to allow an operator to select the region of the plate to be scanned. Obviously, the smaller the area that is selected, the faster the raster scan. Another modification was to ask the operator the minimum size of object that could possibly be a target on the plate under investigation. This second improvement reduces the amount of debris found, since any object that is obviously too small to be a target is not recorded for the final location algorithm to work on. The total time taken to measure each of the remaining three plates was reduced to 8½ hours. In that time, an operator was required for about 5 minutes before the raster scan to select the target size, the area of interest, find the fiducial marks, and calibrate the field of view. A further five minutes of operator time was required before starting the final location routine to allow for re-calibration of the field of view and remeasuring the fiducial marks.

Measurement of each of the plates produced a large number of debris co-ordinates, even with the modifications outlined above. In theory, the location of these spurious points is unimportant since the target matching algorithm should eliminate many of the surplus points. However, a further modification was made to the target finding system to eliminate totally the debris from the plate. An additional option was made available to the operator initialising the final high resolution routine. He is now asked whether he wishes to monitor visually the objects being found by the algorithm and decide whether to reject any debris. Plate 1 was re-examined using this new option, so that the target matching algorithm would have at least one plate free from noise. Figure 3.1.4(a) shows the points that were found by the fully automated scan, while figure 3.1.4(b) shows the points found when the scan was monitored manually.

3.1.5 The Results Obtained

Following the measurement of the plates, there are several procedures that have to be executed before the final survey results are obtained. Each of these procedures eliminates some of the measured co-ordinates corresponding to debris. Figure 3.1.5 shows the raw scan data from plate 2. From this plate it is apparent that much debris was found by the automated process.

Figure 3.1.6 shows how the number of targets diminish following the use of the target matching algorithm. On plates 2 and 4, the spurious points began to vanish and the shape of the boat starts to become apparent. Unfortunately, it proved difficult to use the target matching program effectively with plate 3. The reason for this problem is that the fiducial marks on the plate were badly over-exposed, due to a problem with the

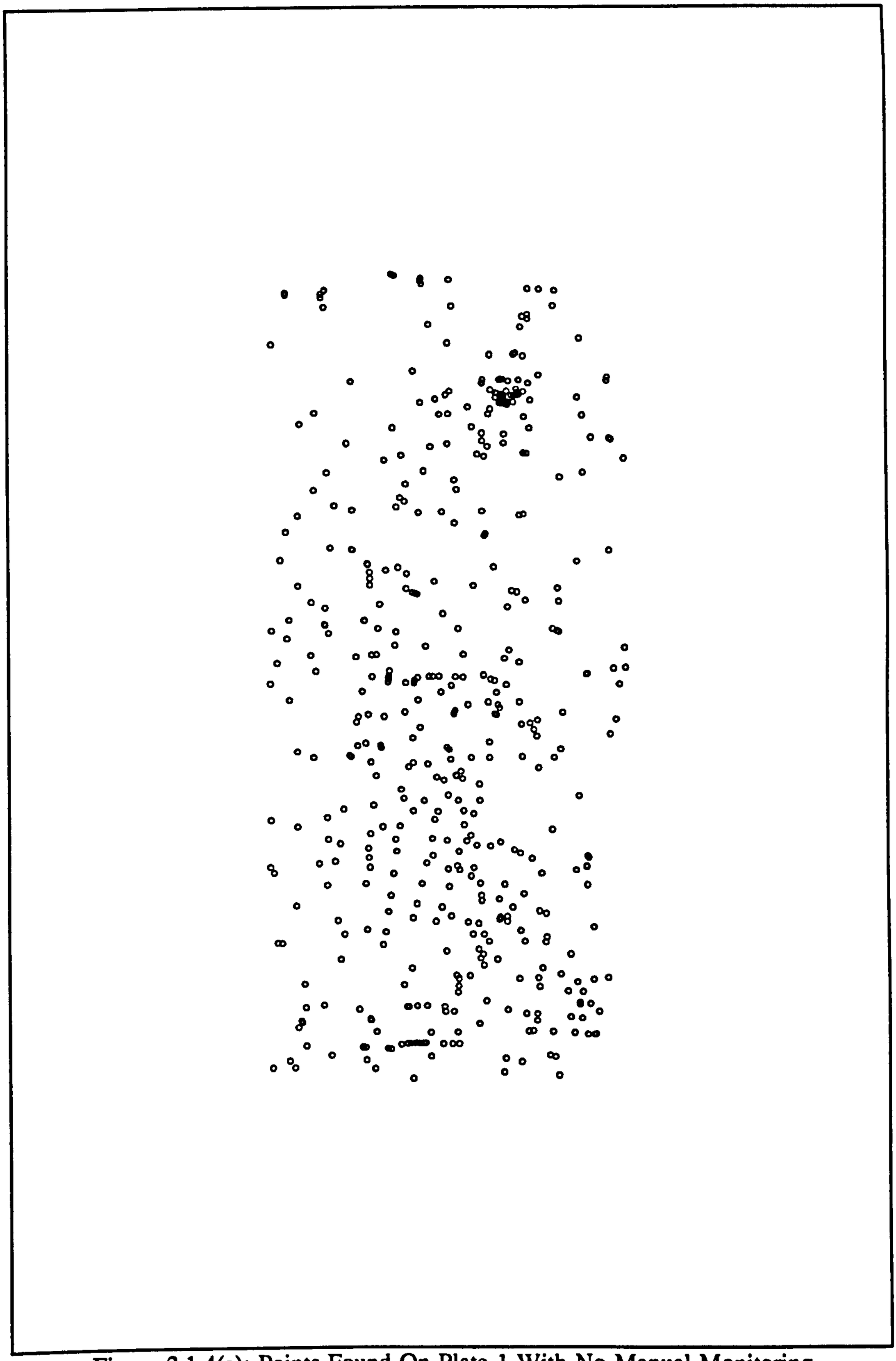

Figure 3.1.4(a): Points Found On Plate 1 With No Manual Monitoring

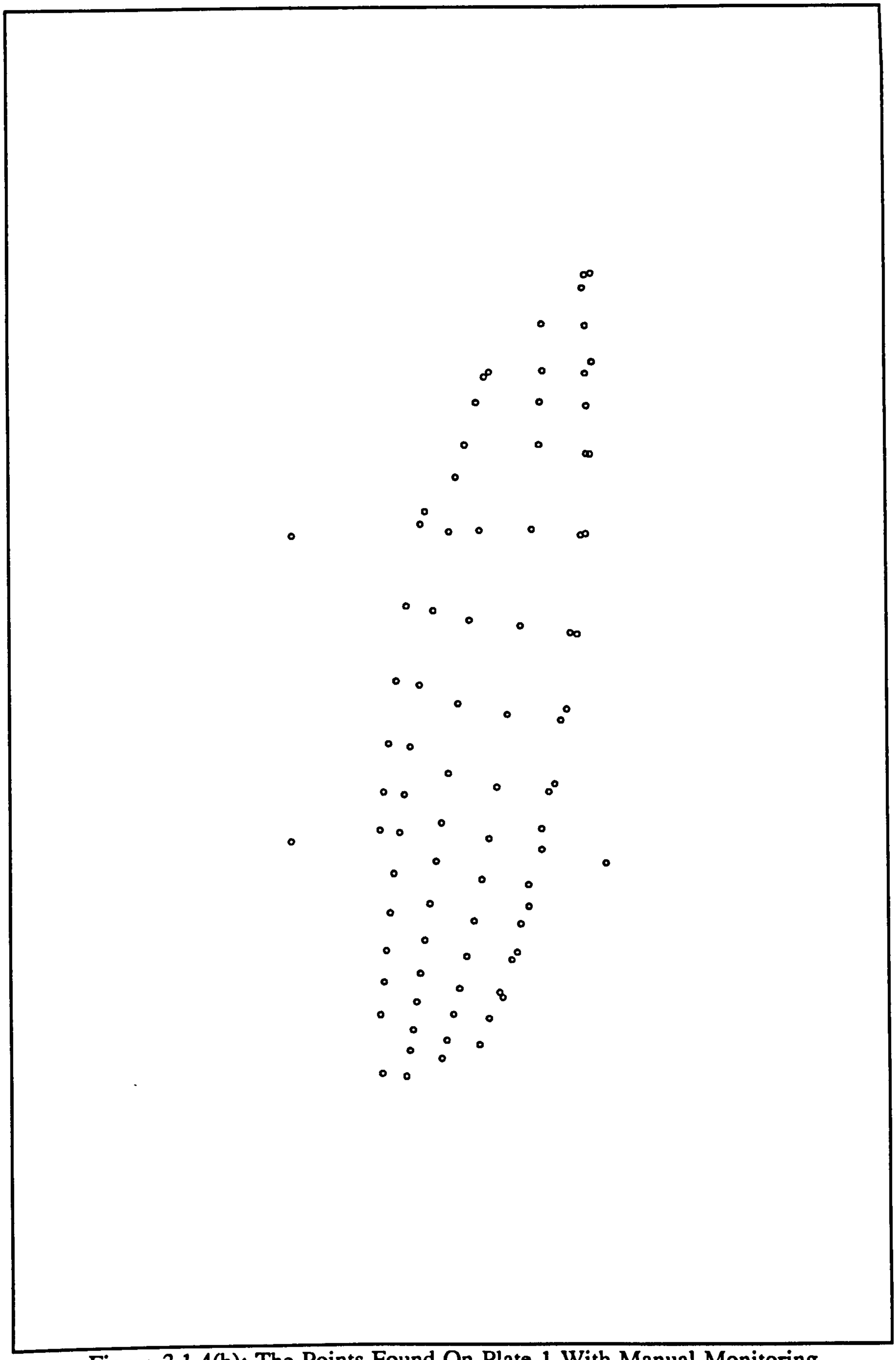

Figure 3.1.4(b): The Points Found On Plate 1 With Manual Monitoring

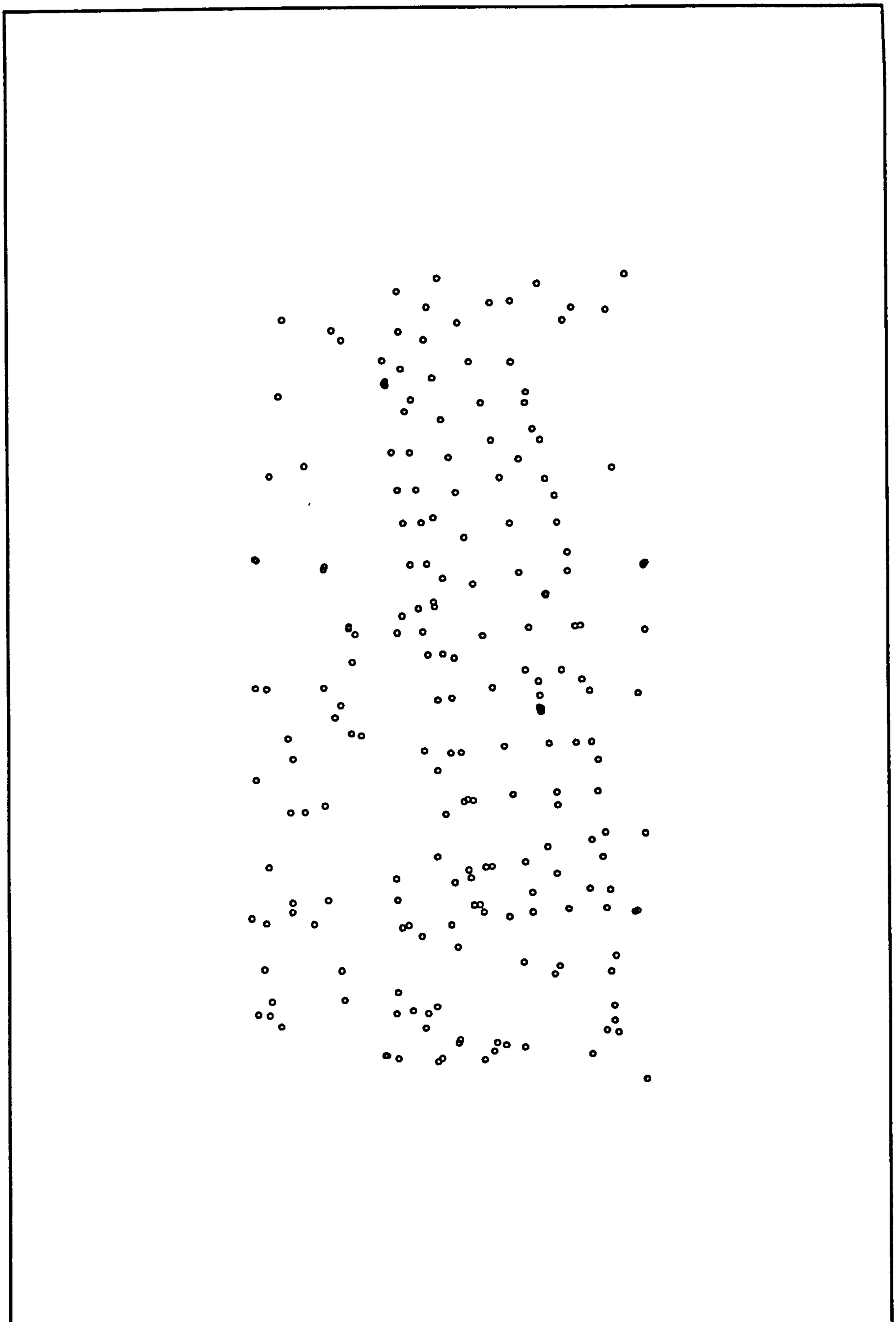

Figure 3.1.5: Raw Data From Plate 2

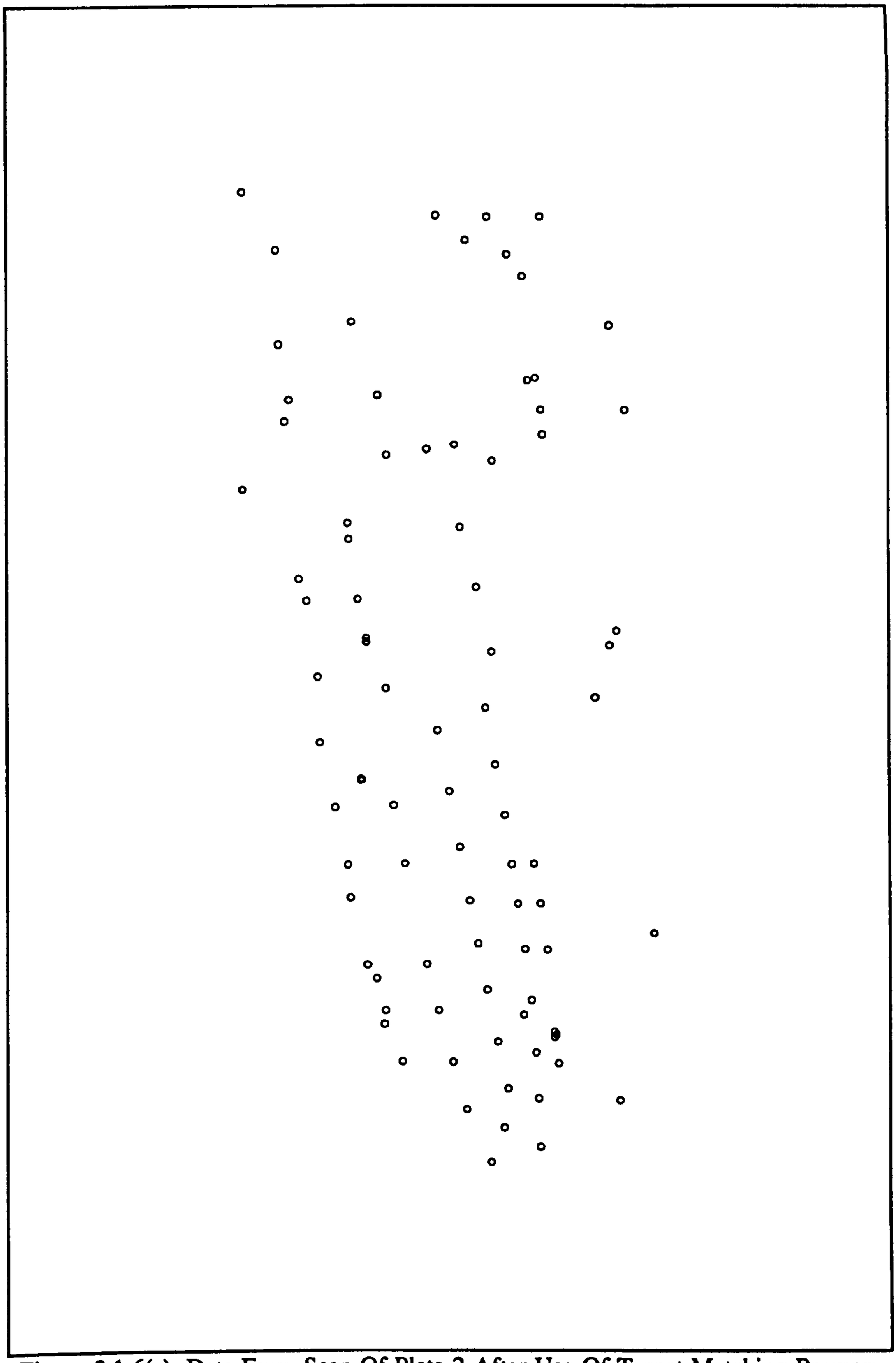

Figure 3.1.6(a): Data From Scan Of Plate 2 After Use Of Target Matching Program

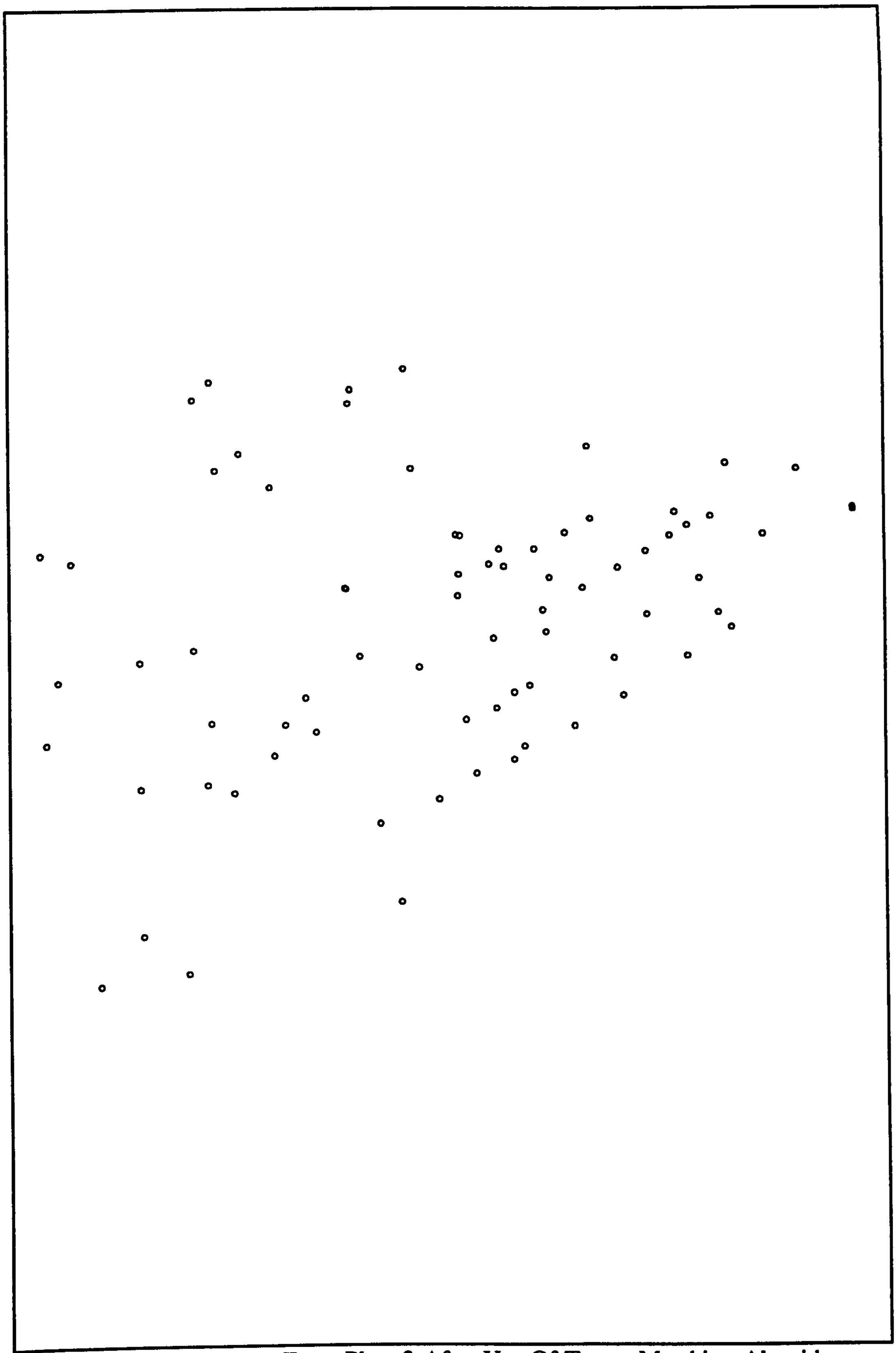

Figure 3.1.6(b): Data From Plate 3 After Use Of Target Matching Algorithm

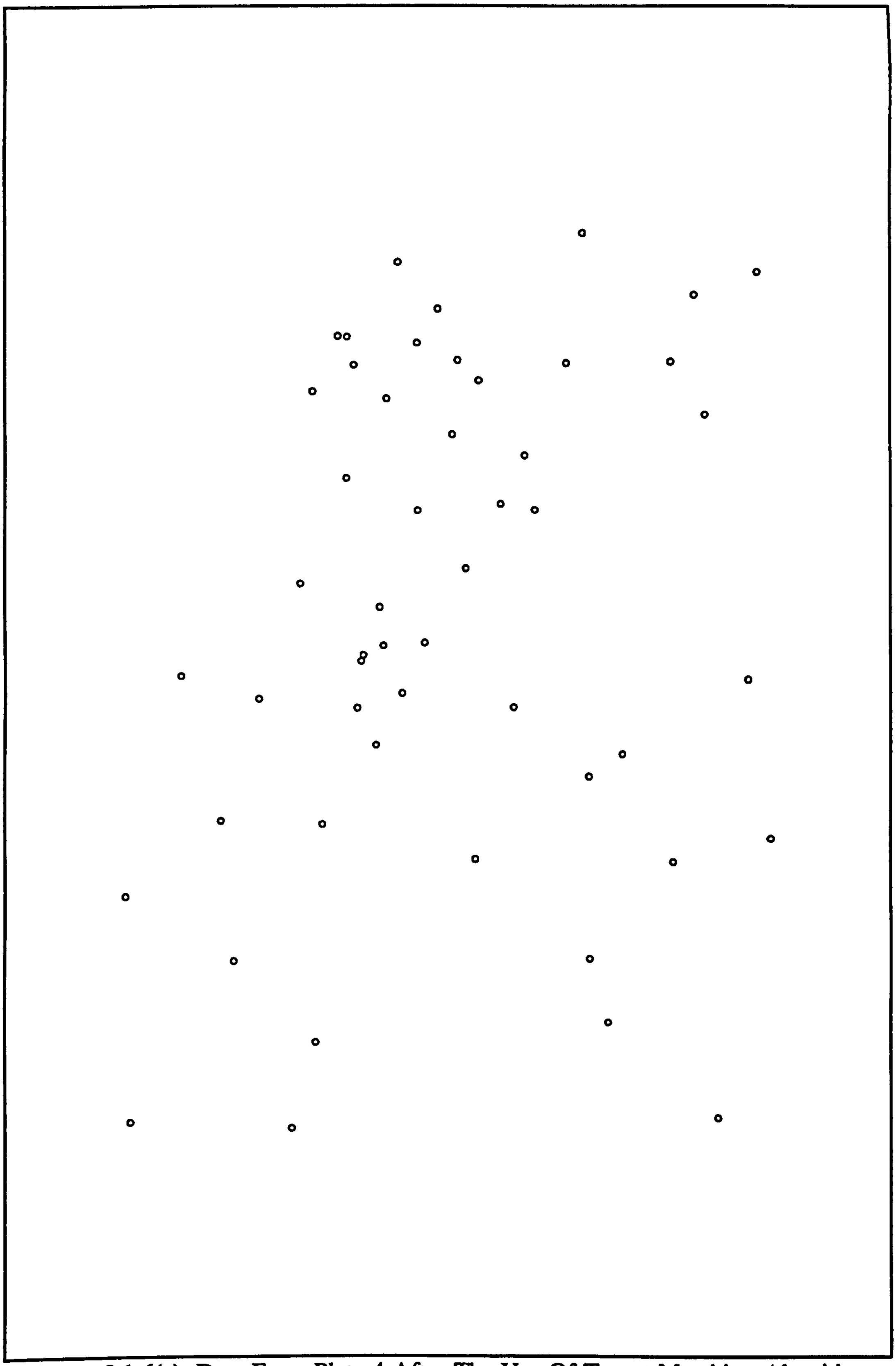

Figure 3.1.6(c): Data From Plate 4 After The Use Of Target Matching Algorithm

camera control box, so making it impossible to locate the principal point accurately. Therefore, a coordinate reference point for the image position could not be established on this plate. Relaxing the tolerance in the target matching program, so that each epipolar line had a large error bound, did allow a few points on plate 3 to be matched, but it also produced an unacceptably high number of false matches with other plates. At this point, it was decided omit plate 3 from the subsequent photogrammetric analysis.

Following the matching of the points, the next step is to optimise the data using a least squares bundle solution. The three dimensional coordinates of all the points that have been successfully matched are calculated, along with the residual error in each point location. The bundle solution re-calculates the camera positions and orientations so that the residual error between matched points on the plates is minimised. Once the bundle solution has been run, the user can look at the plate residuals and eliminate any points with errors above a certain threshold value. In this survey, any points with residuals of greater than 10μm were eliminated. Such points will correspond to items of debris that have been improperly matched, or possibly to targets that have been found badly by the scanning program. In either case the point is erroneous and needs to be excluded from a high accuracy survey.

Figure 3.1.7 shows the plate coordinates of the matched points on plate 2 once the poorly matched points have been rejected. These are all genuine points that have been matched and numbered by the target matching program. From the figure it can be seen that the shape of the boat has become clear.

Figure 3.1.7:The Final Plate Data From Plate 2

The 3-dimensional coordinates calculated by the bundle solution are shown in figures 3.1.8(a),(b) and (c). Each one of these figures shows a projection of the boat in a different plane. The diameter of the circle representing the points shows how far from the observer the point is. Decreasing size corresponds to the point being more distant. From the three dimensional plots of the boat it may be seen that one end of it is very badly defined by the survey. The poor results in this region are due to the removal of plate 3 from the survey. All of the missing points will have been imaged by plates 2 and 3 only. Therefore, although the points will have been recorded and found on plate 2, it proved impossible to match them with points on any other plate. Hence it is not possible to calculate their three dimensional coordinates.

3.1.6 Calculation of The Object Coordinates

At NPL there are two programs available for calculating the three dimensional coordinates of points, given their image positions on two or more photogrammetric plates.The first of these, the NPL bundle solution, has been in use at NPL for approximately ten years for the analysis of photogrammetric data, and runs on a VAX computer. More recently a program known as the "General Adjustment Program" (GAP), written in the Division of Photogrammetry, The Department of Civil Engineering, at City University, London, has been obtained. Both have been used in conjunction with the data obtained from the boat survey.

Both of these programs require initial estimates of the three-dimensional coordinates of all the points before they start their iterative refinement of them. The

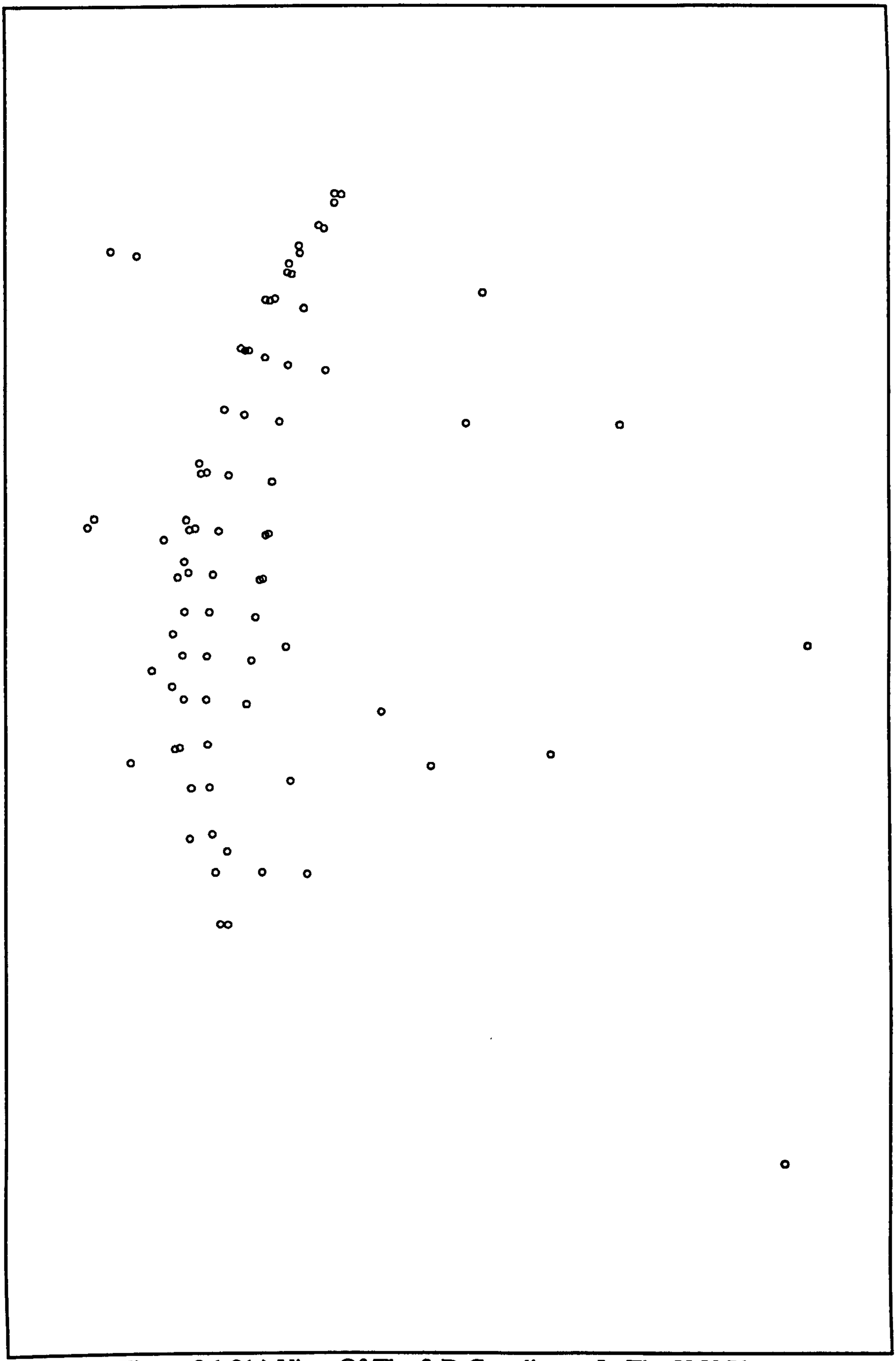

Figure 3.1.8(a):View Of The 3-D Coordinates In The X-Y Plane

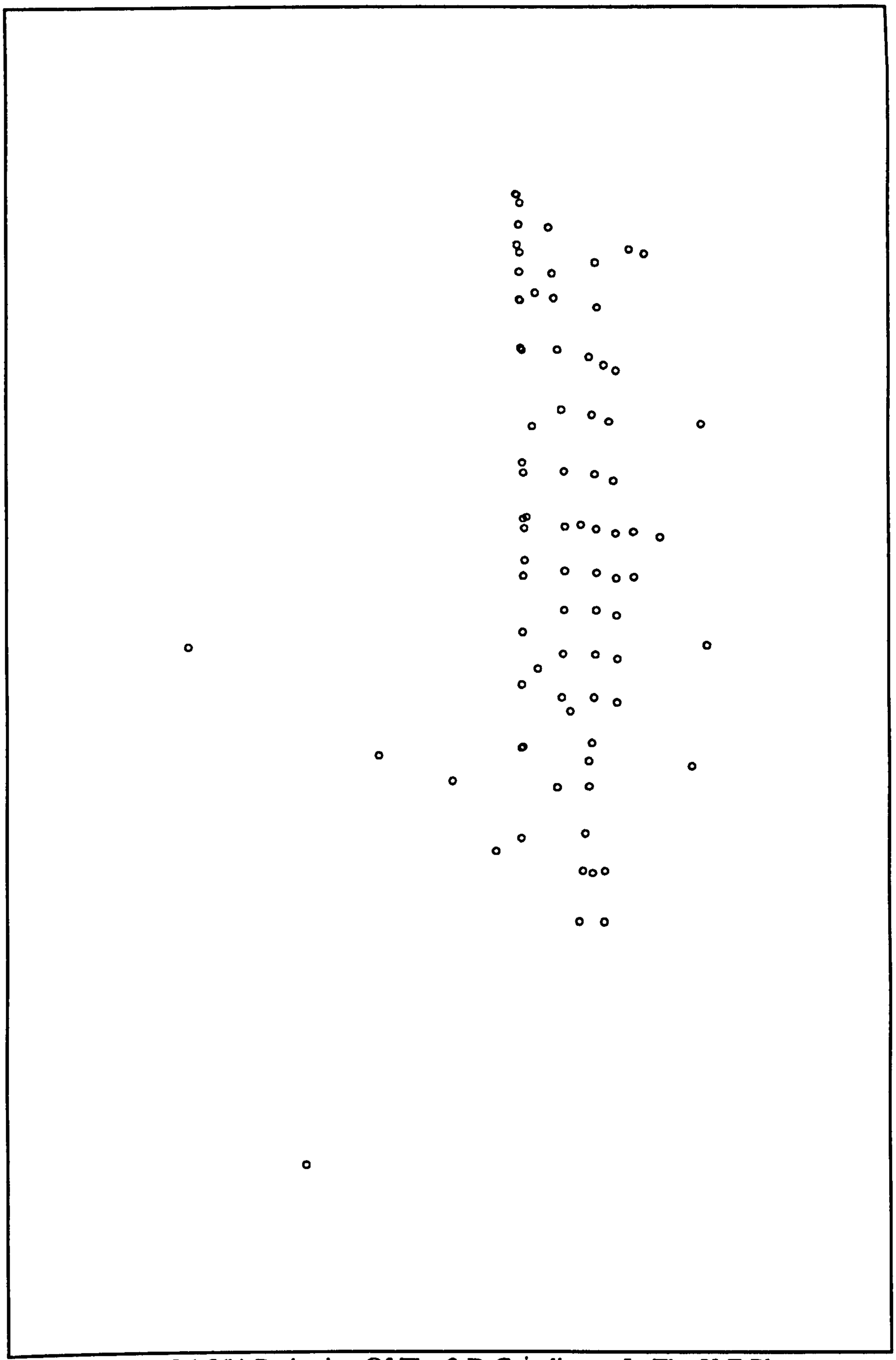

Figure 3.1.8(b):Projection Of The 3-D Coordinates In The X-Z Plane

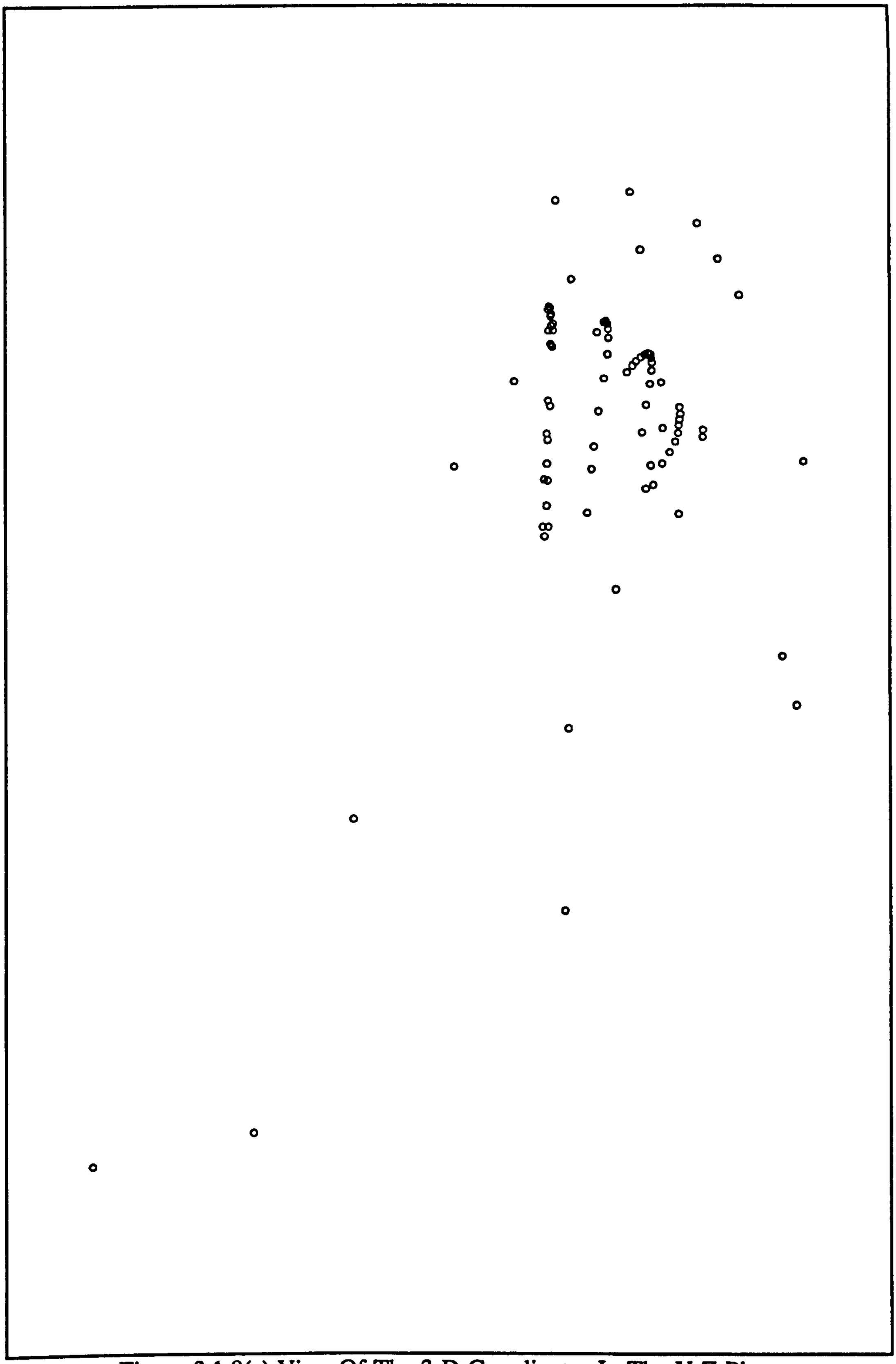

Figure 3.1.8(c):View Of The 3-D Coordinates In The Y-Z Plane

same program, written by R.A.Hunt, was used, in this study, to provide the estimates for both programs. A brief outline of the production of the initial estimates is given here. A more detailed description may be found in Hunt(1983,1984). The three dimensional positions of the ground points are known from the results of the theodolite survey. These are used to calculate the position of each camera, as outlined in appendix 1. The initial estimate of the three dimensional coordinates of a particular point is then calculated as follows. A line is projected through space from the image on the photogrammetric plate, through the perspective centre of the camera, to infinity. This process is repeated for the corresponding points on each plate. The point of intersection of the lines is the initial estimate of the three dimensional coordinates for that object point. It should be noted that the lines will generally not all intersect in space at a common point due to measurement errors, so a point of nearest approach is used. A maximum tolerance is placed on the point of nearest approach to ensure that incorrectly matched points are not used.

The output of this program is in the form of initial estimates of the camera positions as well as the initial estimates of the three dimensional coordinates of the targets. In the first analysis of the data from the survey the NPL bundle solution was used to calculate the final three dimensional coordinates. This program iteratively refines the estimate of the three dimensional coordinates to minimise the plate residuals. The plate residual of a point is the distance between the measured position of the target image and the projection of the estimate of the object position through the camera's perspective centre onto the photogrammetric plate. A weakness of the NPL analysis program is that it keeps the three dimensional coordinates of the ground points fixed.

This means that any error in their measurement from the theodolite survey will adversely affect the calculation of the coordinates of all the points in the survey.

GAP does not suffer from this problem. It can keep the ground points fixed in the same way as the NPL program, or it can be requested to treat the ground points in the same manner as any other point. This means that it can adjust the whole three dimensional structure to minimise the residuals in the three dimensional coordinates. The data was analysed using GAP with the ground points fixed in the same way as they had been when the NPL bundle solution was used. As expected there was no difference between the three dimensional coordinates calculated by the two packages. The root mean square of the plate residuals were also in agreement. Having established the compatibility of the two systems, GAP was then used on the data with no constraints on position of the ground points.

The root mean square plate residuals for the case when the ground points were fixed are shown in table 3.1.1.

Plate	RMS plate residual for x (μm)	RMS plate residual for y (μm)
1	1.16	2.41
2	1.06	2.49
3	1.64	3.08

Table 3.1.1:RMS Plate Residuals

The root mean square three dimensional coordinate residuals from this treatment

of the data are shown in the first column of numbers in table 3.1.2. The right hand column shows how these residuals were reduced by the removal of the constraints on the ground points. The root mean square of the plate residuals were not changed by this modification.

Axis	Ground points constrained(mm)	Ground points unconstrained(mm)
x	0.99	0.32
y	7.81	0.29
z	11.61	0.19

Table 3.1.2:RMS 3-d coordinate residuals

These plate residuals are comparable to those of similar photogrammetric survey where the plates have been measured manually. This success, however, is tempered by the fact that only 70 of the 100 points on the boat were found by the survey. As was stated earlier, most of these points were lost owing to the problems with plate 3. Further points were lost around the keel and rim of the boat due to the very oblique angle at which they were seen by the cameras. With hindsight, these targets were viewed from a far more oblique angle than is normally the case, and more care should have been taken in positioning the cameras.

The targets used in this survey were found to be easily centred under the microscope by a human operator, but a solid disc rather than a ring pattern is more suited to this automated image finding routine. This point is illustrated by figure 3.1.9

which shows how the ring targets were imaged when viewed obliquely. The apparent change of shape of the target causes a problem since the algorithm does not know which of the three features it should attempt to centre. If it chooses to find one of the features corresponding to the ring there will be an error of about 50μm in the position. The simplest way to overcome this problem is to use solid targets.

A further unexpected problem arose with two points. The targets were so large that each one of them more than filled the field of view of the microscope system when viewed at high magnification. Obviously, this lead to their centres of gravity being found erroneously. Once more this problem could be overcome by a careful choice of target size.

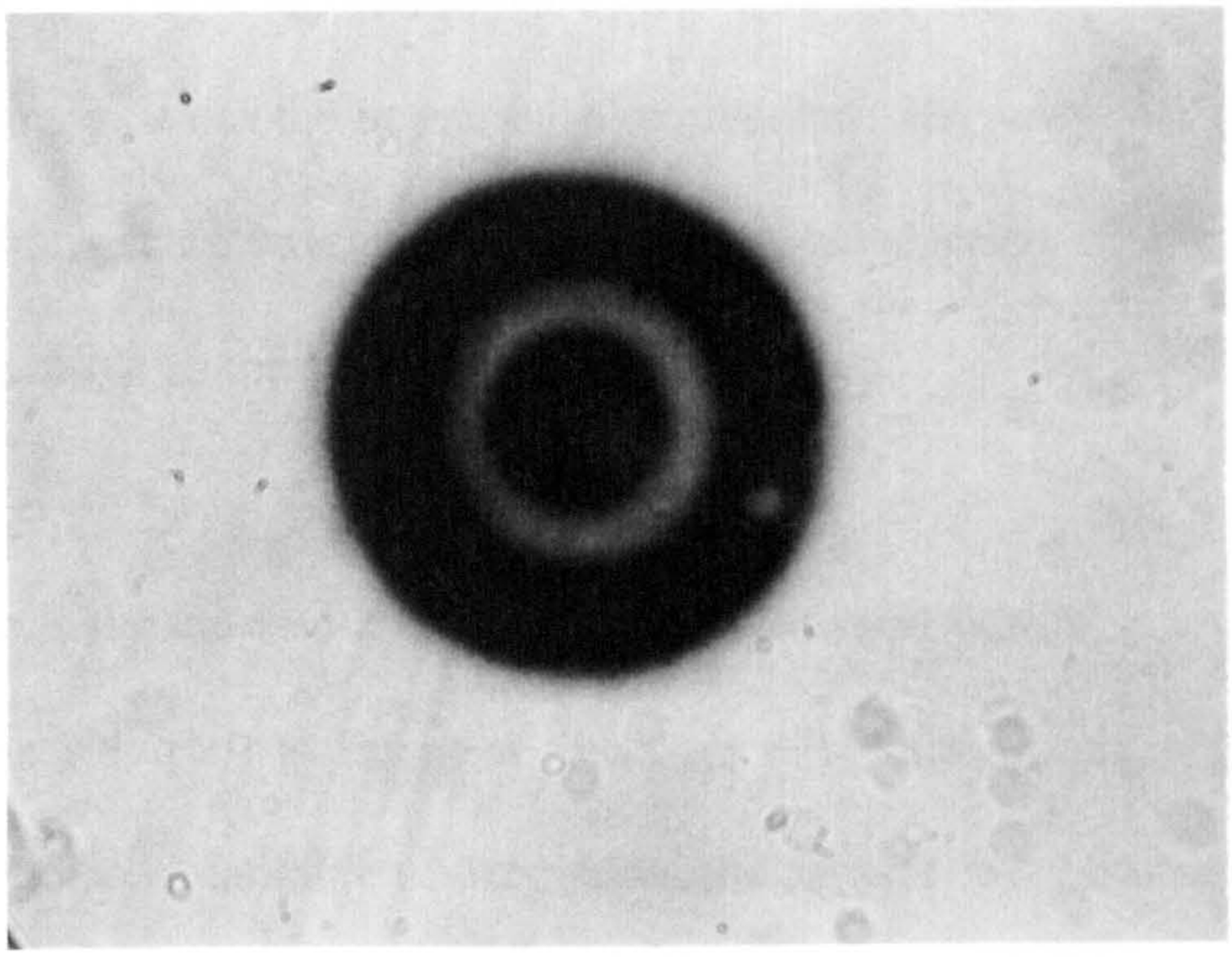

Figure 3.1.9(a):A Target Viewed Normally

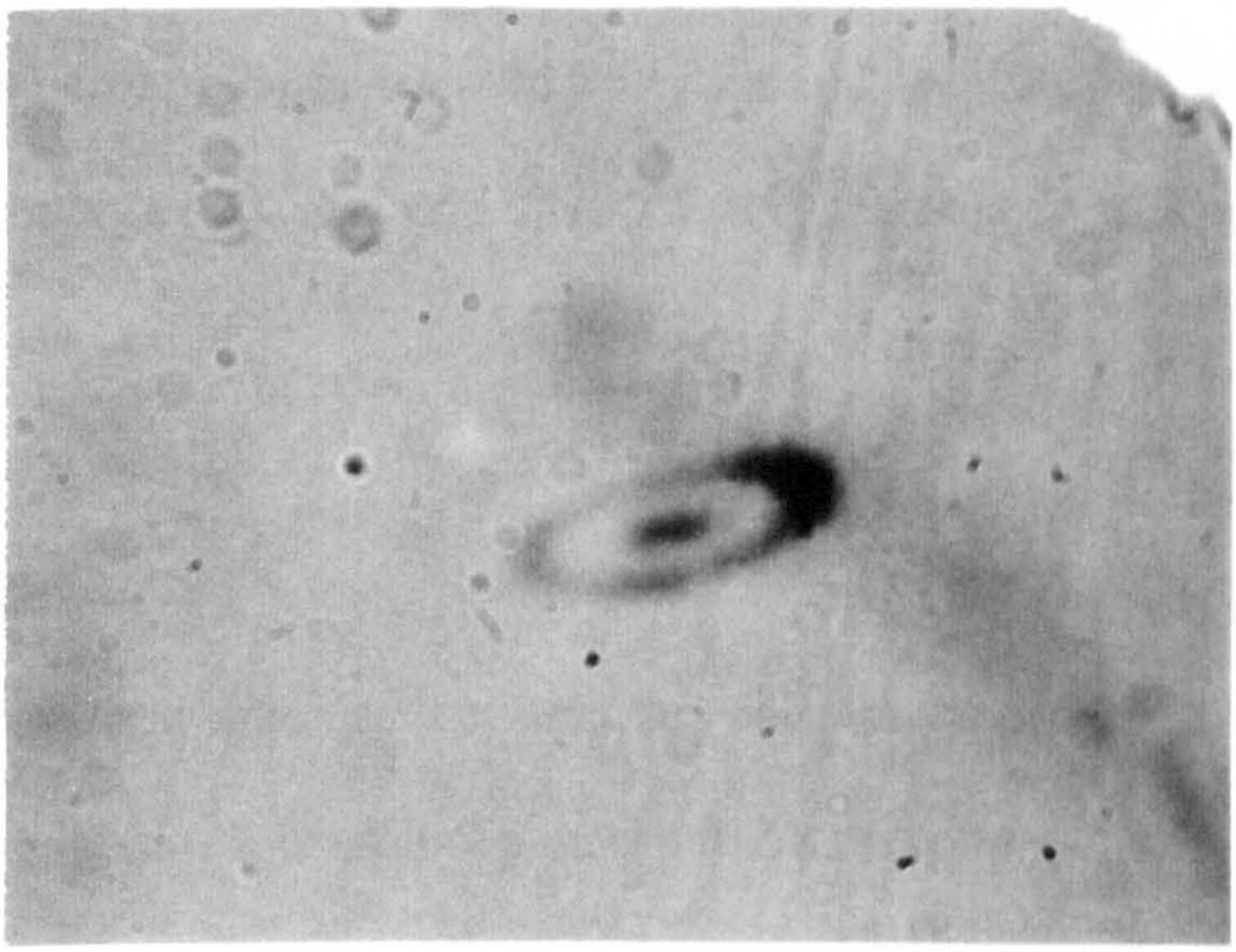

Figure 3.1.9(b):A Target Viewed Obliquely

3.1.7 Improvements To The System

The automated system developed here meets the criteria that were initially set out in terms of accuracy. It has the potential to reduce drastically the cost of performing a high accuracy photogrammetric survey due to the elimination of the need for an operator to be present while the plates are being measured.

However, as is the case with all new systems, several problems arose during its implementation. The solutions to many of these are relatively simple, with the key to success being the choice of suitable photogrammetric targets and camera positions.

Perhaps the biggest improvement could be made by adjusting the target finding algorithm to reject more debris. Most of the debris corresponds to long features, such as scratches on the plate. One simple way to eliminate such flaws is to calculate the ratio of the area of the object to its perimeter. For scratches and similar features this ratio will be much lower than in the case of targets. Therefore, by setting a threshold for this quantity much of the debris could be eliminated from the subsequent analysis. However, as may be seen from figures 3.1.5-3.1.7, the target matching program performs well in rejecting bad points.

3.1.8 Conclusions

An ambitious new automated system has been developed for the measurement of photogrammetric plates. It is has been shown to obtain results of an accuracy similar to a manual survey performed with the same equipment. The algorithm developed appears to be robust in that it can be left to measure a plate reliably without any

operator intervention, but as with all new programs, it will gradually be developed in use as more potential improvements are investigated.

4. THE MEASUREMENT OF CENTRAX PLATES

The Centrax camera has been shown to be capable of recording photogrammetric information that may be reconstructed to give the three-dimensional coordinates of a point, within a $1m^3$ volume, to a precision of $2\mu m$ (Fomo 1991). In order to achieve this high accuracy, it is necessary to measure the position of the features, over the 50mm diameter image field, on the photographic plate to an accuracy of 50nm, or better. The Zeiss ZKM microscope used for measuring conventional photogrammetric plates at NPL has an accuracy of $1\mu m$ (Oldfield 1986), so a different microscope system is required to examine the Centrax plates.

A second two axis measuring microscope, known as 'Gandalf', has been in the possession of the NPL photogrammetry group for several years. The design specifications of the machine stated that it should have a repeatability of better than $0.2\mu m$. However, the stage displacement measurement system was found to be unreliable, due to aberrations in the motion of the stage. In particular, the linear interferometric measurement system was found to be incapable of correctly monitoring a yaw in the stage motion, of $1.2\mu m$ in amplitude, at a pitch of 5mm (Brown 1991). Unfortunately, it was not possible to apply any reliable form of compensation to the interferometer readings to eliminate this error. Owing to this problem the interferometer system was removed from Gandalf, and the microscope was not used for three years.

Gandalf was seen as a useful test-bed for the development of a new high precision x-y displacement transducer potentially suitable for the measurement of

Centrax plates.

4.1 Techniques For High Precision Displacement Measurement

There are several methods by which a microscope stage position may be monitored. Two of the most popular methods, linear interferometry and moiré fringe devices, are outlined below.

4.1.1 Linear Michelson Interferometers

The most popular high precision measurement technique involves Michelson interferometry. Figure 4.1.1 illustrates this well known method. A corner cube is attached to the stage. Laser light enters a beam-splitter, which sends half of the light to the corner cube on the stage, and the other half to a second corner cube which is fixed relative to the beam-splitter. The light returns from the corner cubes, to be re-combined in the beam-splitter. Interference occurs between the two returning beams due to the change in phase between them as the path length to the stage mounted corner cube changes. As shown in the diagram there are two output beams from the beam-splitter. These signals are both modulated, but are 90° out of phase. Therefore, combining the two signals produces a quadrature signal, of the type described in section 4.2.3, which may be used to monitor the direction of motion of the stage.

There are two axis measurement systems based on this form of interferometry which satisfy the accuracy criteria required to make full use of the Centrax system. Indeed, a Zeiss ZKM 05-150 machine has been modified, in the NPL micro-metrology section, with such a measurement system to give a resolution of 20nm. Great care is

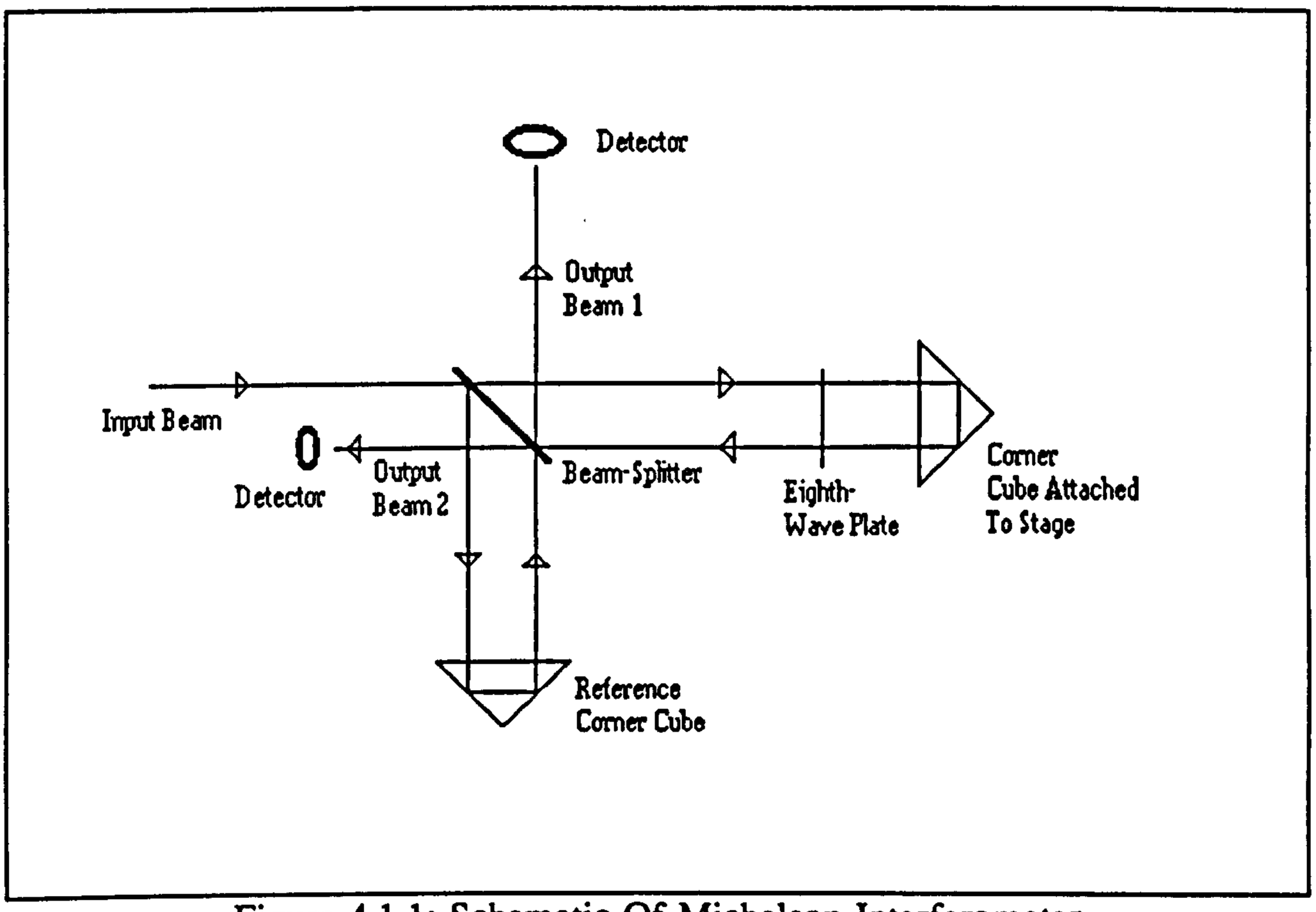

Figure 4.1.1: Schematic Of Michelson Interferometer

taken to monitor any pitch, roll and yaw in the stage motion. This microscope has been used to measure Centrax plates to an accuracy of 60nm (Forno 1991).

However, it is not easy to build a measurement system to meet such demanding requirements. This point is illustrated by the original linear interferometer system that was installed on Gandalf. Figure 4.1.2 shows schematically how the interferometer systems were arranged on the machine. There was a relatively large distance (≈10cm) between the axis of microscope objective lens, and the measurement point of each interferometer. Such a situation leads to problems in making high accuracy measurements, as is explained in section 4.3. In fact, Gandalf's original instrumentation is particularly poor in design since the measurement centre shifts relative to the objective lens as the stage is moved. Therefore, the sensitivity of the system to problems such as roll and pitch may vary with position.

4.1.2 Moiré Grating Systems

Many microscopes, including the ZKM-01-250D used at NPL, for examining conventional photogrammetric plates, use the moiré effect to monitor stage position. The simplest implementation of such a system is illustrated in figure 4.1.3. One grating is fixed to the stage, while a reference grating is held stationary. As the stage moves relative to the reference grating the light from the source reaching the detector is modulated according to the relative positions of the gratings. If the clear areas of one grating correspond to the opaque lines on the other, the transmitted light will be at a minimum. If the clear sections of both gratings coincide the transmitted light intensity will be maximum. Therefore, the intensity of the output light is an indication of position.

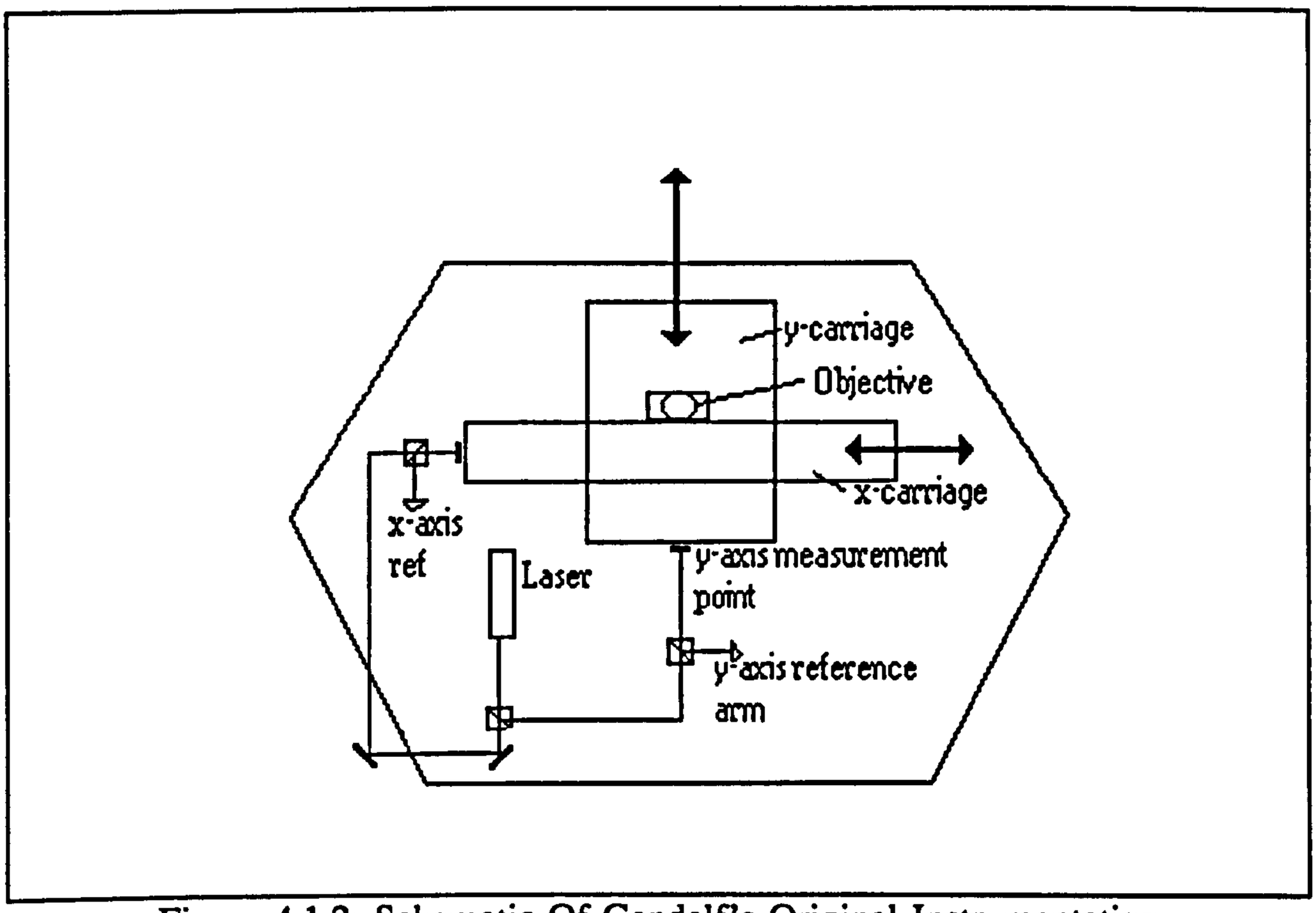

Figure 4.1.2: Schematic Of Gandalf's Original Instrumentation

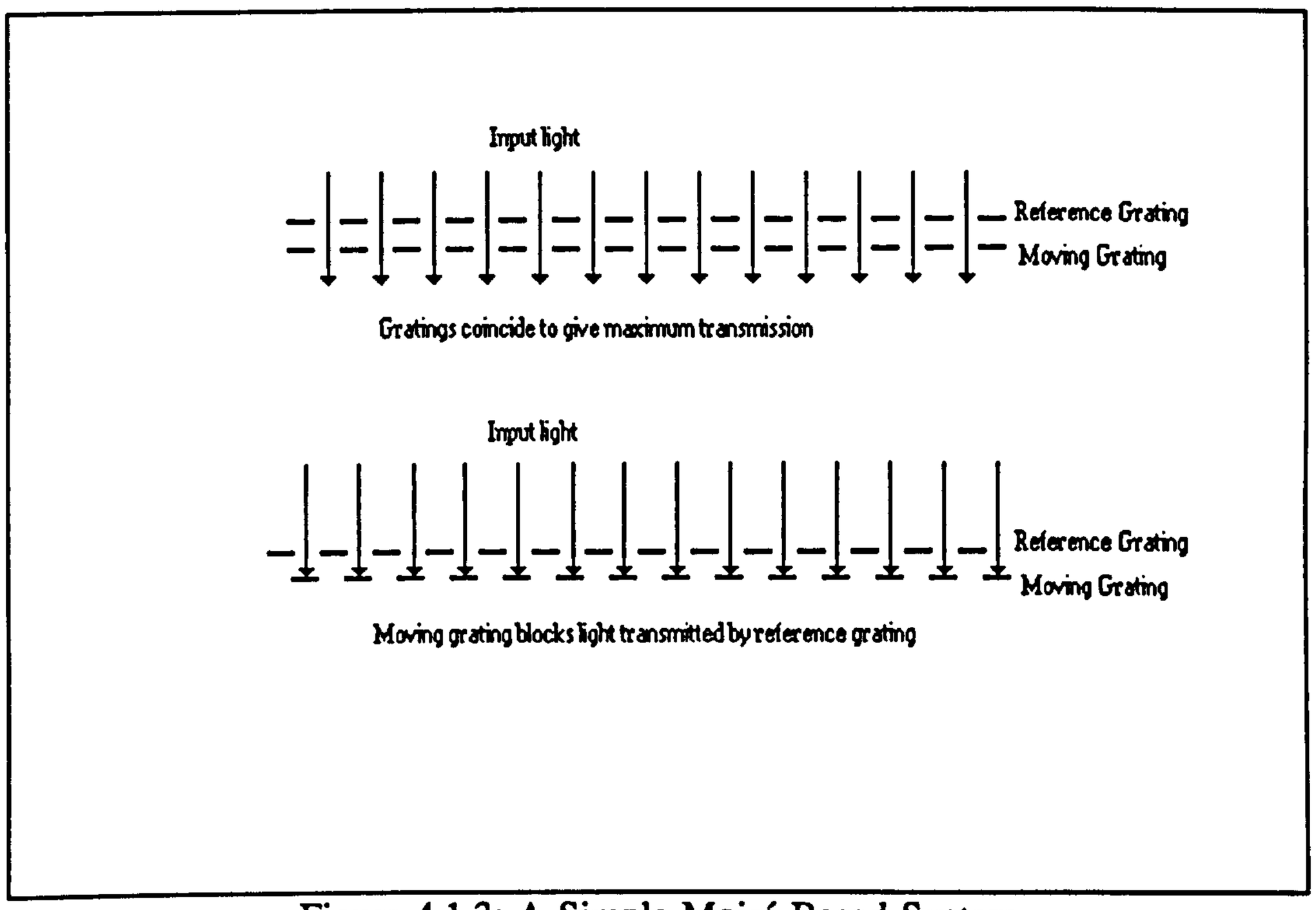

Figure 4.1.3: A Simple Moiré Based System

A different pair of gratings is used for each axis of motion.

Directional counting is achieved by fixing two gratings of similar pitch side byside to make the reference grating. They are positioned such that there is a 90° phase difference between there lines. Two sets of light sources and detectors are used to monitor the motion on each axis, with a set interacting with each half of the offset grating. Hence, the output from the two detectors is 90° out of phase, so producing a quadrature signal.

The fundamental accuracy of such a device is dependent upon the pitch of the gratings, and the degree of interpolation used on the transmitted light intensity. It is not possible to satisfy the Abbé criterion (see section 4.3.1), while having the measurement centre of the system on the optical axis of the microscope, with an instrument such as this. Hence high precision measurement is not possible.

4.2.1 The Proposed Novel Interferometer

A novel two grating instrument for the measurement of Centrax plates, in keeping with the innovative nature of the Centrax project, was proposed some time ago by Dr.J.M.Burch (Forno 1991). Modifications to eliminate the need for a second grating have since been made by Dr.C.Forno (1991). The design of the device is shown schematically in figure 4.2.1.

A simple way to explain its operation is as follows. Light is incident normal to the surface of the diffraction grating. The two first diffraction orders are intercepted by 90° prisms which return the beams to the grating surface. Figure 4.2.2 illustrates how two coherent beams shows how the two such beams interfere to produce a sinusoidal interference of pitch p, where:-

$$p=\frac{\lambda}{2\sin\theta} \qquad 4.2.1$$

In this case θ is the diffraction angle from the diffraction grating, which for normal incidence is given by:-

$$\sin\theta=\frac{n\lambda}{d} \qquad 4.2.2$$

where d is the pitch of the original grating, λ is the wavelength and n the order of diffraction. Substituting 4.2.2 into 4.2.1 gives:-

$$p=\frac{d}{2n} \qquad 4.2.3$$

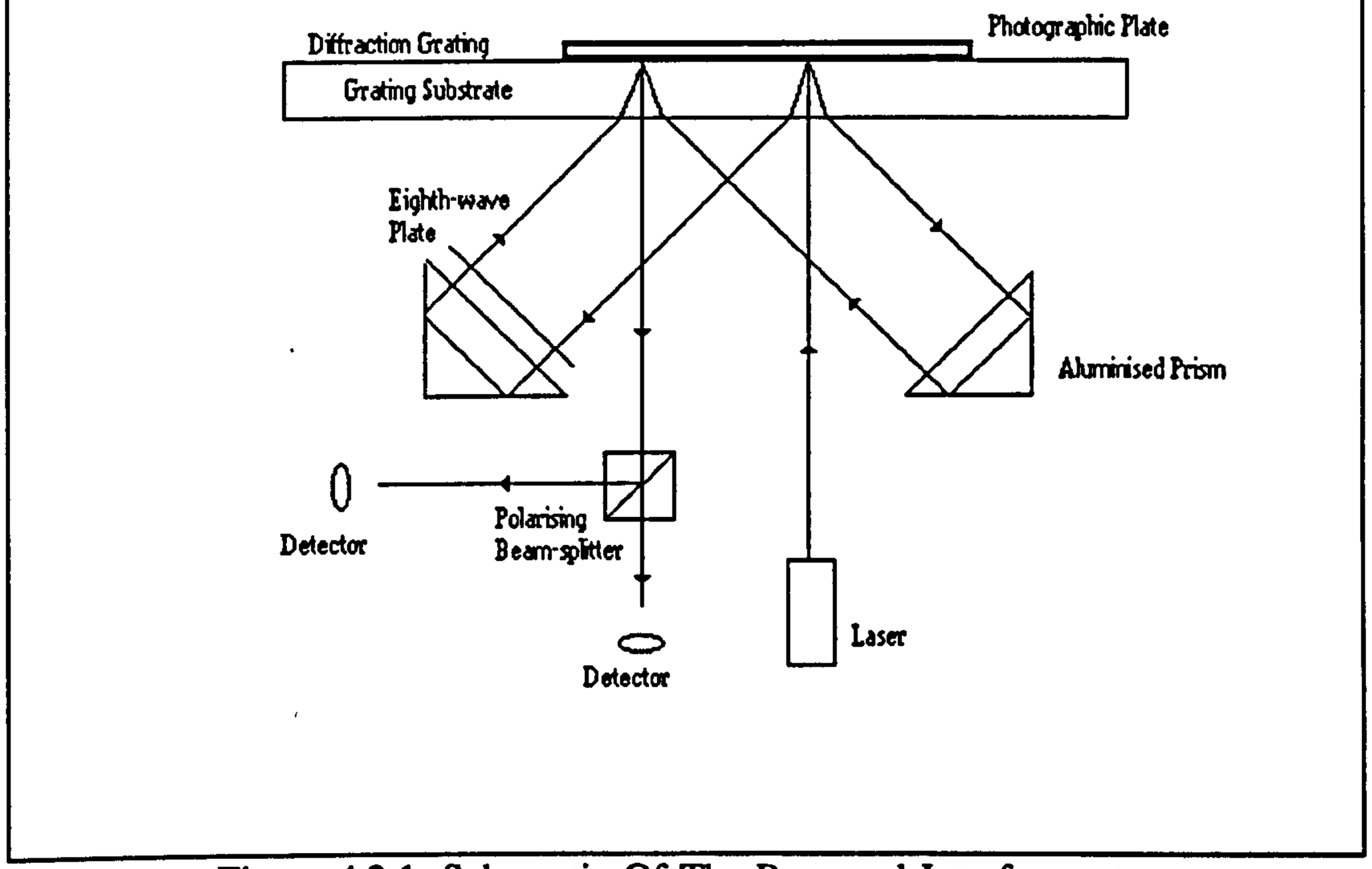

Figure 4.2.1: Schematic Of The Proposed Interferometer

Therefore, the pitch of the light grating formed is half that of the original grating if the first diffaction order is used.

The intensity of the returning light, diffracted by the grating to be parallel to the input beam, is dependent upon the relative positions of the real and virtual gratings. If the brighter areas of the light grating coincide with the non-reflecting portions of the reflection grating, the output light is a minimum. The modulation for interference between two sinusoidal gratings, one having twice the pitch of the other is at the pitch of the finer grating.

A further doubling in the output modulation frequency occurs in this interferometer owing to the virtual grating moving in the opposite direction to the actual grating. Hence, for a grating motion equivalent to its pitch, the intensity of the output light passes through four cycles of modulation. If a 1200 line/mm grating is used then the displacement predicted to cause one cycle in output intensity is 208nm. Directional counting is made possible by changing the polarisation states of one of the returning beams using an eighth-wave plate. This process is described further in section 4.2.3.

An alternative, more rigorous way to consider the operation of the instrument is based entirely on interference, rather than a geometric moiré effect. In the region of overlap between two coherent beams a virtual grating, whose pitch is dependent on the half angle between the beams, is formed. The relationship between pitch and angle is shown in equation 4.2.1. Figure 4.2.3 illustrates how the operation of the interferometer may be described in terms of interference. In the region bounded by the triangle A'B'C

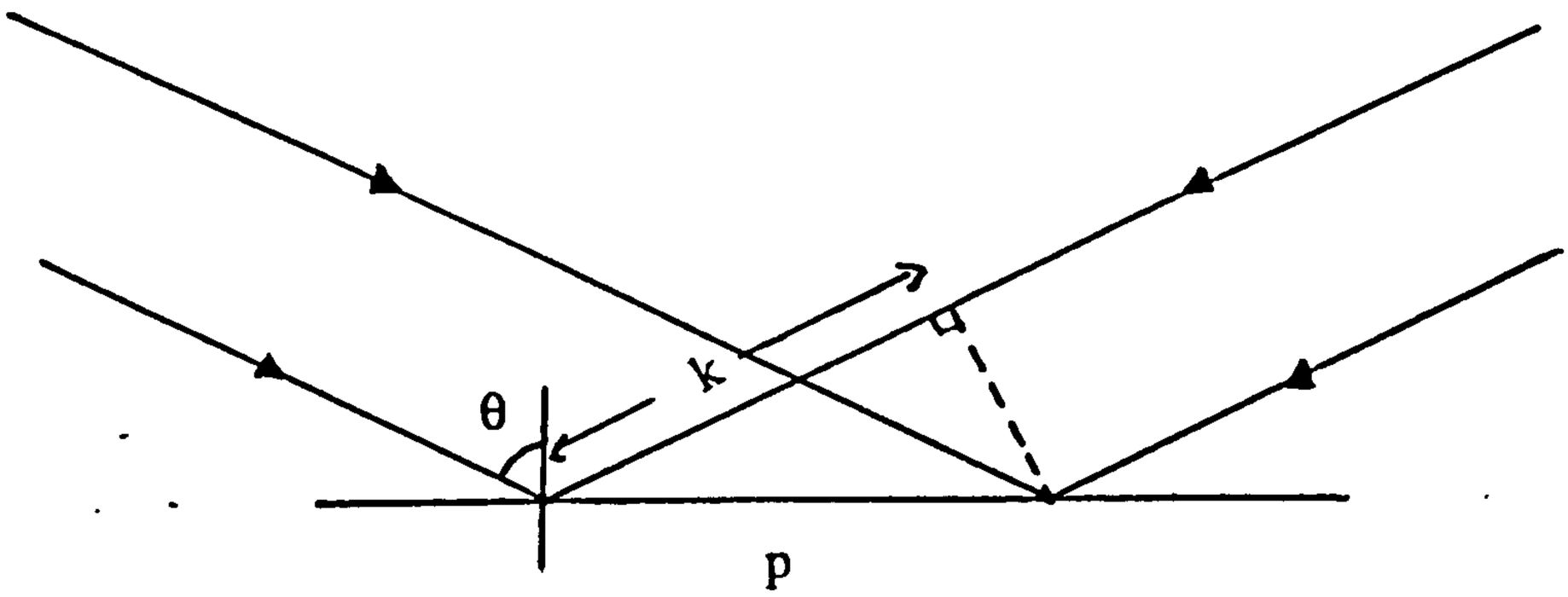

$$k=n\lambda$$

$$p=\frac{n\lambda}{2\sin\theta}$$

Figure 4.2.2: Formation Of A Light Grating

the angle between the interfering beams is θ, and a virtual grating of twice the pitch of the diffraction grating is formed. However, the angle between the two interfering beams is 0° in the whole of the area of overlap from triangle A'B'C to the detector. If two interfering beams travel along the same path in this manner, the interference grating formed has a pitch of zero lines/mm (This may be seen by substituting θ=0° into equation 4.2.1). Hence, at any particular time there is a constant light intensity across the field viewed by the detector. As the diffraction grating is moved relative to the input beam, in a direction perpendicular to the lines on the grating, there is a change in the phase between the two returning beams. Therefore, the output light intensity varies.

As the grating is translated normal to its lines by a distance equal to its pitch, the diffracted light is subject to a phase change of 2π (Hutley 1982). Consider the beam diffracted into the +1 order, towards prism 2, as the grating moves to the right by its own pitch. This light undergoes a $+2\pi$ phase change on diffraction. On returning from prism 2 to the grating the light is subjected to a further phase change of $+2\pi$ by diffraction parallel to the input beam. Therefore, there is a total phase change of $+4\pi$. Similarly, the light diffracted into the negative order is subjected to a total phase change of -4π. The total change in phase between the two beams interfering to produce the output light intensity is 8π if the grating moves by one pitch. The direction of motion determines which of the diffracted beams leads in phase. A phase difference of 2π between the beams would lead to one cycle in the output intensity. Therefore, for a motion equal to the pitch of the grating the output light intensity will pass through four cycles of modulation.

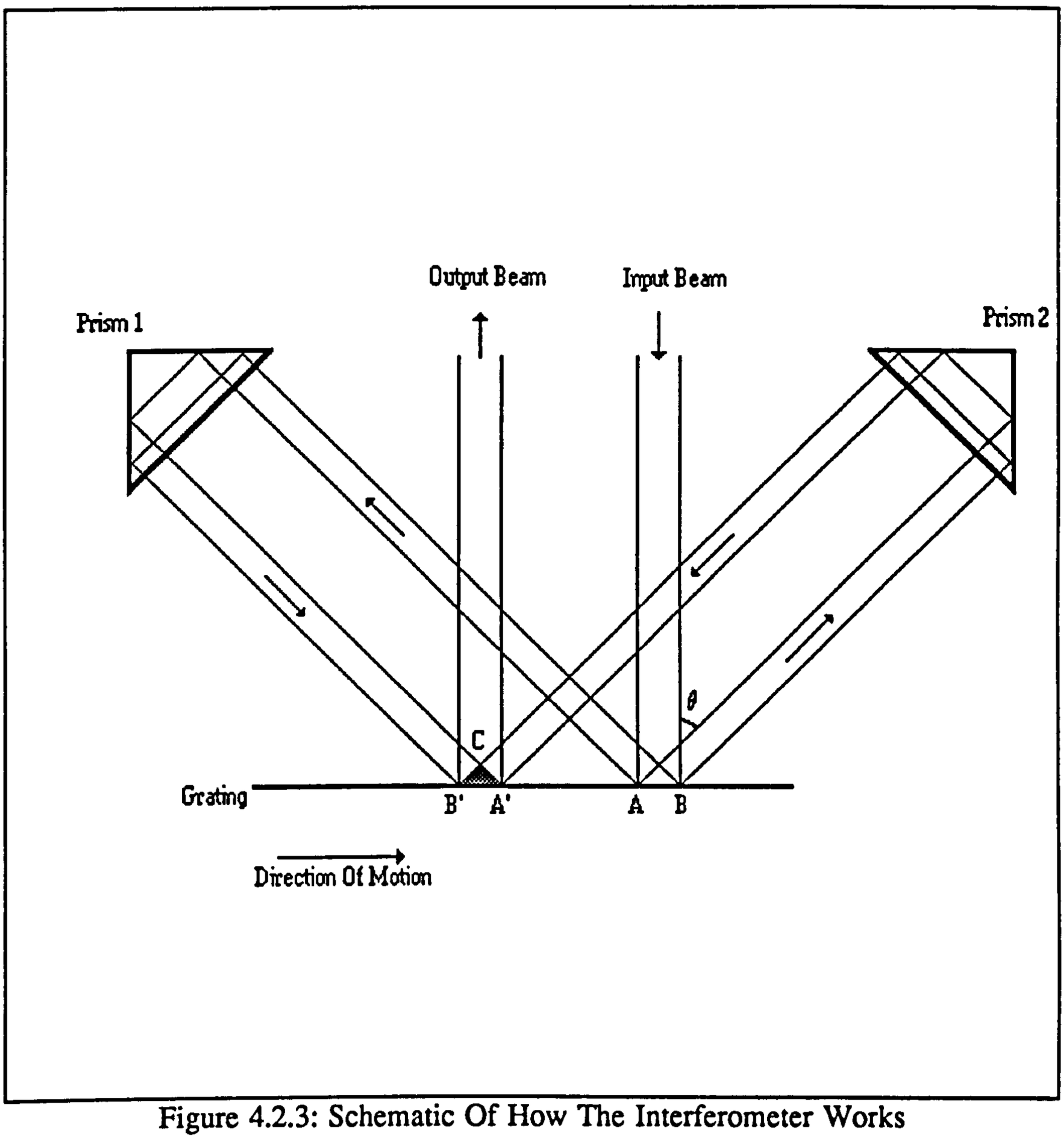

Figure 4.2.3: Schematic Of How The Interferometer Works

The device described so far is a single axis measuring system. However, it is relatively simple to adapt the idea to produce a two axis measurement system. Rather than using a normal diffraction grating, a crossed grating with two sets of lines running perpendicular to each other can be used. Such a diffraction grating has the effect of producing a second pair of first order diffraction beams, propagating in a plane perpendicular to that containing the original pair. A second set of prisms arranged as in figure 4.2.4 return the beams to the grating surface in the same manner as the first set, so providing a second orthogonal measurement axis.

4.2.2 A Simple Single Grating Moiré Device

An experiment was conducted to illustrate the feasiblity of a moiré fringe displacement transducer based on a single diffraction grating. Figure 4.2.5 is a schematic of the arrangement used. Parallel light is transmitted through the diffraction grating onto a concave spherical mirror. The grating is held on a micrometer stage in a plane, perpendicular to the optical axis of the mirror, containing the centre of curvature of the mirror. An inverted image of the grating is projected back onto itself. As the grating is moved the image moves in the opposite direction, so causing the the output light to be modulated. When the dark lines in the image overlap with the opaque grating areas the output intensity is a maximum. Conversely, when the the dark image areas are coincident with the transmitting lines on the grating, the light output is at a minimum. Since the real and light gratings travel in opposite directions, the output modulation is expected to be at twice the pitch of the grating.

The displacement corresponding to 20 cycles in the output light intensity was

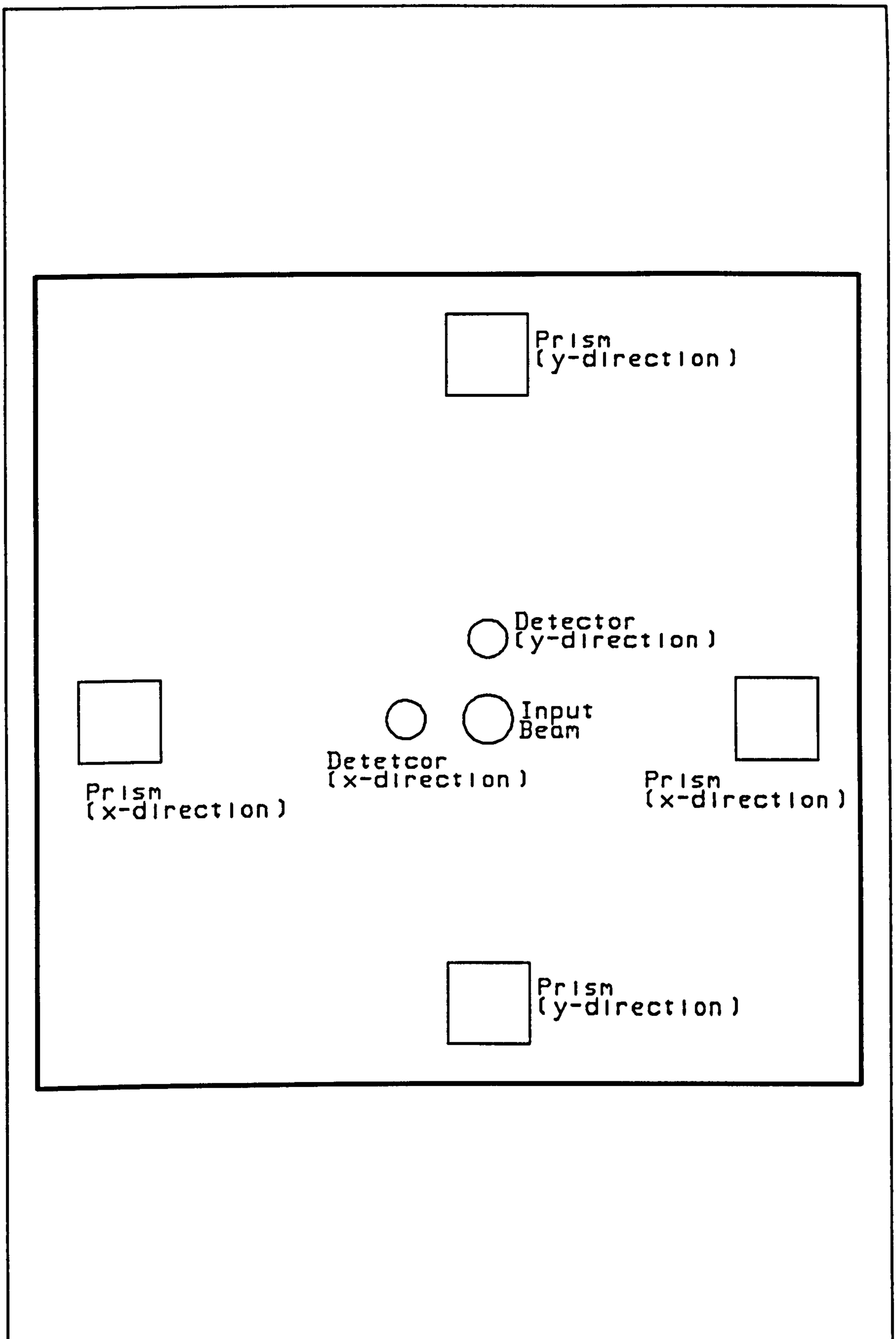

Figure 4.2.4: Schematic Of 2-Axis System

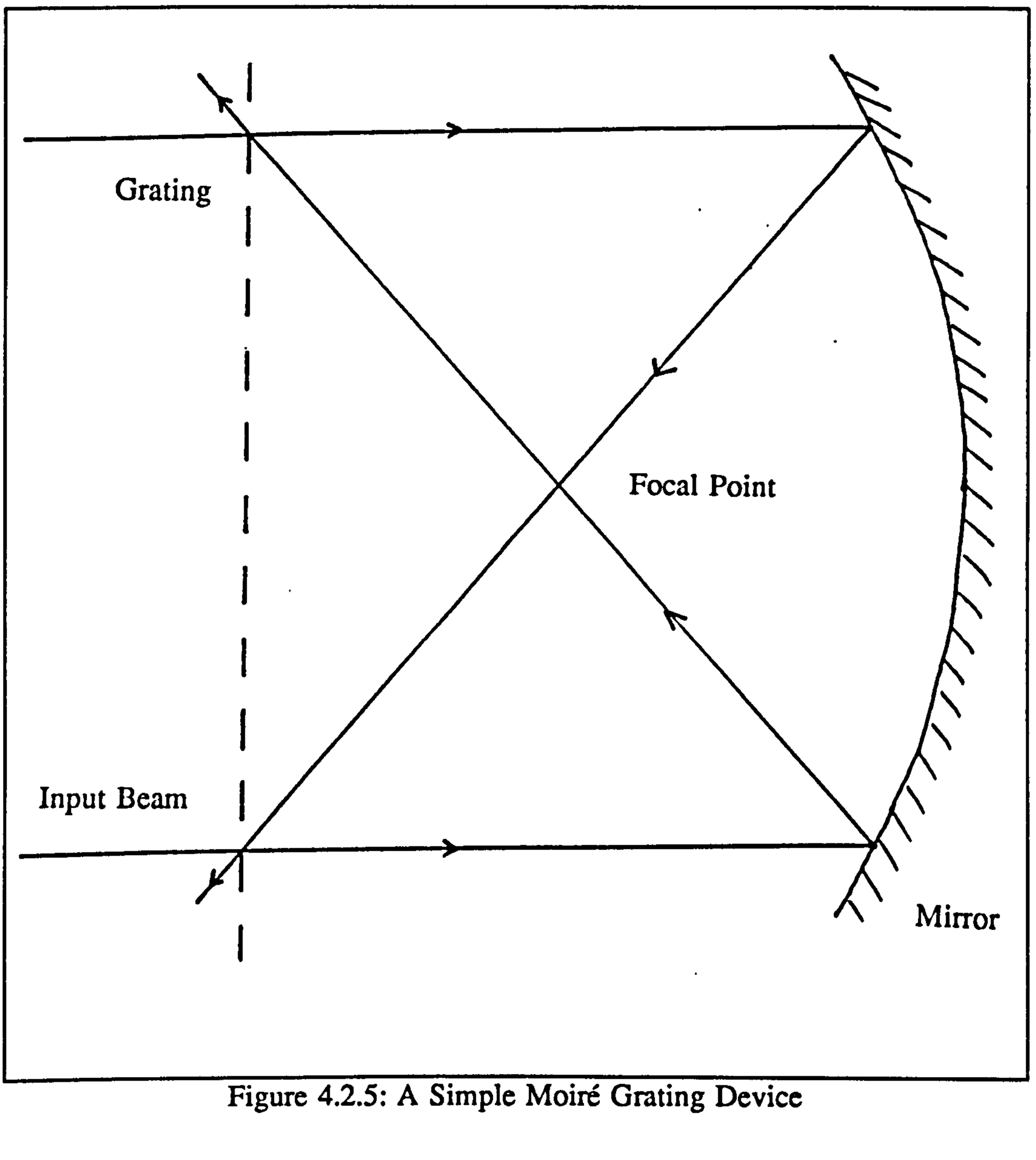

Figure 4.2.5: A Simple Moiré Grating Device

recorded for both a 1 line/mm grating and a 500 lines/inch grating. In the case of the 1 line/mm grating this movement was found to correspond to 10mm which implies an output modulation frequency of 2 cycles/mm. Similarly the other grating had to be moved by 0.02 inches to produce a similar number of fringes. The modulation frequency was found to be 1000 cycles/inch for this grating, which like the other result is what is predicted by theory.

The experiment described above is useful in its demonstration of a moiré effect between a real and an imaged light grating, but it would not be a realistic to base a high precision measurement system on this simple system for a number of reasons. When used with gratings of pitch 100 lines/mm, or greater, modulation of the light is adversely affected by the off axis lines in the image becoming curved. The image no longer maps perfectly onto the object. This difficulty could be eliminated if a cylindrical rather than a spherical mirror was used. However, a problem that would be considerably more difficult to solve is that of the grating moving out of focus. Once more this problem is more serious for high pitch gratings. A factor that further diminishes the possibility of building a displacement transducer based on this design is the lack of information about the direction of motion.

4.2.3 Directional Counting

The basis of a microscope stage monitoring system has been outlined above. However, in such an application, it is not sufficient to measure absolute displacement. Before a system can be of any practical use it must be able to sense the direction of motion and hence count in a reversible manner.

The most convenient way to achieve bi-directional counting with this sensing system is to cause the output signal to take the form of a quadrature signal. A quadrature signal is produced by combining two sinusoidal signals that are 90° out of phase. The direction of motion is determined by which of the two signal leads in phase. Feeding the two signals onto the two channels of an oscilloscope provides a simple illustration of this. The resultant Lissajou figure is a circle, with the direction of progression around the circle being determined by the relative phases of the signals.

A quadrature signal may be produced in the device described here by causing one of the diffracted beams to be linearly polarised, while the other is converted to circularly polarised light(Downs & Raine 1979). Circularly polarised light may be obtained by passing linearly polarised light through a quarter wave plate once, or an eighth wave plate twice (in each case the incident linear polarisation state should be at 45° to the fast axis of the retardation plate). In this system the simplest approach is to place an eighth wave plate on the front of one of the prisms as shown in figure 4.2.1.

The resultant output light beam is made up of a combination of circularly and linearly polarised light. A polarising beam-splitter may be used to separate the output beam into two orthogonally polarised components which can be monitored by photo-detectors. There is 90° phase difference between the two output signals. Which signal leads is determined by grating motion relative to the prism associated with the eighth wave plate.

4.3 Problems Associated With Microscope Stages

There are several important considerations that must be borne in mind when designing a microscope monitoring system. Incorrect readings can easily be obtained if care is not taken to eliminate the many problems that can arise during stage motion.

4.3.1 The Abbé Criterion

One of the most important factors that must be taken into account is the Abbé criterion. This condition states that,

"The object to be measured, and the measuring standard must be in contact or lie in the same plane." (Ghosh 1979).

Figure 4.3.1 shows how a tangential error may be introduced if the measurement point is not co-planar with the object.

The Abbé criterion is almost satisfied by the proposed interferometer. If the object is to be viewed in reflection, it is possible to use the measurement grating surface as the microscope stage. In the proposed application of this microscope, measuring photographic plates, the photographic emulsion will be put in very close contact with the grating. Using the interferometer in this manner, as illustrated in figure 4.2.1, has only one minor disadvantage. Since all of the measurement system light beams have to pass through the grating substrate, it is necessary to ensure that the substrate is of good optical quality. However, this is a slight inconvenience rather than a serious problem. An additional advantage of viewing the photographic plates in reflection is an increase in image contrast (The light has to pass through the plate twice, so enhancing the attenuation caused by optically dense areas).

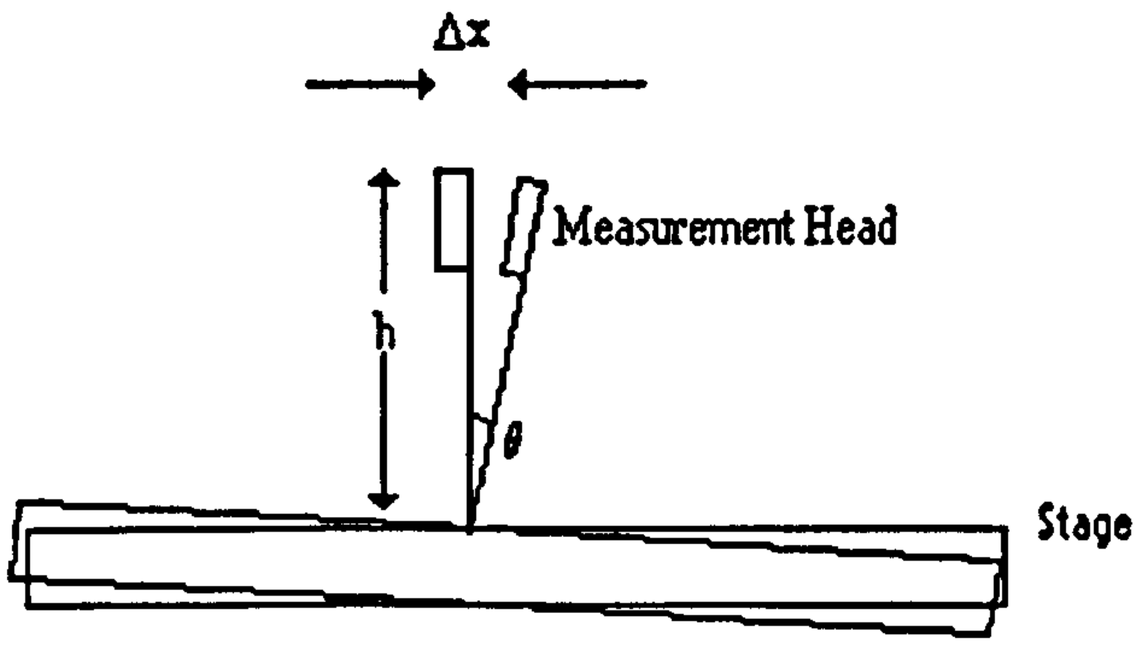

With the measurement point out of the plane containing the object under interrogation there is an error Δx between the point under observation, and that being measured.

$$\Delta x = h \tan\theta$$

Figure 4.3.1: Illustration Of The Abbé Criterion

4.3.2 Problems Associated With Motion

The microscope stage motion is likely to exhibit three types of aberration;- pitch, roll and yaw. If not properly dealt with, each of these problems can introduce a cosine-type error into the measurement process, as shown in figure 4.3.2. Ideally, to minimise any errors of this type, the measurement centre should be on the optical axis of the microscope objective. If this condition of the two axes being co-linear is satisfied, the point under observation is at the point being measured. This instrument's two measurement axes do not have a common measurement point. In this case it is not easy to construct the device so that the measurement centres of the two axes both always lies directly beneath the objective. Section 5.4.1 outlines how the design of the instrument may be modified to allow for a common measurement point between the two axes.

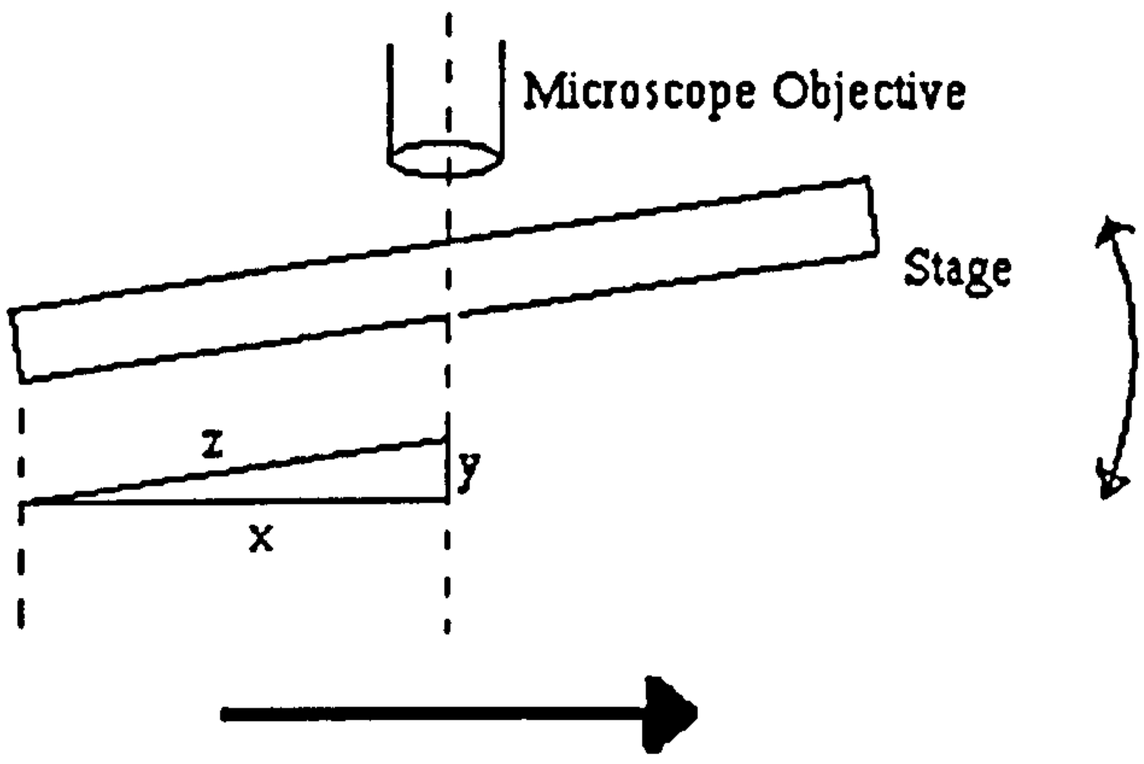

Pitch

In this case the measurement head is at the left of the stage. The horizontal distance to the objective is x but in actual fact the point under interrogation is z distant from the measurement point.

Figure 4.3.2(a): The Error Introduced By Pitch

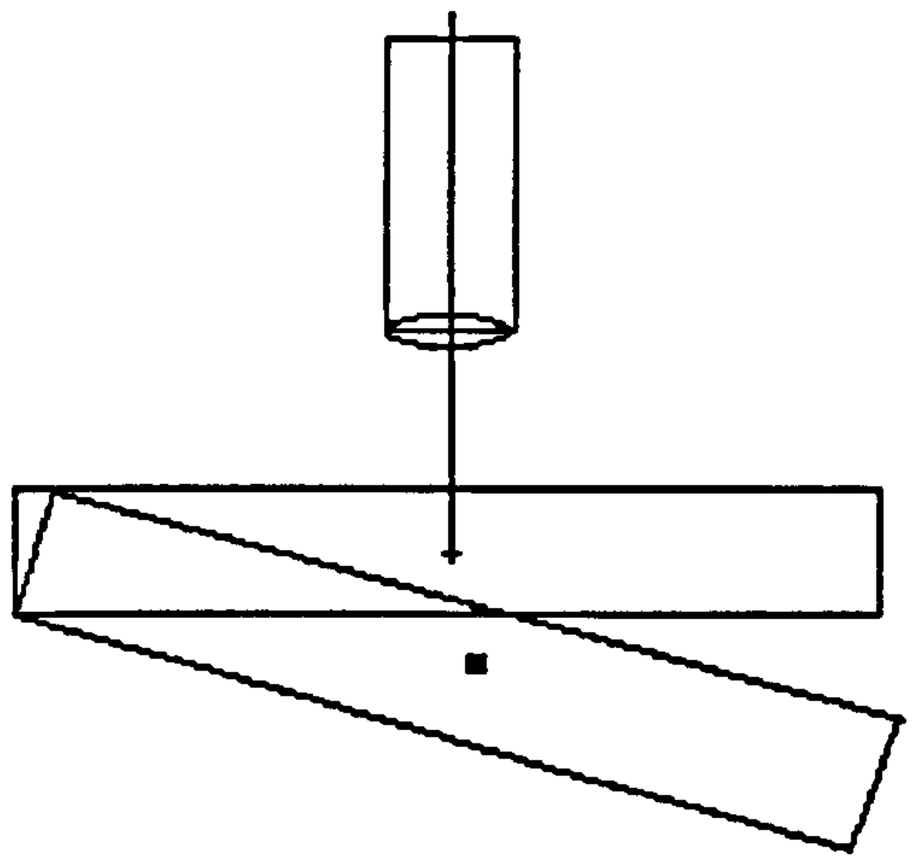

Roll: Once more the point of observation, denoted by a cross, is moved away from the measurement centre.

Figure 4.3.2(b): The Error Introduced By Roll

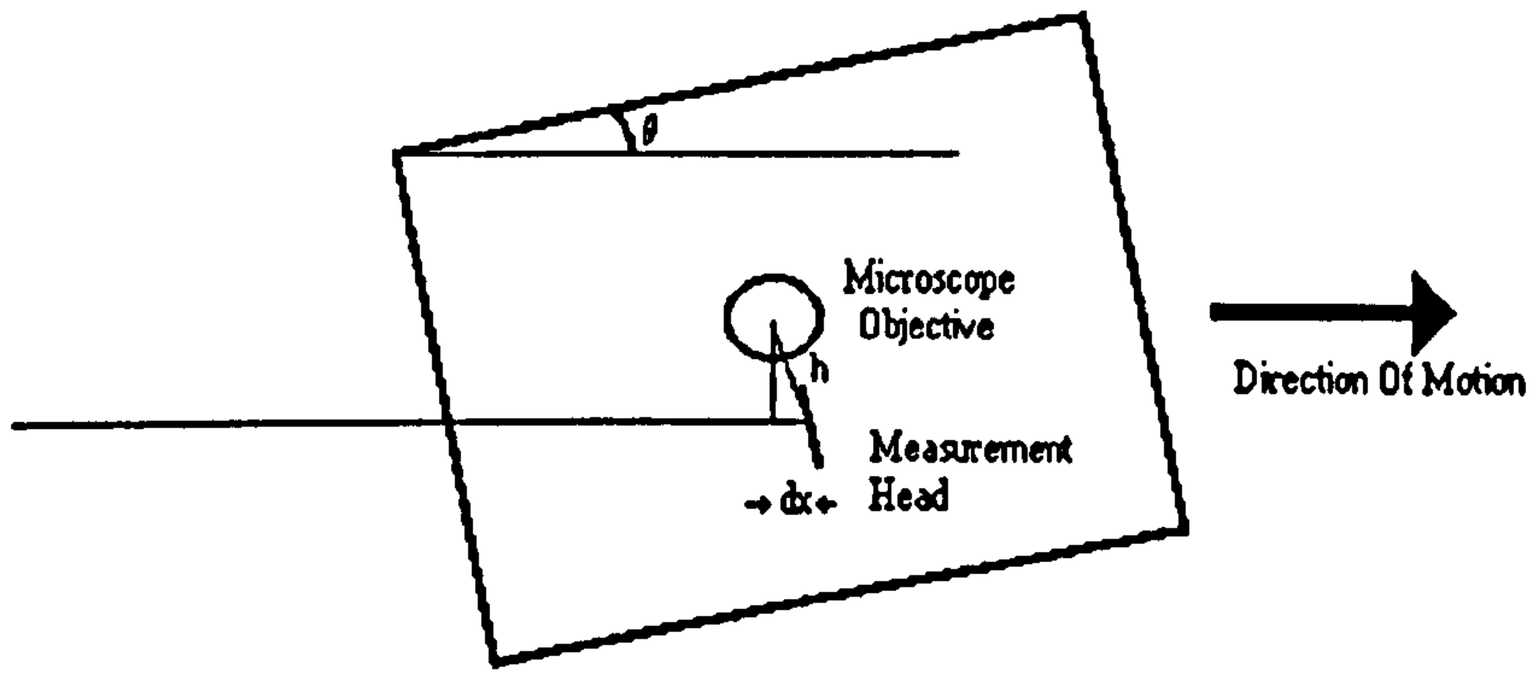

Yaw leads to the error shown above. The microscope stage rotates in the plane of motion so producing a cosine error in displacement along the direction of motion.

The error (dx) is given by:-

$$dx = h\cos\theta$$

Where h is the distance between the measurement centre and the optical axis of the microscope.

Figure 4.3.2(c): The Error Introduced By Yaw

4.3.3 Sources Of Error In The New Instrument

There are several potential sources of error that can affect the accuracy of the system under development. These problems may be divided into two broad categories, those specific to this instrument and those which affect all microscope stage position transducers.

The first of these classes of error are mainly due to errors in the production of the diffraction grating. The number of counts per unit distance moved is determined by the line spacing of the diffraction grating. Any systematic problem of this type, (ie. the grating being of the wrong pitch) is eliminated by calibrating the instrument against a standard device.

The grating is manufactured by a two beam interference technique, described by Hutley (1982). Light from an argon-ion laser of wavelength 458nm is split into two beams. These two beams are deflected by mirrors so that they are brought together. An interference pattern of constant pitch is produced throughout the region of overlap between the two beams. If a plate coated in a photo-resist material is placed in this region it will record the interference pattern. This method is analogous to the way that the virtual grating is produced in the novel interferometer, see figure 4.2.2 for a schematic diagram. The formula relating the grating pitch with the input angle of the two beams is:-

$$\sin\theta = \frac{\lambda}{2p} \qquad 4.3.1$$

To produce a 1100 line/mm grating requires θ=14°35', where θ is half the angle made between the two beams as in figure 4.2.2. The beam angles can be set to ±15' in the grating manufacturing process. Such a tolerance corresponds to an uncertainty in the grating of ±19 line/mm. However, this is a systematic error and is eliminated by calibration. A more serious source of error would be local blemishes in the line structure, but there is no evidence to suggest that the production technique used to produce the gratings used here is susceptible to such problems. Even local variations in the grating pitch can be removed by careful calibration. Damage to small areas of the diffraction grating during use is also not likely to have any affect on the operation of the instrument, as long as the damaged area is small relative to the interrogation beam.

The orthogonality of the measurement axes is determined by the orthogonality of the two sets of lines on the diffraction grating. The crossed grating is produced by exposing the photo-resist on the substrate to the interference pattern twice, but with the substrate being rotated by 90° between exposures. Hence, the orthogonality is determined by the precision with which the rotation can be performed. Ultimately this depends on the 'squareness' of the substrate as its edges are used to locate it on a flat metal holder. The substrate was manufactured with sides that were specified as being right angled to better than 10 seconds of arc. Therefore, this problem should be of little consequence. Any error in orthogonality may be checked by measuring the positions of features on plate twice, with a 90° rotation of the plate between the two measurements.

Apart from the potential sources of error described above, those due to the aberrations in the motion of the microscope stage must also be considered. An

approximate value for the magnitude of the pitch, roll and yaw of Gandalf's stage may be calculated in order to estimate the likely effect of these parameters on the accuracy of the measurement system.

Both axes of motion are carried on air bearings, which means that the pitch and roll are determined by the flatness of the carriageways. Across the 600×600mm span of interaction between the stage and the carriageway, the surfaces are expected to be machined within a 2μm tolerance. Therefore, the magnitude of the pitch and roll may be approximated by the angle Δ where

$$\tan\Delta=\frac{2.10^{-6}}{600.10^{-3}}=\frac{1}{300000}$$

$$\Delta\approx 0.0002°$$

The magnitude of the yaw has been found during a previous study (Brown 1991). A transverse motion error of 1.8μm repeating every 5mm was found. The magnitude of this yaw has since been reduced to approximately 0.5μm by the addition of anti-yaw bars beneath the drive screws.

4.3.3(a) Pitch

Appendix 4 contains a model which provides an estimate of the error introduced into the measurement process due to the stage motion exhibiting problems of pitch.

When a pitch of 0.0002° is used in the calculation an error of 240nm is predicted. The magnitude of this error is reduced as the prisms are moved towards the surface of the diffraction grating.

4.3.3(b) Roll

A rolling motion has much less influence on the accuracy of the interferometer than pitch. If the stage is subject to a pure rolling aberration, the beams returning to the grating from the prisms are displaced perpendicular to the direction in which the stage is being driven. Such a displacement means that the lines in the virtual grating produced by the returning beams move up and down the lines on the real grating, but do not move across them. Hence no change in the output beam intensity results. If there was a relatively large roll there could be a small movement of the output beam across the diffraction grating lines. The magnitude of this movement would only be approximately 0.36nm for a roll of 0.005°, which is over twenty times larger than the amplitude of the roll expected on Gandalf. This small movement is due to light beams being incident upon the prism sides closer to the angle of the prism (ie. a rotary motion when projected onto a plane produces an arc.). Figure 4.3.1 illustrates this effect, with the unbroken line showing the path of the light when there is no roll, and the broken line showing the case of roll. Before the error became large enough to produce on count on the new interferometer a roll of 0.09° would be necessary.

4.3.3(c) Yaw

Yaw is fully compensated for by the proposed interferometer. As the orientation of the grating rotates in this manner the two diffracted beams being returned from the

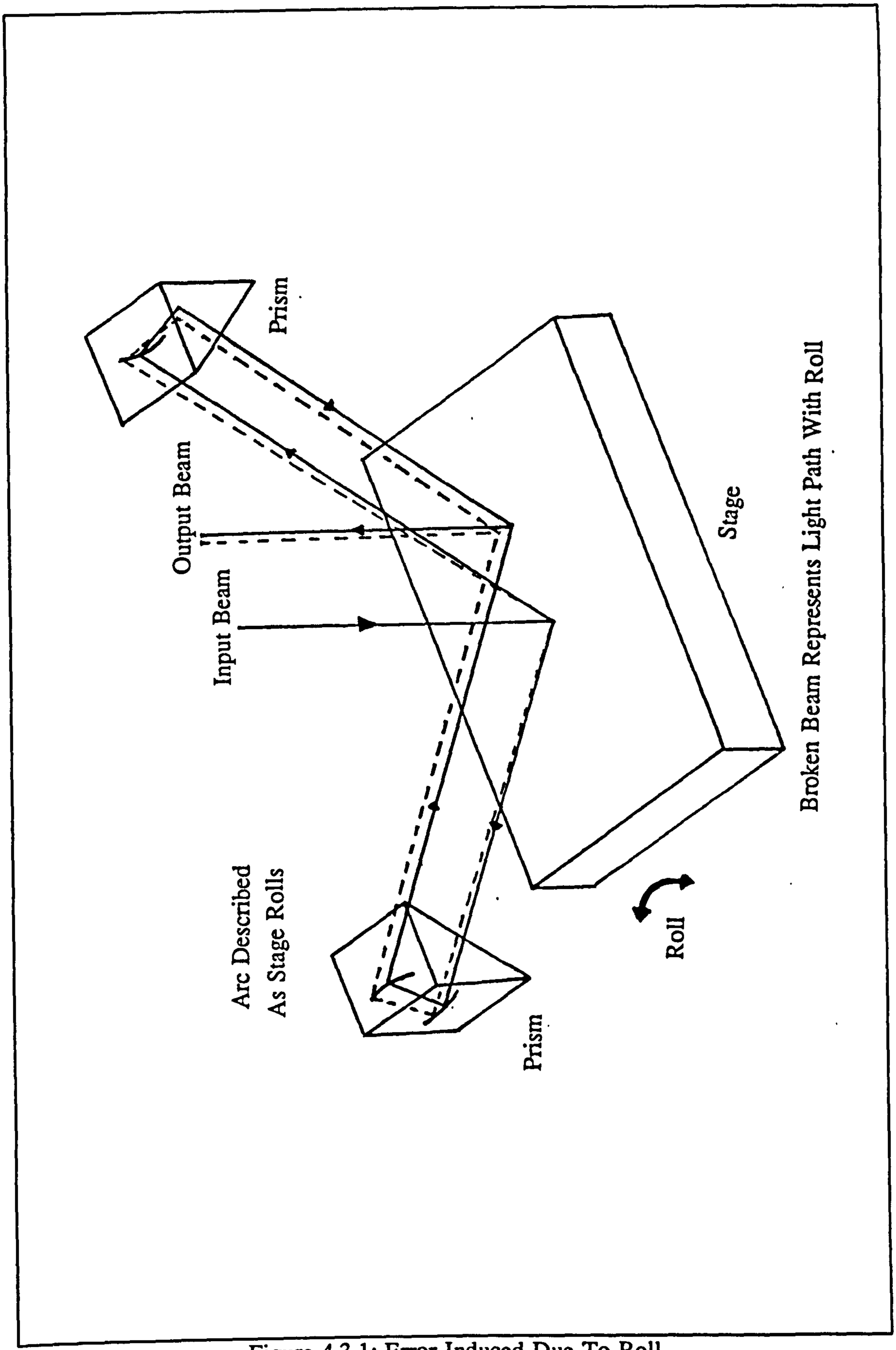

Figure 4.3.1: Error Induced Due To Roll

prisms gradually separate, but the centre of their region of overlap remains at the same point. Tilt fringes will be produced by this process, so reducing the fringe contrast, but the overall modulation frequency will remain constant. The interferometer should be immune to all rotary displacements due to this type of motion unless the output modulation intensity is dramatically reduced because of tilt fringes. For a yaw of 1.8μm at a pitch of 5mm two tilt fringes are produced, which will have no discernable on the output intensity. In an extreme case the two interfering beams could separate to the extent that they no longer overlap to produce a diffraction grating. However, this would require an unrealistically large yaw (approximately 1.5° for the anticipated dimensions of the proposed system).

4.4 Preliminary Interferometer Results

Several experiments were conducted to test the viability of building the instrument. Initially a single axis version was constructed on an optical bench to test the resolution attainable using the device. Once the operation of the single axis device had been proved a two axis test system was built.

4.4.1 Results From The Single Axis System

Figure 4.4.1 shows a schematic of the system used to test the interferometer, with a photograph of the apparatus being shown in figure 4.4.2. A 1200 lines/mm diffraction grating was mounted on a two axis stage. One axis was used to move the grating in its own plane, perpendicular to the lines, while the other axis was used to move the grating towards the prisms. A linear displacement transducer with a resolution of ±0.05μm was placed in contact with the grating substrate to monitor the actual displacement of the diffraction grating. At this first stage of development a helium-neon laser of wavelength 633nm was used. In subsequent experiments a Toshiba 9211 Gallium-Arsenide laser diode operating at a wavelength of 670nm was used.

Once the components had been adjusted to give a good fringe contrast, the grating was moved while the number of cycles of light modulation were counted. The displacement of the grating after every five counts was noted. Table 4.4.1 shows these results while they are displayed graphically in figure 4.4.3.

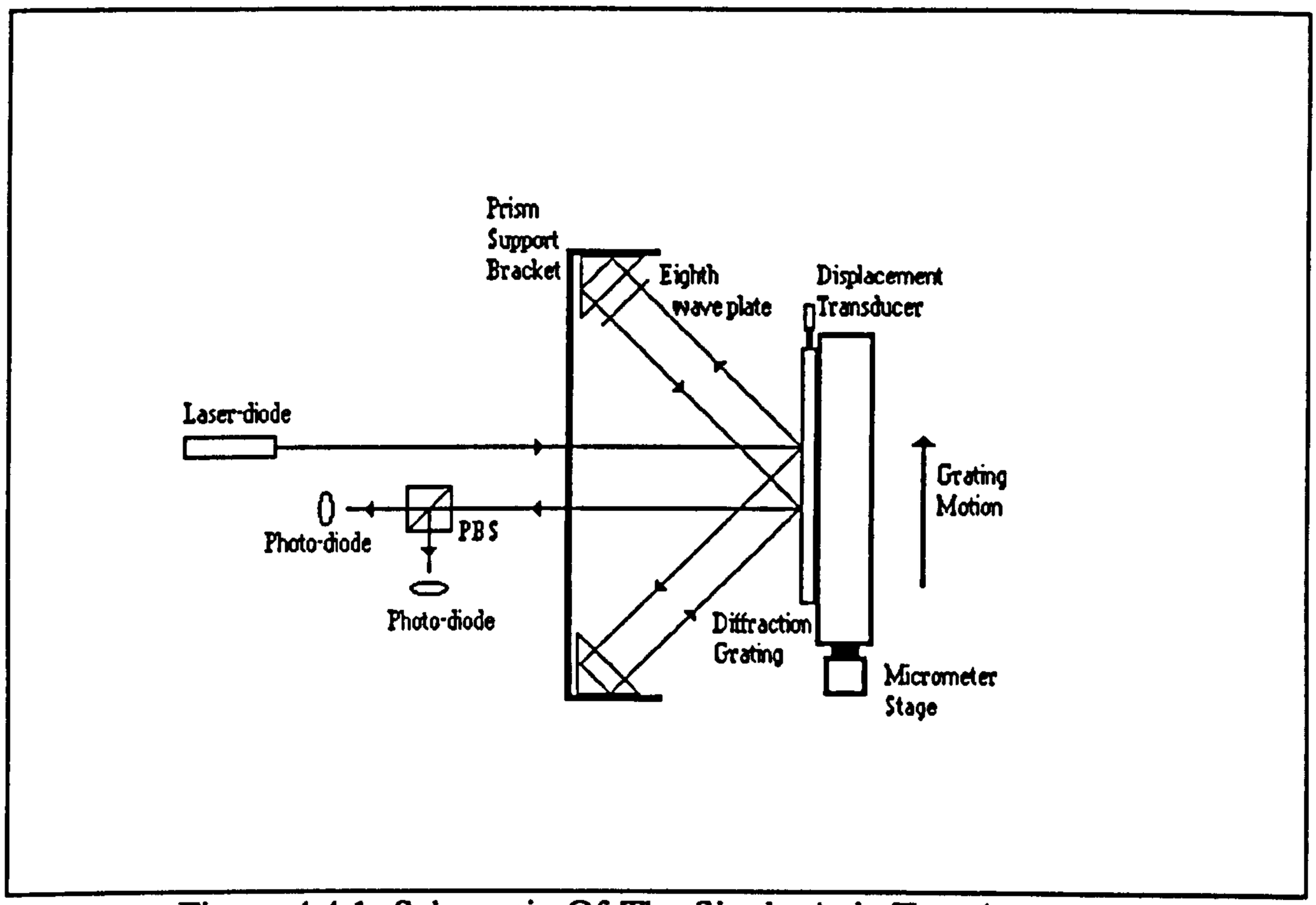

Figure 4.4.1: Schematic Of The Single Axis Test Apparatus

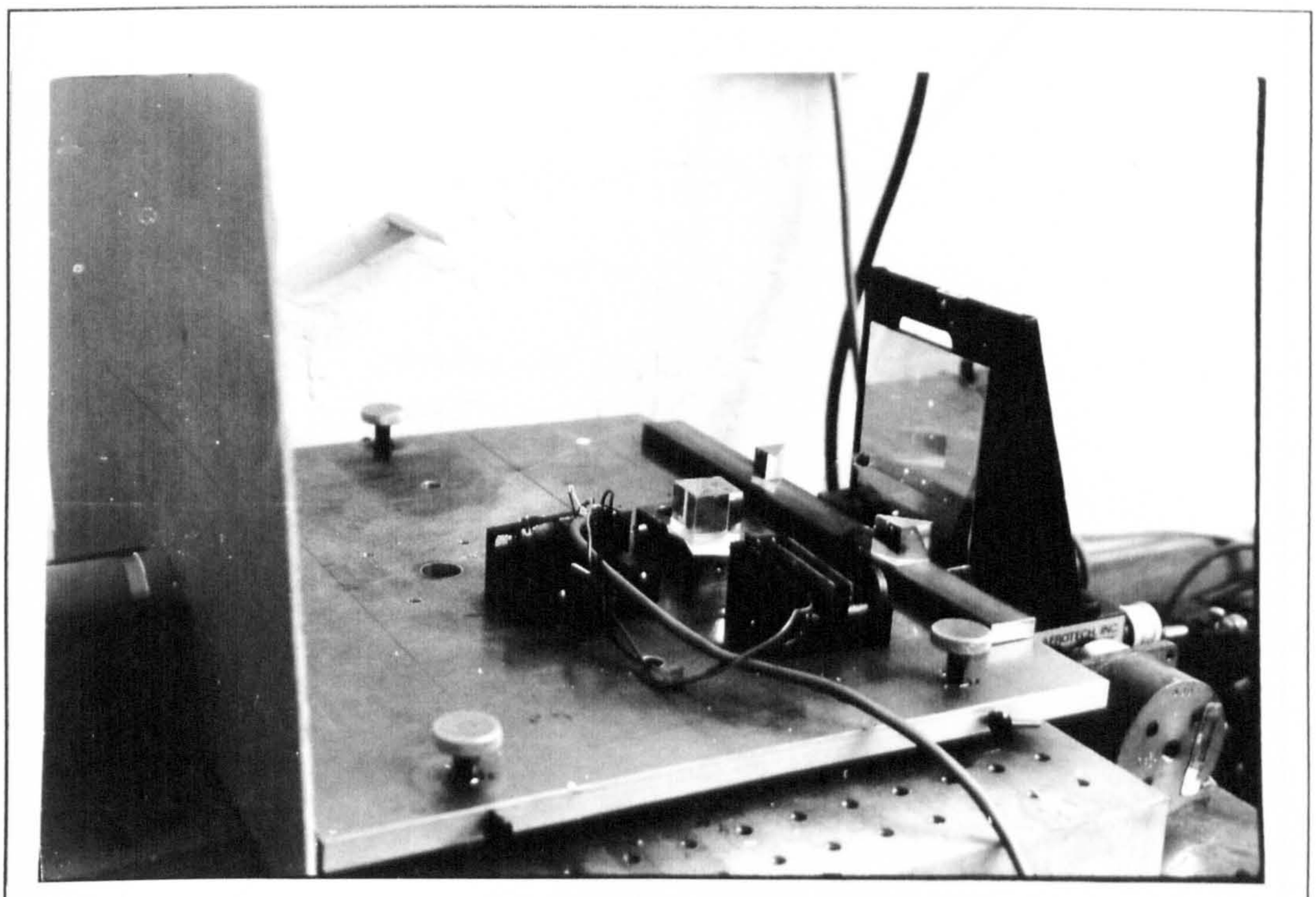

Figure 4.4.2:Photograph Of The Apparatus Used To Test The Instrument

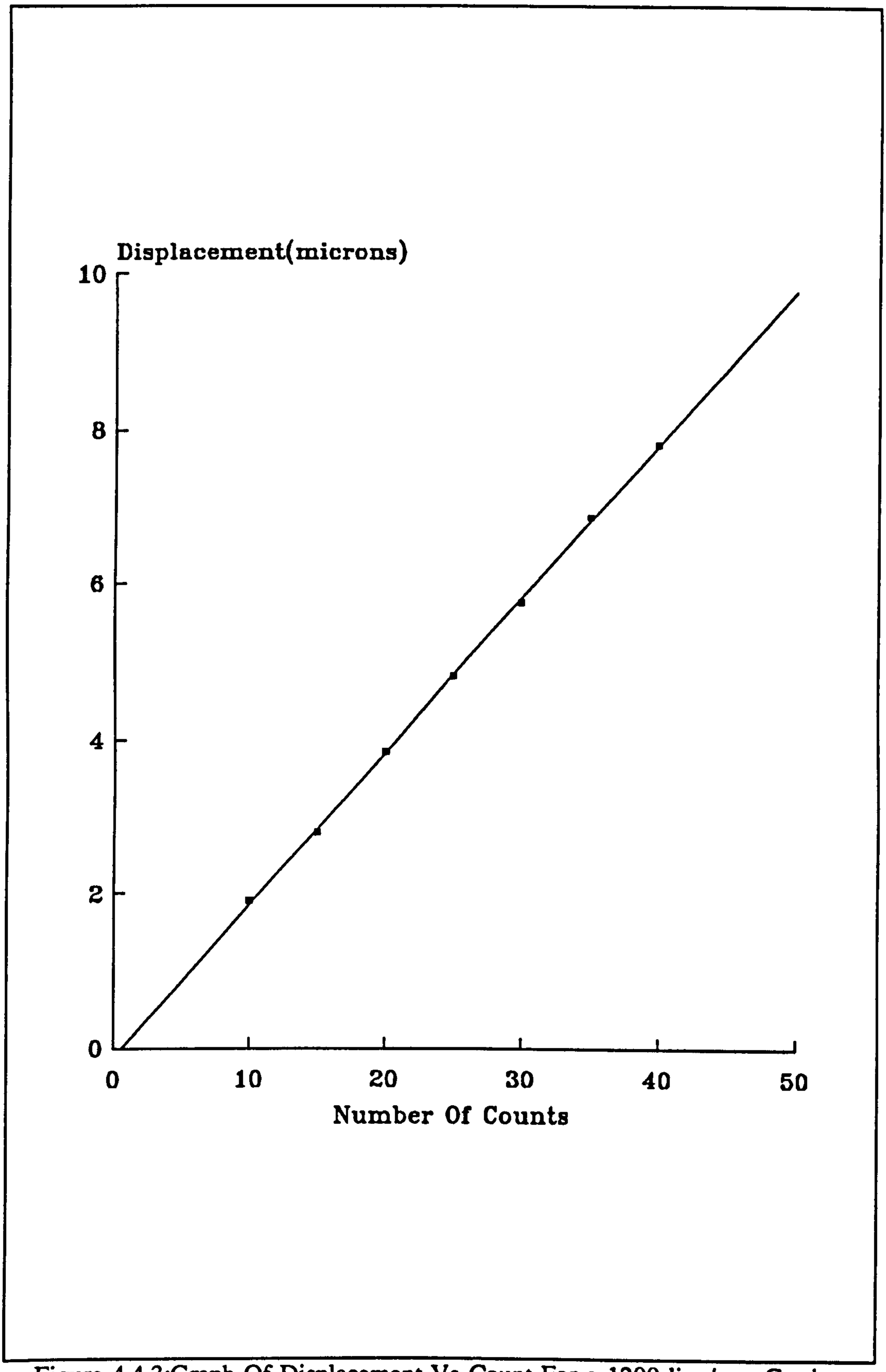

Figure 4.4.3:Graph Of Displacement Vs Count For a 1200 line/mm Grating

Number Of Fringes	Displacement (μm)
10	1.90
15	2.80
20	3.80
25	4.80
30	5.75
35	6.85
40	7.75

Table 4.4.1: Displacement Versus Number Of Fringes For A 1200 Lines/mm Grating

Theoretically, the displacement corresponding to one cycle in the modulation of the output light should be one quarter the pitch of the grating. The gradient of the graph in figure 4.4.3 gives the displacement for one period of modulation. Using a least squares graph fitting program the equation of the line was found to be:-

$$y=0.197x-0.121$$

For perfect agreement with the theory the gradient should be 0.208μm/count. Although experimental results do not agree exactly with the theory, they may be considered to confirm the divide by four nature of the device. The accuracy of the displacement transducer, as well as the possibility of introducing an error due to misalignment of the transducer, explain the slight deviation from theory.

The above experiment was repeated using a 600 line/mm grating. For a grating of this pitch the displacement corresponding to each count is predicted to be 0.416μm. The gradient of the results taken using the new grating, shown in figure 4.4.4 and table 4.4.2, was calculated to be 0.474μm. Once more, the result is as near to agreement with theory as the experimental apparatus would allow.

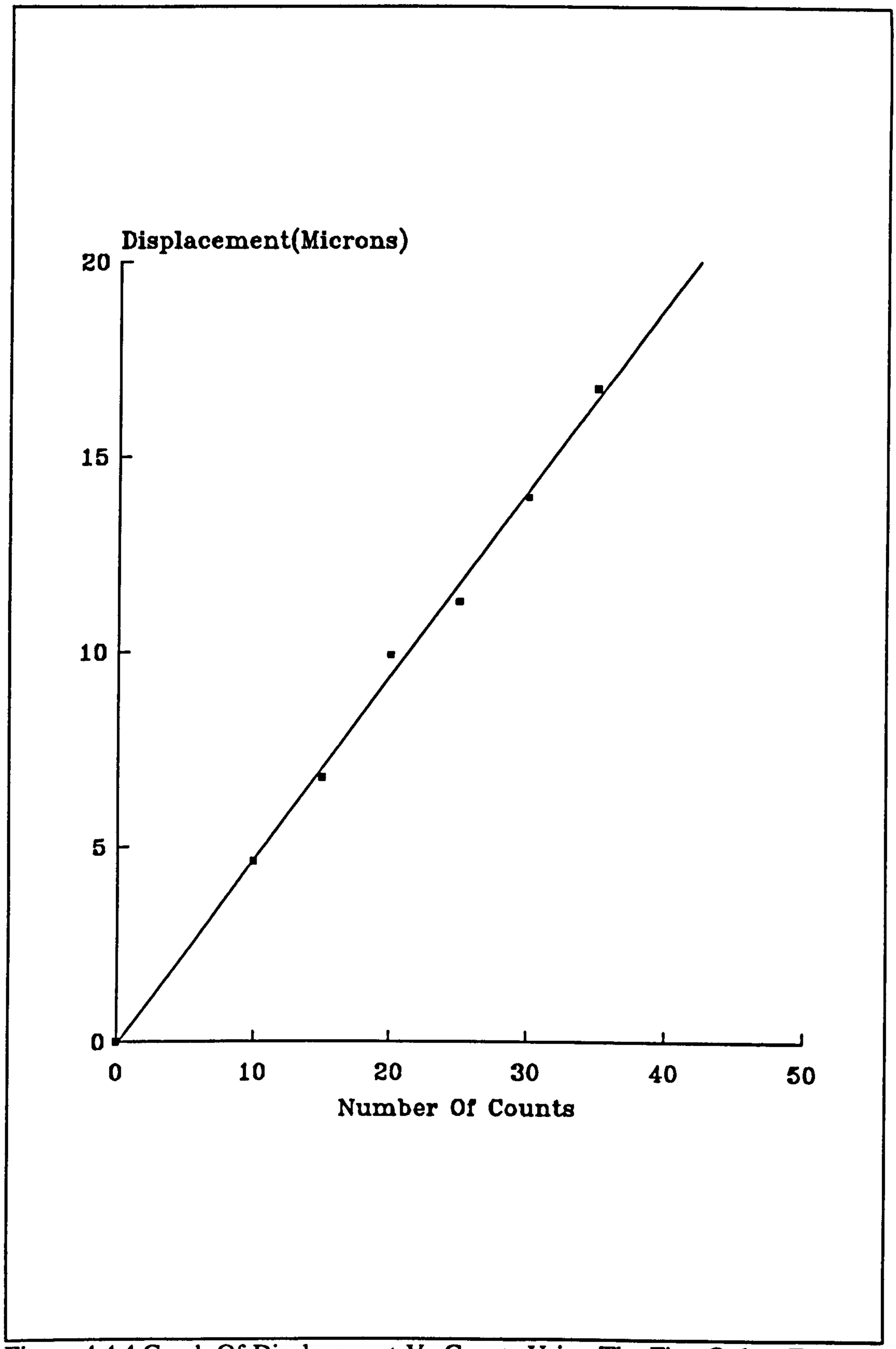

Figure 4.4.4:Graph Of Displacement Vs Counts Using The First Orders From A 600 Line/mm Grating

Number Of Fringes	Displacement (μm)
10	4.55
15	6.85
20	9.95
25	11.40
30	13.95
35	16.60

Table 4.4.2:Displacement Versus Number Of Fringes For A 600 Lines/mm Grating

From the theory of the operation of the interferometer, it is apparent that the resolution of the device can be increased for a particular grating by using higher diffraction orders (ie the pitch of the virtual grating produced is halved when the second order is used). For example, recombining the two second orders of diffraction should half the grating displacement required for one count. To test this aspect of the theory the experimental arrangement was re-arranged to recombine the second order beams from the 600 lines/mm grating. The virtual grating in such a configuration should be four times that of the real grating. Therefore, there should be one count for every movement of one eighth of the grating pitch (0.208μm), equivalent to using a 1200 line/mm grating in the first order mode. However, in practise it is better to use a grating of finer pitch as more lines interact with the beam, so reducing noise due to the contribution of any flawed lines.

The results for the second order experiment are shown in table 4.4.3 and figure 4.4.5.

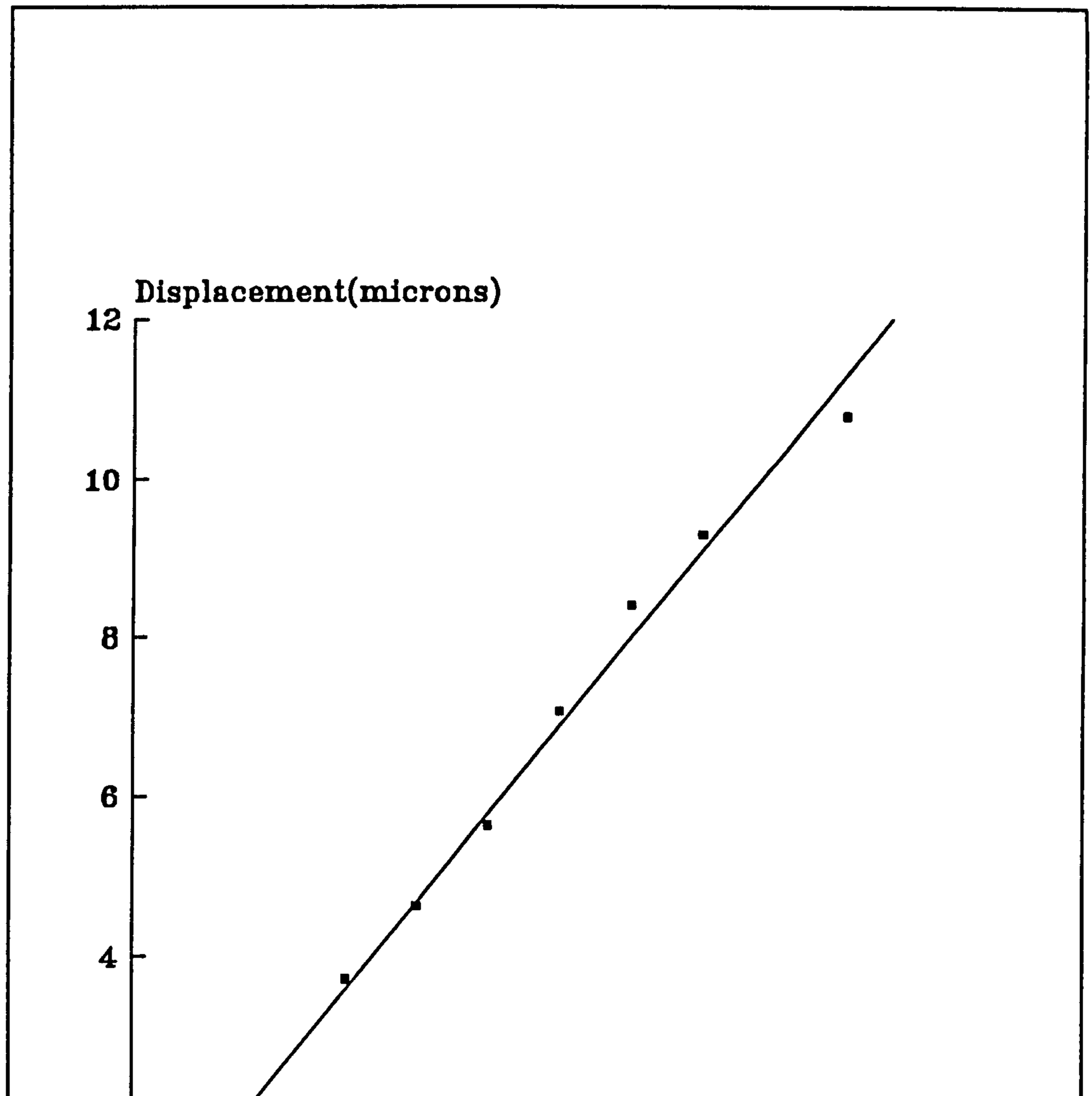

Figure 4.4.5:Graph Of Displacement Versus Counts For The Second Order Configuration Of A 600 Line/mm Grating

Number Of Fringes	Displacement (μm)
15	3.70
20	4.75
25	5.50
30	7.10
35	8.30
40	9.40

Table 4.4.3:Displacement Versus Number Of Fringes For A 600 Lines/mm Grating Used In The 2nd Order

The results from this experiment are higher than predicted, as was the case when the grating was used in the first order. The gradient is predicted to be 0.208μm/count, while the equation of the line was found to be:-

$$y=0.232x+0.055$$

This value for the gradient is approximately half that for the first order experiment, which is what the theory predicts. All of the above results demonstrate the fact that the proposed instrument produces fringes at predictable intervals that are suitable for counting.

4.4.2 Directional Sensing

It is essential that any device used for monitoring the displacement of a microscope stage should be able to count bi-directionally (ie. it should sense whether the stage is moving backwards or forwards). In order to satisfy this condition it is necessary to produce a quadrature signal for interpretation by an electronic fringe

counter.

The next stage of the initial trials was concerned with establishing that it is possible to produce a quadrature signal from the grating interferometer, in the manner outlined in section 4.2.3.

For these initial tests the eighth-wave plate was manufactured by splitting discs of mica. The discs were split by placing a sharp blade into the material, and then putting a few drops of distilled water between the two separating sheets. The two sheets then simply slide apart to give two thin discs of mica. Each time that a sheet was split its ability to act as an eighth wave plate was tested using the apparatus illustrated in figure 4.4.6. Plane polarised light passes through the mica, strikes a prism, and is transmitted by the mica for a second time. The beam is then passed through a rotating polariser onto a photo-diode whose output is consistently monitored. The mica sheet was slowly rotated until the output signal was most consistent. If the output of the photo-diode remains constant as the polariser rotates, the mica is of the correct thickness, and is at the correct orientation relative to the polarisation of the input light to behave as an eighth wave plate. Once a suitable piece of mica had been cleaved it was placed in front of one of the prisms as shown in figure 4.4.1.

The modulated light returning from the grating surface is split by a polarising beam splitter. If the polarisation elements of the interferometer have been correctly orientated there should be a 90° phase difference between the two beams emerging from the beam splitter.

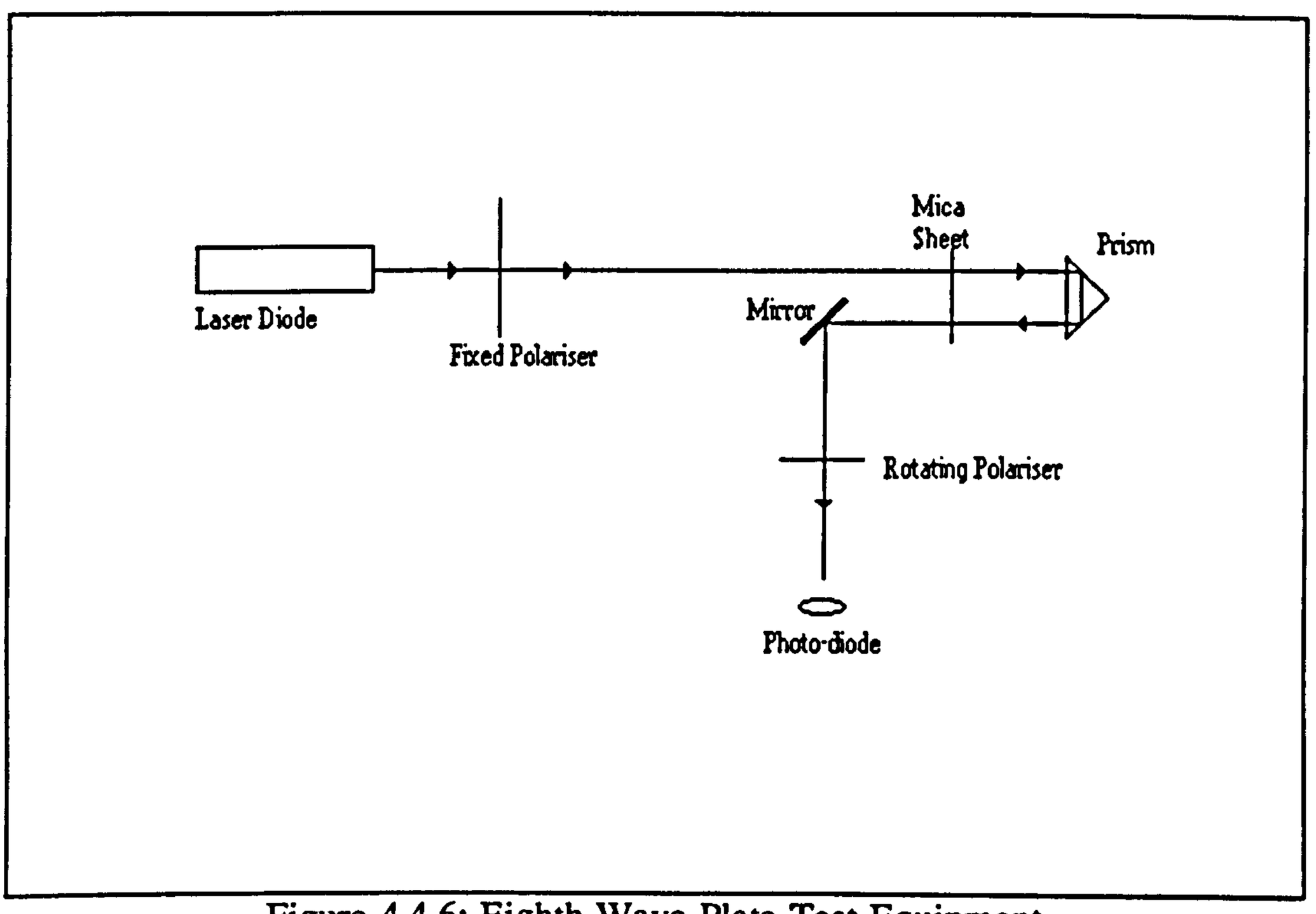

Figure 4.4.6: Eighth Wave Plate Test Equipment

To test the phase difference a BPX-65 photo-diode was placed in each of the output beams. The two electrical signals produced were amplified and fed into the two channels of an oscilloscope which drive the x-y deflector plates. If a quadrature signal has been produced by the interferometer, a circular Lissajou figure should be described on the oscilloscope as the grating is moved.

The Lissajou figure produced by moving the grating is shown in figure 4.4.7. As may be seen the output from the instrument is in the form of a quadrature signal. If the direction of motion of the grating is changed then the direction of rotation of the Lissajou figure also changes. Hence the output is suitable for the monitoring of a microscope stage.

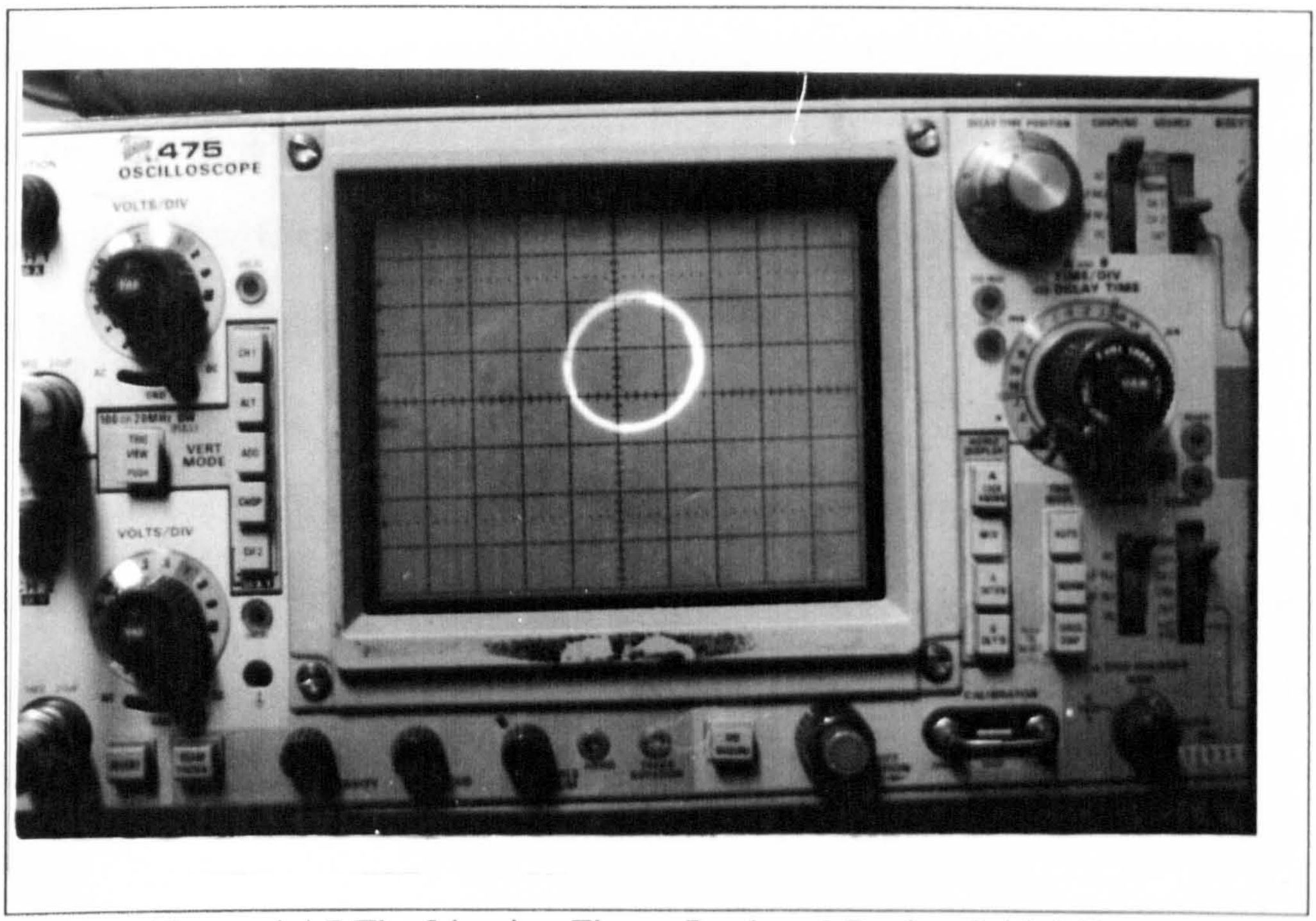

Figure 4.4.7:The Lissajou Figure Produced During Initial Tests

4.4.3 The Trial Dual Axis System

Having established that the novel system can be implemented as a single axis system, it only remains to test whether it is practical to develop a two-axis device. A plate to hold the two sets of prisms and detectors was built in the NPL workshops. The plans for these parts are shown in appendix 3.

Each component was attached to the base plate by two bolts passing through slits in the plate. Crude motion of all of the components can be achieved by sliding them along the slits. Small screws at each corner of the prism holders allow for a small amount of rotation relative to the base plate. Figure 4.4.8 is a photograph showing a prism holder with its simple rotary adjustment screws.

A structure to hold all of the components was constructed from Dexion as illustrated in figure 4.4.9. As can be seen from the photograph the structure allowed for the use of a two axis stage, so that simultaneous motion along two axes could be produced.

The main purpose of this experiment was to verify that correct polarisation states could be obtained simultaneously on both axes of the interferometer to give two independent quadrature signals. It proved possible to achieve this objective with the procedure described above. The experiment also allowed for the first use of one of the 1100 line/mm crossed gratings that were manufactured for the interferometer. Unfortunately, the Dexion structure did not prove stable enough to take any meaningful measurements of displacement against the number of fringes.

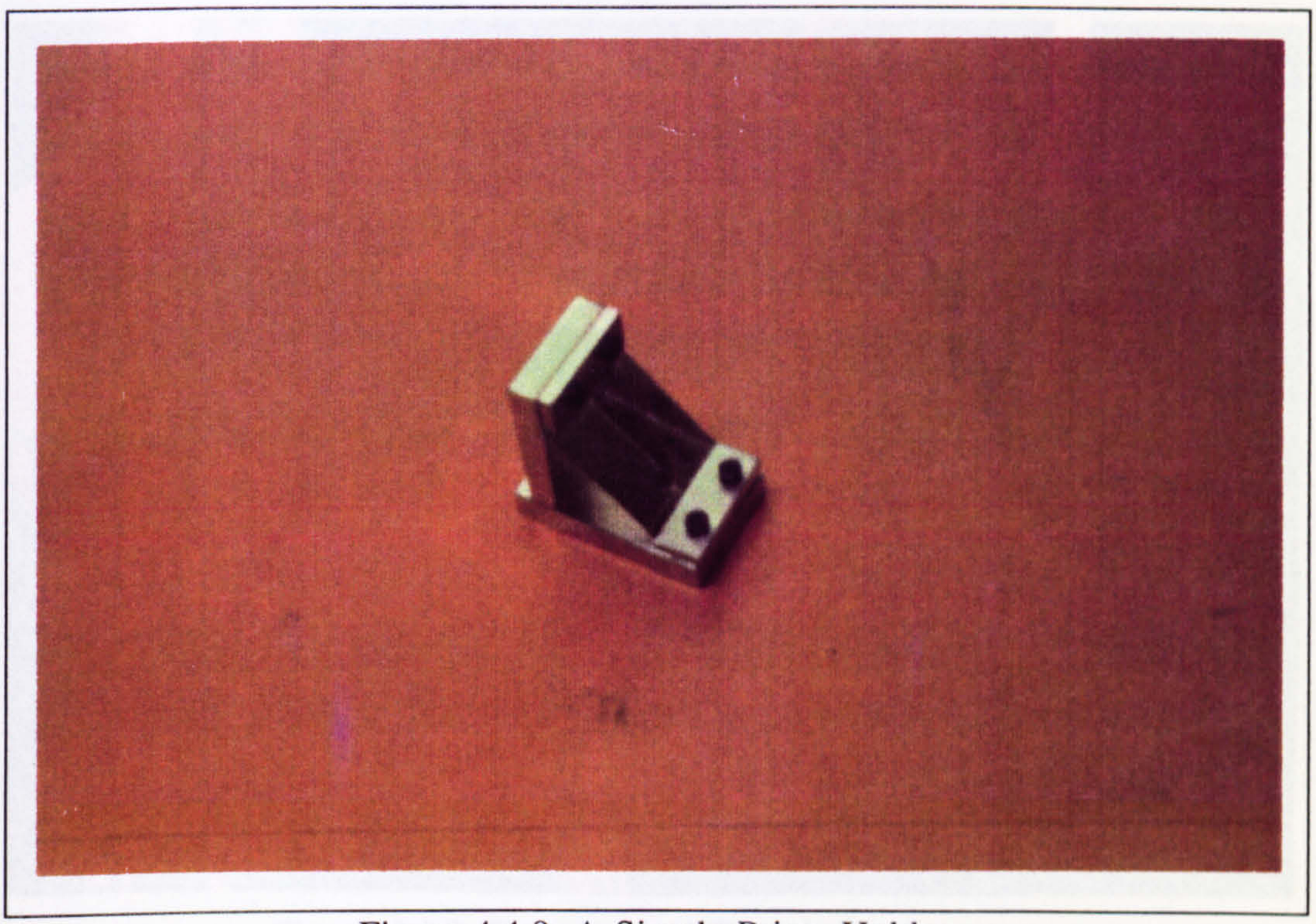

Figure 4.4.8: A Simple Prism Holder

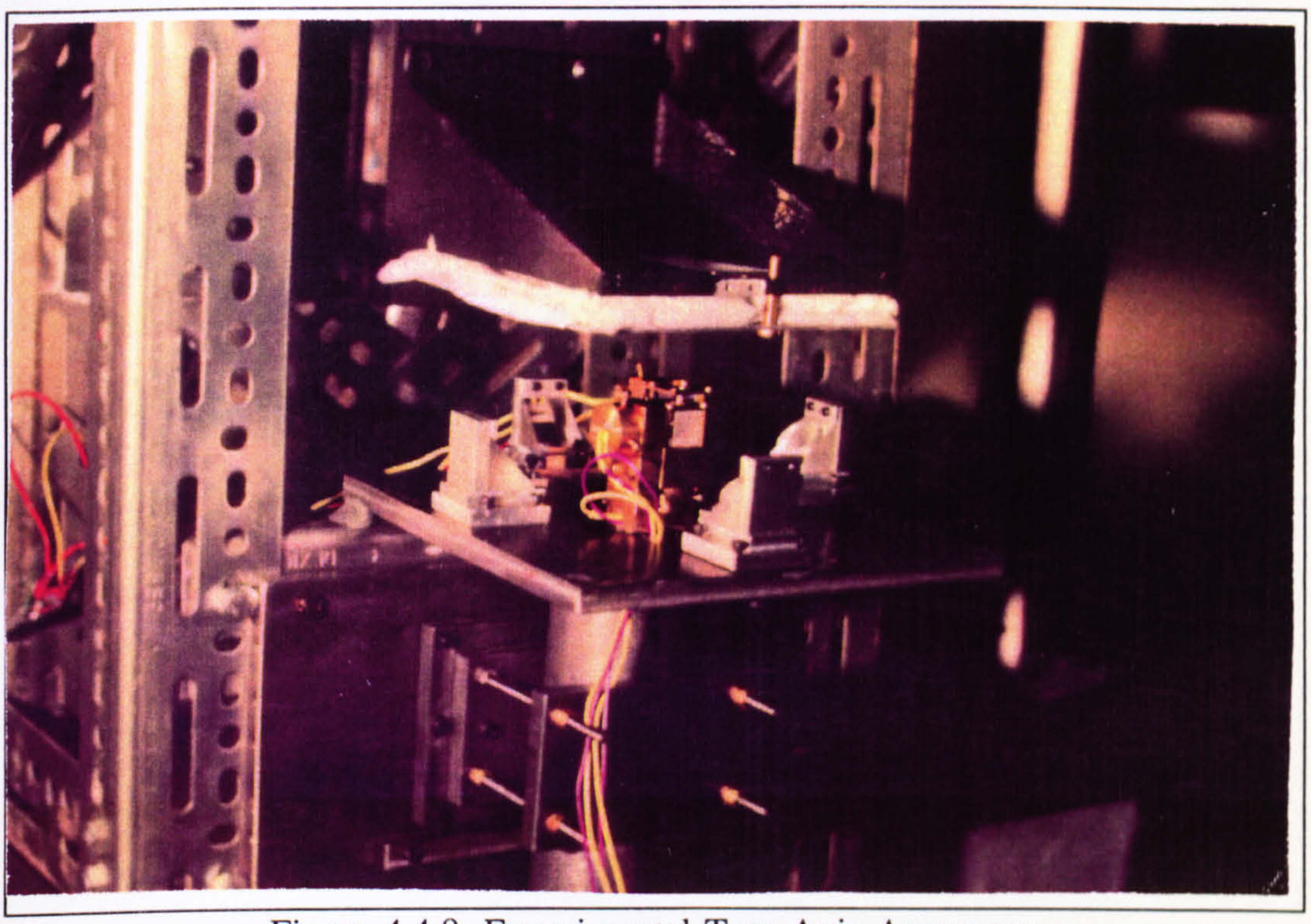

Figure 4.4.9: Experimental Two Axis Apparatus

Having demonstrated that the interferometer could potentially work as a two-axis system, it was decided to proceed with the installation of the measurement system on Gandalf's microscope stage. The final implementation is described in Chapter 5.

5. INSTALLATION OF THE INTERFEROMETER

5.1.1 Initial Installation

The same components that had been used to hold the prisms, laser diode and detectors in the preliminary two axis test were re-assembled on the microscope (known as Gandalf). A kinematically mounted plate, a photograph of which is shown in figure 5.1.1, was designed to hold the diffraction grating. Figure 5.1.2 is an overall view of Gandalf.

Naturally, the alignment of the optics proved much more difficult on Gandalf than had been the case on the test frame. After much adjustment fringes were obtained from both axes. However, the fringe contrast was very poor in comparison to that achieved on the one axis system. The lack of contrast arose because tilt fringes were produced due to the real and virtual gratings not being parallel. The crude adjusters, fitted to the prism holders, did not allow for the prisms to be aligned with sufficient precision to overcome this problem. Therefore, a more elaborate component adjustment system was designed.

5.1.2 The New Alignment System

A set of four kinematically supported prism holders that allow each prism to be rotated about two axes with greater sensitivity were designed. The rotation is achieved by having two round ended screws pushing against a spring loaded plate to which the prism is rigidly clamped. As with all kinematic location devices there are three points of contact; one screw pushes against a flat, the other into a groove, and in this case the

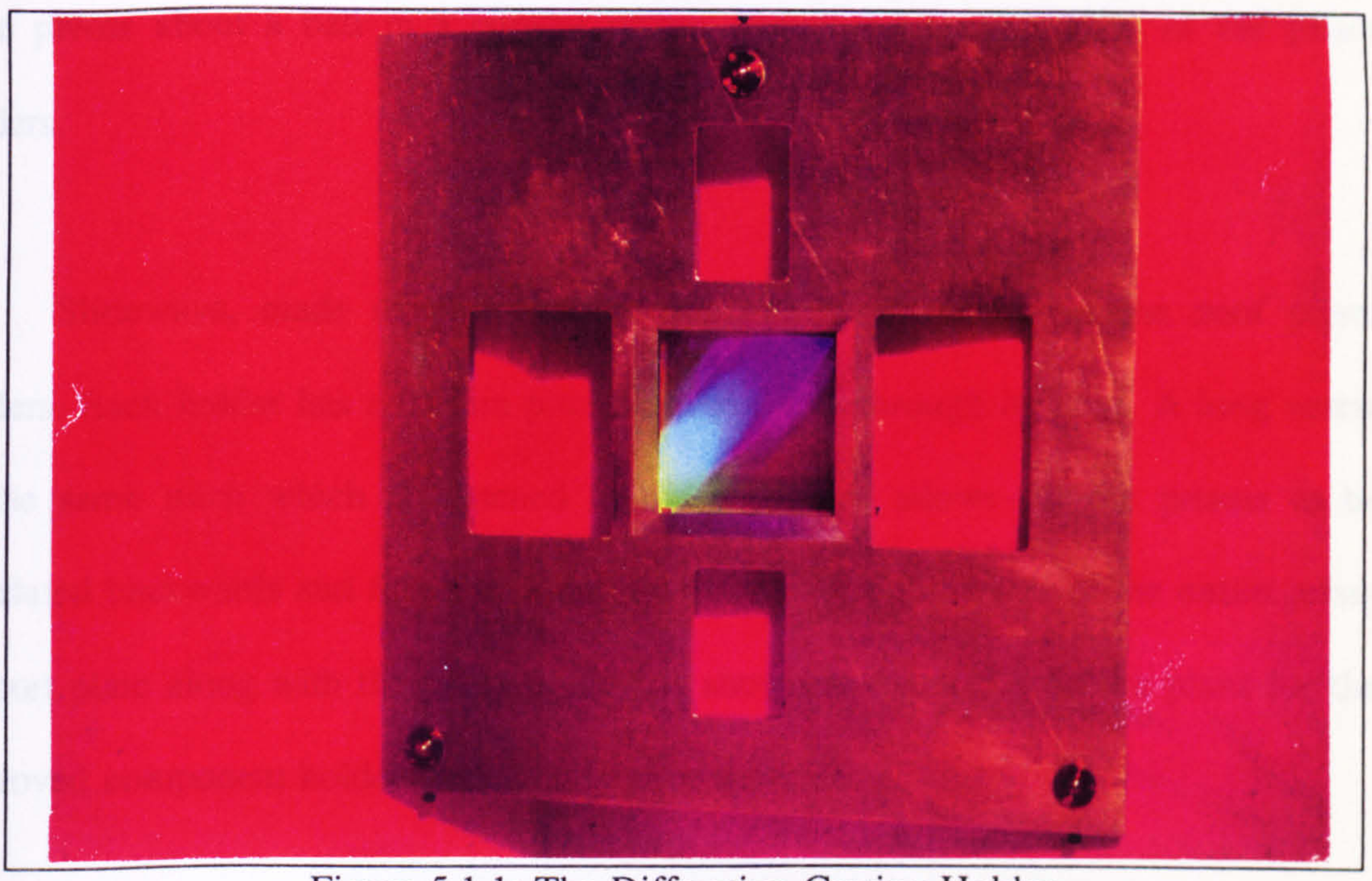

Figure 5.1.1: The Diffraction Grating Holder

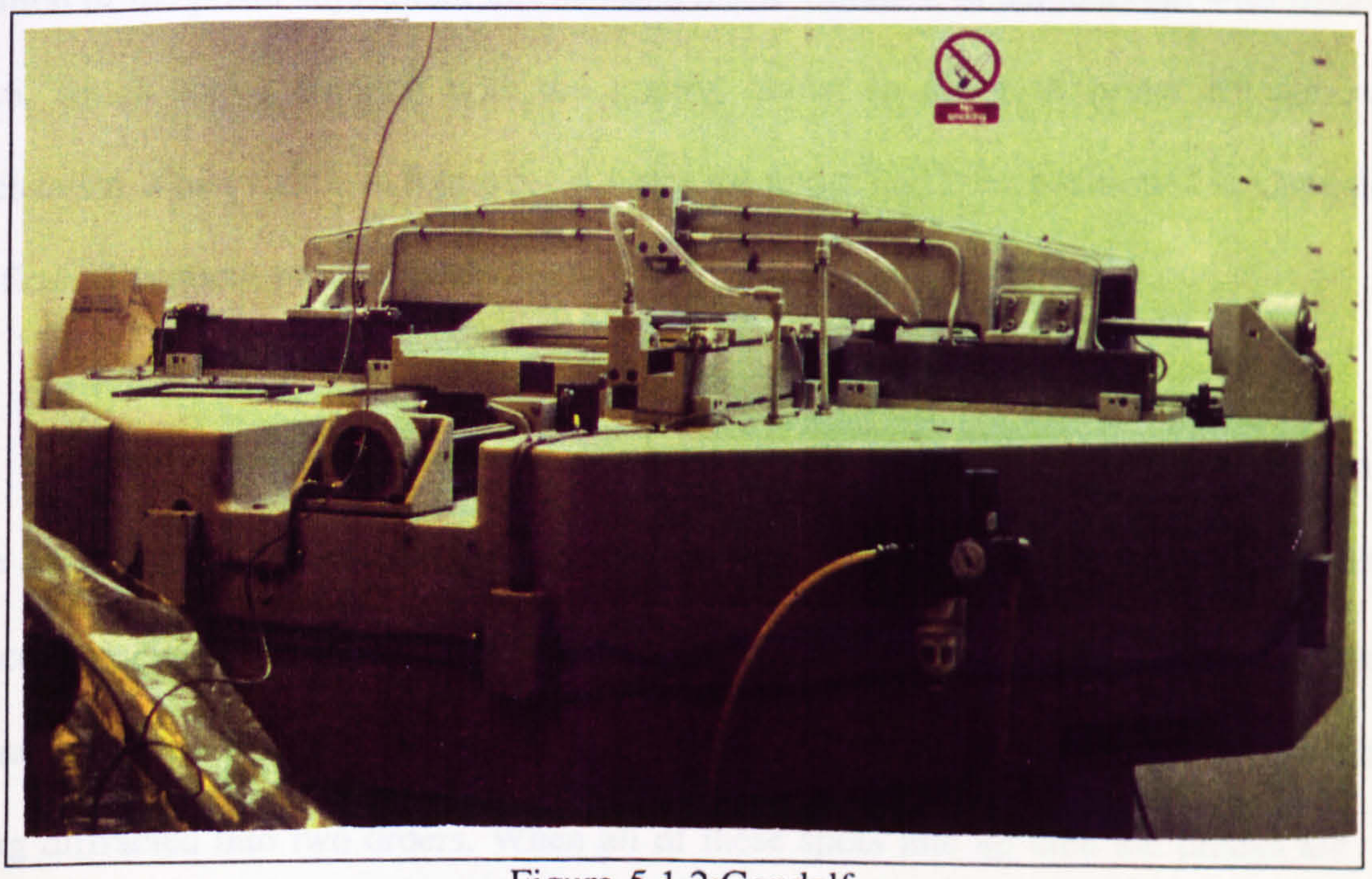

Figure 5.1.2:Gandalf

plate pivots about a ball in a conical recess. Figure 5.1.3 shows one of the prism holders.

Slideways, made of phosphor-bronze, were constructed for the roof prism holders. Each holder has a 0.5mm pitch threaded hole through its base. A long screw of the same pitch which is fastened to the base-plate allows for the prisms to be translated backwards and forwards along two tracks. A photograph of the entire prism support plate along with the prism holders is shown in figure 5.1.4. The plans for the improved component holders are contained in appendix 3.

5.1.3 The Final Installation

The new components were assembled and installed on Gandalf. To allow access to the prism adjustment screws three large apertures were cut in the grating holder. Some idea of the access difficulties may be seen in figure 5.1.5, which shows the location of the prism adjustment mechanisms inside Gandalf, in conjunction with figure 5.1.6, which shows Gandalf with the grating holder in place. A prism adjustment mechanism is just visible in figure 5.1.6. Once the optics had been positioned in Gandalf the fine adjustment process began.

The angular alignment of the prisms was greatly simplified by the new adjusters. One advantage of the interferometer system is that it is relatively easy to judge when the components are at approximately the correct orientation to produce fringes. Several diffraction spots are produced on the base plate due to reflected light from the prisms being diffracted into two orders. When all of these spots line up then the prisms are

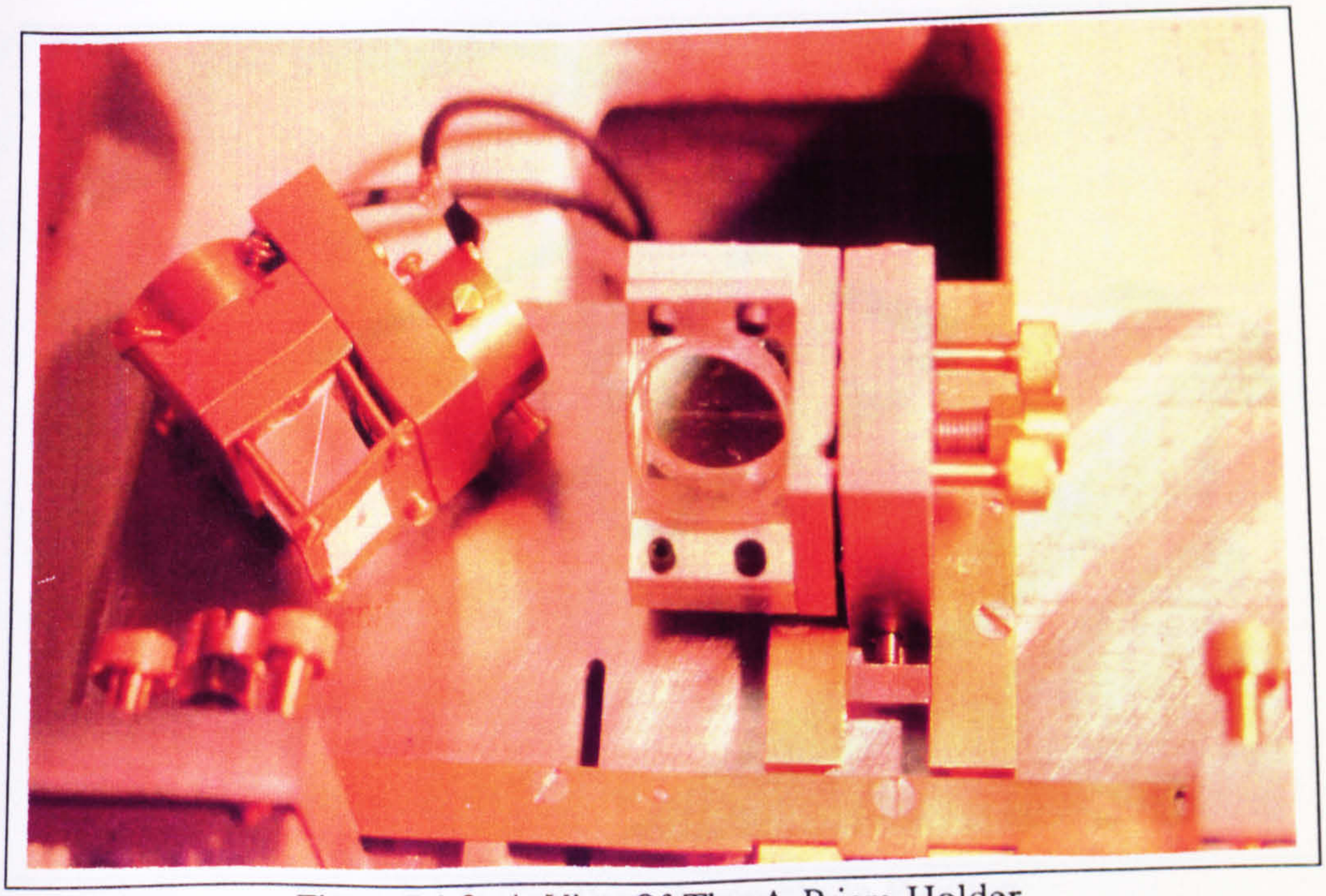

Figure 5.1.3: A View Of The A Prism Holder

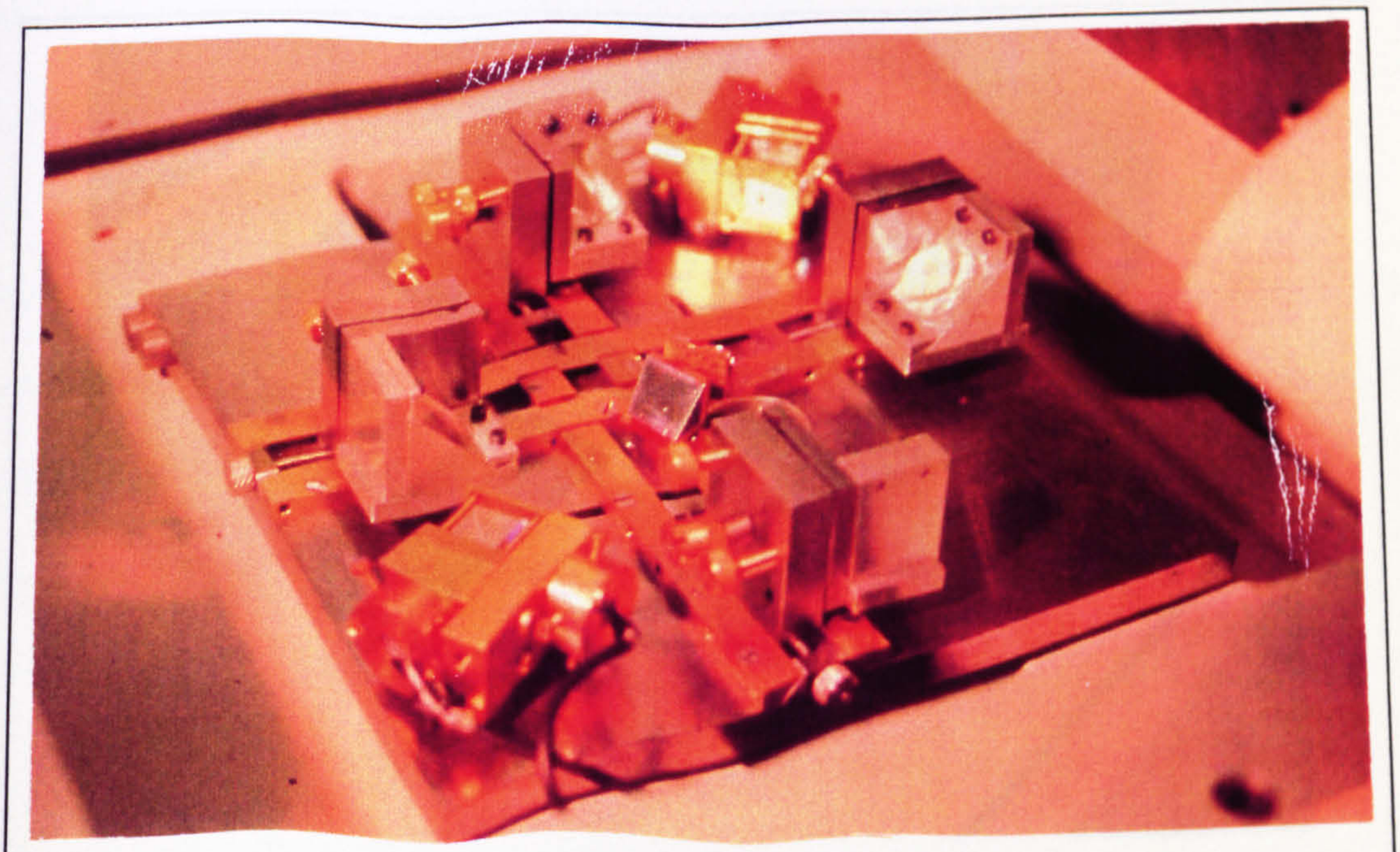

Figure 5.1.4: The Base Plate And Optical Components

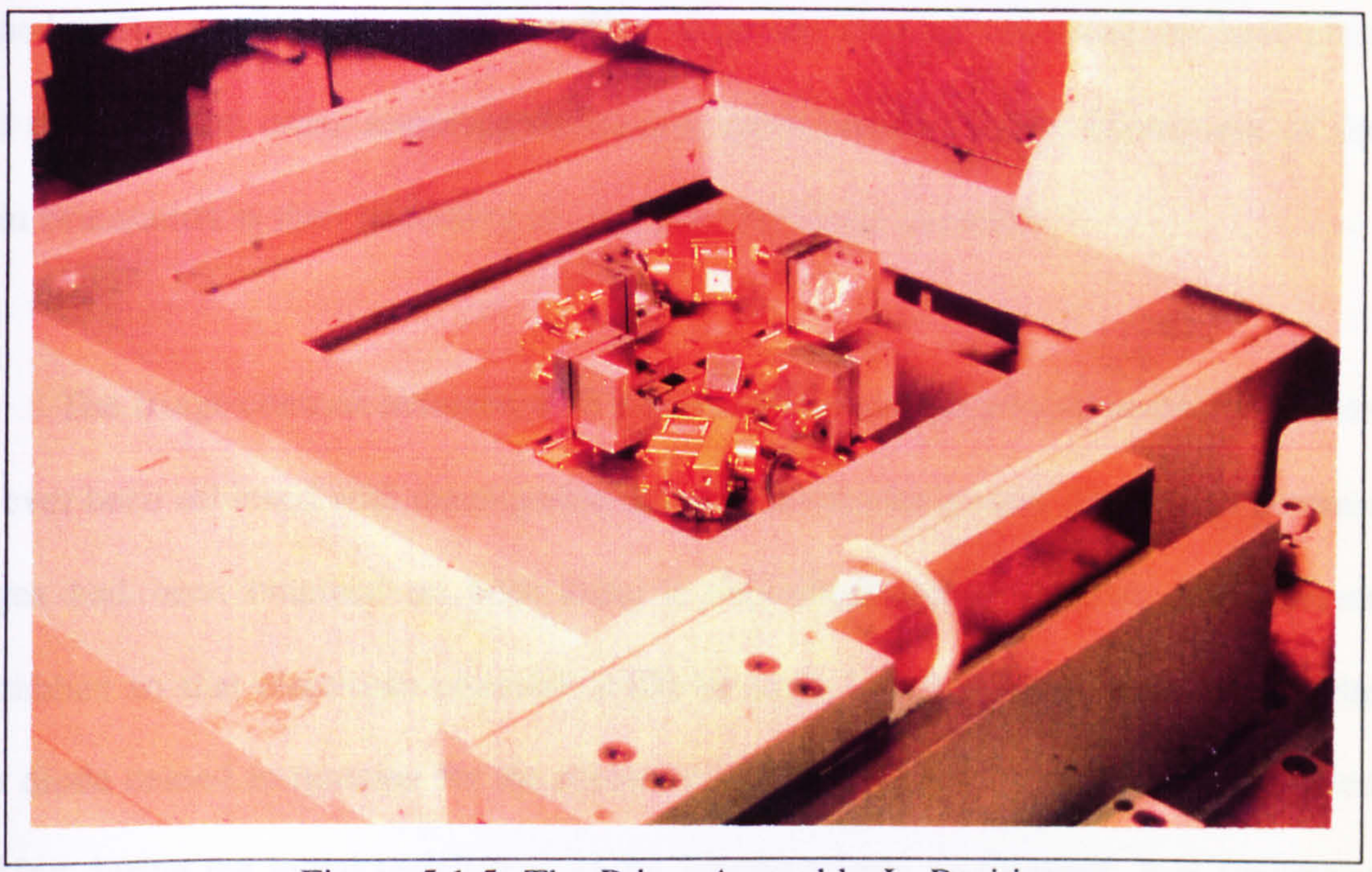

Figure 5.1.5: The Prism Assembly In Position

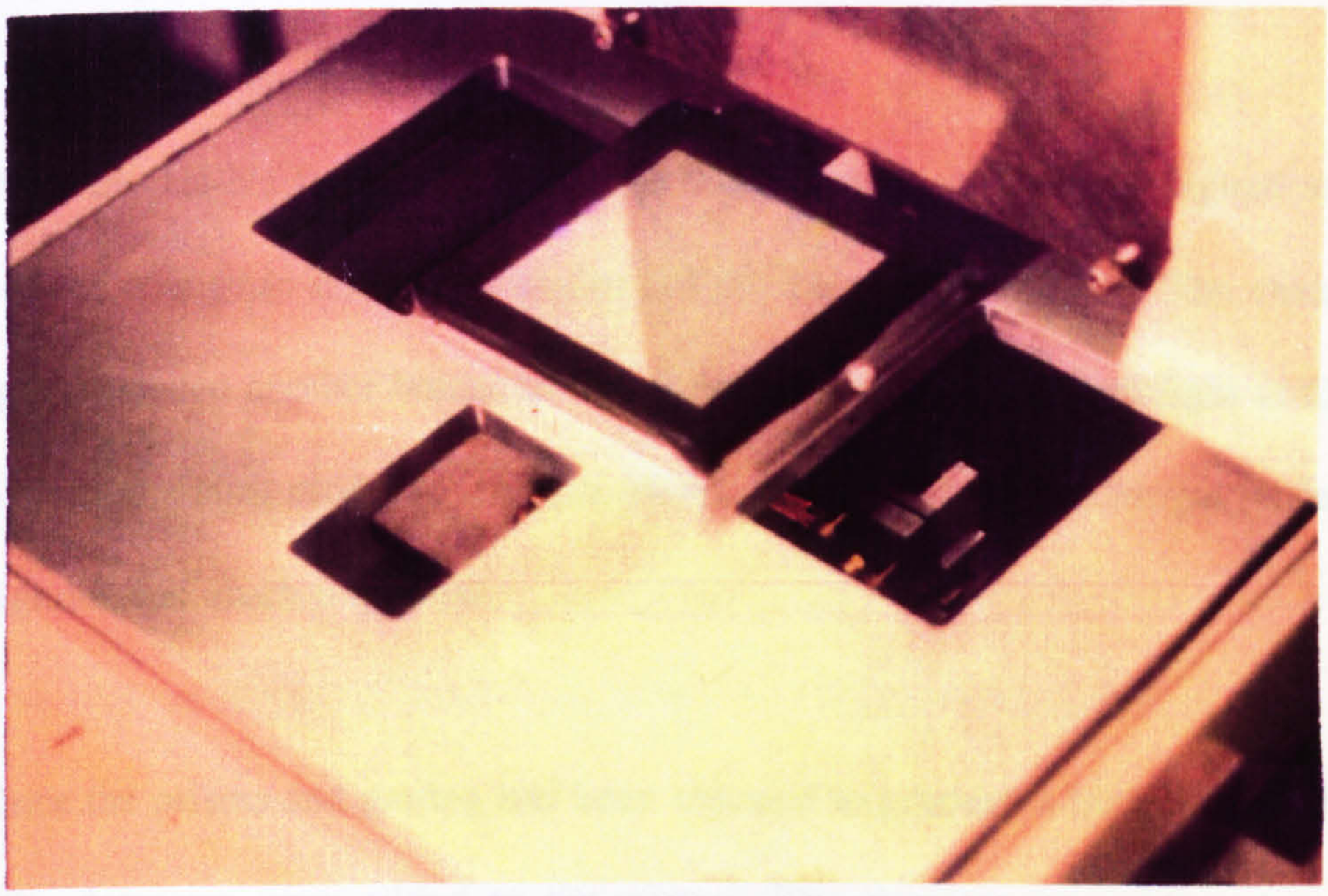

Figure 5.1.6: The Grating Holder In Place

aligned well enough to obtain fringes. The prisms are then moved along the base plate until the two first order returning diffraction spots overlap. Slight adjustment of the prism orientation is then necessary to optimise the fringe contrast.

The fringe contrast obtained with the new prism holders proved much better than had ever been achieved with the experimental interferometer system. Once high contrast fringes had been obtained on both axes, it only remained to position the detector assemblies so that electronic counters could be used. Unfortunately, at this point the laser diode ceased to function for the second time. The original laser diode had stopped working during the initial installation of the interferometer on Gandalf. It is important that a scientific instrument should be robust and reliable, so when the second diode developed a fault a decision was made to replace it with a Helium-Neon laser (wavelength 633nm). When the plans were made for the construction of the base plate provision was made for the use of a Helium-Neon laser as an alternative to the laser diode, so the replacement was only a minor set-back.

With the He-Ne laser in place the optical components were re-aligned to take account of the change in diffraction angles (44°08' rather than 48°29'). The change in wavelength produced another bonus, in that the eye is more sensitive to light at 633nm than at 670nm, the laser diode wavelength. Hence the visibility of the fringes during the initial alignment is much improved.

Once the prisms and grating had been adjusted to produce a high contrast fringe pattern, the detectors were added to the system. The detector assemblies that were

designed for the original base plate were used. However, the effect of stage motion aberrations, such as pitch, roll and yaw, is reduced in this system by having the output beam as near as possible to the input beam. The size of the assemblies meant that there would have to be a minimum gap between the input and output beams of 10mm, in order to position the detectors as originally planned. A simple solution to this problem was implemented. A small mirror, angled at 45° to the base plate, was placed in each of the output beams so as to reflect each beam parallel to the plate surface. It proved possible to reduce the beam separation to the input beam width. Three small magnets were glued to the side of each of the detector assemblies to allow the detectors to be mounted horizontally.

5.1.4 Addition Of The Electronics

The output from each of the photodiodes on both axes were fed into an amplifier circuit of the design shown in figure 5.1.7. The amplified pairs of outputs were each fed into an oscilloscope so as to produce a Lissajou figure. To produce a quadrature signal it is necessary for the polarisation direction of the input beam to be at the correct angle relative to the one-eighth wave plates that are fixed to the prisms. Rather than rotating the entire laser to change the polarisation angle, hence causing the whole system to need re-aligning, it is more practical to use a half wave plate to rotate the polarisation state. Plane polarised light incident at angle θ to the fast axis of the half wave plate is rotated so that the angle of polarisation makes an angle 2θ with the fast axis on output. Hence, rotating the half wave plate changes the orientation of the plane polarised light. The half-wave plate was rotated until a circular Lissajou figure was obtained on each oscilloscope.

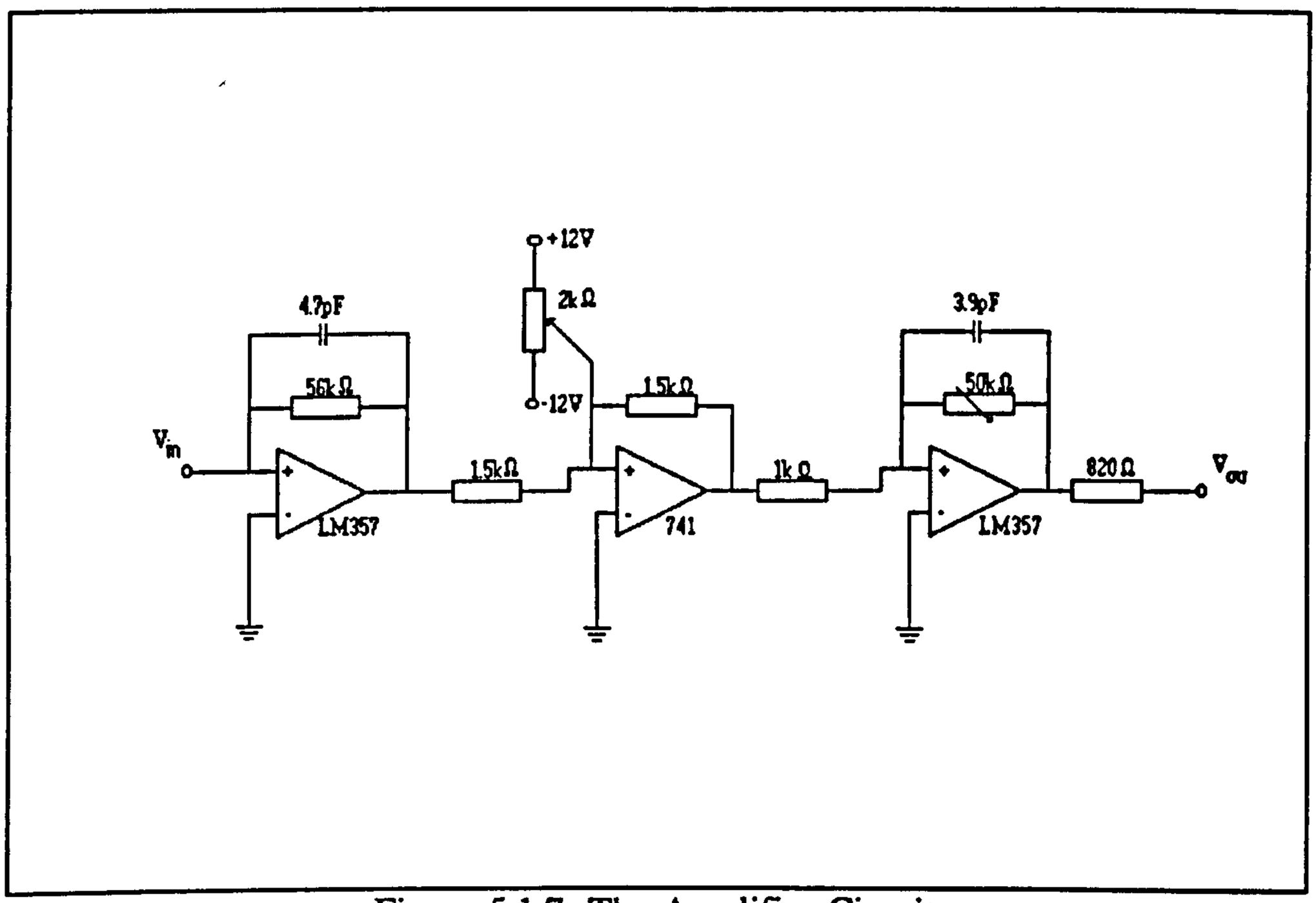

Figure 5.1.7: The Amplifier Circuit

The quadrature signal from each axis was fed into a Unimetrics counter with a divide-by-four capability. A count is recorded by the counter each time one of the two photodiode signals that produce the quadrature signal, crosses the zero volts level.

5.2.1 Calibration Procedure

When any new measurement system is developed it is necessary to calibrate it against an instrument whose performance is known to a higher accuracy than that required for the new application. Both axes of the new device were calibrated in turn against a Hewlett-Packard linear interferometer. While one axis was being calibrated the other was held stationary. The Hewlett-Packard instrument is based on a Michelson interferometer, and has a resolution of 10nm.

Ideally, the measurement centres of the two interferometers should be coincident to avoid any misreadings. Unfortunately, it did not prove possible to satisfy this condition in this case. The measurement points lay approximately in the same plane, so meeting the Abbé criterion. However, as is shown schematically in figure 5.2.1, the measurement point of the Hewlett-Packard interferometer was offset by approximately 10cm from that of the new system. Initially, problems with air turbulence reduced the stability of the commercial instrument to an unacceptable level. This was overcome by shielding its beams with piping. The new system is not susceptable to this problem owing to its short pathlengths, and shielding effects of the prism base plate and diffraction grating that lie relatively close together.

The x-axis was calibrated using the following procedure. The microscope was

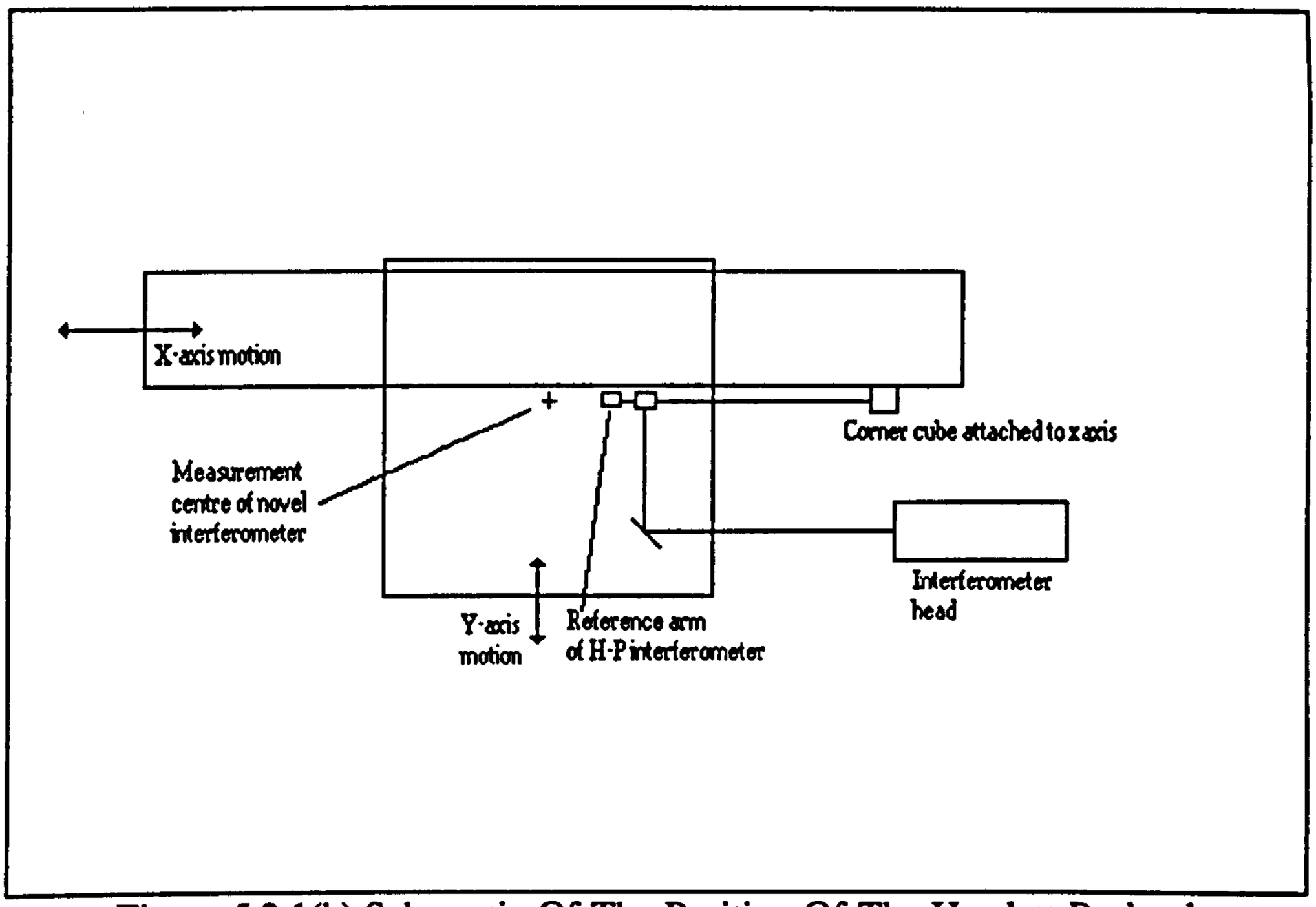

Figure 5.2.1(b):Schematic Of The Position Of The Hewlett-Packard Interferometer Relative To The Instrument Under Calibration

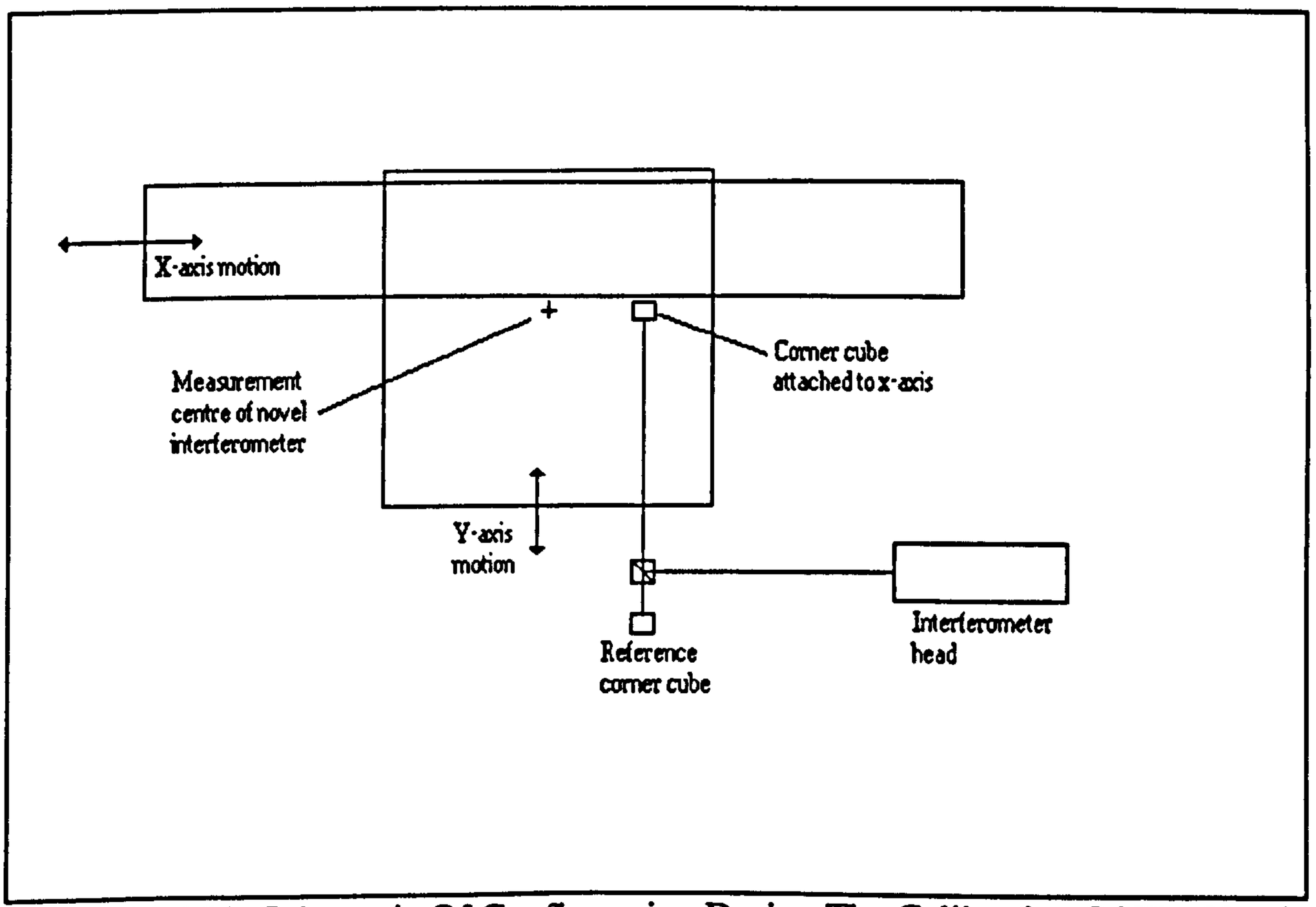

Figure 5.2.1(b): Schematic Of Configuration During The Calibration Of The Y-axis

moved to one extreme corner of its range. Steps of approximately 1mm were made along the x-axis until the end of the microscope travel was reached. Both the moiré and Hewlett-Packard interferometer systems were read at each step. To check for any hysteresis in the system, the stage was then returned to its original position in steps of 1mm. Having completed a run along the x-axis, the y-axis was then moved by approximately 5mm and the x-axis calibration repeated. This process was repeated until the y-axis reached the end of its travel.

Once the x-axis calibration was complete, the configuration of the Hewlett-Packard interferometer was adjusted to monitor the y-axis. Again, the calibration started in an extreme corner of the stage motion, with movements of 1mm being made to the axis being calibrated. The x-axis was advanced by 5mm after each y-axis calibration run.

5.3.1 Results From The Calibration

If the Hewlett-Packard interferometer and the novel transducer both behaved in an ideal manner there would be a linear relationship between the displacement shown on the commercial instrument and the number of counts produced by the new device. The gradient of the graph produced by plotting these two quantities against each other indicates the number of counts produced by the new interferometer per millimetre of movement. Figure 5.3.1 shows the results obtained from a typical run along the x-axis. A gradient of 17.647 counts per micron, with a standard deviation of 0.0123 counts per mm, was calculated from the data using a least squares line-fitting routine. The predicted gradient for an exact 1100 lines/mm grating is 56.8nm/count, as opposed to 56.7nm which is obtained by taking the reciprical of the best fit gradient. All of the runs along

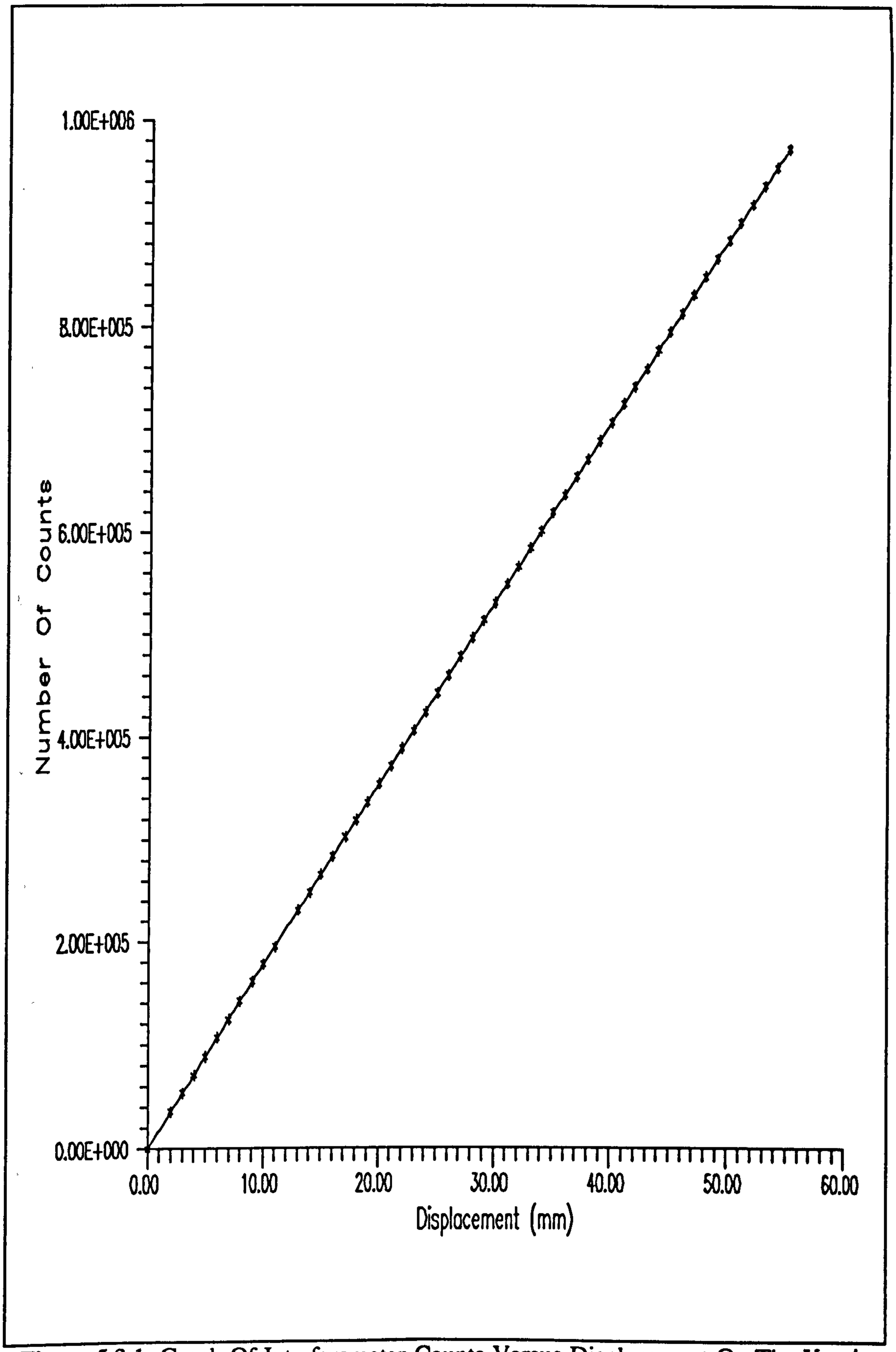

Figure 5.3.1: Graph Of Interferometer Counts Versus Displacement On The X-axis

the x-axis produced the same value for the displacement per count. The slight difference can be interpretted as the diffraction grating having 1103 lines/mm instead of 1100. This agreement indicates that on average, taken across the full range of the stage motion, the two instruments show a consistent relationship. However, when a high precision instrument is being calibrated it is important to consider the agreement on a smaller scale. The residual displacement of data point i (r_i) from the best fit line was calculated using the following formula:-

$$r_i = mx_i + c - y_i \qquad 5.3.1$$

Where m and c are the best fit line gradient and constant respectively, x_i is the number of counts at data point i and y_i is the displacement at point i.

Plots were made of r_i against x_i for each set of data. Figure 5.3.2 is a typical example of how the residuals varied across the range of the stage. A return trip along the same line produced the results shown in figure 5.3.3. The two figures lack consistancy because the microscope stage could not be driven sufficiently precisely to return it to the same point. From the available data it is impossible to determine whether or not hysteresis exists in the system, again, because it was impractical to reposition the stage at exactly the same points on the return trip as on the outward motion. There is no reason to believe that there should be any hysteresis but the graphs cannot be taken as conclusive proof that none exists at the high level of accuracy that this device was intended to perform at.

Figure 5.3.4 shows the residuals results obtained from a run along the y-axis. In

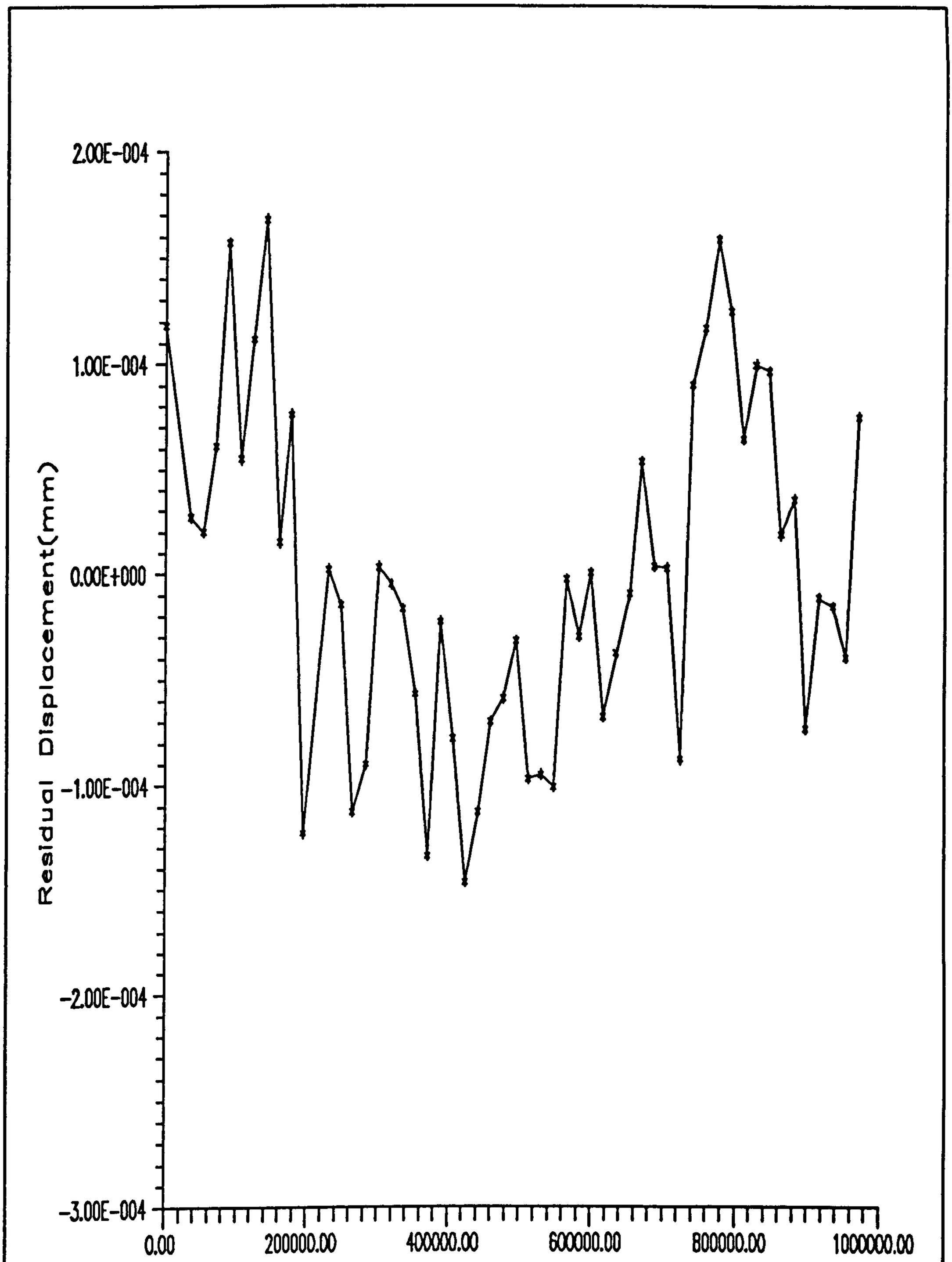

Figure 5.3.2:Plot Of Residual Displacement For Motion Along X-axis

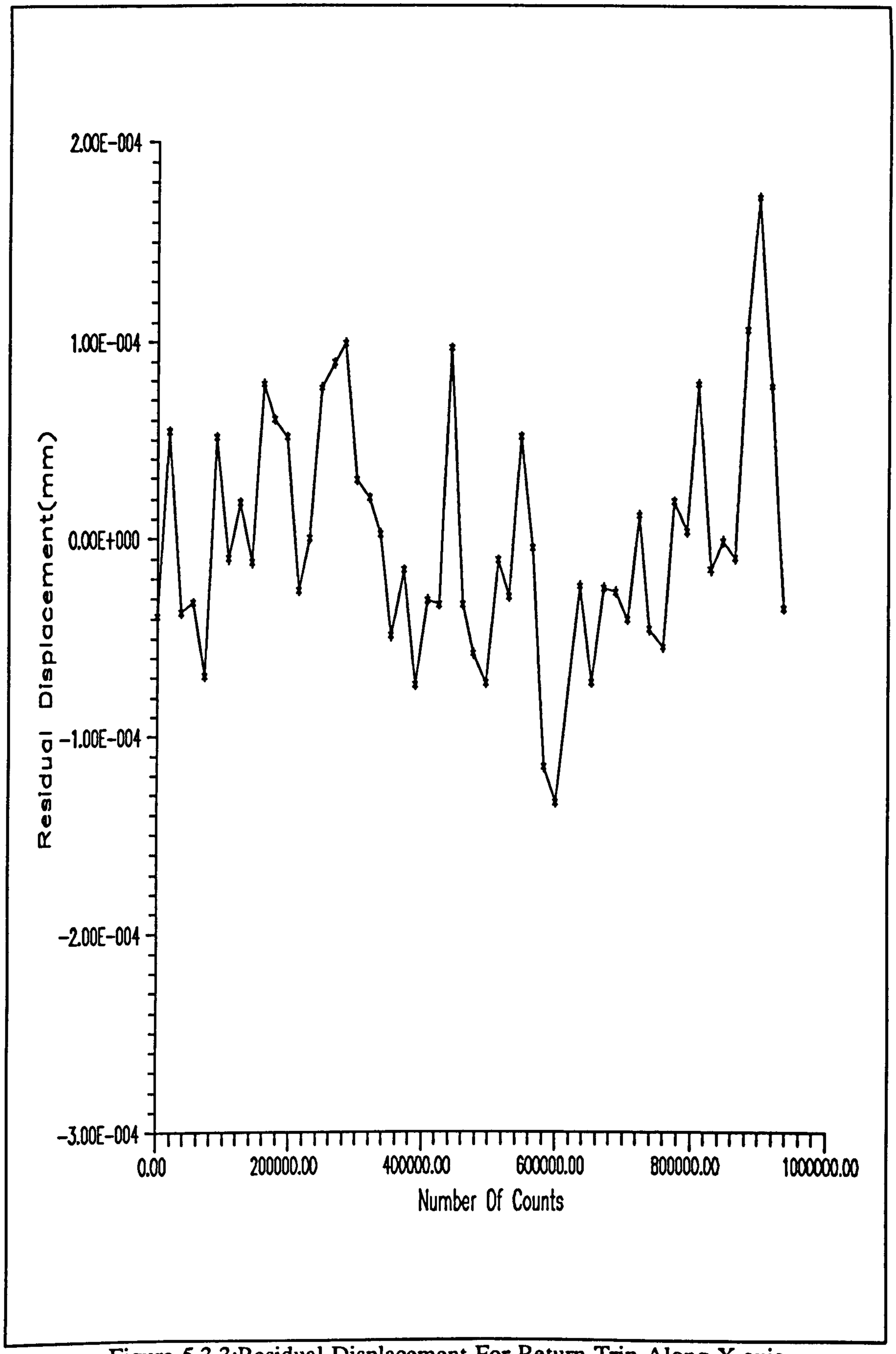

Figure 5.3.3:Residual Displacement For Return Trip Along X-axis

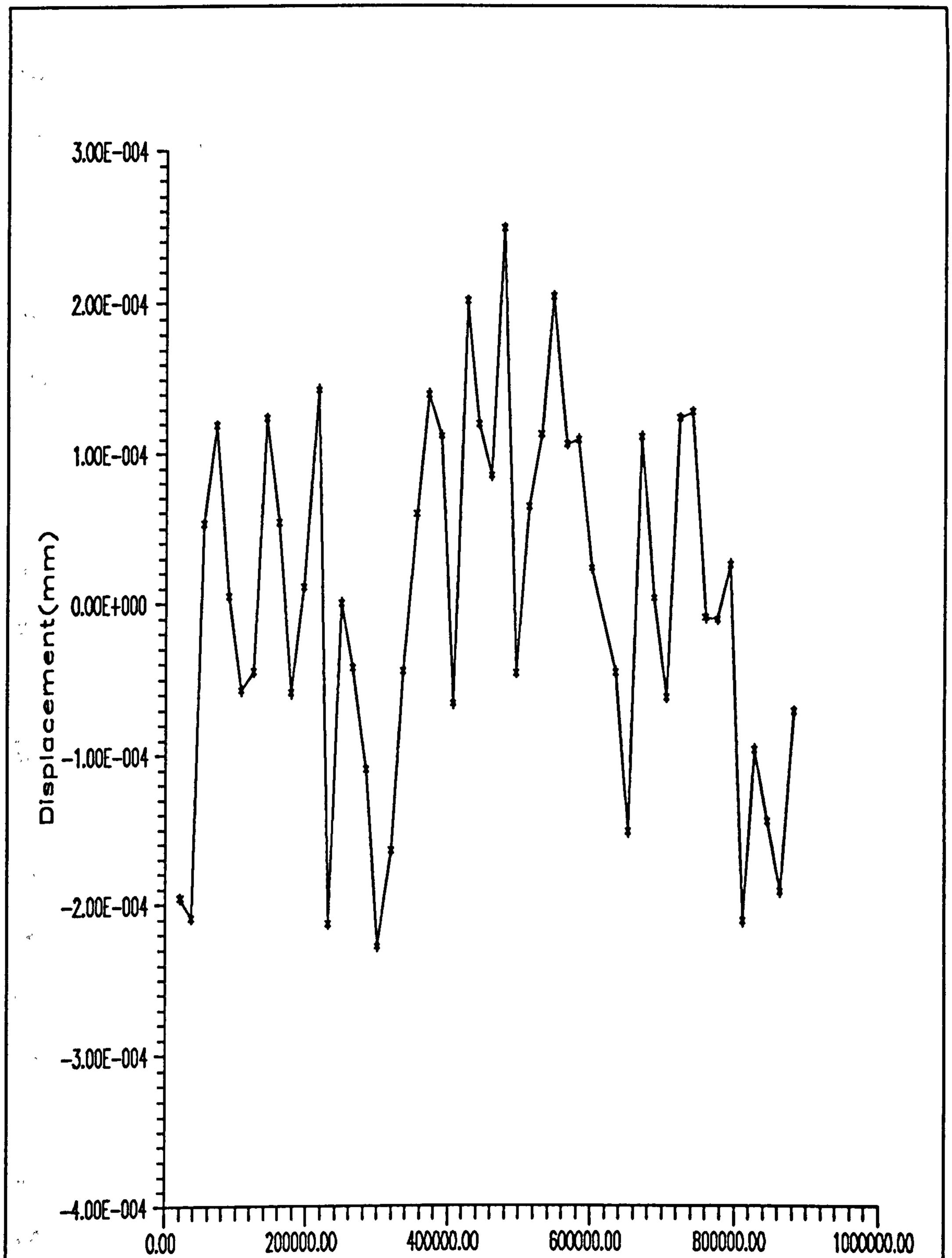

Figure 5.3.4: Residuals From A Typical Run Along The Y-axis

this case, the gradient of the best fit line was 17.644 counts/μm with a standard deviation of 0.0216 counts/mm. Once more the experimental result agrees with theory for a grating having 1103 lines/mm rather than 1100 lines/mm.

The maximum residual obtained on the x-axis lies within the range ±200nm for all of the calibration runs made along the x-axis. Similar results were also obtained when the y-axis was tested in the same manner.

The repeatability of the instrument is as good as could be realistically anticipated at this stage in its development. The disparities are similar to the errors predicted by the model for stage pitch described in section 4.3.3.

5.3.2 Further Development

There are limits to how far the instrument can be developed using Gandalf as the motion system. To take full advantage of a high precision measurement system it is necessary to be able to position the microscope stage to an accuracy commensuate with the resolution of the measurement system. The motor drive system on Gandalf is very basic, with provision for stage movement under joystick control. It proved impossible to position the stage with the precision required for a proper calibration process using the current system, and motion was achieved by manually turning the motors. However, the measurement of real objects could not be performed using such manual driving, as it still proved impossible to position the stage with a precision greater than ±0.1mm. To overcome these problems would require the development of a new control system for Gandalf, based around the output from the new interferometer, but this would involve

a large financial cost as well as a considerable investment of time. Gandalf was only a test bed for the instrument, so such investments would be better made on a new more suitable machine.

The measurement behaviour of each of the axes of motion have been investigated independently by the calibration process already described. However, in practice the microscope would be used to measure photographic plates in two dimensions. Therefore, it would be essential to test both axes simultaneously. The best way to execute such a test would be to measure the position of known features on a calibration plate. An example of a suitable test object for this purpose is one of the chrome-on-glass line standards, developed at NPL, for the measurement of line thickness in the electronics industry. Unfortunately it did not prove possible to locate microscope optics of sufficient power on Gandalf to make meaningful measurements of the standard. This problem illustrates once more that while Gandalf was a suitable test bed for the instrument, any further development, and the eventual use for serious measurement, would have to be done on a different microscope stage.

5.4 Points To Be Considered In Future Development

Much has been learnt about the operation of the new interferometer system during its development to the stage of an instrument whose basic operation has been proved. As potential problems have been discovered solutions for them have been considered which should be incorporated into any subsequent designs.

5.4.1 Elimination of Error Due To Pitch

The aberration in the stage motion that leads to the most serious error in the measurement of position is pitch. It is also the problem which requires the most elaborate solution to overcome. Figure 5.4.1 shows how the measurement system may be modified to eliminate the effect of pitch.

Rather than using prisms to return the light to the grating as in the original design, a hemispherical mirror should be placed over the grating. An aperture in the top allows light to enter and leave the system. If the centre of curvature of the mirror coincides with the point where the input beam is incident on the grating, then the light will always be returned to the same point on the grating, as shown in figure 5.4.1. This solution eliminates problems associated with pitch, roll and yaw since the measurement point may be kept exactly beneath the centre of the microscope objective, so meaning that the position being measured is always the position being observed.

There are several complication that arise owing to this modification. The major problem is that the light from both axes is returned to a common point on the grating. A method has to be found so that the light corresponding to each of the axes can be separated. The simplest solution to this problem is that shown in figure 5.4.1. A different wavelength of light is used to monitor each of the axes. The two different colours may then be separated at the output stage by means of interference filters used in conjunction with beam-splitters. Polarising beam splitters may then be used to produce a quadrature signal from each axis in the same way as in the original system. Care would have to be taken to ensure that the two wavelengths were far enough apart so that it is possible to

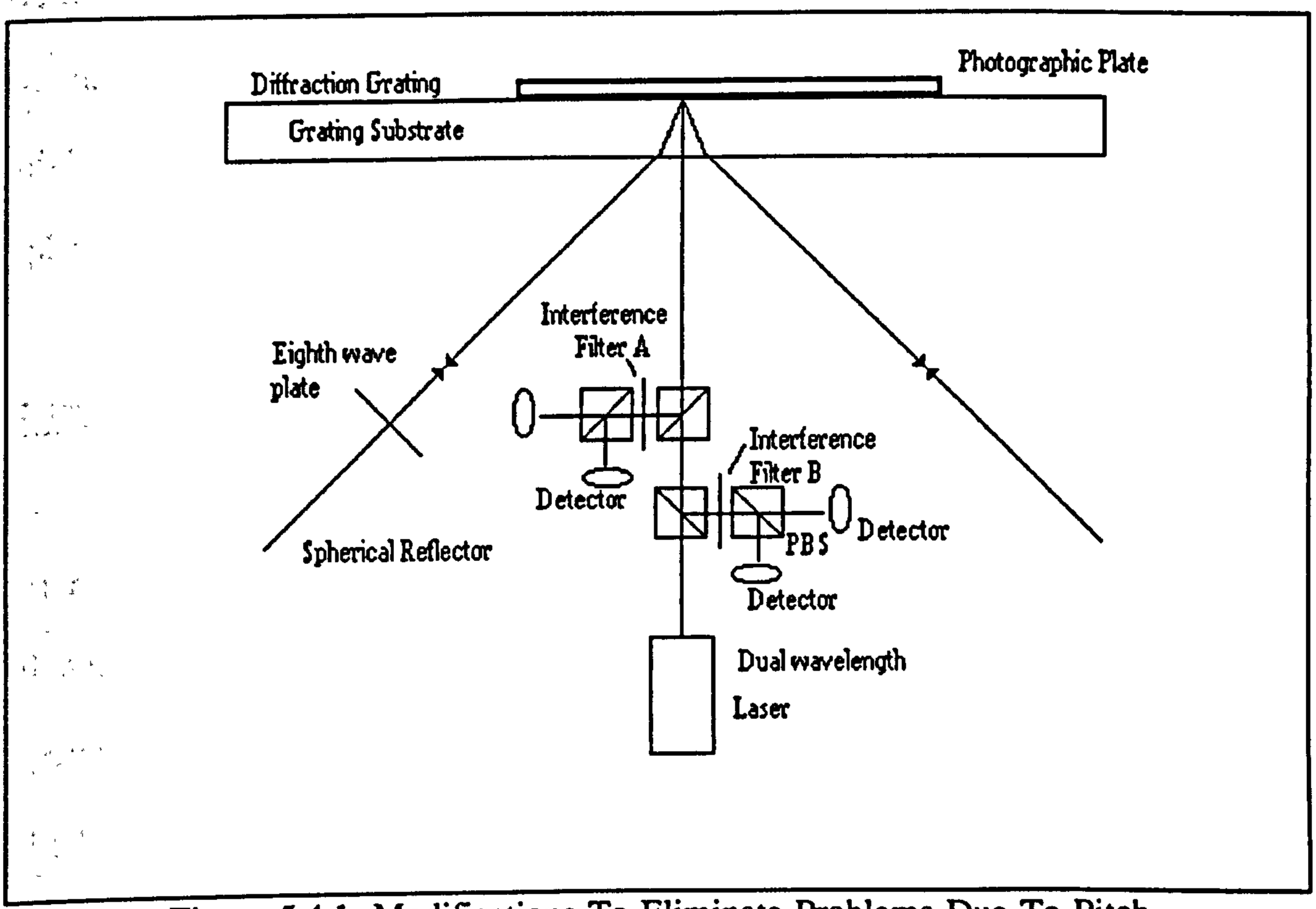

Figure 5.4.1: Modifications To Eliminate Problems Due To Pitch

ensure that the measurement system on each axis only returns light of one colour. If this is not the case, counts due to motion along one axis could also be recorded on the other axis as well. A difference in wavelength of 20nm would be sufficient to guarantee that the interference filters eliminated any possiblity of cross-talk between the axes.

The main additional expenses involved in making the modified system would be that of the dual wavelength light source and the manufacture of a spherical mirror of suitable dimensions. It would be possible to use four smaller spherical reflectors in slightly modified versions of the prism holders, if the cost of manufacturing a large spherical mirror proved prohibitive.

5.4.2 Simplifying The Building Of The Interferometer

The viability of commercially producing an instrument based on this interferometer is restricted by the care required to align the various components to obtain a suitable output fringe pattern. Although the interferometer proved robust in operation, it is possible that if care is not taken in its use, the prisms could move out of alignment. A solution to this potential problem is outlined below. There are two similar proposals outlined, one based on the interferometer already built, and one based on the system that eliminates the error due to pitch. The former of these designs is described first.

Rather than using four separate prisms to return the diffracted light to the grating, there is no reason why a solid block should not be used in the manner shown in figure 5.4.2. The block should be silvered on all of its surfaces, except for the one nearest the

grating, with an apertures being left in the top surface to allow light to enter and leave the system. The detectors and polarising beam-splitters can be cemented to the top of the block, so eliminating any possibility of components moving relative to each other. The quarter-wave plate can be cemented onto the surface of the glass block, as shown in figure 5.4.2.

There is one difficulty with this modified system. It is essential that the lines in the diffraction grating are parallel to the sides of the glass block that has replaced the prisms. If this condition is not satisfied it will prove impossible to achieve a good fringe contrast in the output beam. However, there is a simple solution to this problem. The diffraction grating substrate and the block should be manufactured as part of one large block. The sides should be polished to make all of the corners 90° to within a tolerance of two seconds of arc. The large glass block can then be sliced into two pieces, a thinner slice for the substrate and a more substantial one for the main block. Due to the way that the grating is made, described in section 4.3.3, this should ensure that the grating lines are parallel to the edges of the block.

The system to eliminate the error due to pitch may be modified in similar manner to that described above. Figure 5.4.3 shows the proposed device. A solid hemisphere is manufactured to replace the spherical reflectors. A thin slice must be cut off the bottom of the hemisphere so that its centre of curvature can coincide with the point on the grating that the input beam interacts with. The top of the hemisphere should also be flattened so that the components responsible monitoring the output of the device can be cemented to it. The curved surface area of the glass block should be silvered to reflect

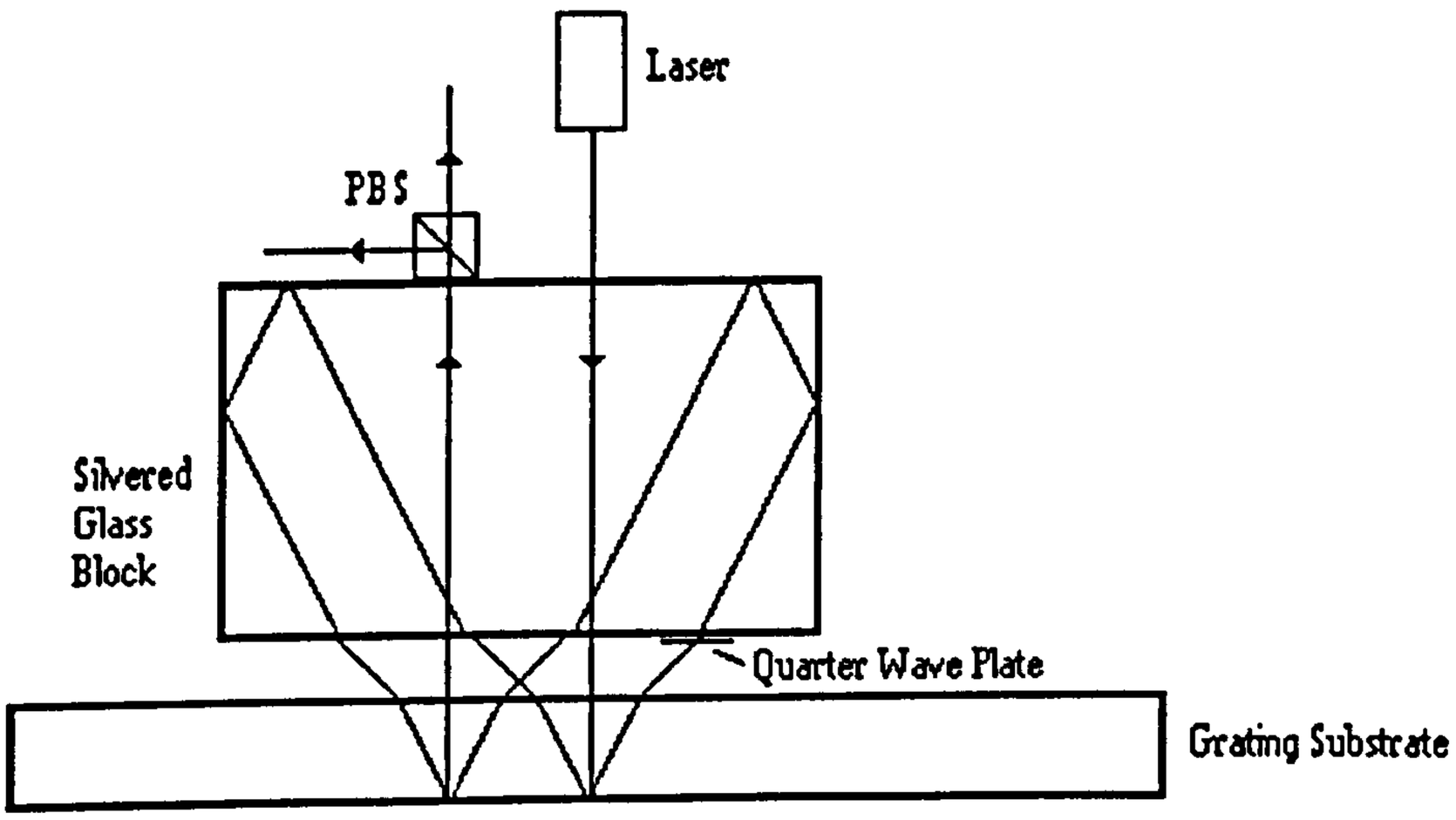

Figure 5.4.2: Solid Block Interferometer

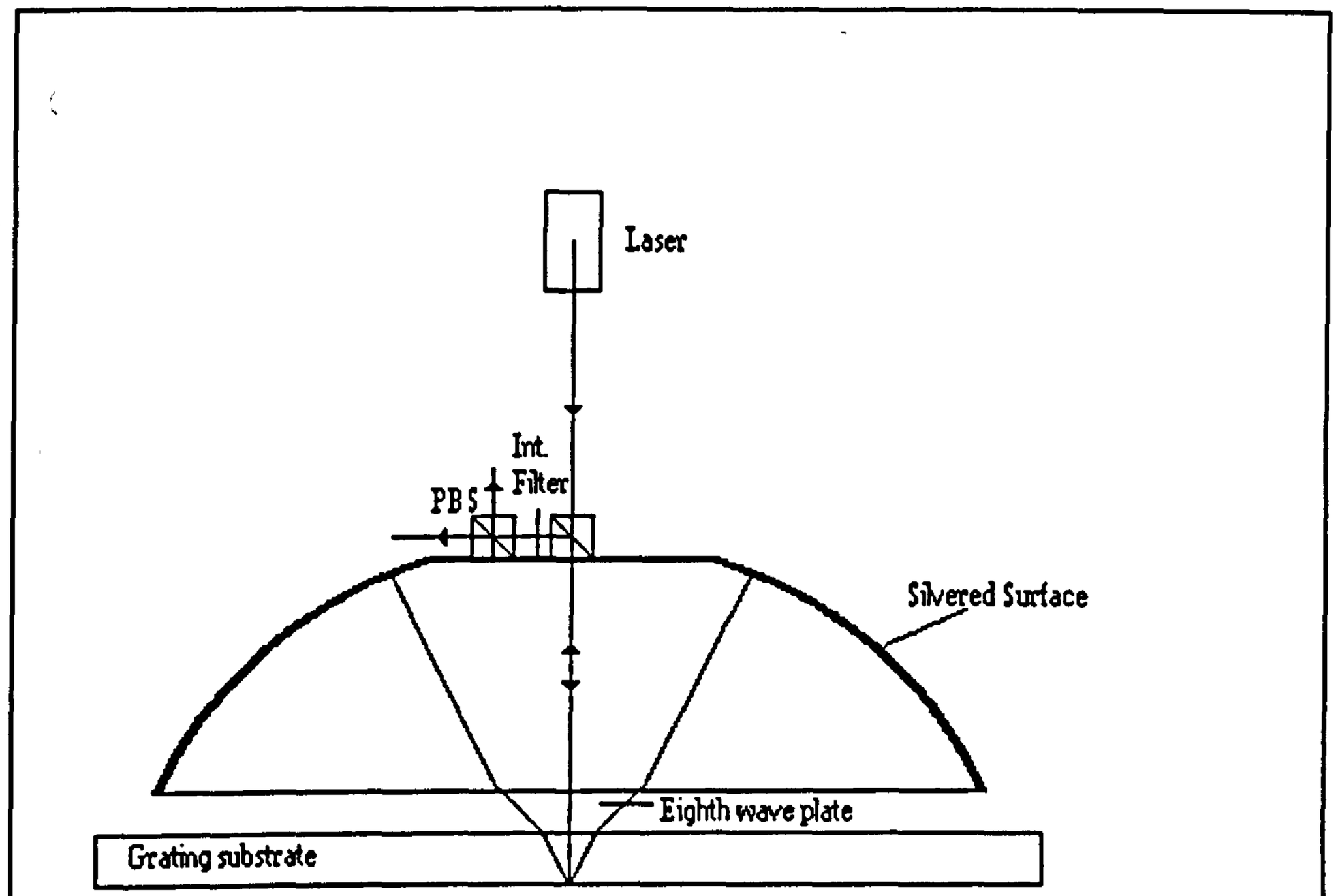

Figure 5.4.3: Hemisphere Version Of The Interferometer

the diffracted light back to the grating. This system is implemented more easily than the square glass block version since the problem of getting the grating lines parallel to the edges of the block does not arise. It is more straight-forward to make a hemisphere of this type than the spherical reflectors suggested in the original modification. Hence, this system would be the most easily manufactured of all of the devices proposed so far, and has the most potential as a commercial, high precision, displacement sensor.

6. CONCLUSION

A number of factors that influence the accuracy with which photogrammetric plates can be measured have been investigated. In Chapters 4 and 5 the development of a novel two axis interferometer system is described. The interferometer is used to monitor the position of microscope stage on which a photogrammetric plate may be measured. The prototype instrument developed here is able to measure displacement along both axes with a repeatability of better than 200nm over a 50mm × 50mm area. The fundamental precision of the interferometer is 57nm, and there is no theoretical reason why the repeatability should not be improved to reach this level. In order to achieve an increase in performance it will be necessary to implement the modifications outlined in Chapter 5, so that measurement errors due to aberrations in the stage motion are eliminated. The repeatability of the prototype is already more than adequate for the requirements of even the most demanding conventional survey. Measurement of the target positions to a precision of 1-2μm would give an acceptable accuracy in such a high precision photogrammetric survey, since camera distortion limits the survey accuracy. Only for special application such as Centrax image analysis does the interferometer require further development. The advantages of the device may be summed up as follows:-

a) The interferometer is compact. A reduction in size to a 5cm square could be achieved without a radical redesign of the components.

b) The device is much cheaper to construct than a Michelson type interferometer, or a moiré grating transducer offering measurement with the same resolution.

c) The operational area of the device is only limited by the dimensions of the diffraction grating, so it has potential in a wide variety of larger applications.

d) Owing to the compact and enclosed nature of the interferometer, there is little potential for any of the light beams to be obstructed. Hence, there is a very low risk of positional information being lost. This contrasts with some implementations of Michelson interferometers which have relatively long exposed optical paths.

e) The instrument is based on the interference of two beams which have equal path lengths. This property means that a short coherence length light source can be used.

f) During the trials and calibration process, the interferometer proved to be extremely robust. Once the instrument had been aligned it required no further adjustment.

Overall, the novel interferometer has proved to be satisfactory, and it has met all of the performance targets that were attainable with the available equipment.

Automation of the plate measurement process eliminates the need for human involvement in the most tedious and time consuming part of photogrammetric work. Searching a photographic plate for features approximately 100μm in size is extremely tiring, and mistakes may occur due to fatigue and loss of concentration. A system has been developed that is able to find and record the positions of all clearly observable targets on a photogrammetric plate with virtually no human supervision. A further program is used to match each point on a plate with the corresponding points on all of

the other plates. No loss in the accuracy of the survey is caused by the use of this target finding routine. When a survey was conducted to test the program, the target positions were found with an uncertainty of approximately 2μm. This result is in keeping with the accuracy of similar surveys conducted manually. It is hoped that the plate analysis program will be used extensively in future photogrammetric surveys. The use of such an effective labour saving package should reduce the cost of conducting a survey, so making photogrammetry an even more attractive technique for the three dimensional measurement of large structures.

After an initial investigation into the process of measuring photogrammetric plates, two distinct areas were identified as being suitable for improvement. Experiments were performed in each of these areas which led to results that can be used to improve the accuracy of photogrammetric surveys. Most of the work described has been carried out with the specific intention of improving the accuracy and efficiency with which the National Physical Laboratory can offer a photogrammetry service, but all of the aspects discussed could be adapted for wider use.

This thesis constitutes a record of two years practical work by the author at the National Physical Laboratory in the field of high precision metrology. A summary of the main areas to which the author has been contributed to during this time is shown overleaf.

The development of a set of computer programs to automatically measure photogrammetric plates has included the development of algorithms and the writing of programs for the following:-

Edge tracing around binary images
Calculation of the centre of gravity of an image
Calculating the centre of an ellipse
Controlling the microscope stage and reading its position
Calculating the position of cameras
Calculating the epi-polar line corresponding to a point
Matching corresponding image points (using epi-polar line fitting)

An automated survey was then carried out to test the system.

The basic concept of the interferometer was devised by Dr J.M. Burch. The development of a working instrument has involved the following:-

Development of the theory of how the interferometer works
Analysis of the likely measurement errors
Constructing a simple moiré device
Building a simple prototype to test the idea
Design of the optical and mechanical components
Use of a laser diode in a precision measurement environment
Manufacture and testing of eighth wave plates
Aligning the components
Building an electronic circuit to monitor the output of the interferometer
Proposals for alternative instruments based on this principle
Testing the interferometer using a commercial instrument

All these developments have culminated in a verification of their performance with the both the plate measurement programs and the interferometer system giving the desired performance.

Appendix 1: Calculation Of Camera Position

The camera positions may be calculated using a space resection technique developed at the NPL by Dr.R.A.Hunt(1983,1984). The first step in this method is to determine which known points to use (assuming more than 3 are available) in the resection calculation. For the resection process to work well it is important that these points should not be collinear. A simple test of the collinearity of 3 points is to calculate the area of a triangle bounded by the points. The three points which produce the triangle of largest area may be considered to be the least collinear. Hence these are the points selected for the resection.

The next step is to determine the distance of the 3 chosen points from the perspective centre of the camera. Here the distance to a point $\underline{X}_k$ is denoted by S_k and the perspective centre of the camera is represented by $\underline{X}_0$.

Figure a1.1 shows how the rays from the standard object are projected through the perspective centre onto the photographic plate. The angle between two rays may be expressed in terms of the object coordinate system by equation A1.1.

$$\cos\theta_{12}=\frac{(\underline{X}_1-\underline{X}_0).(\underline{X}_2-\underline{X}_0)}{S_1S_2} \qquad \text{A1.1}$$

$$\textit{where } S_i=|\underline{X}_i-\underline{X}_0|$$

In the camera coordinates the angle is given by:-

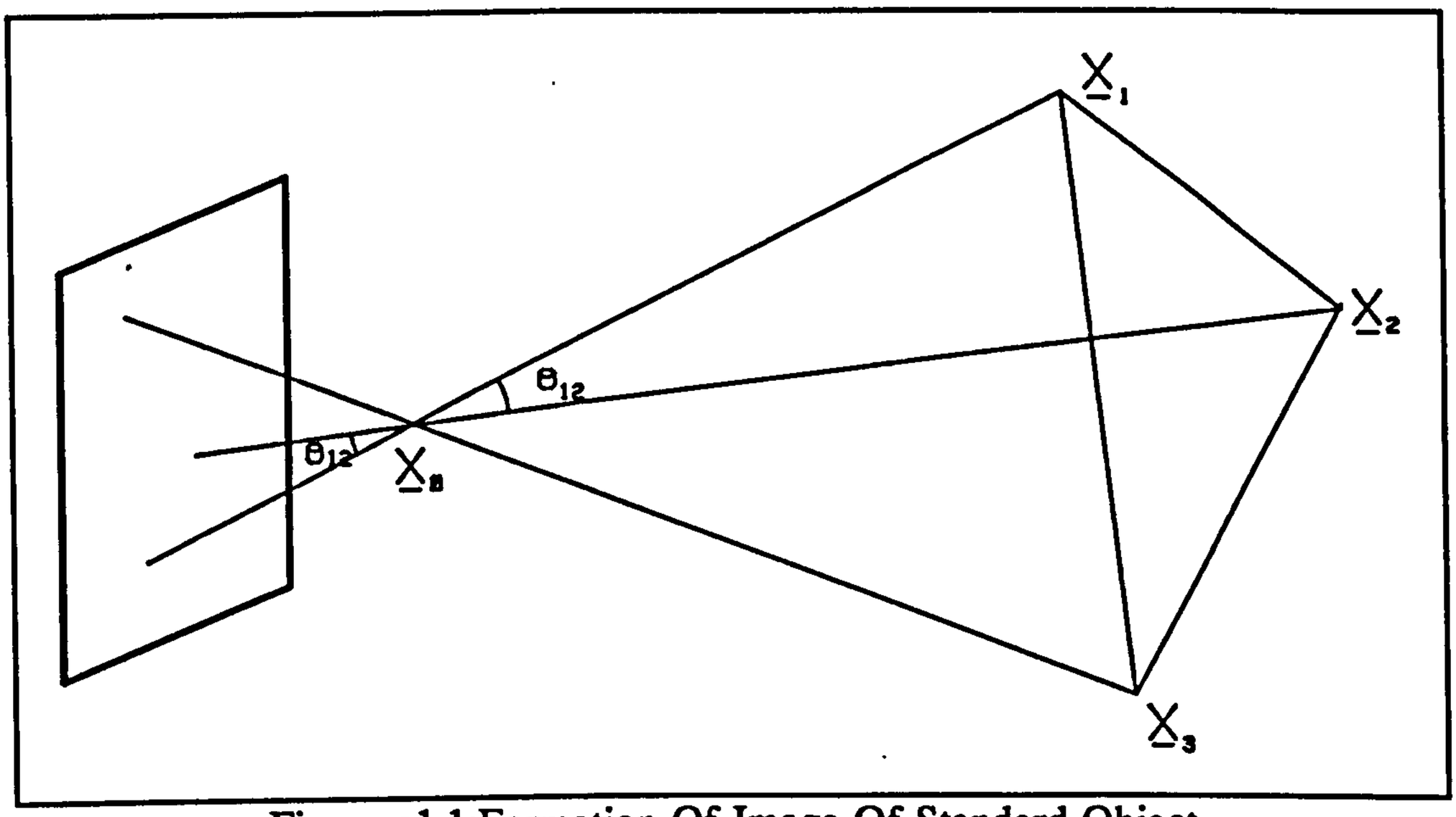

Figure a1.1:Formation Of Image Of Standard Object

$$\cos\theta_{12}=\frac{\underline{y}_1.\underline{y}_2+f^2}{\sqrt{\underline{y}_1.\underline{y}_1+f^2}\sqrt{\underline{y}_2.\underline{y}_2+f^2}} \qquad \text{A1.2}$$

Where $\underline{y}_i$ is the coordinate of point i in the interior system.

The diagram shown in figure a1.1 may be projected onto a single plane to give figure a1.2. Any two of the known points lie on a circle whose radius also contains the principal point of the camera. The radius of the circle containing points $\underline{X}_i$,$\underline{X}_j$ and $\underline{X}_0$ is given by:-

$$2r_{ij}=\frac{|\underline{X}_i-\underline{X}_j|}{\sqrt{1-\cos^2\theta_{ij}}} \qquad \text{A1.3}$$

From figure a1.2 it may be shown that:-

$$S_i=r_{ij}\sqrt{2+2\cos(\theta_{ij}-\alpha_{ij})}$$
$$S_j=r_{ij}\sqrt{2+2\cos(\theta_{ij}+\alpha_{ij})} \qquad \text{A1.4}$$

Considering the case i=1, j=2, α_{12} may be replaced by a variable α to give:-

$$S_1=r_{12}\sqrt{2+2\cos(\theta_{12}-\alpha)}$$
$$S_2=r_{12}\sqrt{2+2\cos(\theta_{12}+\alpha)} \qquad \text{A1.5}$$

The labels can be swapped cyclically so that r_{12} is less than or equal to both r_{23} and r_{31}. When this condition is satisfied the following equations always exist in the range $0\leq\zeta_{31}\leq\pi$, $\zeta_{31}(\alpha)=\theta_{31}-\alpha_{31}$ and $\pm\zeta_{23}(\alpha)=\theta_{23}-\alpha_{23}$ are made then $S_3(\alpha)$ may be written as

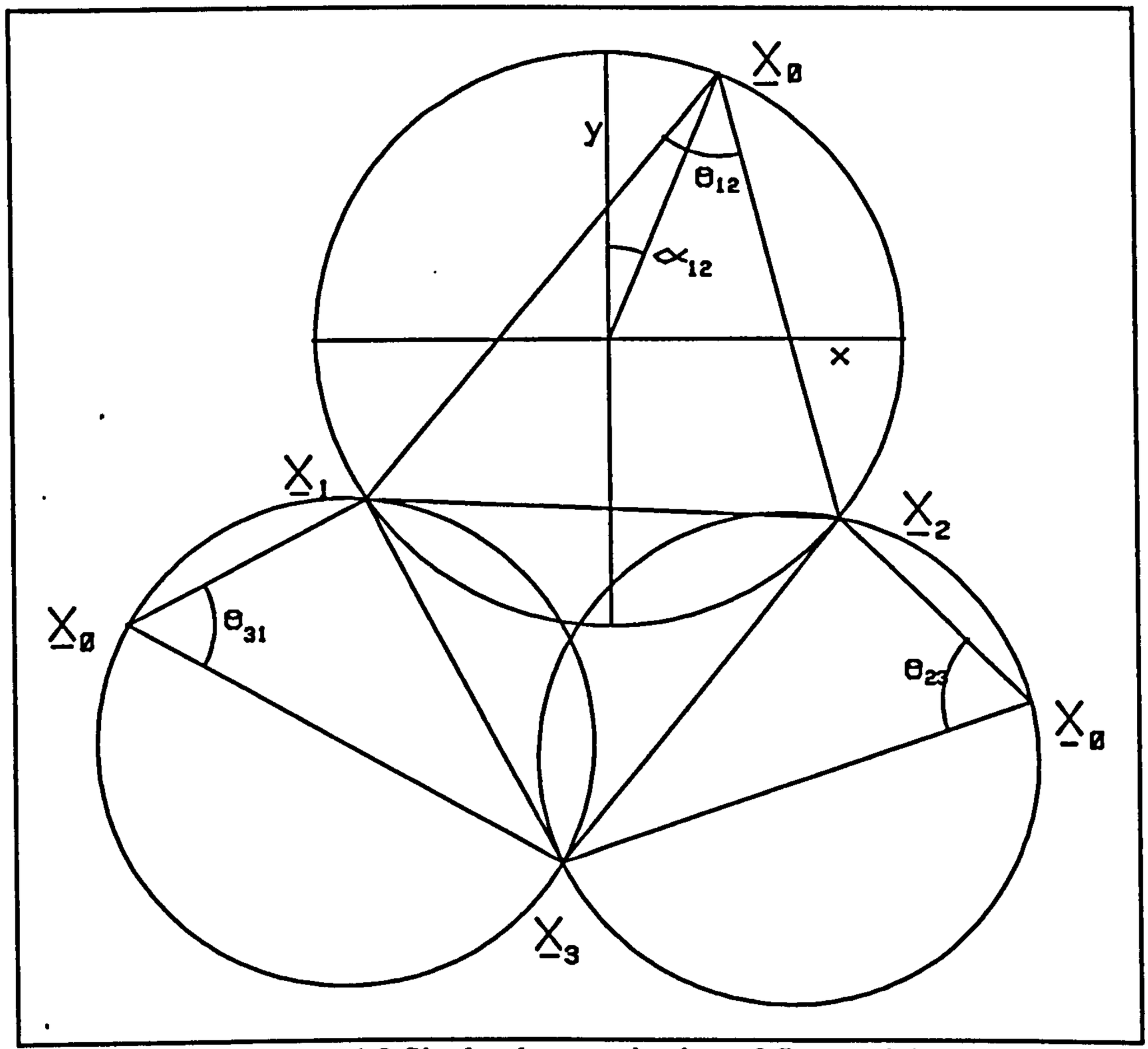

Figure a1.2:Single plane projection of figure a1.1

either of the following two equations:-

$$\zeta_{31}(\alpha)=\cos^{-1}(S_1^2(\alpha)/2r_{31}^2-1)$$

$$\zeta_{23}(\alpha)=\cos^{-1}(S_2^2(\alpha)/2r_{23}^2-1) \qquad \text{A1.6}$$

A1.4 may be rearranged to give A1.7:-

$$\cos(\theta_{31}+\alpha_{31})=(S_1^2(\alpha)/2r_{31}^2)-1 \qquad \text{A1.7}$$

By comparison of A1.6 and A1.7 it is apparent that:-

$$\pm\zeta_{31}(\alpha)=\theta_{31}+\alpha_{31} \qquad \text{A1.8}$$

$S_3(\alpha)$ may be calculated from either equation A1.9 or A1.10, depending upon which circle is used in the calculation.

$$S_3(\alpha)=r_{23}\sqrt{2+2\cos(2\theta_{31}+(-1)^k\zeta_{31}(\alpha))} \qquad \text{A1.9}$$

where $k=1$, $k=2$

$$S_3(\alpha)=r_{23}\sqrt{2+2\cos(2\theta_{23}+(-1)^l\zeta_{23}(\alpha))} \qquad \text{A1.10}$$

where $l=1$, $l=2$

If α is such that $S_3(\alpha)$ is the same when both of the above equations are evaluated, α is a possible solution of equation A1.4 The solutions are tested by calculating the quantity F_{kl} as defined in equation A1.8 below.

$$F_{kl}(\alpha)=r_{31}^2(1+\cos(2\theta_{31}+(-1)^k\zeta_{31}(\alpha)))-r_{23}^2(1+\cos(2\theta_{23}+(-1)^l\zeta_{23}(\alpha))) \quad \text{A1.11}$$

α is varied in equation A1.8 to find all the zeroes of the function. The values of S_1 and S_2 are then calculated by substituting the value for α back into equation A1.5, while S_3 is calculated from equation A1.6.

Once the distances of the ground points from the camera are known, it is possible to calculate the location of the camera perspective centre in the object space coordinate system. The perspective centre is the point of intersection of three spheres centred at $\underline{X}_1$, $\underline{X}_2$ and $\underline{X}_3$ having radii S_1, S_2 and S_3 respectively.

The equations of the three spheres are:-

$$(\underline{X}-\underline{X}_1)^2=S_1^2 \quad \text{A1.12}$$

$$(\underline{X}-\underline{X}_2)^2=S_2^2 \quad \text{A1.13}$$

$$(\underline{X}-\underline{X}_3)^2=S_3^2 \quad \text{A1.14}$$

Subtracting A1.13 from A1.12 gives:-

$$2\underline{X}.(\underline{X}_1-\underline{X}_2)=\underline{X}_1^2-\underline{X}_2^2-(S_1^2-S_2^2) \quad \text{A1.15}$$

Which is the plane containing the circle of intersection of spheres 1 and 2. While subtracting A1.14 from A1.13 gives the equation of the plane containing the intersection between spheres 2 and 3:-

$$2\underline{X}.(\underline{X}_2-\underline{X}_3)=\underline{X}_2^2-\underline{X}_3^2-(S_2^2-S_3^2) \qquad \text{A1.16}$$

The line where these two planes meet is perpendicular to the plane containing the triangle whose vertices are at $\underline{X}_1$, $\underline{X}_2$ and $\underline{X}_3$. The normal to the triangle is:-

$$\underline{K}=\underline{X}_1\times\underline{X}_2+\underline{X}_2\times\underline{X}_3+\underline{X}_3\times\underline{X}_1 \qquad \text{A1.17}$$

The plane containing the triangle is represented by equation A1.18:-

$$\underline{X}.\underline{K}=\underline{X}_1.(\underline{X}_2\times\underline{X}_3) \qquad \text{A1.18}$$

Using equations A1.15 and A1.16 in conjunction with A1.18 allows the calculation of the point in the plane of the triangle where it is crossed by the line joining the intersections of the three spheres ($\underline{X}_p$). The plane of the triangle may also be written as the perpendicular bisector of the line joining the two points of intersection of the spheres, so allowing $\underline{X}_0$ to be expressed as:-

$$\underline{X}_0=\underline{X}_p\pm t\underline{K} \qquad \text{A1.19}$$

Equation A1.19 may now be substituted back into A1.12 to give:-

$$t^2=\frac{S_1^2-(\underline{X}_p-\underline{X}_1)^2}{\underline{K}.\underline{K}} \qquad \text{A1.20}$$

From this equation it is possible to calculate $\underline{X}_p$, and hence calculate $\underline{X}_0$ from equation A1.19. Two solutions for $\underline{X}_0$ are obtained for each calculation of $\underline{X}_0$.

Once the possible locations of the cameras have been determined in the above manner, it is necessary to evaluate which is the best solution. A good test of the relative merits of the various solutions is to compare the angle subtended by each point in the interior camera coordinate system with that subtended in the exterior system. In an idealised case the two sets of angles are identical for the correct solution.

In the interior coordinate set the angle may be calculated from:-

$$\cos\theta_{ij}=\frac{(\underline{X}_i-\underline{X}_0).(\underline{X}_j-\underline{X}_0)}{S_iS_j} \qquad \text{A1.21}$$

While in the interior system the angle is given by:-

$$\cos\theta_{ij}=\frac{\underline{y}_i.\underline{y}_j+f^2}{\sqrt{\underline{y}_i.\underline{y}_i+f^2}\sqrt{\underline{y}_j.\underline{y}_j+f^2}} \qquad \text{A1.22}$$

Hence the best perspective centre solution is the one which minimises equation A1.23.

$$T(\underline{X}_0)=\sum_{i>j}\left\{\frac{(\underline{X}_i-\underline{X}_0).(\underline{X}_j-\underline{X}_0)}{S_1^2S_2^2}-\frac{\underline{y}_i.\underline{y}_j+f^2}{\sqrt{\underline{y}_i.\underline{y}_i+f^2}\sqrt{\underline{y}_j.\underline{y}_j+f^2}}\right\} \qquad \text{A1.23}$$

The only property of the camera still to be determined is its rotation. The interior and exterior coordinates are linked by the following equation:-

$$\underline{\hat{G}}_i = -R\underline{\hat{P}}_i$$

A1.24

$$\underline{\hat{P}}_i = \frac{\underline{P}_i}{|\underline{P}_i|} \qquad \underline{\hat{G}}_i = \frac{\underline{G}_i}{|\underline{G}_i|}$$

Where $\underline{G}_i$ is the exterior coordinate of the object, $\underline{P}_i$ is the interior coordinate of the image, and **R** is the rotation matrix. Equation A1.24 may be rearranged to give A1.25 which may be solved for any point i to give the rotation matrix.

$$\boldsymbol{R} = -\underline{\hat{G}}\,\underline{\hat{P}}_i^T$$

A1.25

where $\underline{P}_i^T$ *denotes the transpose of* $\underline{P}_i$

Appendix 2: Paper from
"Sensors: Technology, Systems & Applications",
Vol 5 p299 (Ed. K.T.V. Gratton) September 1991

A Novel Diffraction Based X-Y Position Transducer

I Severn[1] and C Forno[2]

1.BCMM, Brunel University,Uxbridge,Middlesex
2.The National Physical Laboratory, Teddington, Middlesex

ABSTRACT: A robust position sensing transducer, with a resolution of better than 60nm, has been developed for the monitoring of a microscope stage. A prototype with an operating field of 8×8cm has been developed.

1.INTRODUCTION

Photogrammetry is a well established technique in which 3-dimensional information is extracted from multiple photographic views of an object. Features are marked on the object, their relative positions on the photographic plates measured and the 3-dimensional coordinates of the object calculated.

A novel type of photogrammetric camera, known as Centrax (Burch and Forno 1983,1984), has been developed at NPL for the calibration of Coordinate Measurement Machines. To be of any use for this purpose the accuracy of the photogrammetry must be 1 part in 10^6. The total image produced by the centrax camera is 5cm in diameter. To meet the accuracy criteria the individual Centrax features must be located to better than 50nm. It has been demonstrated that, given a suitable microscope and image location system, the images can be relocated with a repeatability of 20nm. This paper describes an innovative microscope stage position monitoring system which has been designed to allow Centrax plates to be measured.

2.THE BASIS OF THE NEW DEVICE

Figure 1 shows a schematic of a single axis version of the novel transducer. Light is normally incident on the diffraction grating and is split into its characteristic orders.

The two first orders are then returned to the grating surface where they are recombined. If all of the orders were to be recombined then a virtual light grating of the same pitch as the original would be formed. Each order would contribute a term to the image to produce a virtual grating made up of the following Fourier sum.

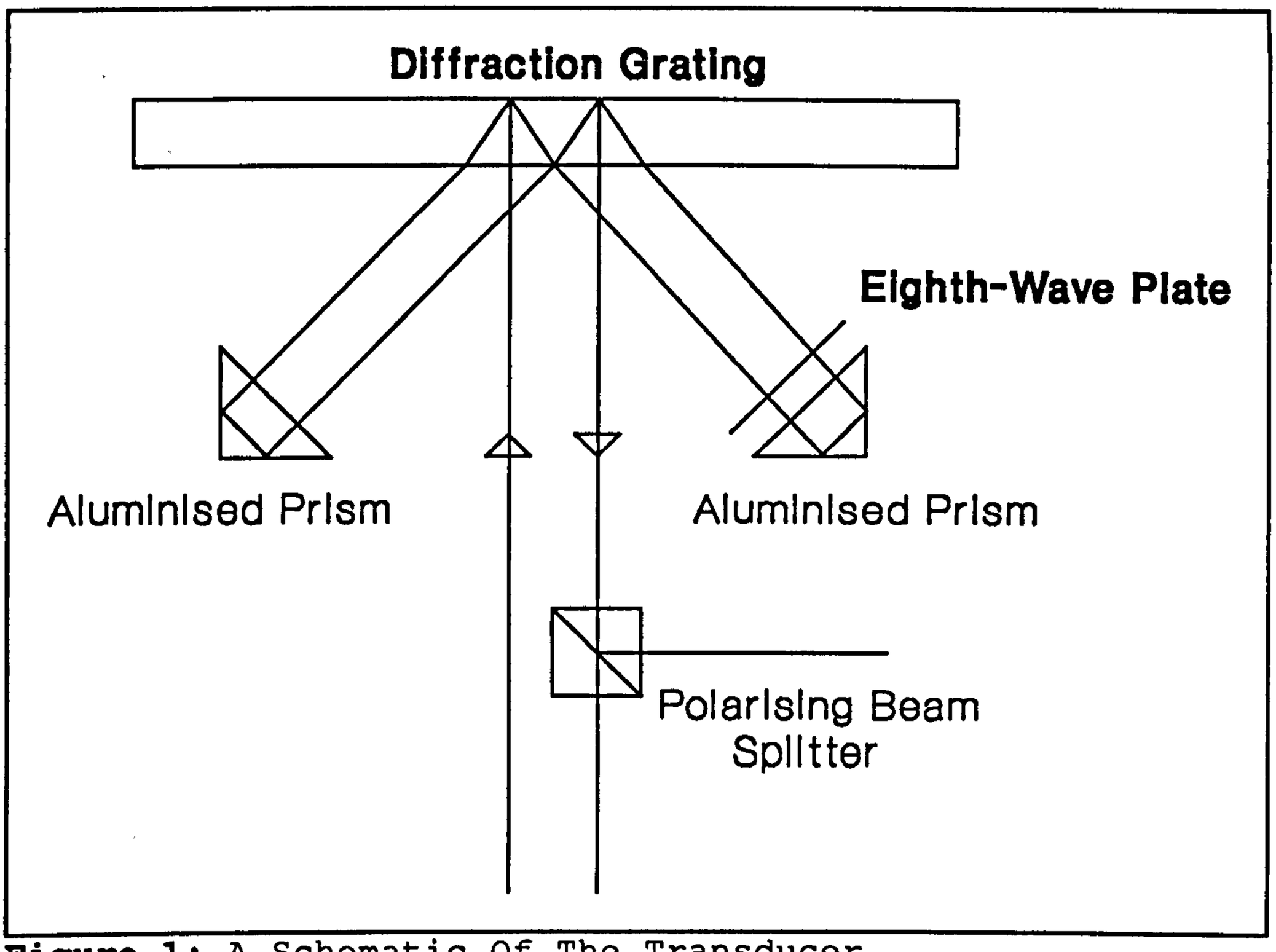

Figure 1: A Schematic Of The Transducer

$$B(x) = 1 + b_1 \cos\{\frac{2\pi x}{W}\} + b_2 \cos\{\frac{4\pi x}{W}\} + b_3 \cos\{\frac{6\pi x}{W}\} + \ldots$$

Where B(x) is the brightness at distance x from the centre of a grating strip, and W is the pitch of the grating.

If however, as in this case, only the two first orders are present, only the second sinusoidal Fourier component contributes to the virtual grating. Therefore, the profile of the light grating will be of the form:-

$$B(x) = 1 + b_2 \cos\{\frac{4\pi x}{W}\}$$

Hence the virtual grating formed has twice the pitch of the real grating. A moiré effect occurs between the two gratings, so causing the light returning to the zero order to be modulated at the pitch of the virtual grating(Guild 1956). moving the grating a distance equal to its pitch causes the output light to pass through two modulation cycles.

The modulation frequency is further doubled since the virtual grating is moving in the opposite direction to the original. Hence the output intensity is modulated through four cycles for a grating motion equivalent to its own period.

To allow the device to sense the direction of motion as well as the distance, a quadrature signal is produced by converting one of the beams into circularly polarised light. Passing a linearly polarised beam through a quarter-wave plate once, or an eighth-wave plate twice produces circularly polarised light.

The recombined beam is now made up of a combination of plane and circularly polarised light. A polarising beam splitter is then used to divide the light into two orthogonally polarised beams, so producing two modulated outputs with a phase difference of 90° between them. The direction of motion is determined by observing which beam is ahead of the other in phase.

Commercial counters are available which can interpolate the quadrature signal to give a resolution much better than the 50nm required for this application.

If the linear grating is replaced by a crossed grating x and y motion may be monitored simultaneously. Two axis measurement also requires the addition of a second pair of prisms along an axis perpendicular axis to the first.

3.PRELIMINARY RESULTS

A single axis device as shown in figure 1 was constructed with the grating mounted on a micrometer type stage. A linear displacement transducer with a resolution of ±0.5µm was used to monitor the movement of the grating. The stage was moved through distances up to that corresponding to 40 fringes being counted. Figure 2 shows how the distance moved by the grating is related to the number of counts.

The results are slightly lower than predicted by theory. They imply that a movement of 197nm produces one fringe, while theory predicts 208nm for a 1200 line/mm grating. This slight anomaly may be explained by the fact that the fringe counting was done manually, so leading to the strong possibility of some counts are missed. The fact that the results are systematically low tends to support this point of view. Further errors are introduced by the fact that it proved impossible to position the test stage to a greater precision than ±1 count. In spite of these problems it can be said that the basic principle of the device has been successfully demonstrated.

A prototype two axis system has been constructed based on an 1100 line/mm crossed grating. No results are yet available, although initial tests look promising.

4.ADVANTAGES OF THE SYSTEM

The major advantage of this system over an instrument such as a Michelson interferometer is its wavelength independence. The only wavelength limitation is that the first order beams should be intercepted by the prisms.

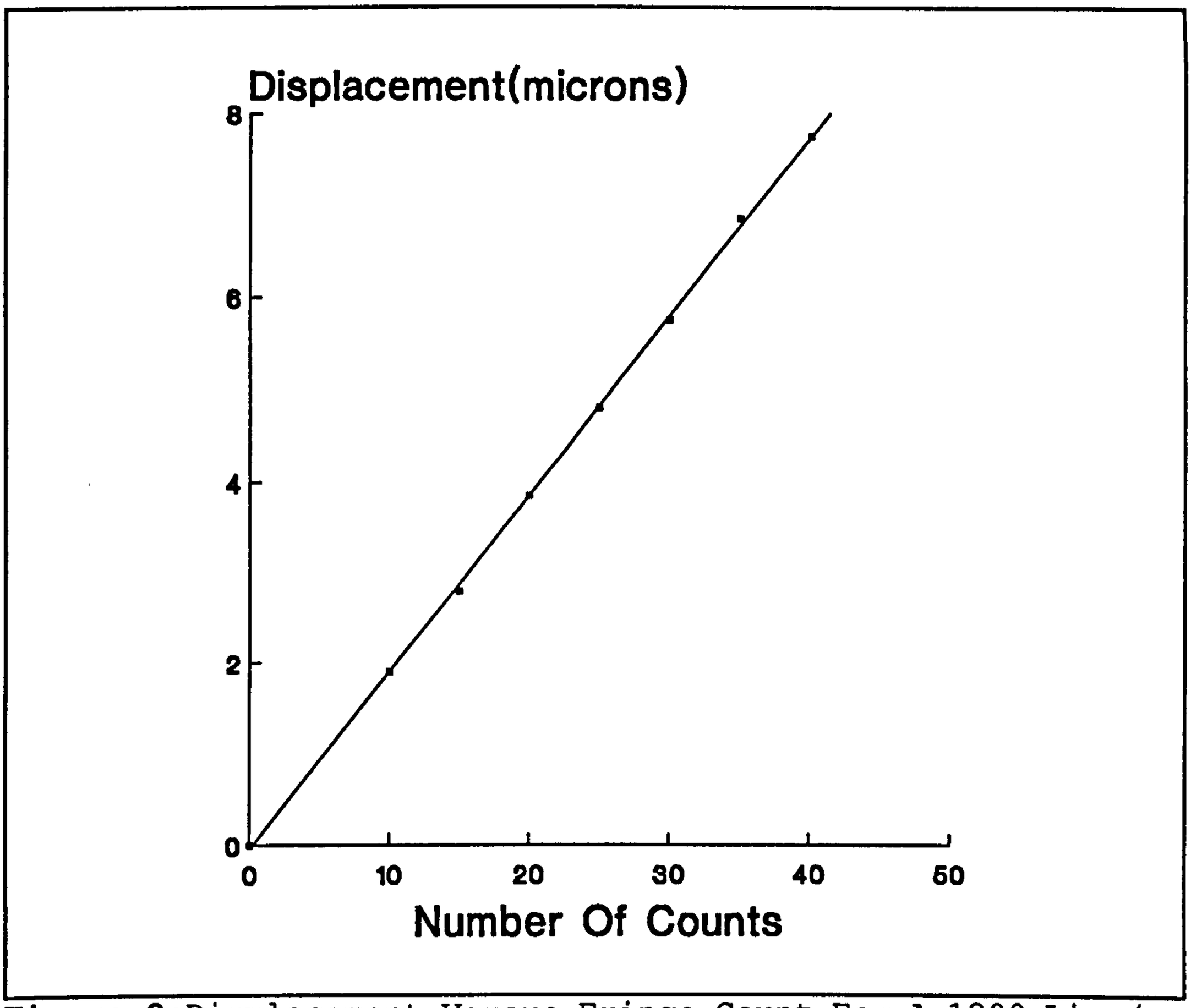

Figure 2:Displacement Versus Fringe Count For A 1200 Line/mm Grating

Another advantage is the ability of the measurement system to satisfy the Abbé criteria. The Abbé criteria states that "The object to be measured, and the measuring standard must be in contact or lie in the same plane" (Ghosh1979). By passing all of the light beams through the grating substrate before they strike the grating surface, as shown in figure 1, it is possible to use grating itself as the microscope stage. Hence the criteria is satisfied.

It is also possible to ensure that the location of the measurement point is as close as possible to the centre of the optical axis of the microscope. This minimises problems due to pitch, roll and yaw. (ie The position that is measured is the actual position being observed by the microscope optics).

5.PRACTICAL CONSIDERATIONS

The wavelength insensitivity of the transducer makes it possible to use a relatively inexpensive laser diode as a light source. Laser diodes provide a low cost way to produce light of sufficient intensity to provide an easily visible output.

The only potential problem with using a diode is the positional stability of its beam. An experiment was conducted to monitor the beam position. After an initial period of approximately 2 hours the beam position was found to stabilise.

A diffraction angle of approximately 45° should be used to reduce problems in aligning the device. Preservation of this angle is possible by either adjusting the wavelength or the grating pitch. The resolution is increased by the use of a higher pitch grating, but the wavelength of the interrogating light should be reduced to give a reasonable diffraction angle.

Unlike a system such as a Michelson interferometer the measurement scale is not directly related to an absolute standard. Rather it is dependent upon the grating pitch. Slight irregularities may occur in the grating structure, so before any meaningful high accuracy measurements can be made the grating must be calibrated.

Fortunately the two beam interference method used to produce modern gratings is likely to cause any deviations to be symmetric, so simplifying the calibration. Non-uniformities are especially likely to occur at the grating edges. However, due to the large size of the interrogation beam (5mm×3mm) relative to the grating pitch (tenths of μm),any small scale blemishes in the grating structure are not critical.

The measurement system itself is compact and will fit into a small space, with the largest component being the grating itself. The limiting factor on the operational area of the microscope is the size of grating that can be manufactured.

6.CONCLUSION

A compact and inexpensive position measurement system has been developed which may well have applications outside the area for which it was built. Once aligned the device is robust and requires little further adjustment. By changing the grating it is possible easily to modify the resolution of the system to meet different requirements.

7.REFERENCES

Burch J M and Forno C 1983 *Optical System Design, Analysis and Production*, SPIE vol 399, (1983) pp412-417.

Burch J M and Forno C 1984 *Proc ISPRS*, Rio de Janeiro pp141-148

Ghosh S K 1979 *Analytical Photogrammetry(1st Ed) The Pergamon Press*

Guild J 1956 *The Interference Systems Of Crossed Diffraction Gratings: Theory Of Moiré Fringes, Monographs On Physics And Chemistry Of Materials. The Clarendon Press*

ACKNOWLEDGEMENTS
This work was carried out under a SERC CASE studentship under the supervision of Professor B.E.Jones and Dr.R.C.Spooncer. The work is based on an idea by Dr.J.M. Burch, and has been assisted by S.Brown, Dr.R.A.Hunt and S.Oldfield.
The gratings were manufactured by Mrs S.Wilson.

Appendix 3: Interferometer Plans

Interferometer Component Holder. All dimensions in mm. Material Steel.

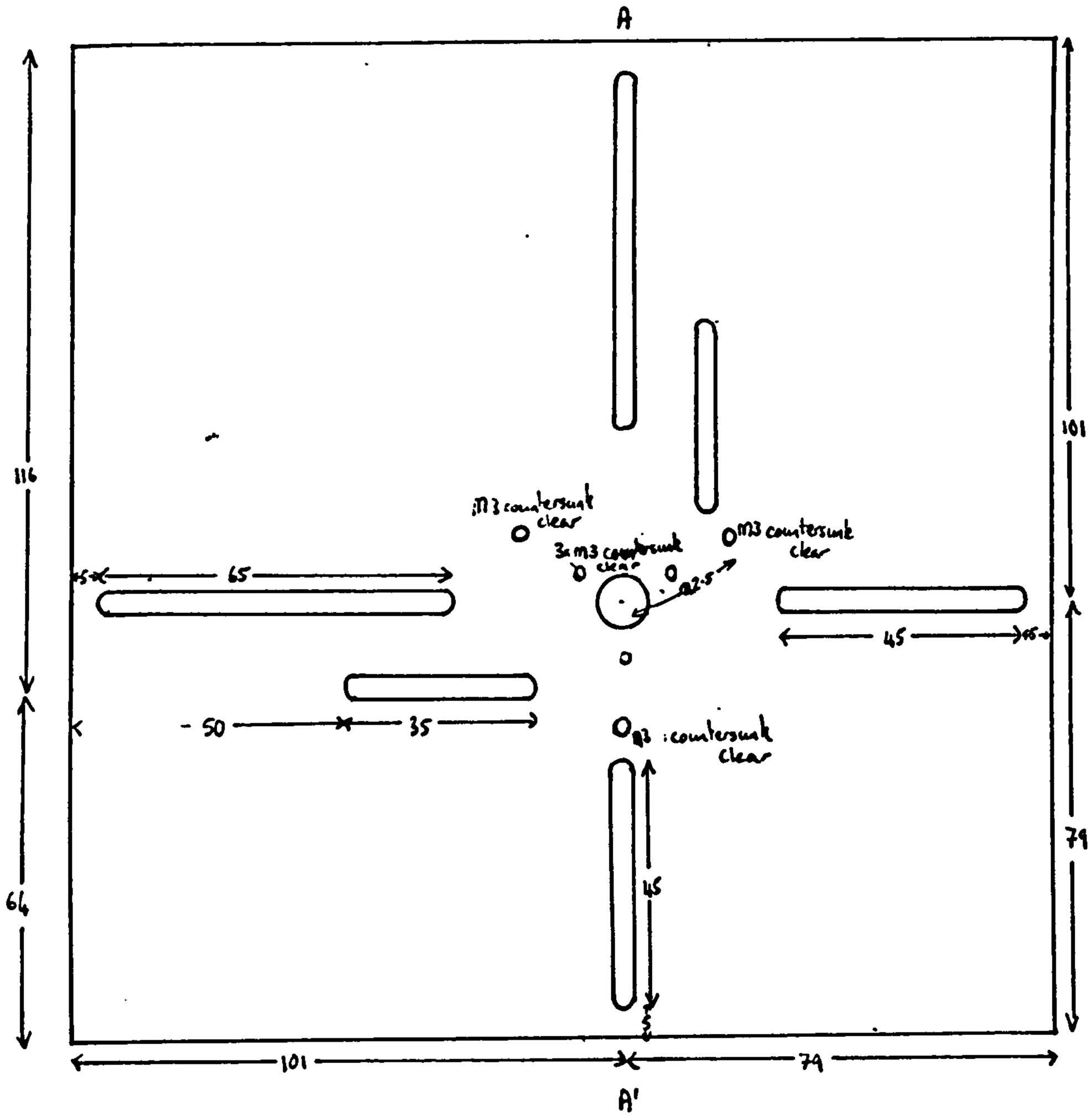

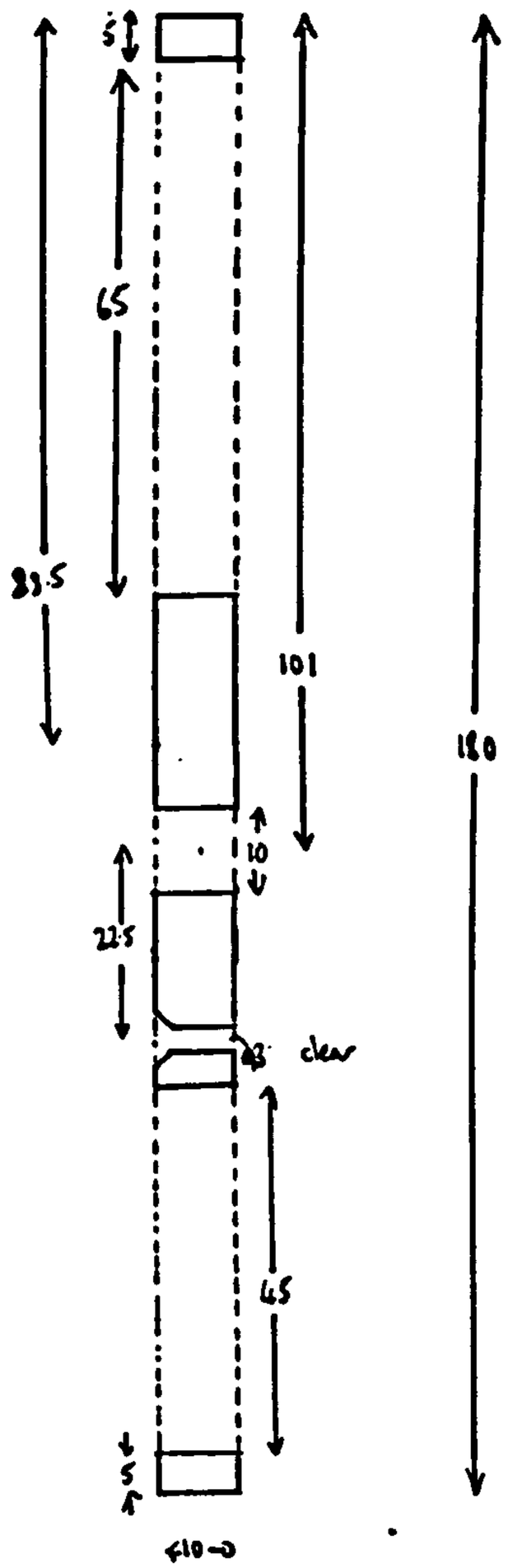

scale 1:1

Interferometer Base Plate

Original

210

Modified Base Plate

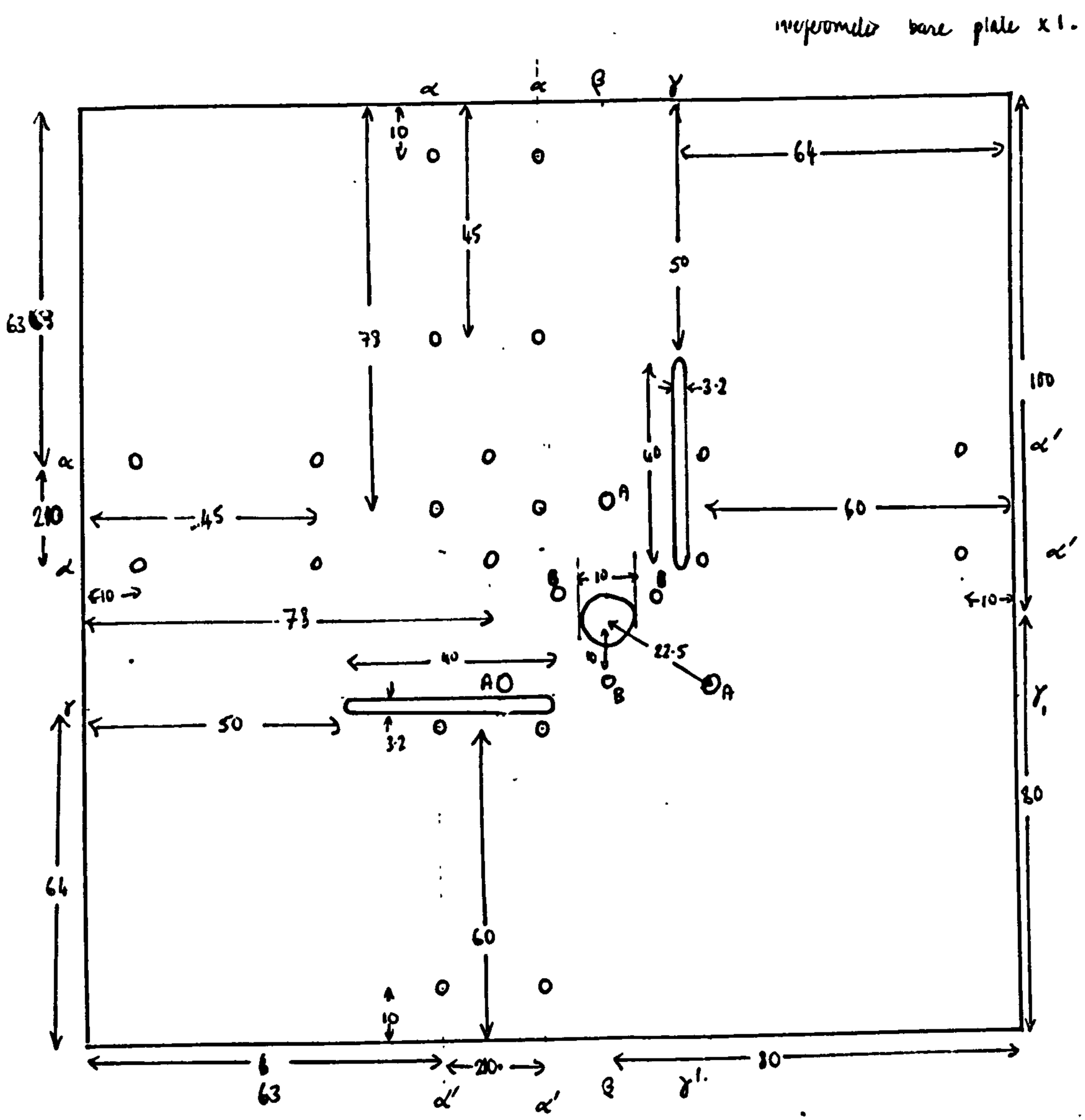

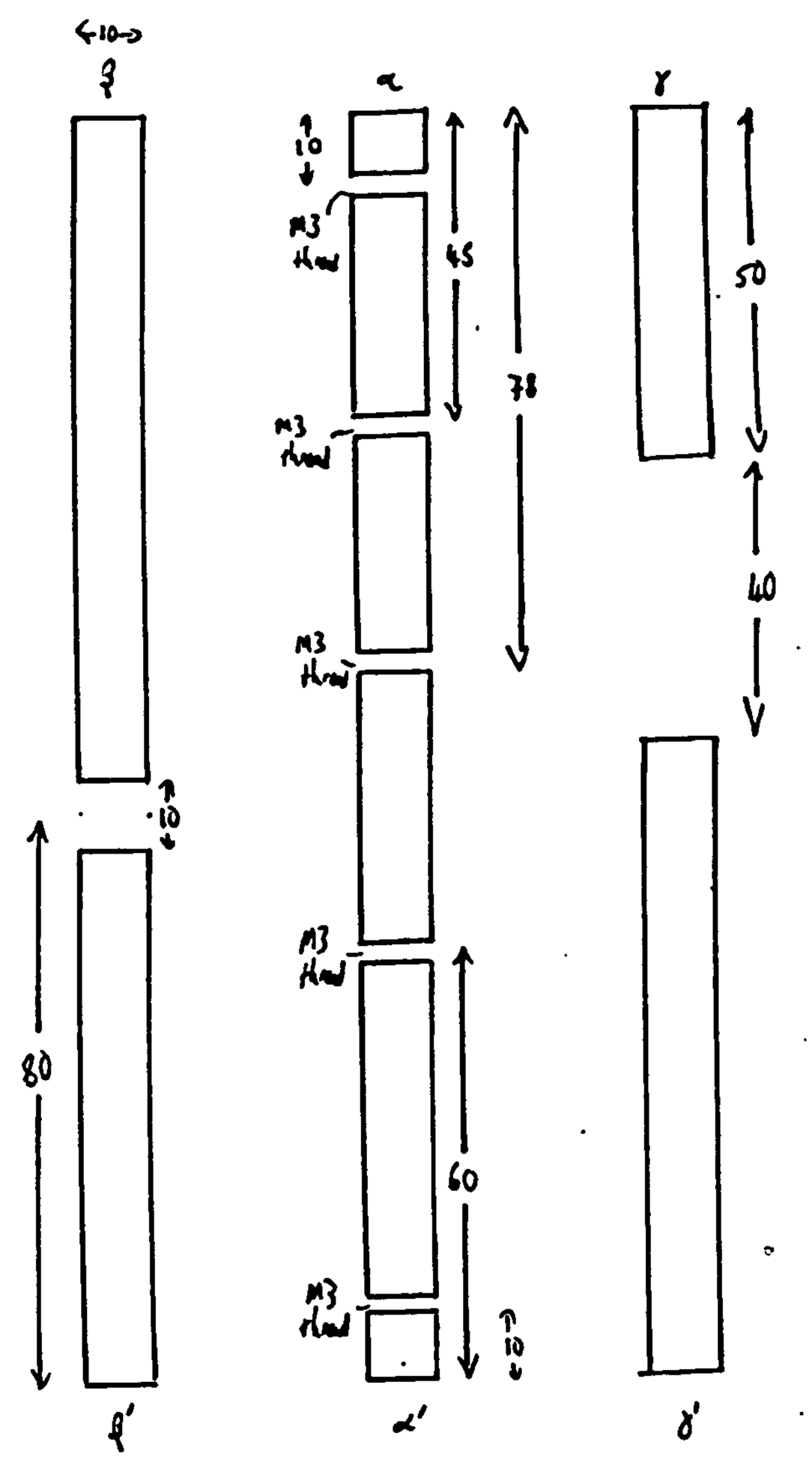

Holes marked A are M3 countersunk clearance and are 22·5mm from the centre of the large hole
Holes marked B are M3 countersunk clearance and are 10mm from the centre of the large hole.
All other holes are M3 threaded.

Top surface (ie surface with countersinking) milled flat. The lines labelled αα' should be as perpendicular as possible.

Tracks for Prism Movement.

212

Track 1

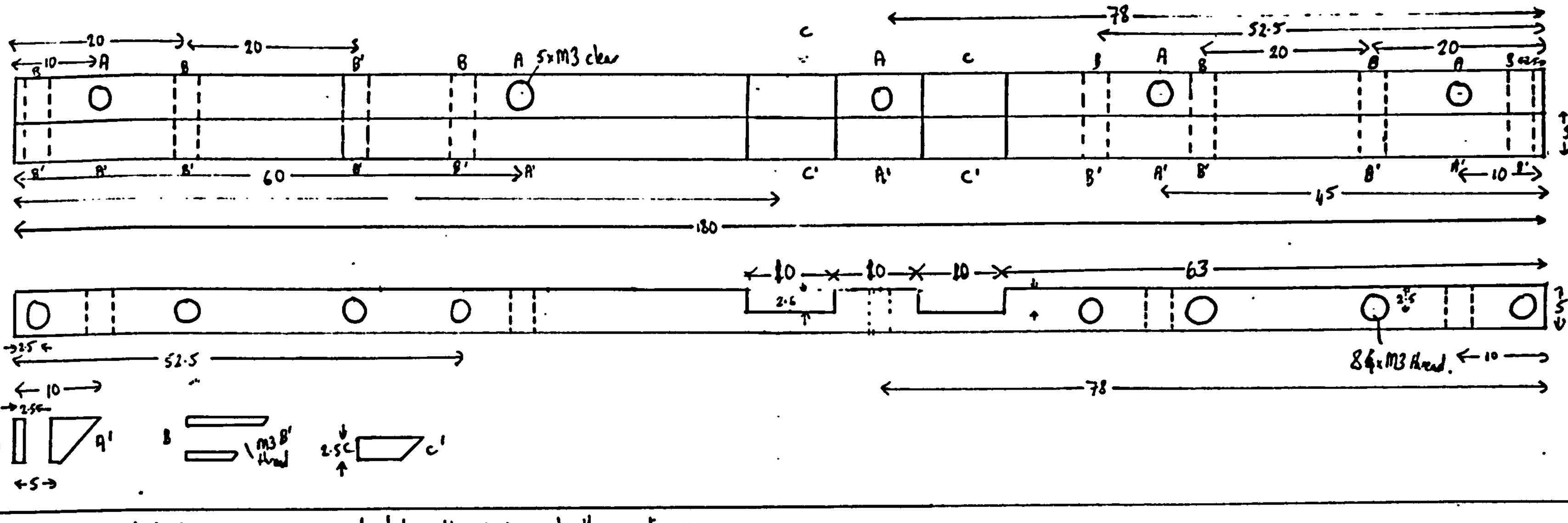

Track 2 ~~is~~ identical to track 1, except that section C is cut the opposite way.

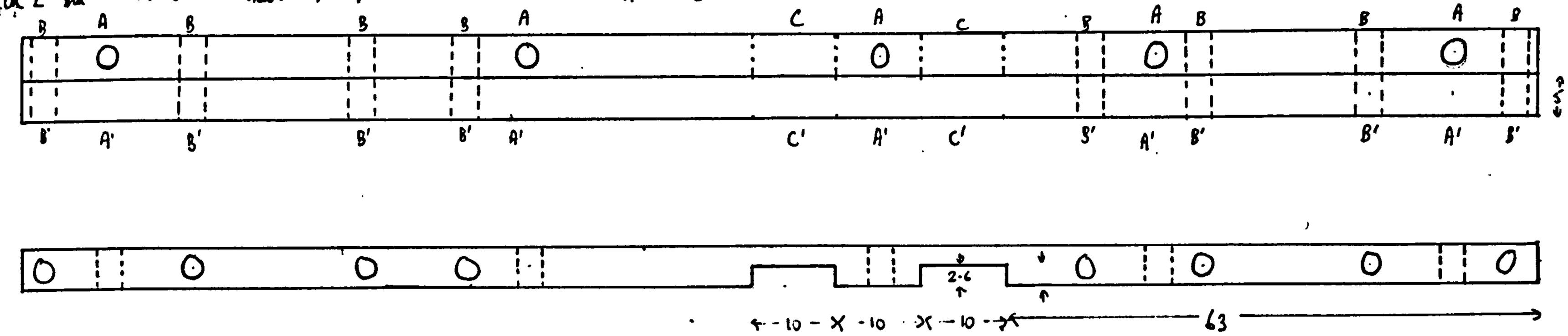

Tracks for Prism Movement

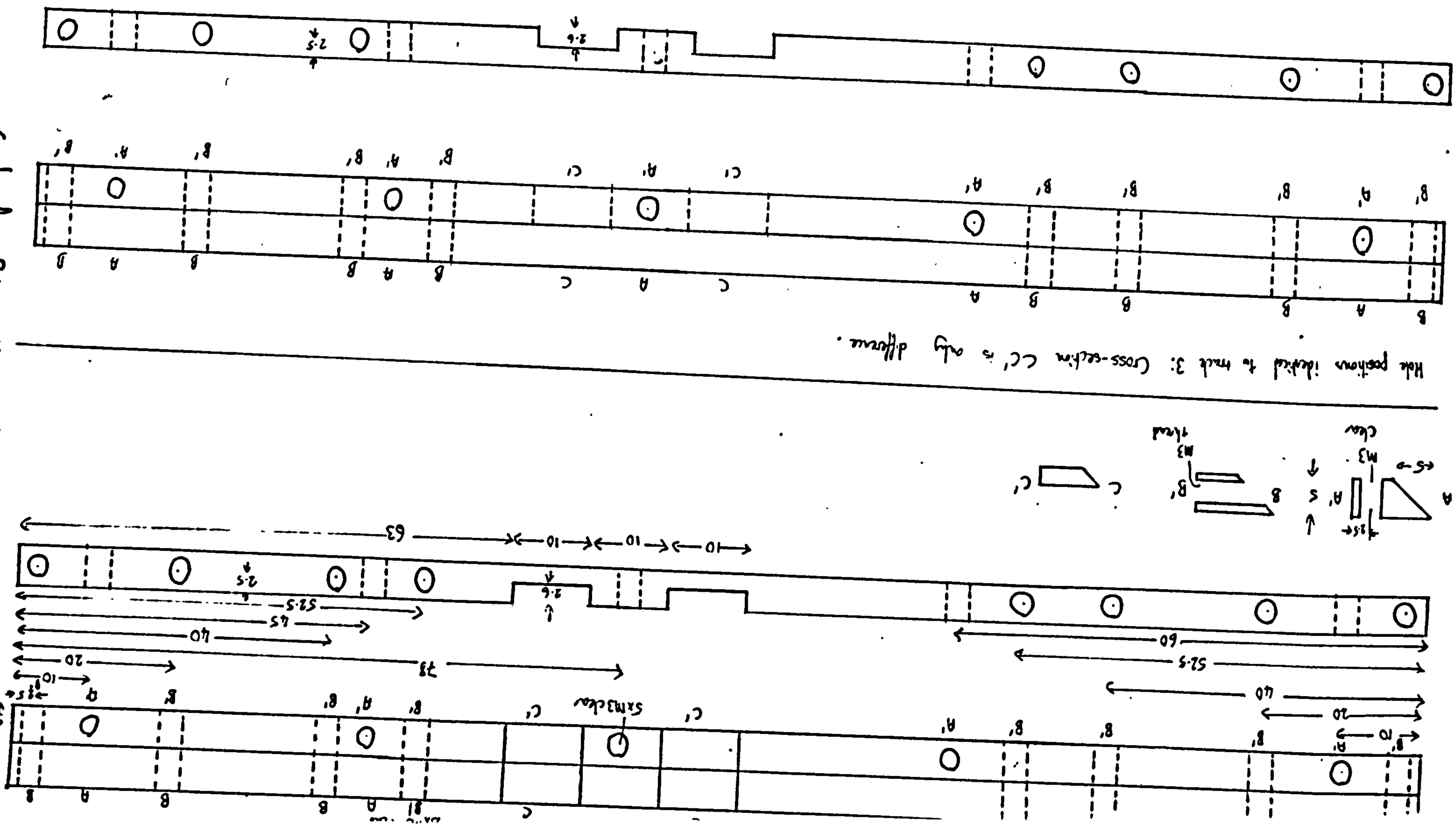

Hole positions identical to track 3: Cross-section CC' is only different.

Interferometer Table Support. Material: steel.
All dimensions in mm.

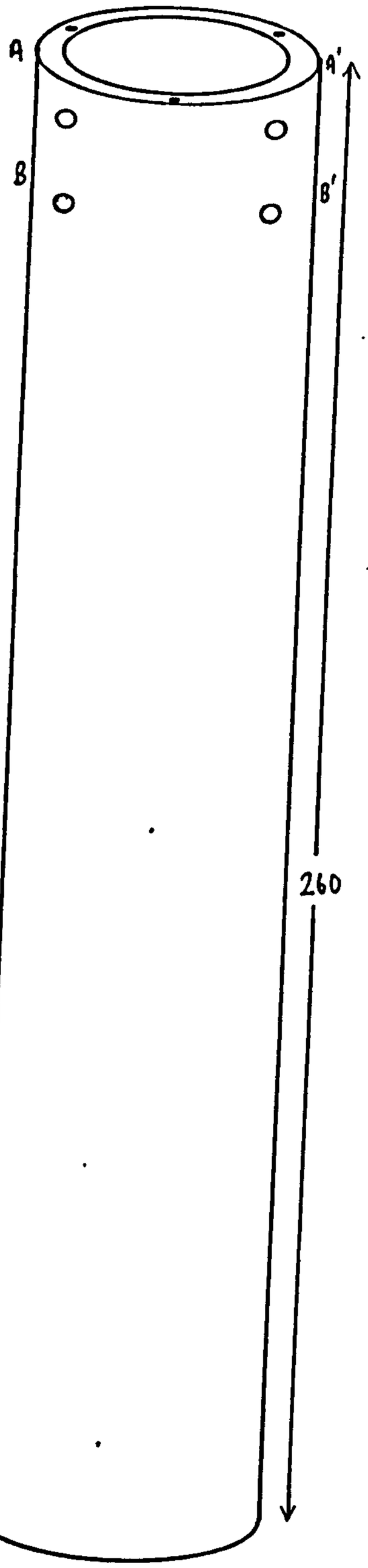

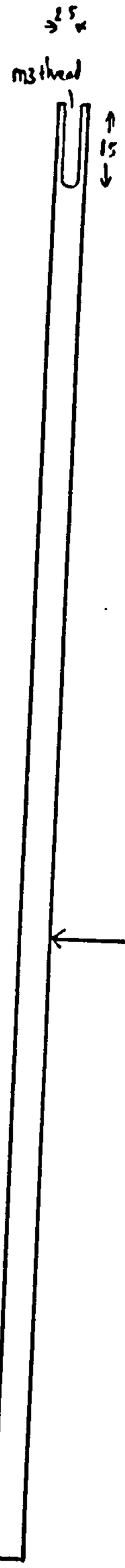

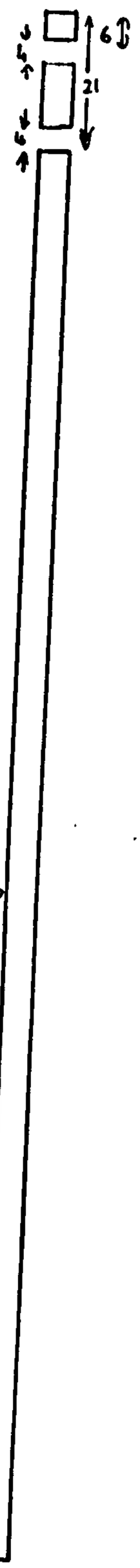

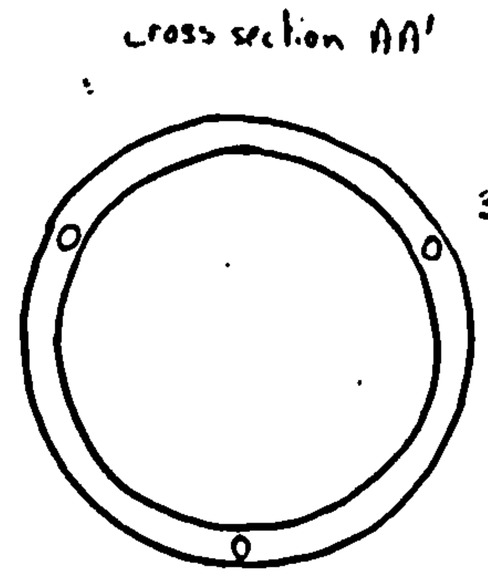

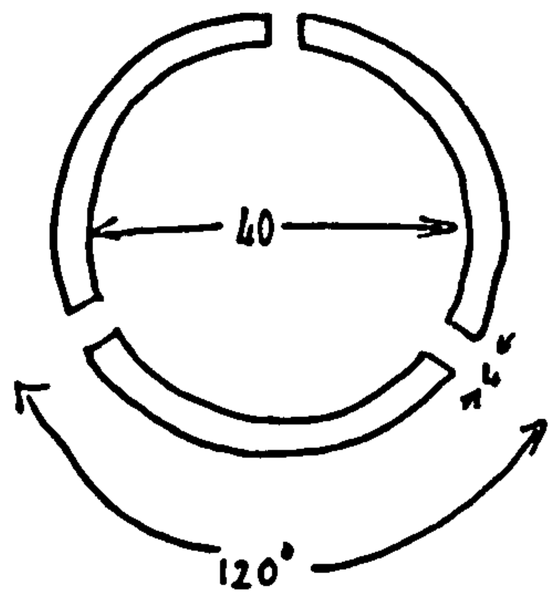

50

This cross-section is repeated every 120°

Column Adjustment. All dimensions in mm. Scale 1:2. Material: steel

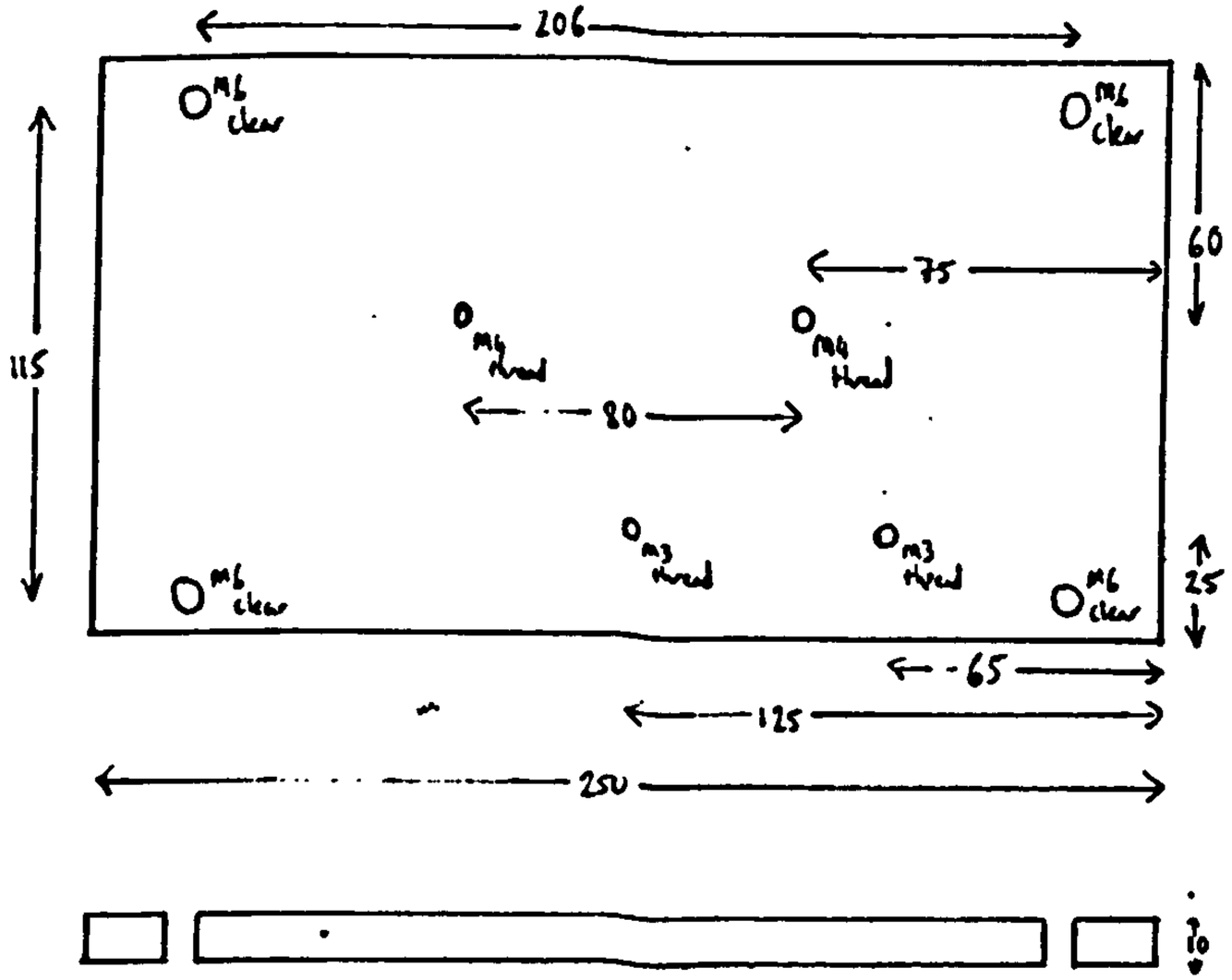

Part A4

Part B4

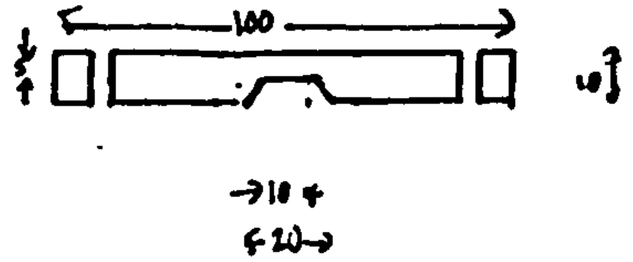

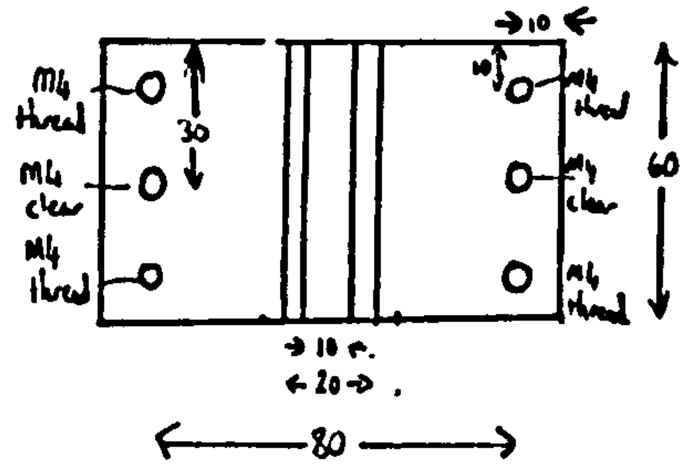

Part D4

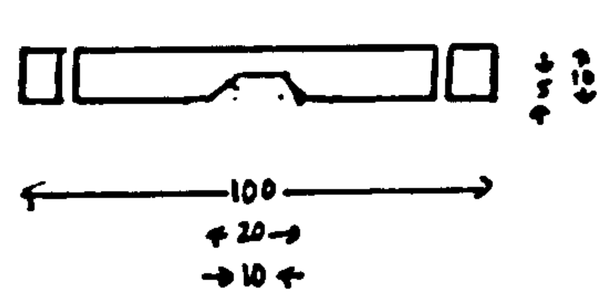

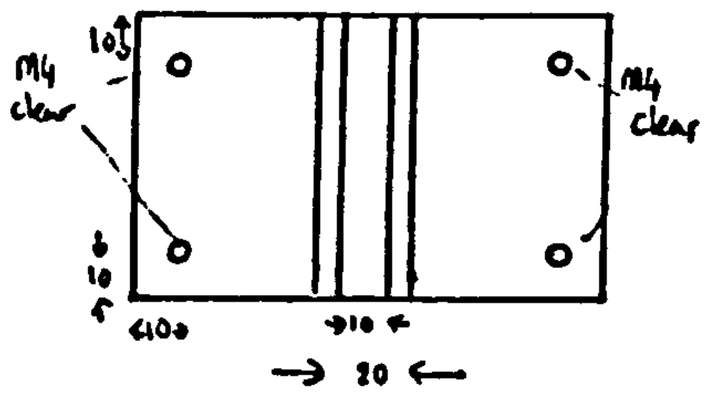

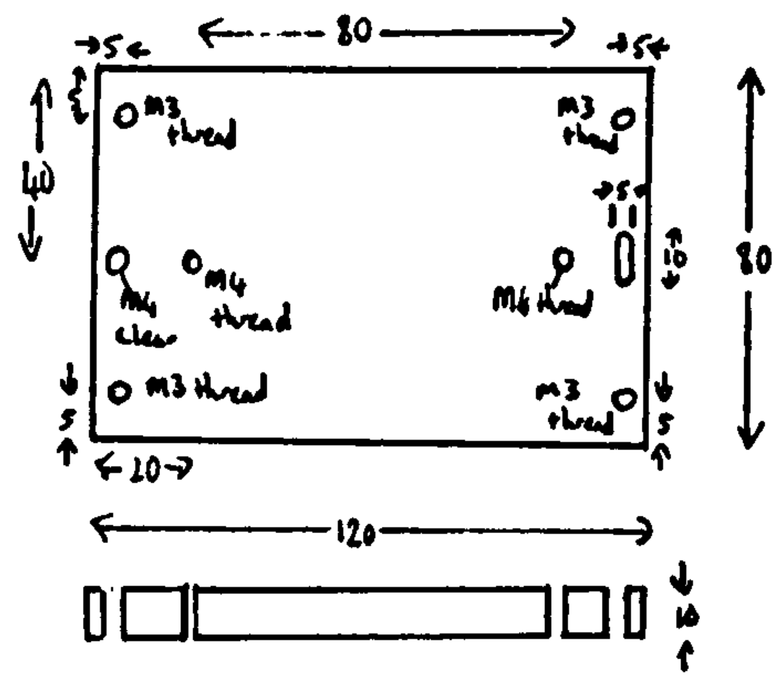

Part C4

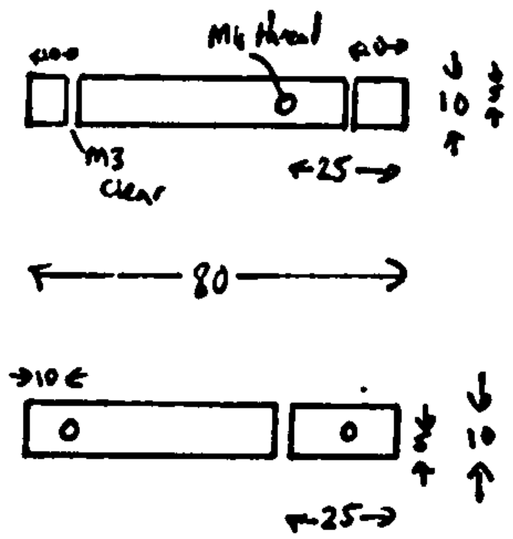

Part E4

Base-plate Height Adjustment.

215

Right handed prism plate

x2.

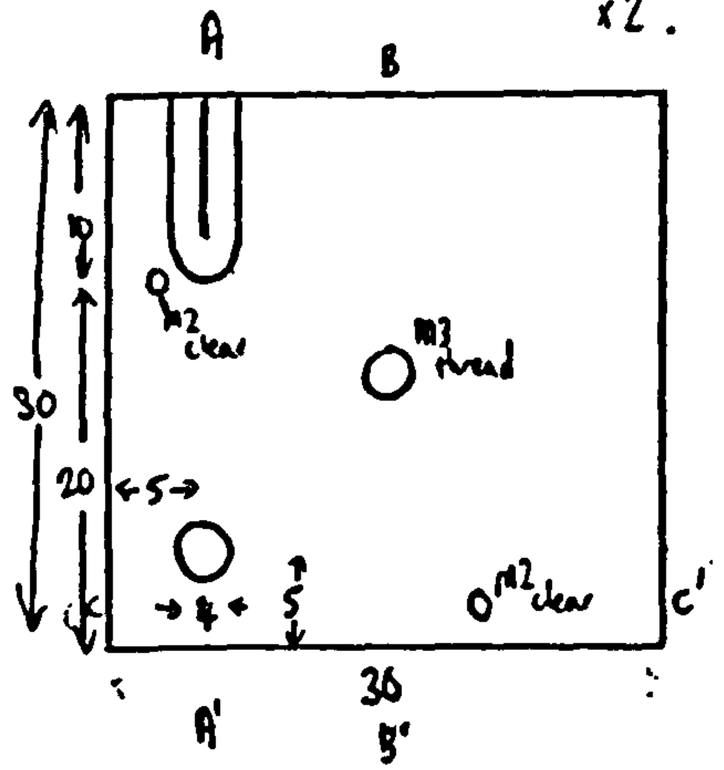

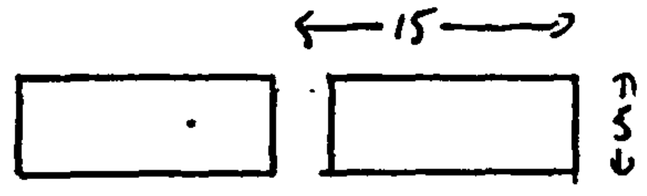

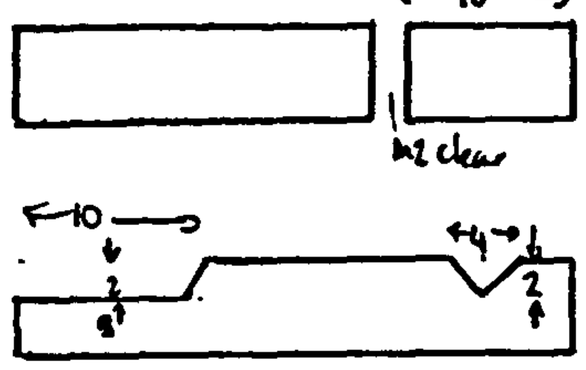

Right-handed interferometer prism holder x2

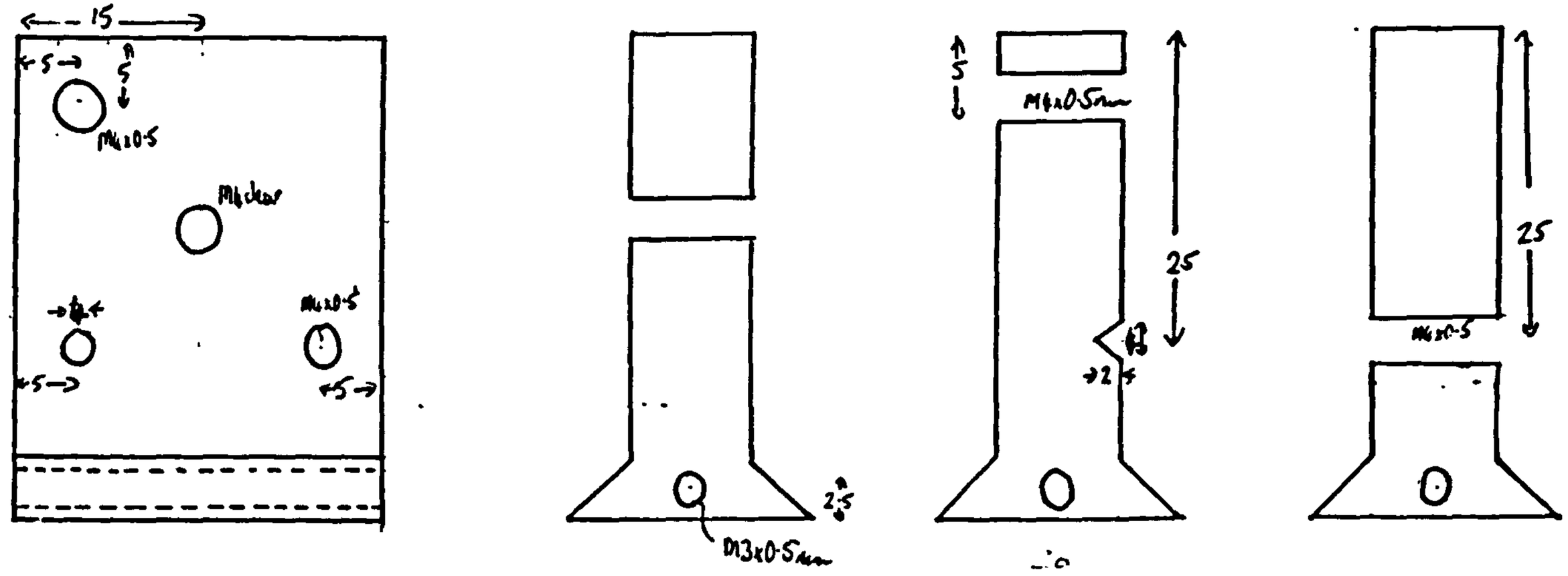

Longitudinal prism adjuster. x4 (made from M3 steel stock)

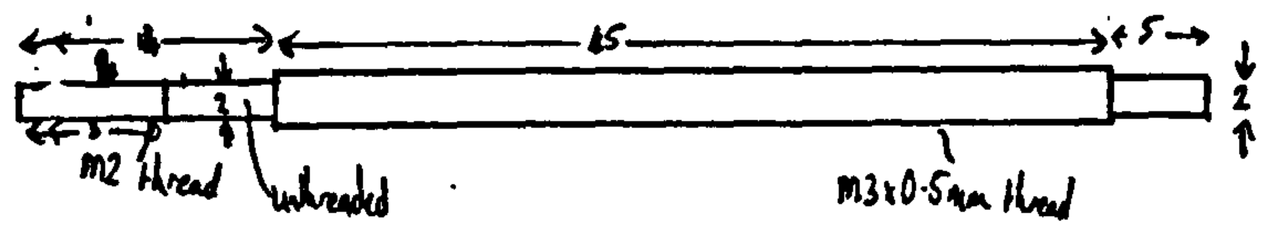

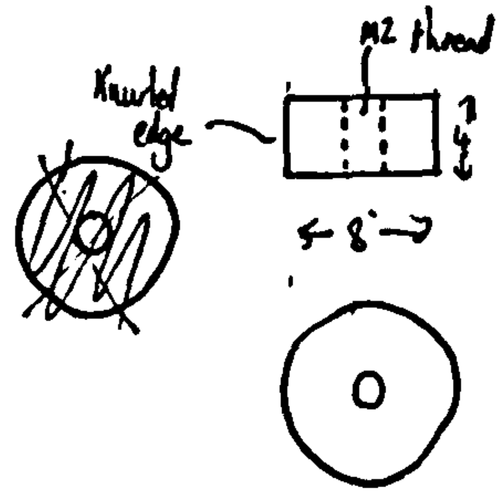

Adjuster-support. x8

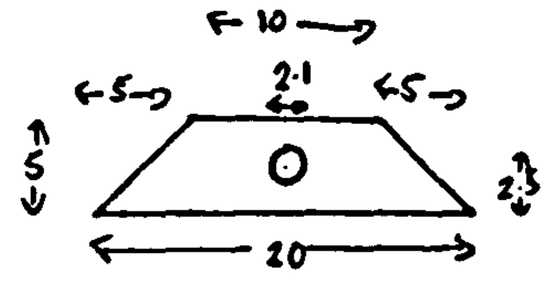

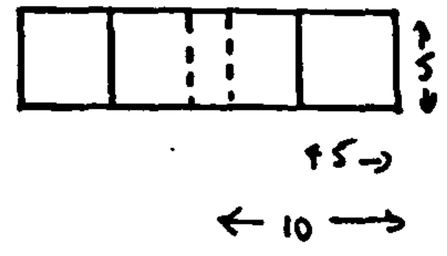

Kinematic Prism Holder

216

Left handed Prism plate x2

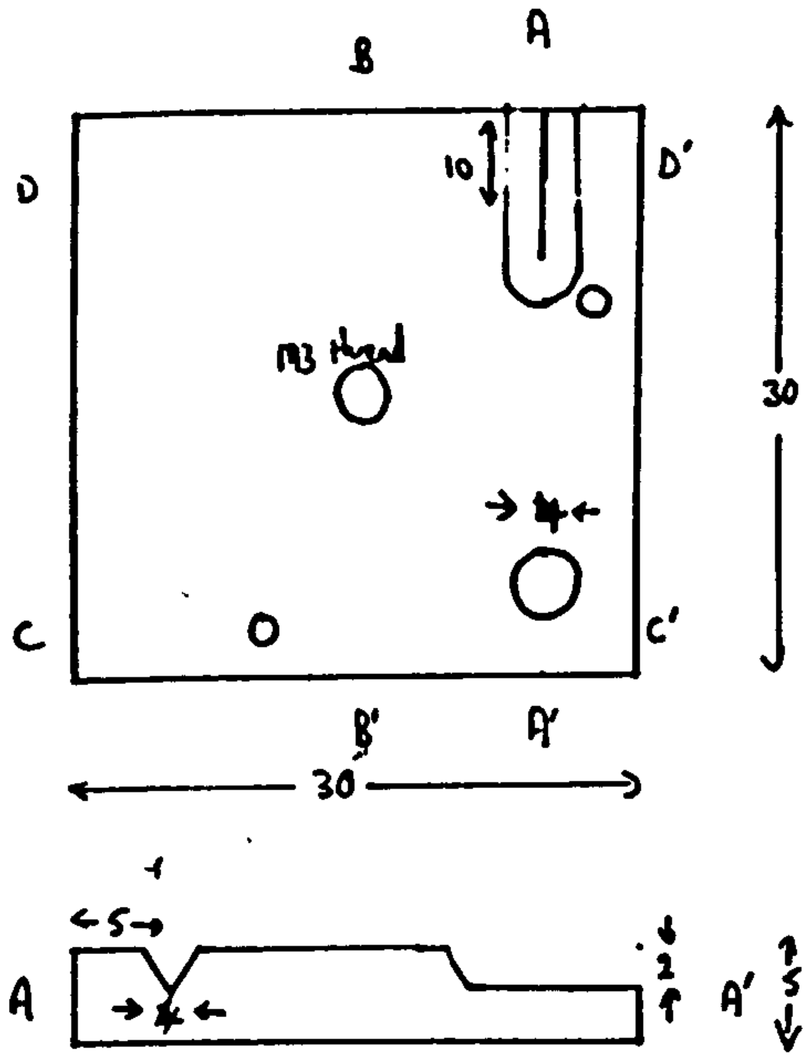

Left-handed interferometer prism holder x2

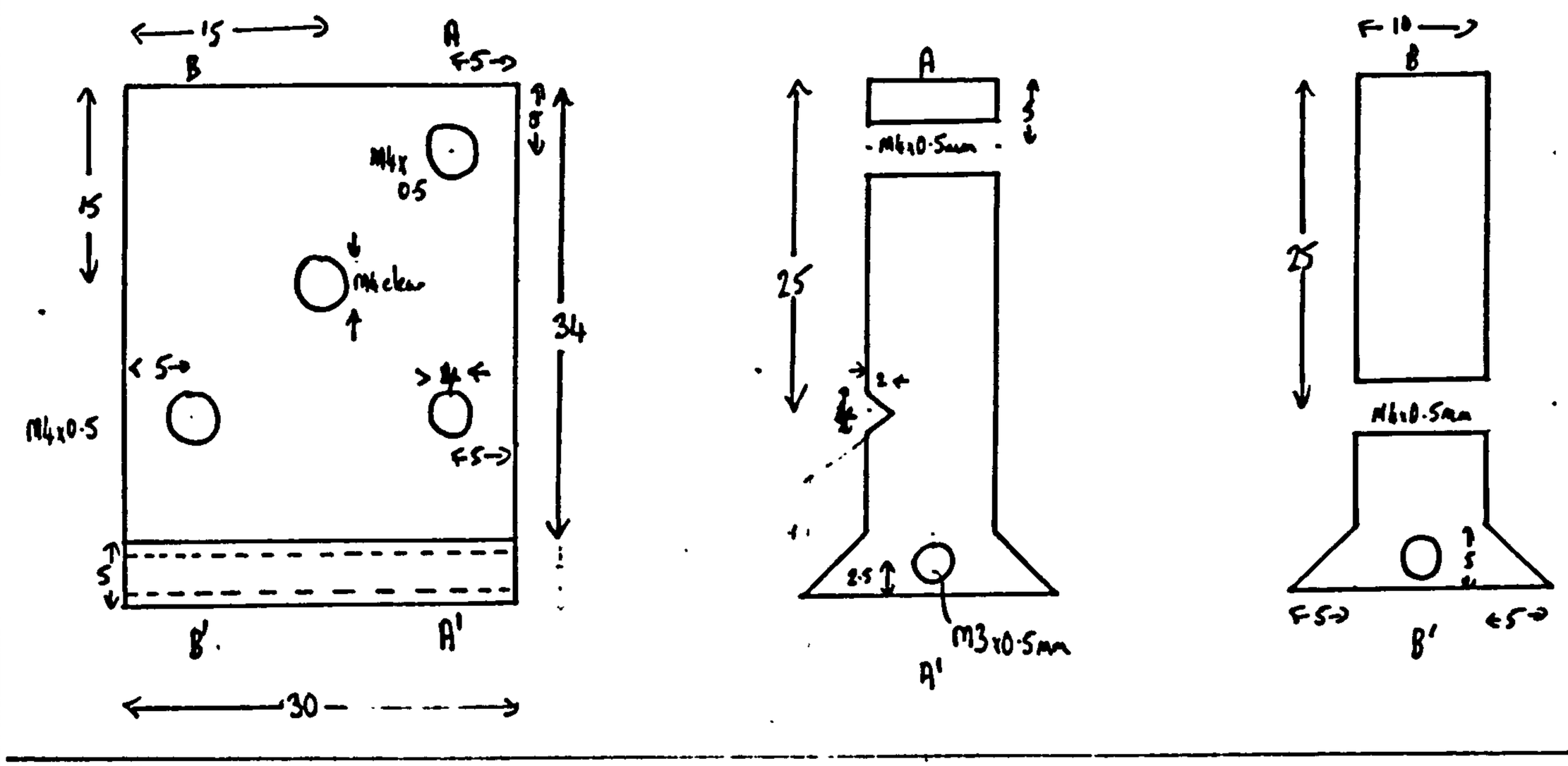

Adjustment bolt x8

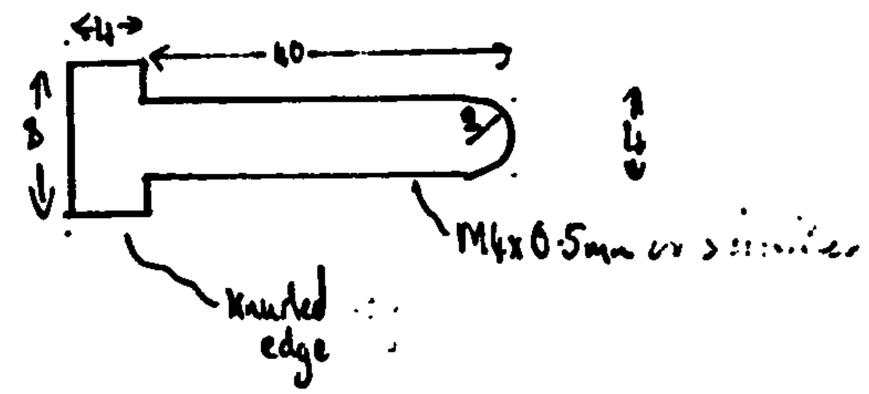

Spring loaded bolt x4.

Part D.

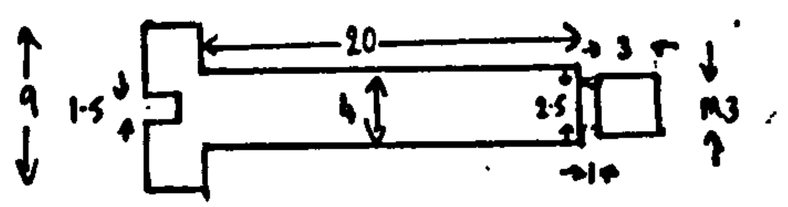

Kinematic Prism Holder

M3 holes x4

All dimensions in mm. Scale 2:1.

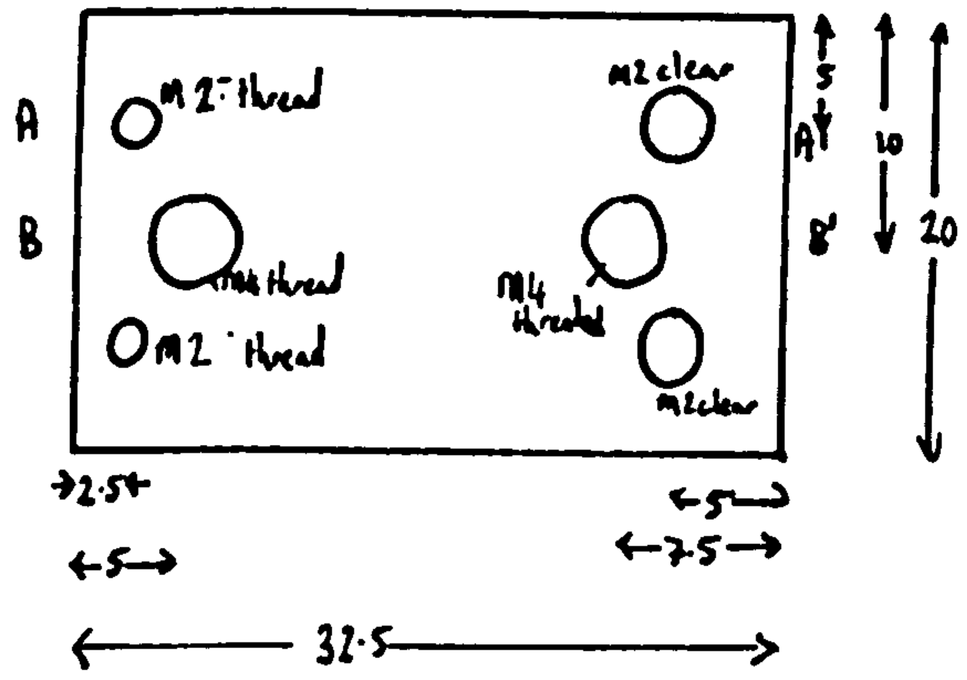

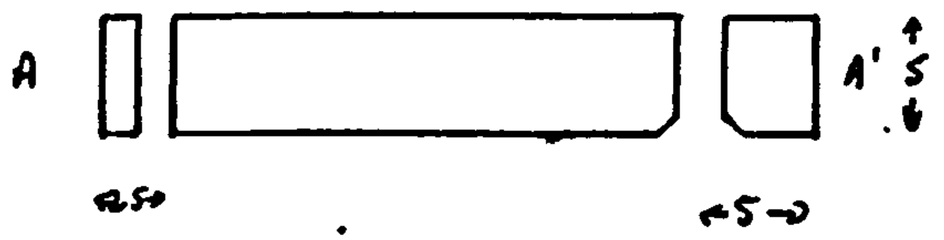

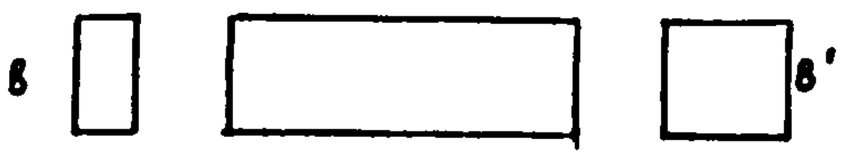

Part A1

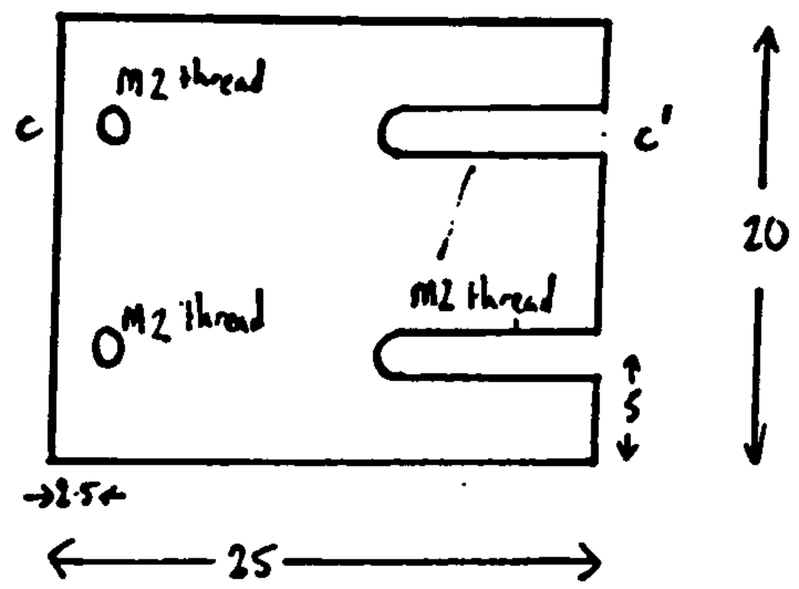

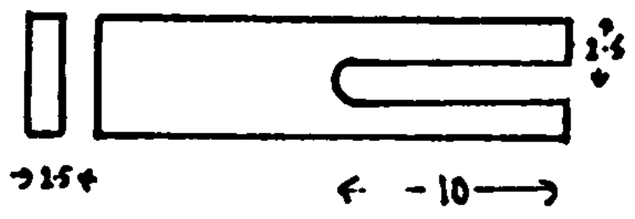

Part B1.

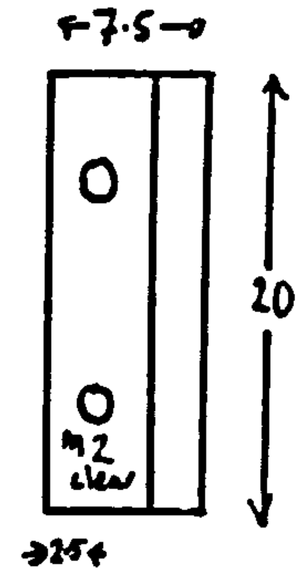

Part C1.

Note 2x C1 for each A1, B1.

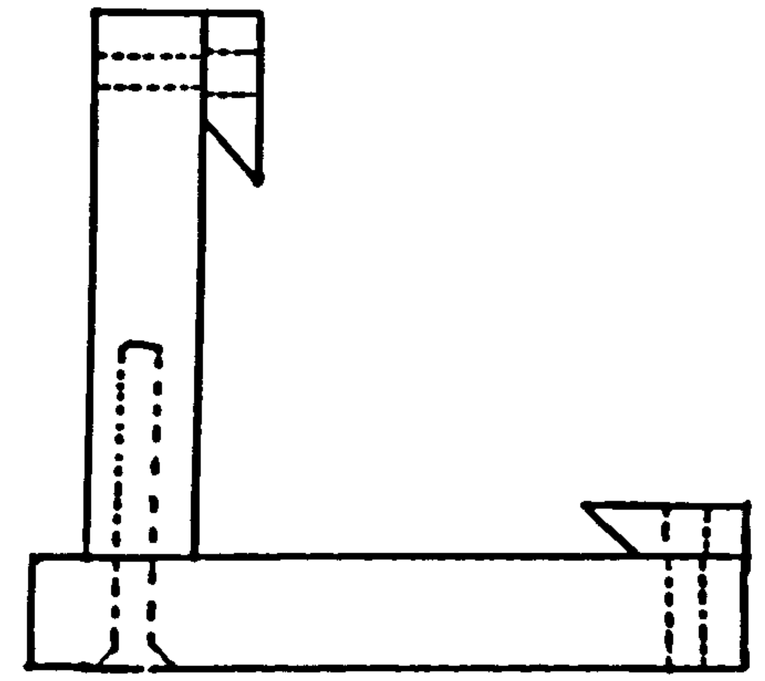

Parts A1, B1, and C1 joined together

Original Prism Holder

218

DETECTOR ASSEMBLY x2. All dimensions in mm.

Part A3

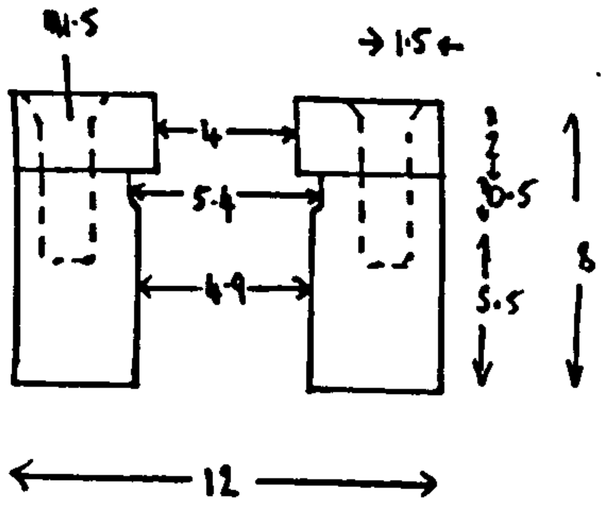

scale 4:1

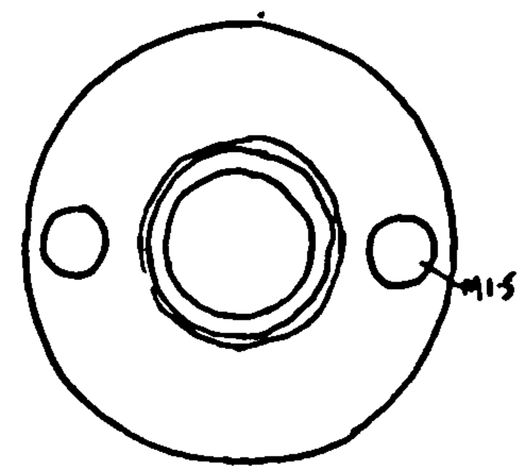

219.

Part F3

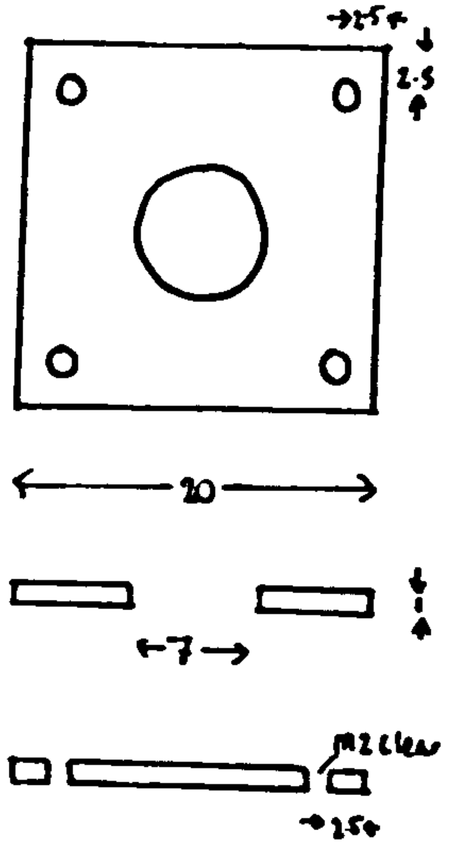

scale 2:1

Cross section AA'

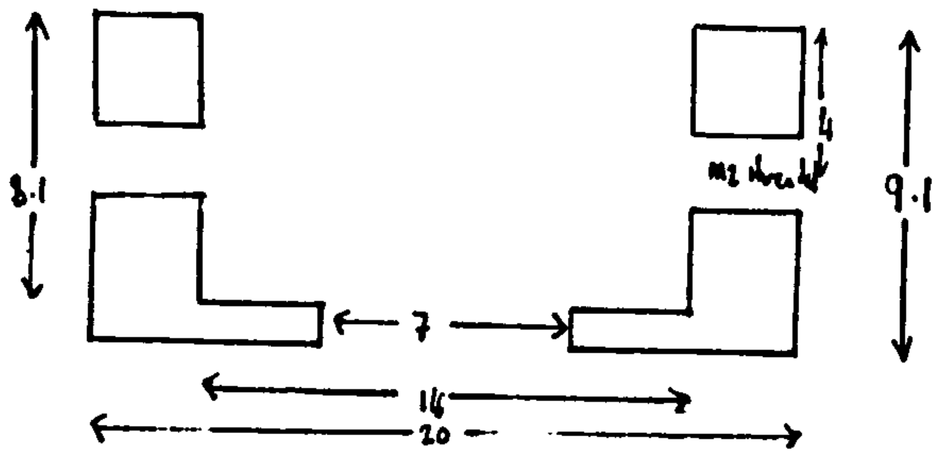

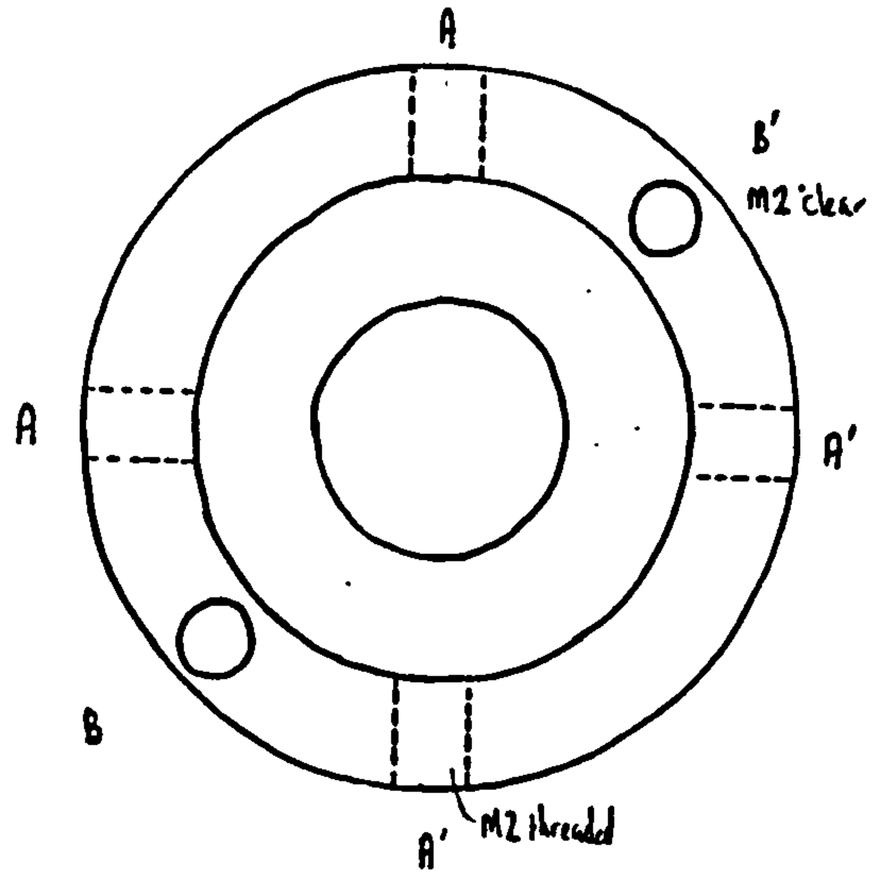

Cross section BB'

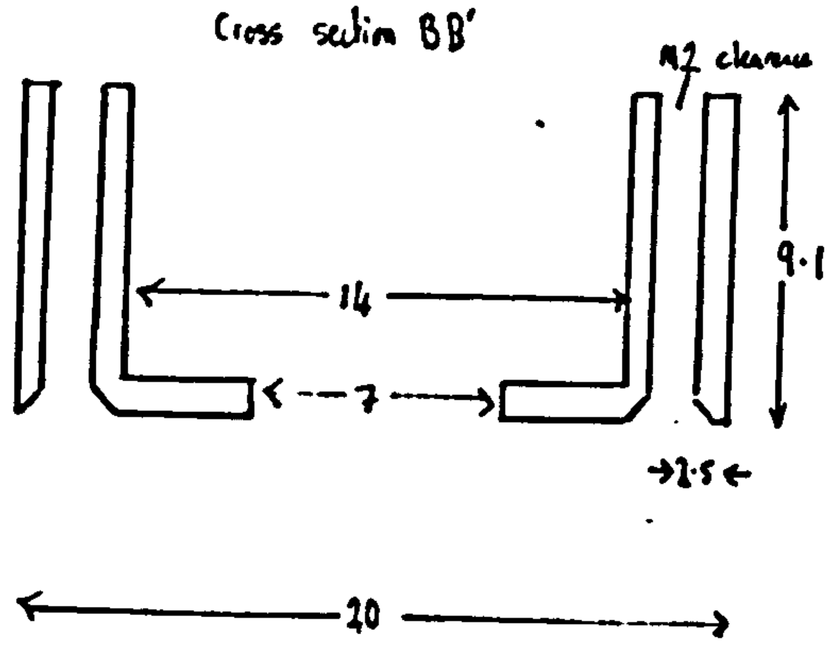

Part B3

scale 4:1

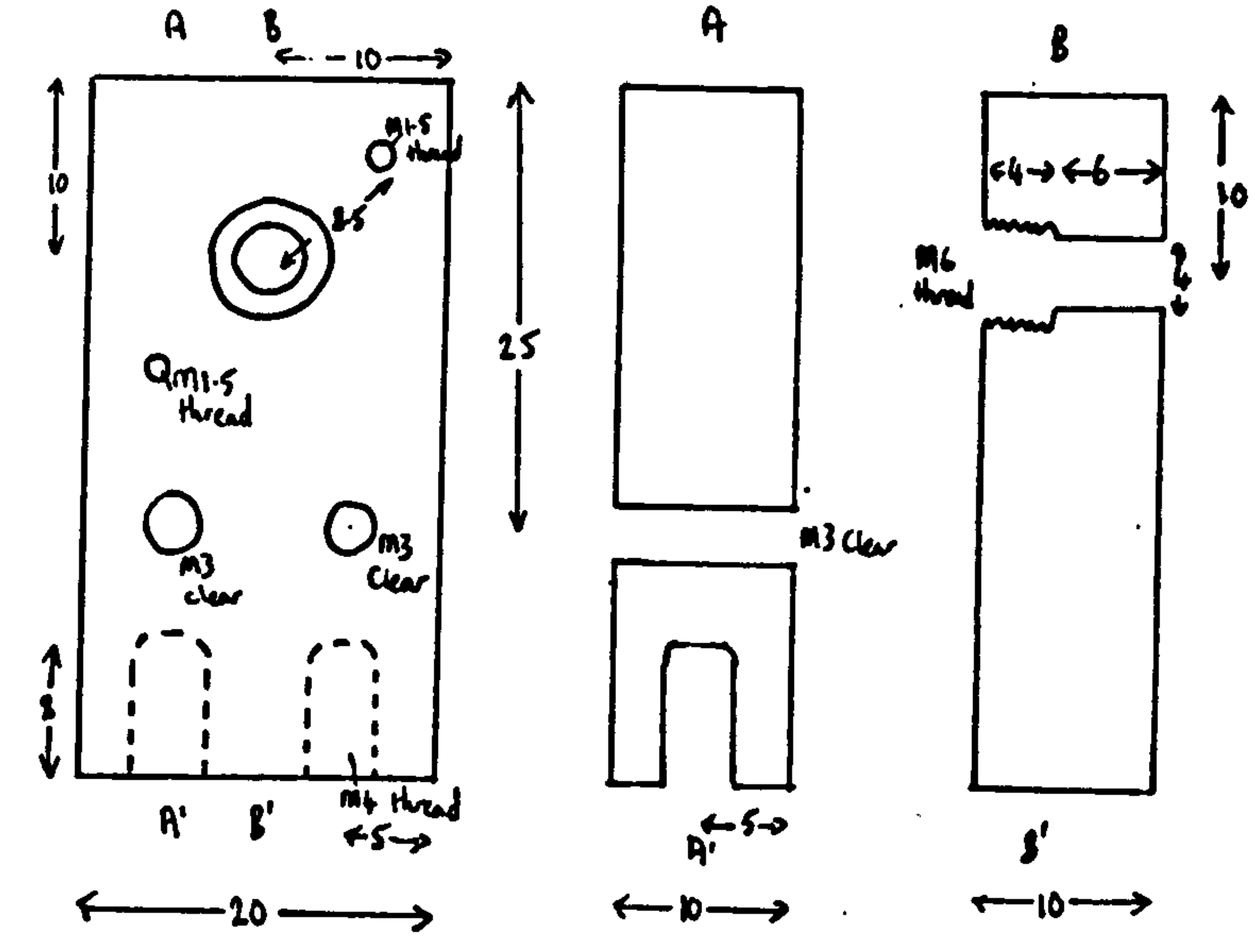

scale 2:1

Part C3

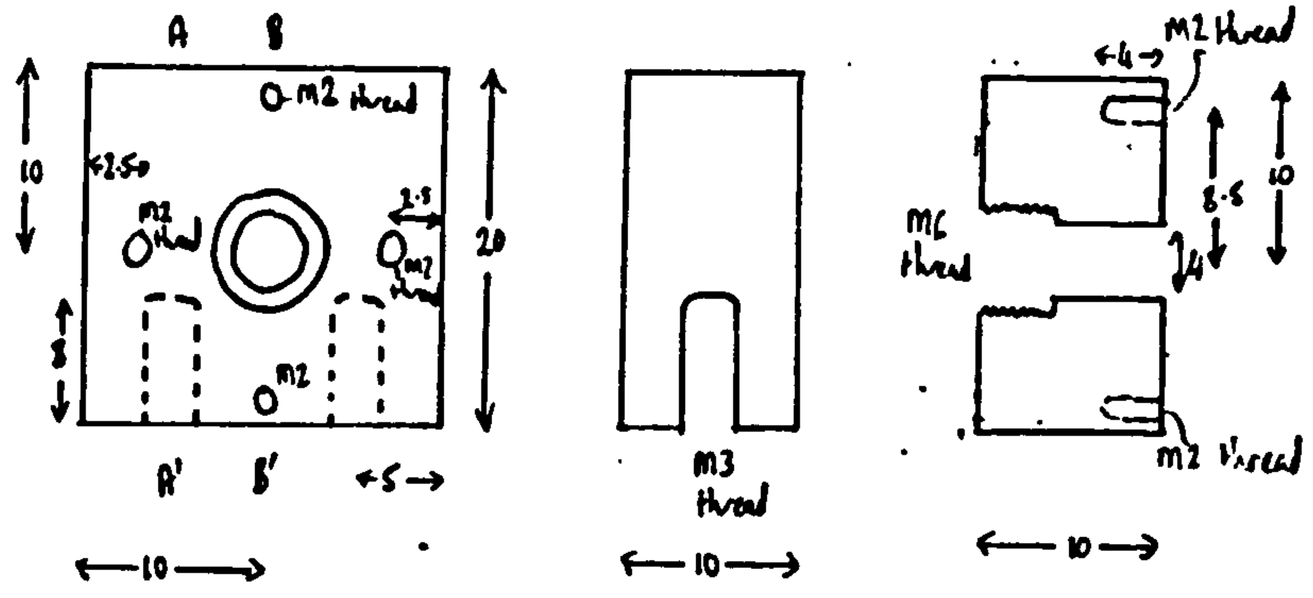

scale 2:1

Part D3

Part E3

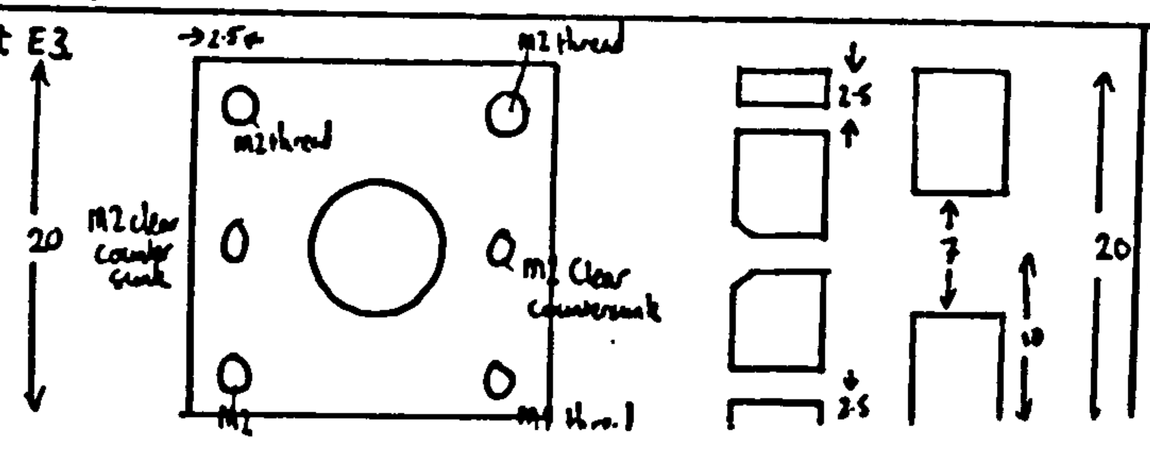

Detector Assembly

Laser Diode Holder. scale 2:1. Dimensions in mm. Material: steel.

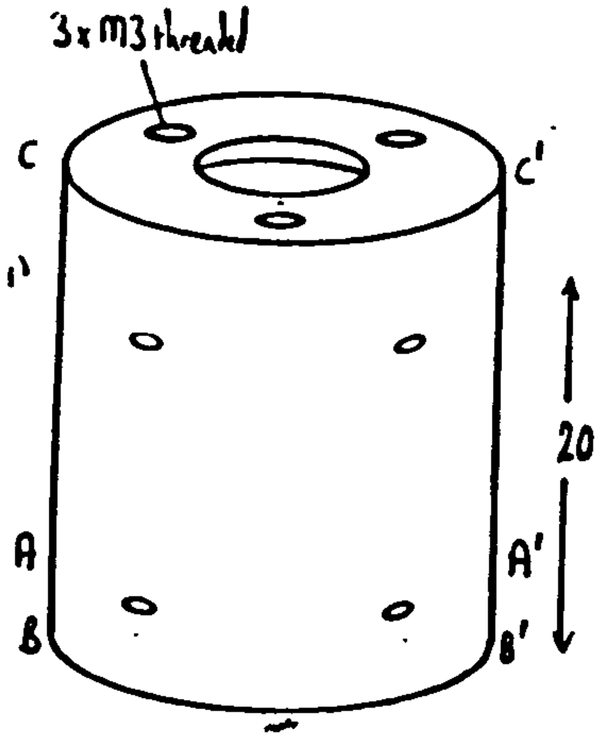

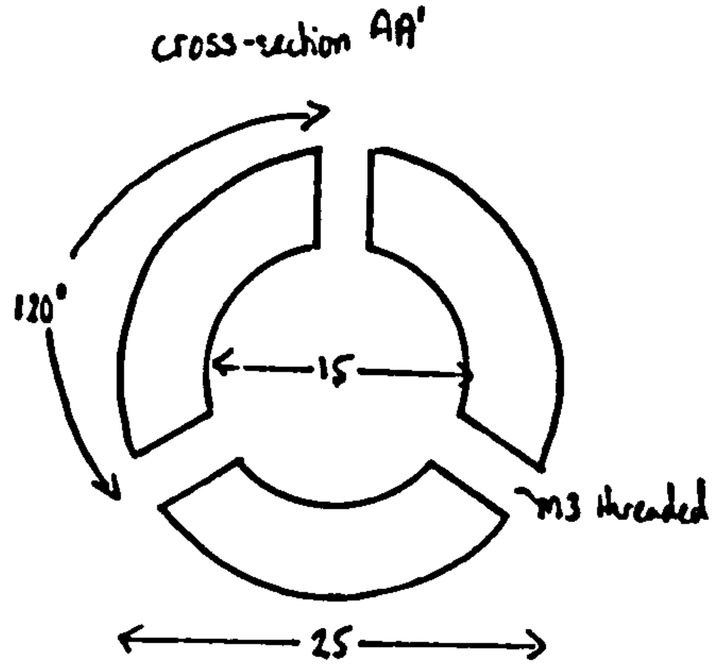

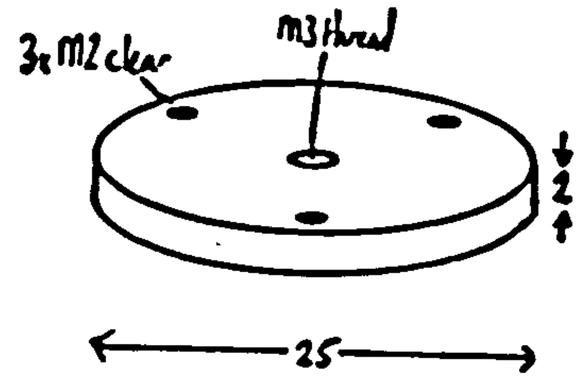

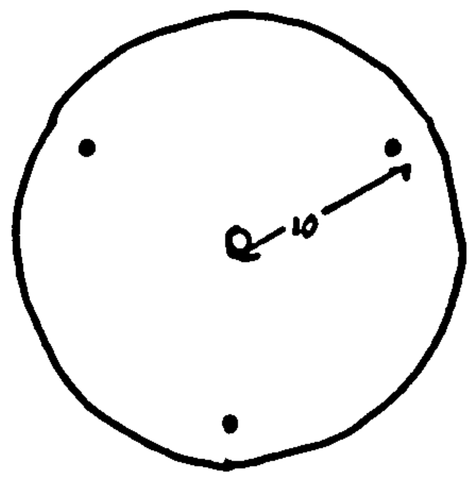

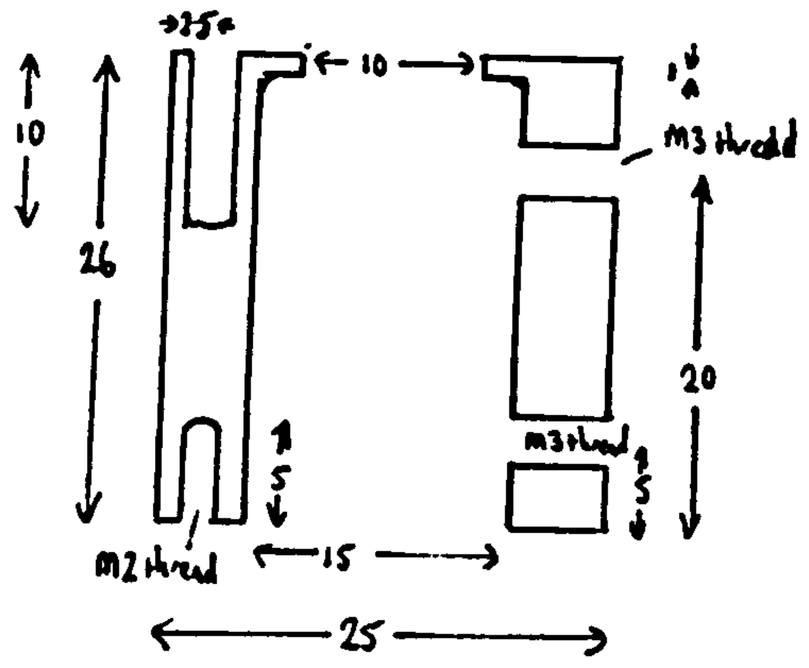

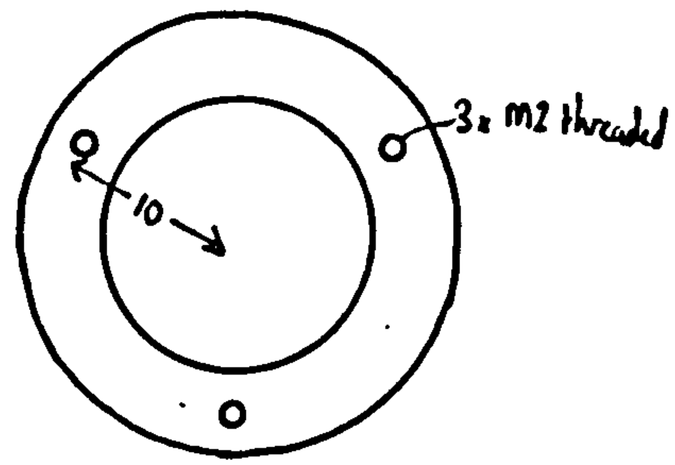

cross-section BB'

cross section CC'

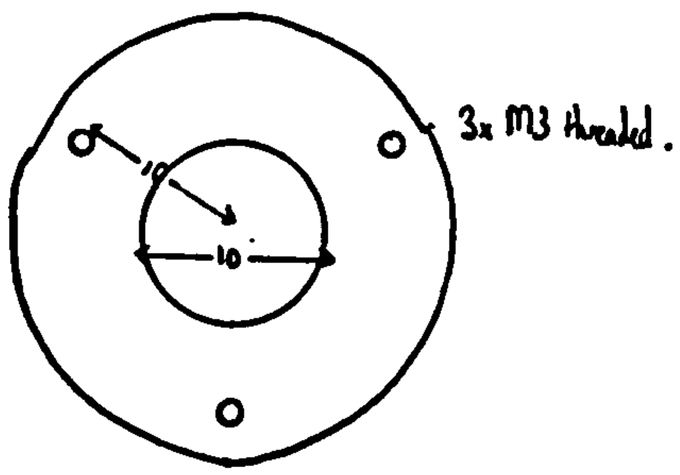

Detector Assembly constructed.

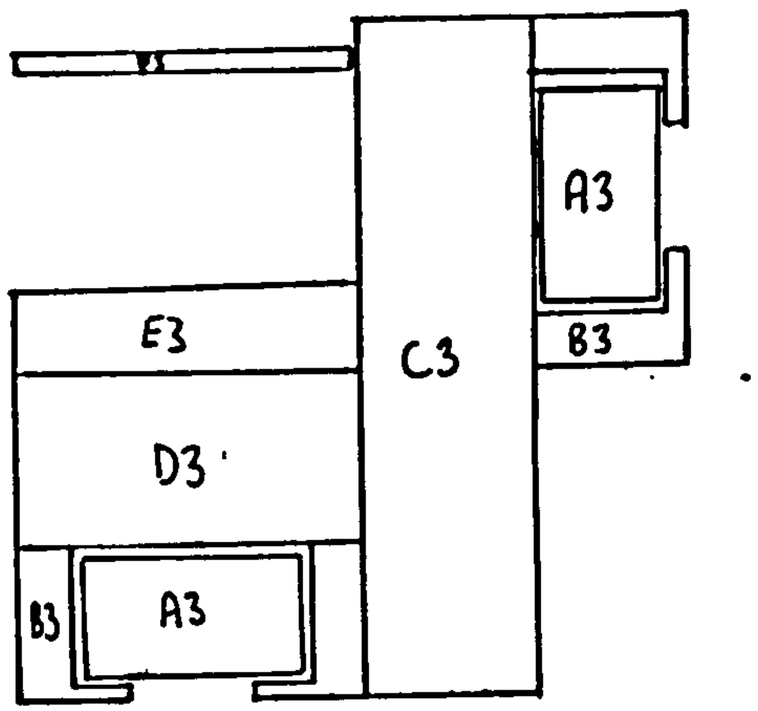

Dimensions in drawing below.

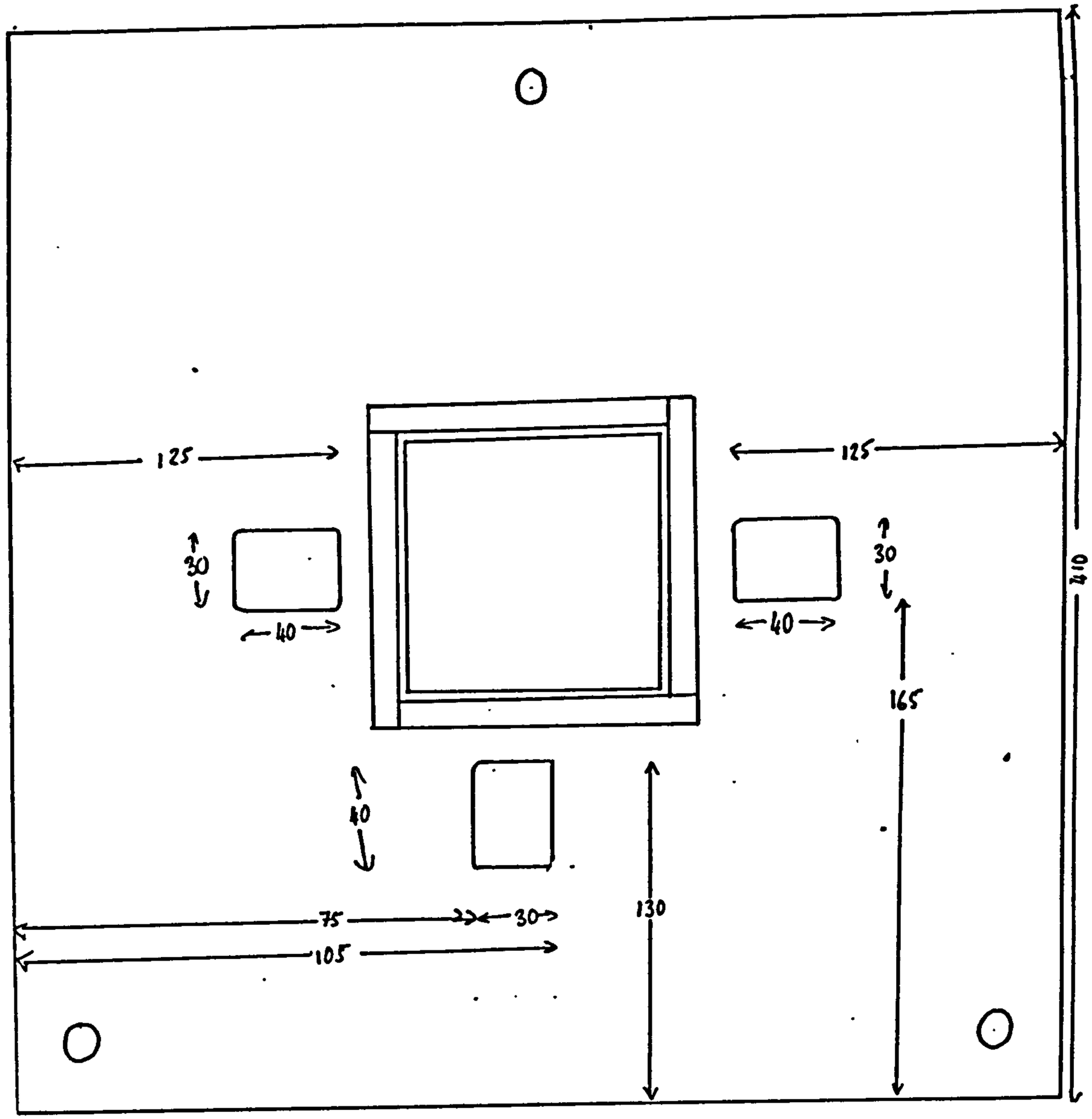

400

Kinematic plate holder.

All tolerances ±0·5mm apart from actual grating area.

Material HE30. 1off each.

part A

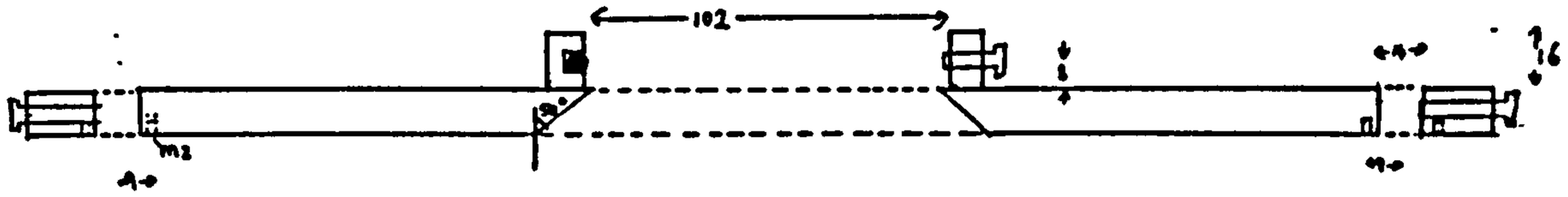

part B

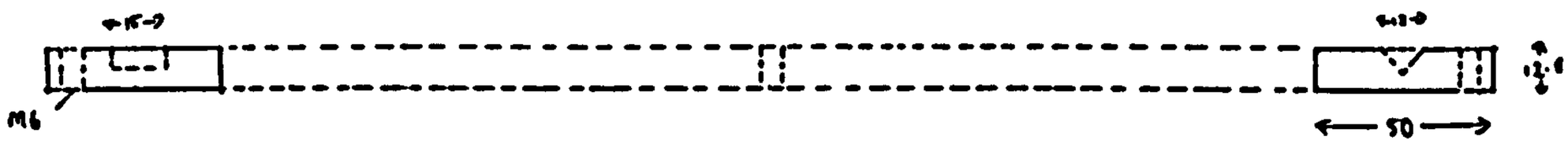

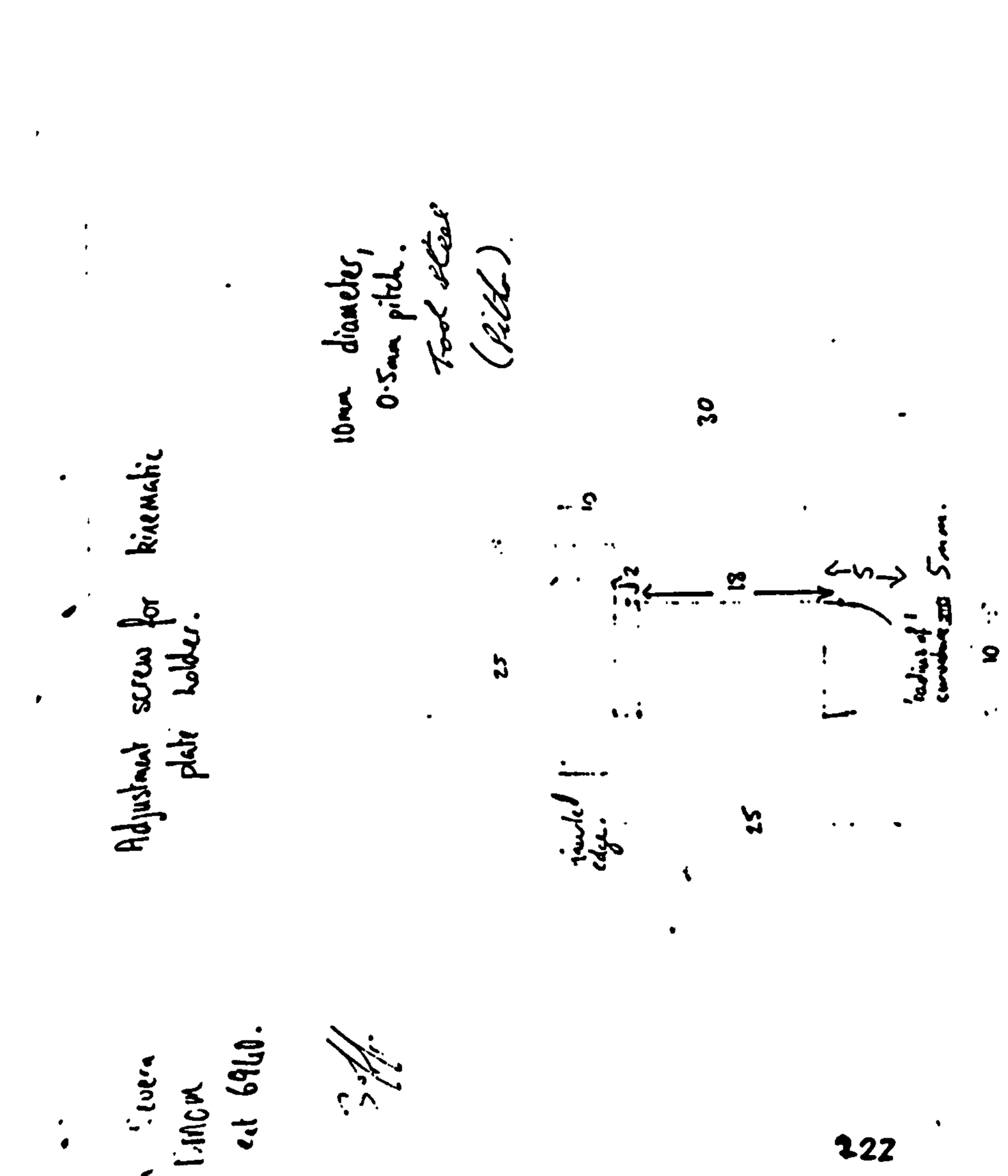

Part 8

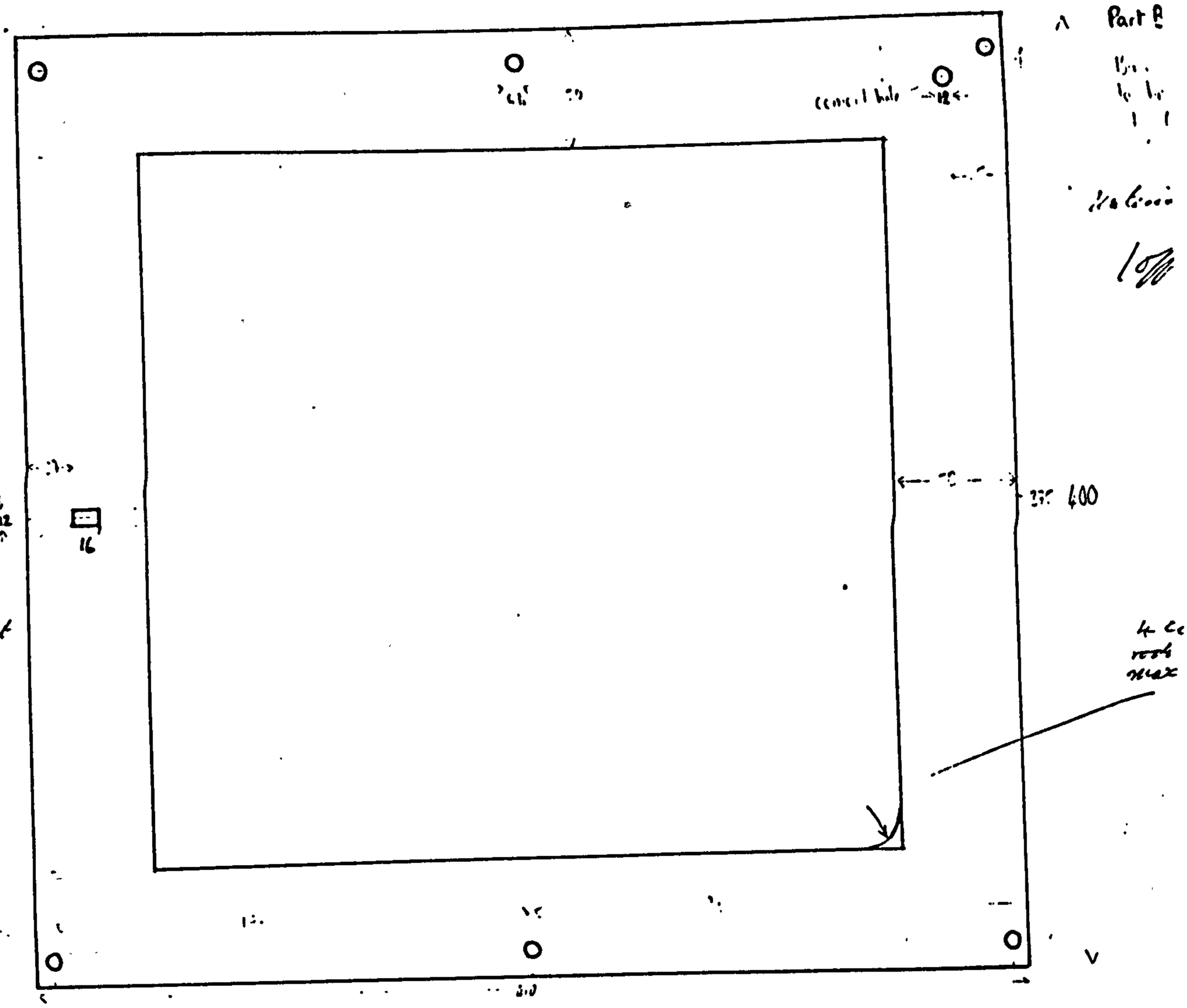

Clamping for height adjustment screws.

Phos. Bronze. 3 off.

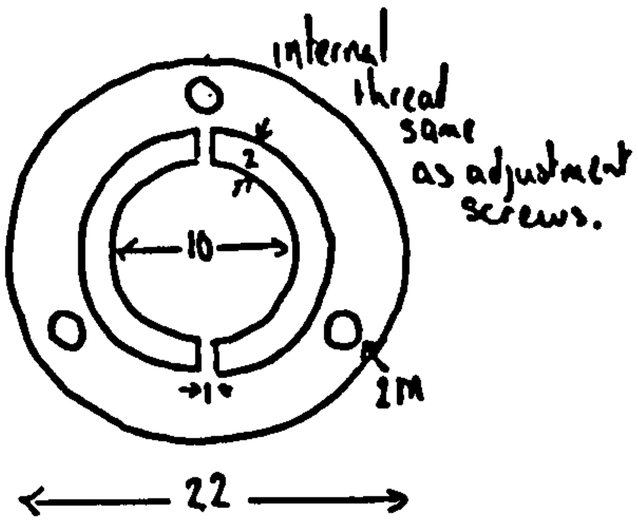

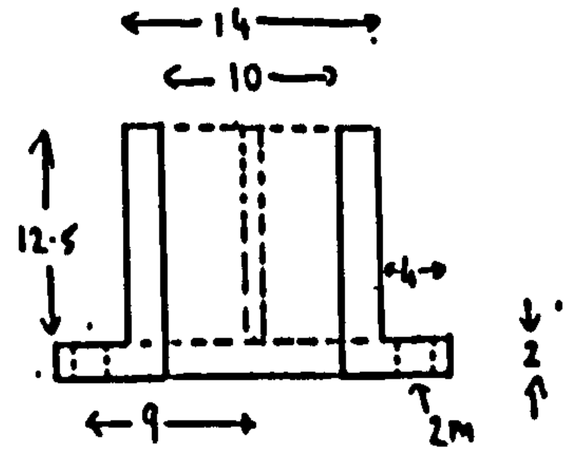

Part A plan.

Material
HE30.
1off

Plan of actual grating holder

1:1 scale

All parts on this sheet
± 0·2mm.

Material HE30.
1 off.

Plan of actual area.

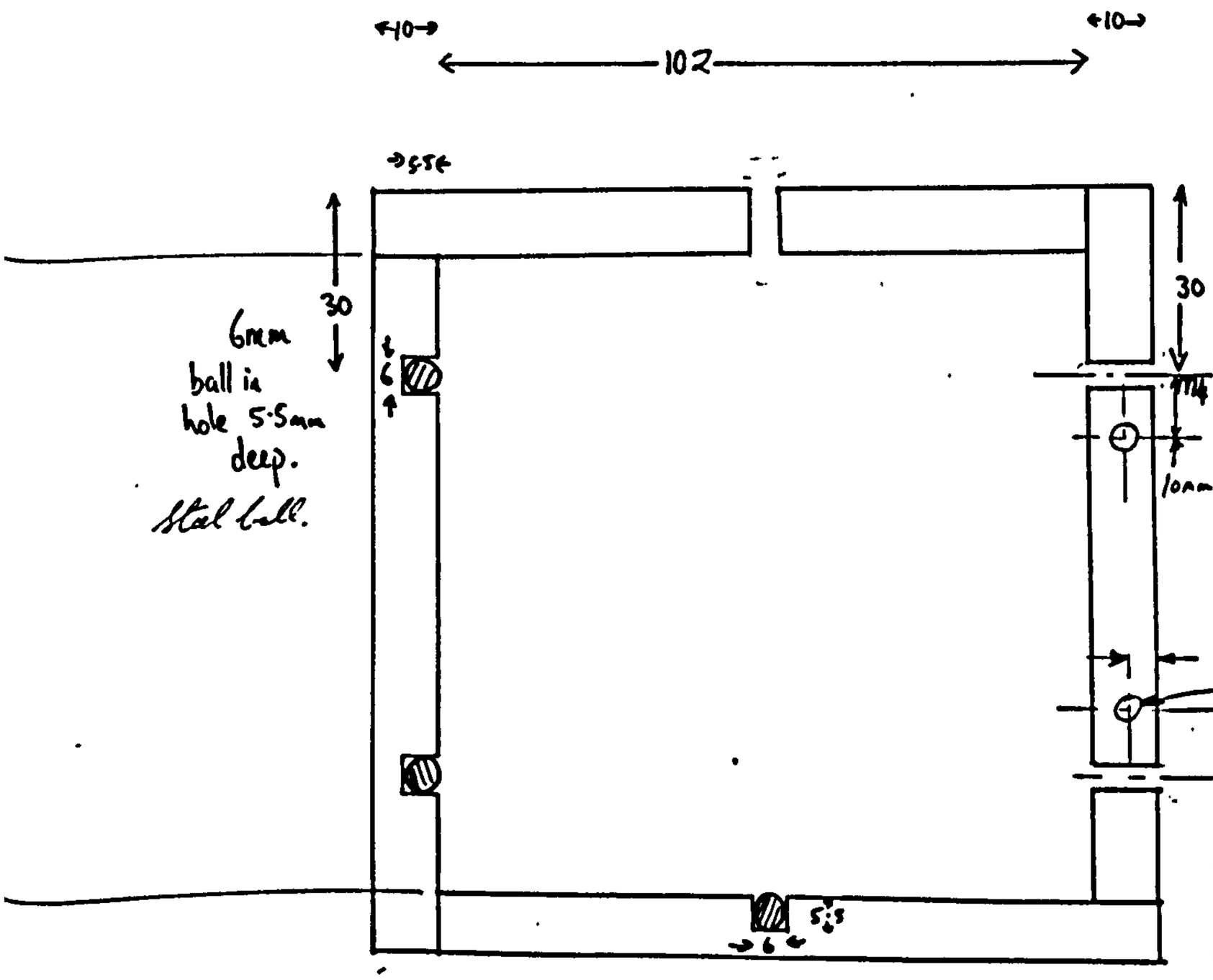

Appendix 4: Calculation Of Measurement Error Due To Pitch

The following model has been developed to predict the effect of pitch on the accuracy of the new interferometer. Figure A4.1 defines the symbols used in this model. The angle of pitch Δ is also the angle of incidence of the input beam on the grating.

$$d(\sin\Delta+\sin\theta)=m\lambda \qquad \text{A4.1}$$

where d=the grating pitch, and m is the order of diffraction.

Consider the positive diffraction order.

$$\alpha=\theta+\Delta \qquad \text{A4.2}$$

$$h_1=\frac{d}{\tan\alpha} \qquad \text{A4.3}$$

$$h_2=H-h_1 \qquad \text{A4.4}$$

$$d_1=h_2\tan\alpha \qquad \text{A4.5}$$

$$d_2=H\tan\alpha \qquad \text{A4.6}$$

The distance between the output beam and the input beam is calculated as follows. The point at which the input beam strikes the grating is given the coordinates (0,0). The gradient of the beam returning to the grating from the prism is cotα.

Therefore the equation of the line of the returning beam can be described by:-

$$y=x\cot\alpha+c \qquad \text{A4.7}$$

The coordinates of point A are $(d-d_1,H)$. Substituting this information into equation A4.7 allows the constant, c, to be calculated and A4.7 becomes:-

$$y=x\cot\alpha+H-(d-d_1)\cot\alpha \qquad \text{A4.8}$$

The equation of the grating surface is:-

$$y=-x\tan\alpha \qquad \text{A4.9}$$

Equating equations A4.8 and A4.9 gives the coordinates of the point at which the beam returns to the grating surface(x_1,y_1).

$$x_1=\frac{(d-d_1)\cot\alpha-H}{\cot\alpha+\tan\Delta} \qquad \text{A4.10}$$

$$y_1=-x_1\tan\Delta \qquad \text{A4.11}$$

The point where the negative order beam returns to the diffraction grating surface may be calculated in a similar manner. The quantity s, the separation between the input and output beams for the case when $\Delta=0°$ can calculated from A4.10 ($s=|x_1|$ when $\Delta=0°$).

$$\sin\theta_2=-\frac{\lambda}{d}-\sin\Delta \qquad \text{A4.12}$$

$$\beta = |\theta_2| - \Delta \qquad \text{A4.13}$$

$$d_3 = H\tan\beta \qquad \text{A4.14}$$

$$d_4 = d + s - d_3 \qquad \text{A4.15}$$

$$h_3 = \frac{d_4}{\tan\beta} \qquad \text{A4.16}$$

$$h_4 = H - h_3 \qquad \text{A4.17}$$

The coordinates of point B are (-d-s,h_4), and the gradient of the beam returning from there to the grating is -cotβ. Therefore, the equation of the returning beam is:-

$$y = -\cot\beta + h_4 - (d+s)\cot\beta \qquad \text{A4.18}$$

Relating this equation with that of the grating surface, A4.9, gives the coordinates at which the negative diffraction order returns to the grating surface.

$$x_2 = \frac{h_4 - (d+s)\cot\beta}{\cot\beta - \tan\Delta} \qquad \text{A4.19}$$

$$y_2 = -x_2\tan\Delta$$

If it is assumed that the midpoint of the two returning beams is taken as the

position where the interference effects occur, then the error due to movement of the output beam along the grating surface(t) is:-

$$t=\sqrt{x_1^2+y_1^2}+\sqrt{x_2^2+y_2^2}-s \qquad \text{A4.20}$$

Typical values for the quantities needed to calculate t are H=45mm, d=40mm, and Δ=0.0002°. Using these values in equations A4.10, A4.11, A4.19 and A4.20 gives an error of 240nm.

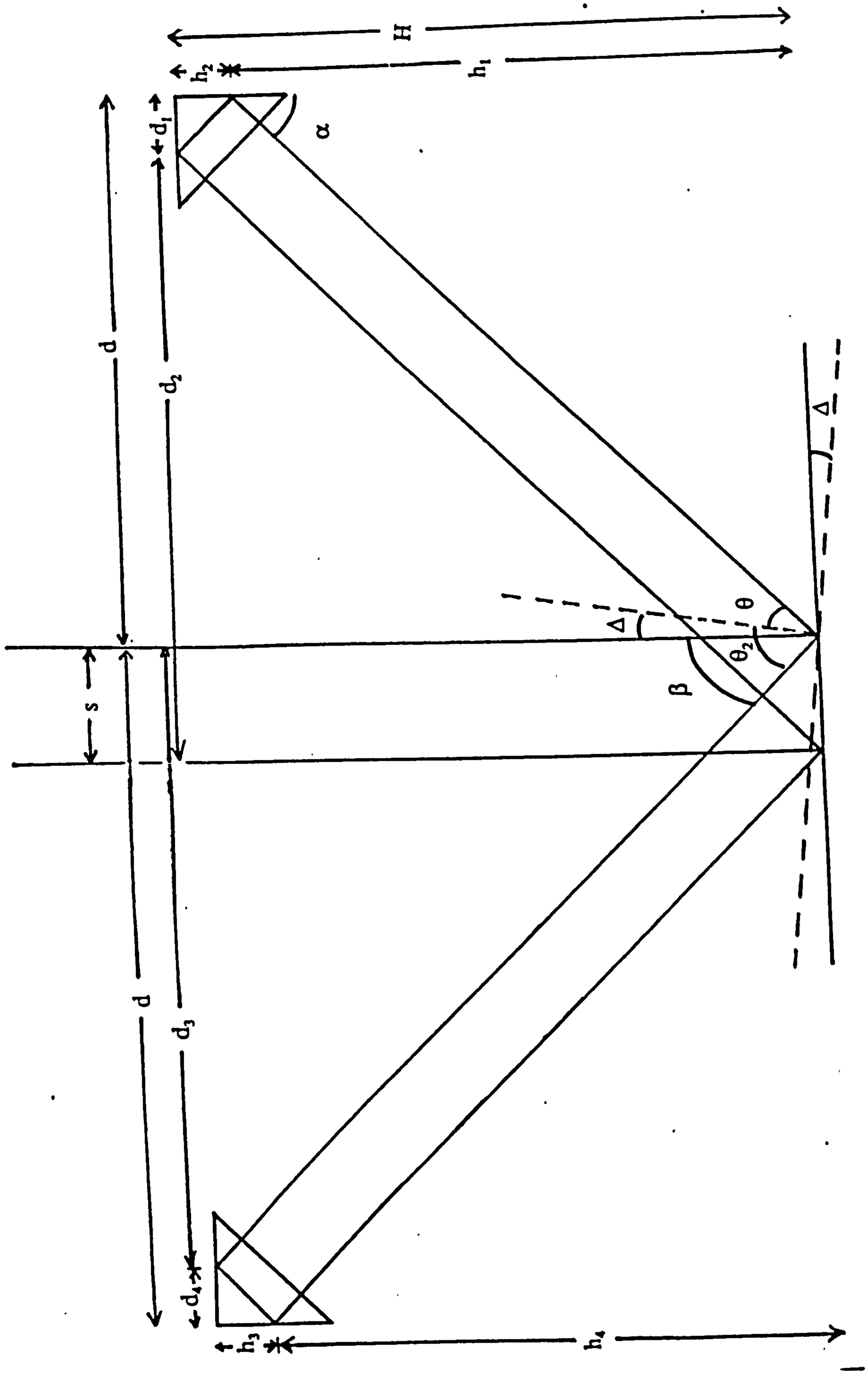

Figure a4.1: Error Due To Pitch

Appendix 5: The 3-Dimensional Coordinates of the Boat

Target	X	Y	Z
5	1.8746	2.5039	-0.6067
6	1.0500	3.5780	-0.2400
7	2.8820	3.3890	-0.2950
8	1.8640	2.0576	-1.1948
12	2.3140	2.4429	-0.6937
13	2.3140	2.4430	-0.6937
14	1.8801	2.4875	-0.7001
15	1.8801	2.4875	-0.7000
16	1.6406	2.5187	-0.7028
17	1.3556	2.5530	-0.7130
18	1.8510	2.2397	-0.8060
19	1.6166	2.2701	-0.8070
20	1.0363	2.5933	-0.7345
21	1.3189	2.3240	-0.8131
22	0.9998	2.4091	-0.8271
23	0.9997	2.4093	-0.8272
24	0.7325	2.6400	-0.7633
25	1.8387	2.1112	-0.9756
27	1.6029	2.1464	-0.9738
28	1.3021	2.2096	-0.9769
29	2.1674	2.0334	-1.1981
30	0.9721	2.3037	-0.9901
32	1.5592	2.1017	-1.1951
33	1.6095	2.1188	-1.1886
34	1.3089	2.1821	-1.1909
37	3.2423	2.3508	-0.7114
38	3.7233	2.3171	-0.7681
39	2.9955	2.3693	-0.7086
41	2.0806	2.4650	-0.6978
42	2.0749	2.4818	-0.6088
43	1.6333	2.5334	-0.6081
44	1.3464	2.5691	-0.6144
45	3.7197	2.2783	-0.8993
46	3.4450	2.2526	-0.8788
47	3.2416	2.2359	-0.8659
48	2.9890	2.2202	-0.8472
49	2.7570	2.2098	-0.8327
50	2.5187	2.2040	-0.8203
51	1.0285	2.6090	-0.6254
53	3.2520	2.1581	-1.0319
54	2.2890	2.2078	-0.8116
55	2.0514	2.2212	-0.8082
58	2.5161	2.0859	-0.9909

60	0.4300	2.7242	-0.7977
61	3.2656	2.1203	-1.2036
62	3.0042	2.0875	-1.1955
63	2.2840	2.0819	-0.9835
64	2.0486	2.0919	-0.9784
65	0.6893	2.5185	-0.8424
67	0.1977	2.7650	-0.8443
68	2.7807	2.0405	-1.2063
69	2.7743	2.0661	-1.1977
70	2.4480	2.0279	-1.2032
71	2.5254	2.0528	-1.2023
73	1.7801	2.0923	-1.1871
74	0.6506	2.4350	-1.0107
76	0.1490	2.7310	-1.0487
78	1.2546	2.1724	-1.1970
79	0.9765	2.2576	-1.2016
80	0.9811	2.2803	-1.1849
81	0.6401	2.3949	-1.2053
84	0.2390	2.6428	-1.2083
85	0.1363	2.7100	-1.2050
86	-0.0114	2.8104	-1.2086
88	-0.1284	2.8935	-1.2011
89	0.3872	2.5259	-1.2101
95	3.7811	2.5188	-0.1161
110	4.5168	7.5414	-2.0958
115	3.9695	5.0026	-2.2655
122	4.2837	7.9747	-4.3406
125	7.0440	7.2991	-4.1210
200	1.0500	3.5780	-0.2400
1	2.8820	3.3890	-0.2950
2	1.8640	2.0576	-1.1949
RMS se	0.00099	0.00781	0.01161
MAX se	0.00494	0.03161	0.03758

References

Ackermann F.	Photogrammetric Record Vol. 11 p429 (1984)
Atkinson K.B.	"Handbook of Non-Topographic Photogrammetry", Chap 3 (Ed. Karara H.M.), Am. Soc. Photogrammetry (1990)
Baltsavias E.P. & Stallmann D.	SPIE Vol.1395 p620 (1990)
Baratin L., Crosilla F. & Paronuzzi P.	SPIE Vol. 1395 p878 (1990)
Beyer H.A.	ISPRS Proc. Intercomm. Conf. Fast Processing Of Photogrammetric Data p68 (1987)
Brown S.B.	NPL Report MOM 104 (1991)
Bruck H.A.,McNeill S.R., Sutton M.A. & Peters W.H.	Exp. Mech. Vol 29 p.261 (1989)
Burch J.M. & Forno C.	SPIE Vol. 399 p412 (1983)
Dold J.	SPIE Vol. 1395 p252 (1990)
Downs M.J. & Raine K.W.	Precision Engineering Vol 4 p85 (1979)
Forbes A.	NPL Report DITC (1987)
Forno C.	PhD Thesis, University Of Surrey (1991)
Forstner W.	ACSM-ASPRS Ann. Conv. Vol IV, Washington (1986)
Fraser C.S. & Shortis M.R.	SPIE Vol 1395 p244 (1990)
Fritsch D.	"Optical 3-D Measurement Tech.",p87. (Ed Grün A. & Kahmen H.) (1989)
Gates J.W.C.,Oldfield S., Forno C., Scott P.J. & Kyle S.A.	Int. Arch. Of Photogrammetry, Vol 24 p185 (1982)
Ghosh S.K.	"Analytical Photogrammetry", Pergamon Press (1979)
Granshaw S.I.	Photogrammetric Record Vol 10 p181 (1980)

Huang Y.D. & Harley I.	SPIE Vol 1395 p1028 (1990)
Hunt R.A.H.	Comm. IV ISPRS Conference Rio de Janeiro (1984)
Hunt R.A.H.	NPL Report MOM 66 (1983)
Hunt R.A.H.	"Optical Methods In Engineering Metrology", Chap 4 (Ed. Williams D.C.), Chapman & Hall (1993)
Hutley M.C.	"Diffraction Gratings", Academic Press (1982)
Jenkins F.A. & White H.E.	"Fundamentals of Optics", McGraw-Hill (1976)
Lambert J.	"Die Perspektive in den Rontgenbildeern und die Technik der Stereoskopie", Fortschritte Rontgenstrahlen (1901)
Laussedat A.	"Recherches sur les Instruments, les Methodes et le Dessin Topographiques", Gauthier-Villars, Paris Vol 1(1898),Vol 2 part 1(1901), Vol 2 part 2 (1903)
Lenz R.	"Optical 3-D Measurement Tech.",p22. (Ed Grün A. & Kahmen H.) (1989)
Luhmann T.	ISPRS Int. Arch. Of Photog & Rem Sensing, Vol 26 part 5 p400 (1986)
Luhmann T. & Wester-Ebbinghaus W.	ISPRS Intercomm. Conf. on Fast Processing of Photogrammetric Data, p35 (1987)
MacLean S.G.,Rioux M., Blais F., Godski J.,Milgram P.,Pinkney H.F.L. & Aikenhead B.A.	SPIE Vol. 1395 p8 (1990)
Morley C.	NPL Report MOM (1990)
Oldfield S.	ISPRS Int. Arch. Of Photog & Rem Sensing, Vol 26 part 5 p541 (1986)
Pinkney H.F.L.,Perratt C.I. & Maclean S.G.	SPIE Vol. 1395 p374 (1990)
Post D.	"Handbook on Experimental Mechanics", Soc. for Exp. Mechanics, Chap 7 (1887)
Robson S.	SPIE Vol 1395 p236 (1990)

Rüther R. & Wildshek R. "Optical 3-D Measurement Tech.",p22. (Ed Grün A. & Kahmen H.) (1989)

Severn I. & Forno C. "Sensors: Technology, Systems & Applications", Vol 5 p299 (Ed Gratton K.T.V.) (1991)

Smith W.J. "Modern Optical Engineering", Mcgraw-Hill (1966)

Tabatabai A.J. & Mitchell O.R. IEEE Trans. Patt. Anal. & Mach. Int. PAMI-6(2) p188 (1984)

Trinder J.C. Photo. Eng & Rem. Sensing Vol 55 no 6 p883 (1989)

Turner-Smith A.R.,White S.P. & Bulstrode C. SPIE Vol 1395 p587 (1990)

van Voorden A. SPIE Vol 1395 p408 (1990)

Wilkinson J.H. & Reisch C. "Handbook For Automatic Computation", Vol 2, Linear Algebra, Springer-Verlag

Wolf P.R. "Elements of Photogrammetry", 2nd Ed (1983)

Wong K.W. & Wei-Hsin H. Photo. Eng. & Remote Sensing Vol 52(1) p67 (1986)

Zhou G. ACSM-ASPRS Annual Conv. Vol IV p256 (1986)

Note: The full title of SPIE Vol 1395 that is frequently referenced here is:-

Proceedings of ISPRS Commission V Symposium, Zurich (Ed Grün A. & Baltsavias E.P.) (1990)